In vitro models to measure antiretroviral drug permeability at vaginal mucosa

Carserides, Constandinos Andreas

Awarding institution:
King's College London

In vitro models to measure antiretroviral drug permeability at vaginal mucosa

A thesis submitted to the University of London for the degree of Doctor of Philosophy in Drug Delivery

by

Constandinos Carserides

Department of Mucosal & Salivary Biology Division

Dental Institute

King's College London

Abstract

This thesis describes an investigation of the permeability of three antiretroviral (ARV) drugs (that are under development as vaginal microbicides) using the human endometrial epithelial cell line, HEC-1A, as an *in vitro* model.

Barrier properties of HEC-1A cells in transwell cultures were determined by measurement of transepithelial electrical resistance (TEER), immunofluorescent staining of tight junctions and determination of the bi-directional permeability of, the paracellular marker, mannitol. Expression of specific uptake and efflux transporters were demonstrated by western blotting and compared with human tissue. Findings indicate that HEC-1A cells provide a physiologically relevant model to investigate permeability of candidate vaginal microbicides. In contrast, the commercially available EpiVagina™ model showed sub-optimal barrier properties.

Permeabilities of three ARV drugs Tenofovir (TFV), Darunavir (DRV) and Dapivirine (DPV) were investigated in the HEC-1A model. Efflux ratios of all drugs were approximately 1 indicating transporter-independent permeability across the epithelium. Apparent permeability (P_{app}) values for TFV were consistent with paracellular diffusion while those for DRV and DPV were indicative of transcellular diffusion. No drug-drug interactions were observed when drugs were co-administered in double combinations. To model the effects of inflammation on drug uptake, HEC-1A cultures were stimulated with a variety of toll-like receptor (TLR) ligands. The TLR-3 ligand Poly I:C stimulated pro-inflammatory cytokine production by HEC-1A cells but did not affect permeability of the drugs and no effect on TEER values was evident.

Permeability of DRV was also assessed using *ex vivo* rat and macaque cervicovaginal epithelial tissue. Consistent with findings from the HEC-1A model, DRV transfer across rat epithelium was transporter-independent although the P_{app} values were significantly lower. Preliminary data from macaque tissue indicate DRV may be effluxed.

Development of a robust and physiologically-relevant *in vitro* model will contribute to development of vaginal microbicides by allowing rapid measurement of drug transporter dependency, drug-drug interactions and testing of formulations aimed at

optimising tissue distribution. In this study, all of the ARVs showed transporter-independent transfer across the epithelium with no drug-drug interactions.

Acknowledgements

I would like to begin by thanking my supervisor Charles Kelly for his continuous guidance and support throughout the course of this journey. It has been a great privilege and I would like to express my gratitude for providing me with such an opportunity. I would like to also thank my second supervisor Ben Forbes and my colleagues at FWB (Abhinav and Magda) for their extremely useful guidance at the beginning and assistance throughout. Additionally, I would like to express my thanks to the team at the University of Aberdeen (Karolin, Kieron and Indrani) for their assistance and supervision with the mRNA expression procedures. I would like to also thank the team at Imperial College London (Robin, Carolina and Julia), for providing me with human vaginal tissue and the team at the CEA (Roger and Delphine) for providing macaque tissue and authorising me to undertake experiments within the facility. This work was part of the MOTIF (Microbicide Optimisation Through Innovative Formulations) project and funded by the European Commission. I thank all partners of the MOTIF consortium for the sharing of ideas. I would like to also thank Ana (FWB, King's College London) for undertaking the LC-MS analysis.

To the "Kelly lab" (Marta, Cherry, Sarah, and Stela) thank you for always being there and making this journey that extra bit more enjoyable. Especially, Carlo for his patience with my random questions and for his contribution to the P-gp transfection, Marta for her general assistance and contribution to the PAMP stimulation assays and Stela for the assistance with the Western blot analysis. I really appreciate your contribution.

Special thanks go also to the other PhD students and staff members whom all provided fantastic assistance/support and contributed to create the friendly environment at Hodgkin Building: Jessica, Yae-eun, Nina, Bushra, Zuraiza, Hersi, Jon, Dave, Shirley, Jemima, Stela, Simona, Mariana and Maria-Jose. I am truly grateful. Also, special thanks to Mahvash for making this happen.

Thank you to my family. As always, continuous support and encouragement throughout, especially by my Mum's famous words of wisdom "whatever will be, will be".

Finally, my girlfriend Charlene, thank you so much for guiding, encouraging and pushing me through this journey. You are amazing. Your turn next!

Table of contents

Figures

Tables

Abbreviations

(A-B)	Apical-to-Basolateral
(B-A)	Basolateral-to-Apical
(ABC)	ATP Binding Cassette
(AC)	Alternating Current
(AIDS)	Acquired Immunodeficiency Syndrome
(AMP)	Adenosine Monophosphate
(ARV)	Antiretroviral
(ATP)	Adenosine Triphosphate
(AUC)	Area under the Curve
(B-A)	Basolateral-to-Apical
(BBB)	Blood Brain Barrier
(BCA)	Bicinchoninic
(BCRP)	Breast Cancer Resistant Protein
(Bq)	Becquerel
(BSA)	Bovine Serum Albumin
(CA)	Capsid
(C_{max})	maximum blood plasma concentration
(C_{min})	minimum blood plasma concentration
(CNT)	Concentrative Nucleoside Transporters
(CVF)	Cervical Vaginal Fluid
(CYP)	Cytochrome P450
(dAMP)	2'-deoxyadenosine monophosphate
(DAPY)	Diarylpyrimidines
(DC)	Direct Current
(DEC)	Dead End Complex
(DMSO)	Dimethyl Sulfoxide
(dNTP)	Deoxyribonucleotides
(DPV)	Dapivirine
(DRV)	Darunavir
(DRM)	Drug Related Material
(EC_{50})	concentration that gives 50% response
(ECL)	Enhanced Chemiluminescence
(EHS)	Engelbreth-Holm-Swarm
(ENT)	Equilibrative Nucleoside Transporters
(Env)	Envelope
(ER)	Efflux Ratio
(ESCRT)	Endosomal Sorting Complex Required for Transport
(EVOM)	Epithelial Voltohmmeter
(FBS)	Fetal Bovine Serum
(FDA)	Food and Drug Administration
(FGT)	Female Genital Tract
(FLA)	Flagellin
(GP120)	Glycoprotein 120
(HBSS)	Hank's Balanced Salt Solution
(HEC)	Hydroxyethycellulose
(HEC-1A)	Human Endometrial Cell-1A
(HEPES)	(4-(2-hydroxyethyl)-1-piperazineethanesulfonic acid)
(HIV)	Human Immunodeficiency Virus
(HRP)	Horseradish Peroxidase
(IC 50)	50% inhibitory concentration

(IN)	Integrase
(IVR)	Intra-Vaginal Ring
(JAMs)	Junctional Adhesion Molecules
(LC-MS)	Liquid Chromatography–Mass Spectrometry
(LCs)	Langerhans Cells
(MA)	Matrix
(MCT)	Monocarboxylate Transporters
(MDR)	Multidrug-Resistant
(MFS)	Major Facilitator Superfamily
(MOTIF)	Microbicide Optimisation Through Innovative Formulation
(MVC)	Maraviroc
(N SITE)	Nucleotide binding site
(NBDs)	Nucleotide Binding Domains
(NC)	Nucleocapsid
(NHP)	Non-Human Primate
(NNRTIs)	Non-Nucleotide Reverse Transcriptase Inhibitors
(NPC)	Nuclear Pore Complex
(Nt/NRTIs)	Nucleotide/Nucleoside Reverse Transcriptase Inhibitors
(OAT)	Organic Anion Transporter
(P loop)	Phosphate binding Loop
(PAMPS)	Pathogen-Associated Molecular Patterns
(P_{app})	Apparent Permeability
(PBS)	Phosphate Buffered Saline
(PC)	Polycarbonate
(PCR)	Polymerase Chain Reaction
(PD)	Pharmacodynamics
(PDB)	Protein Database
(PDZ)	PSD59-D1gA-ZO-1
(PE)	Polyester
(PEP)	Post-Exposure Prophylaxis
(PEPT)	Peptide Transporters
(PFA)	Paraformaldehyde
(P-gp)	P-glycoprotein
(PIC)	Pre-Integration Complex
(PIs)	Protease Inhibitors
(PK)	Pharmacokinetic
(PMTCT)	Prevention of Mother-To-Child Transmission
(POT)	Proton-dependent Oligopeptide Transporters
(PR)	Protease
(PRO2000)	Polynaphthalene Sulphonate
(RPM)	Revolutions Per Minute
(RT)	Reverse Transcriptase
(SD)	Standard Deviation
(SDS)	Sodium Dodecyl sulphate
(SEM)	Scanning Electron Microscopy
(SIV)	Simian Immunodeficiency Virus
(SLC)	Solute Carrier
(SP)	Spacer Peptide
(STDs)	Sexually Transmitted Diseases
(STIs)	Sexually Transmitted Infections
(TAF)	Tenofovir Alafenamide
(TDF)	Tenofovir Disoproxil Fumarate
(TEER)	Transepithelial Electrical Resistance

(TFV)	Tenofovir
(TFV-DP)	Tenofovir Diphosphate
(THF)	Tetrahydrofuran
(TLR)	Tool-Like Receptor
(T_m)	Melting Temperature
(TMD)	Transmembrane Domain
(TMH)	Transmembrane α-Helices
(VMMC)	Voluntary Male Medical Circumcision
(ZO-1)	Zona Occludens-1
(Ω)	Ohms

Statement of work

With the exceptions listed below, all work described in this thesis was my own.

Marta Zinicola (KCL) contributed to the modelling of inflammation in HEC-1A and Epivaginal cultures as well as multiplex analyses of secreted cytokines. Carlo Scala (KCL) contributed to subcloning and expression of P-glycoprotein Kieron Smith (Aberdeen) prepared the primers for the qPCR analysis of drug transporter expression in the Epivaginal model. Determination of drug concentrations in macaque tissue and transport buffers by LCMS was undertaken by Anna Caldwell (KCL).

Chapter 1 Introduction

In 2015, 36.7 million people were estimated to be living with human immunodeficiency virus (HIV) and 1.1 million to have died from HIV [1]. Although the number of deaths has reduced from the peak of 2 million per year over the period 2004-2006, acquired immunodeficiency syndrome (AIDS) remains a major global health concern and new approaches to prevent infection are urgently required. Recently, clinical trials of vaginally applied anti-retroviral (ARV) drug formulations have shown some success in preventing HIV infection.

The demonstration in a phase IIb clinical trial (CAPRISA 004) that vaginal application of a gel formulation of the nucleotide reverse transcriptase inhibitor, Tenofovir (TFV), conferred 39% protection against infection with HIV [2] provided a significant boost to the development of topical microbicides based on anti-retroviral drugs. However, in a subsequent phase III trial of the same vaginal TFV gel (FACTS 001 trial) no overall protection was observed. Adherence was estimated by measurement of drug levels in vaginal fluid in a subgroup of participants. Findings indicated low adherence with women using the product on average in 50-60% sex acts [3]. Subgroup analyses of women with detectable TFV in vaginal fluid in this trial, however, showed significant protection against HIV infection of approximately 52% [4]. These findings suggest that topical microbicides may be effective but emphasise the need for improving use of any product.

More recently two phase III clinical trials (IPM027, RING study and MTN020, ASPIRE study) of the non-nucleoside reverse transcriptase inhibitor Dapivirine (DPV) in an intravaginal ring formulation were completed. These trials demonstrated reductions in HIV infections of 31% (RING) and 27% (ASPIRE), respectively when compared to placebo [5, 6]. Furthermore, in both studies, in women aged >21 higher levels of protection were observed with 37% in the RING study and 56% in the ASPIRE study. Further analyses confirmed higher levels of adherence in this age group compared with women aged 18-21. A phase I study to assess the safety, pharmacokinetics and pharmacodynamics of single and 14 days dosing with two vaginal microbicide formulations containing Darunavir (DRV), or DPV plus DRV presenting no adverse effects.

In contrast to earlier generation microbicides that targeted HIV fusion and entry or aimed at disruption of the virus particle (and which were not effective in clinical

trials), efficacy of ARV-based microbicides requires transfer of ARVs across the mucosal epithelium and uptake by sub-mucosal T cells that form the initial targets for HIV infection. Permeability of ARVs may be influenced no only by physiochemical properties of the drug but also by the activity of drug transporters (solute carrying efflux and uptake transporters) expressed at apical and basolateral surfaces of mucosal epithelial cells. The work described in this thesis aims to characterise the factors that affect permeability of ARVs at vaginal mucosa. It was undertaken as part of a collaborative multi-partner project: Microbicide Optimisation Through Innovative Formulation of Microbicides for Vaginal and Rectal Delivery (MOTIF). Other aspects of the project included characterisation of drug transporter expression in vaginal and rectal mucosae of humans and animal models, development of approaches for co-formulation of ARVs and pharmacokinetic (PK) and pharmacodynamics (PD) studies in animal models and tissue explants.

The overall aim of the work described in this thesis was to investigate factors that influence the permeability of three anti-retroviral drugs TFV, DPV and DRV across vaginal epithelium. Specific objectives were:

1. To develop and optimise an *in vitro* dual chamber model of vaginal epithelium for assessment of drug permeability.
2. To investigate permeability of three ARVs (TFV, DRV and DPV) across model epithelium
3. To develop a model of *in vitro* inflammation and assess effects on drug permeability
4. To compare drug permeability in different models including *ex vivo* epithelial tissue.

The work described in Chapter 4 focuses on the further development of a cell culture model for studies specific of vaginal drug permeability. The Human Endometrial Adenocarcinoma cell line, HEC-1A, was particularly suitable for permeability screening since it forms tight junctions and produces a stable epithelial barrier that forms within 6-10 days of culture. In addition, HEC-1A cells express several uptake and efflux drug transporters with a pattern of expression that, although not identical, is similar to that of human cervical and vaginal tissue. With regard to formation of a barrier epithelium in the dual chamber culture system, the HEC-1A model resembles the well-established, FDA (Food and Drug

Administration) approved intestinal permeability model based on Caco-2 cells [7]. Modelling of inflammation by stimulation of HEC-1A cultures with Toll-like receptor (TLR) ligands in the form of molecules acting as pathogen associated molecular patterns (PAMPS) was also investigated.

Chapter 5 assesses the cellular pharmacokinetics of single and double formulations of the three ARV drugs by measurement of bi-directional apparent permeability (P_{app}), drug distribution and efflux ratio (ER). These experiments demonstrate low TFV permeability via the paracellular pathway, while DRV and DPV show high permeability by passive diffusion via the transcellular pathway. This study also shows that permeability is drug transporter-independent and an absence of drug-drug interactions when drugs are combined. The effect of PAMP stimulation on drug permeability was also investigated

Chapter 6 is a comparison of alternative *in vitro* models to assess ARV permeability. Models investigated were the MatTek EpiVaginal™ primary cell-based model, and rat and macaque *ex vivo* vaginal tissue models.

Chapter 2 Literature Review

2.1 Introduction

This review outlines the epidemiology and origins of HIV/AIDS as well as the events involved in the HIV lifecycle and targets for prevention. Microbicides are described in some detail, including their mechanisms of action. Reference is made to the role of the vaginal epithelium as a barrier to HIV-1 and as a site for drug delivery. Finally, details of drug transporter expression and their mechanisms of action are described as well as the physiochemical properties of the drugs that form the focus of this study.

2.2 Epidemiology of HIV infection

In 1984 a human T-cell lymphotropic retrovirus was linked to the pathogenesis of the earlier discovered AIDS [8-10]. This retrovirus is now known as HIV-1 and AIDS has become a major health issue worldwide. In total, HIV-1 has infected almost 70 million people worldwide and AIDS is accountable for the death of over 34 million people. More than 30 years later, infection rates remain high with an estimated 2.1 million new infections and 1.1million deaths from AIDS-related illnesses during the year 2015 [11]. However, since 1997 there has been a significant decrease in new HIV infections from 3.5 million to 2.1 million in 2014 (Figure 2.1A). Additionally, as illustrated in Figure 2.1A the number of AIDS related deaths is also declining with approximately 1.1 million AIDS deaths in 2015, down from the estimated plateau of 2 million annually between 2004 and 2006. With increasing access to treatment, the number of people living with HIV is increasing and in 2015 was 36.7 million (Figure 2.1B).

HIV can be transmitted through sexual contact, the sharing of contaminated needles, infected mother to child transmission and by blood transfusions. Heterosexual transmission, however, accounts for the vast majority of infections. In 2015 there were approximately 5,700 new infections per day. Of these new infections the majority occurred in the developing world, and in particular Sub-Saharan Africa which remains the region most severely affected by the AIDS epidemic. In this region nearly 1 in every 20 adults is living with the virus. In 2015, an estimated 25.6 million people were living with HIV, (approximately 70% of the global HIV burden). In the same year, there were an estimated 2.1 million new HIV

infections and 1.1 million AIDS-related deaths. Nonetheless, between 2005 and 2015, the annual number of new HIV infections among adults in Sub-Saharan Africa has declined by approximately 40%. Conversely, new HIV infections in the Middle East and North Africa have increased by 4%, between 2010 and 2015. In Eastern Europe and Central Asia, new HIV infections have also increased by 57% during the same period (UNAIDS [1]).

A

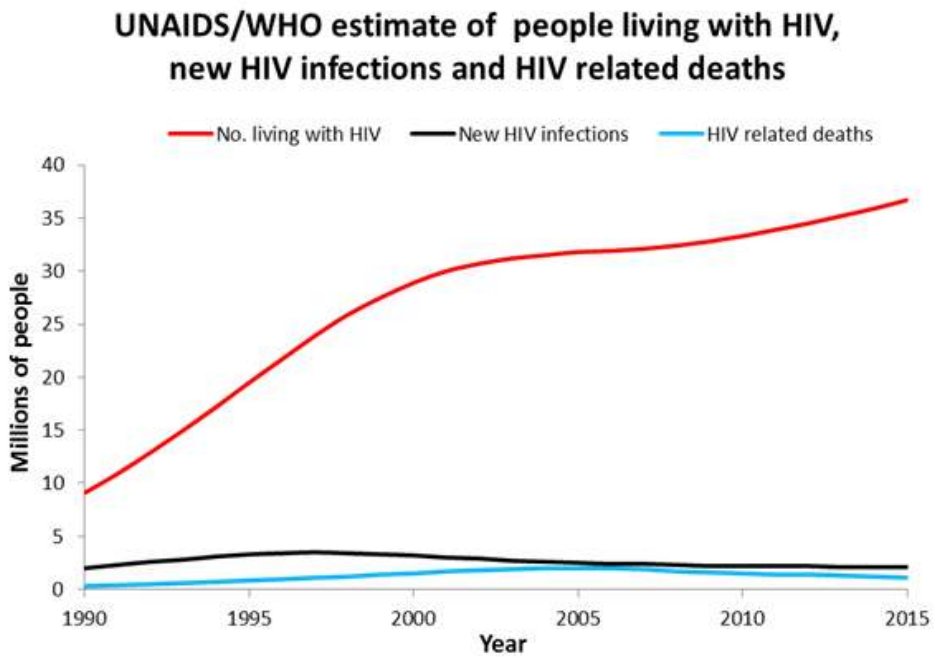

B

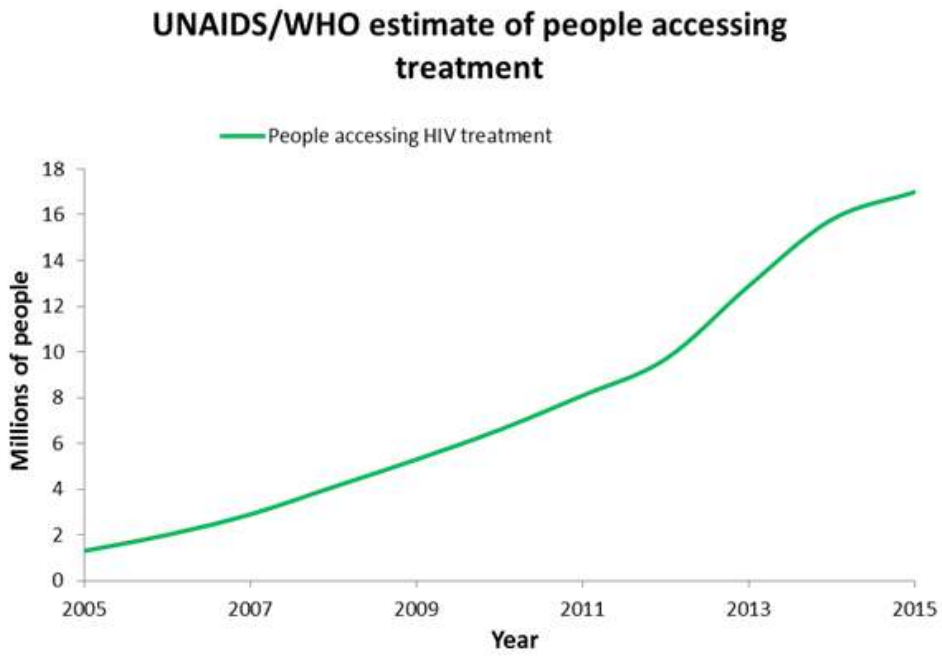

Figure 2.1 Plots of data from UNAIDS/WHO reports showing numbers of people living with HIV, new HIV infections, AIDS related deaths and access to HIV treatment. (A) Numbers of people living with HIV, new HIV infections and AIDS related deaths from 1990-2015. **(B)** Numbers of people accessing HIV treatment from 2005-2015.

2.2.1 Phylogeny and origin of HIV-1

The isolation of viruses, shown to be related to HIV by genome analyses, from several species of non-human primates (as well as other animal species) suggested that HIV originated by zoonotic transfer to humans [12]. These viruses are termed simian immunodeficiency virus (SIV) although not all cause immunodeficiency in the animal host. In particular, a strain of SIV, isolated from a chimpanzee (*Pan troglodytes troglodytes*) and termed SIVcpz showed identical genetic organisation to HIV-1 including the presence of the HIV-1-specific *vpu* gene and the lack of the *vpx* gene common to SIV [13]. Although the divergence in sequence between this strain and HIV-1 did not provide conclusive evidence for SIVcpz as the origin of HIV, subsequent analyses of further SIVcpz strains confirmed the close phylogenetic relationship between SIVcpz and HIV-1 and the significant distance from SIV isolates of species other than *P. t. troglodytes* [14]. Further phylogenetic analyses of SIV from various species of non-human primates demonstrated close clustering of SIVcpz Pol genes (encoding protease, reverse transcriptase and integrase) with those of SIVrcm isolates from red-capped mangabeys (*Cercopithecus nictitans*) while SIVcpz Envelope (Env) genes clustered closely with those of SIVgsn isolates from greater spot-nosed monkeys (*Cerocebus torquatus*) [15]. Acquisition of SIVrcm and SIVgsn by a single chimpanzee is suggested to result from predation [15] and led to recombination resulting in SIVcpz which was transmittable to other chimpanzees and subsequently by zoonotic transfer to humans [16].

The four different groups of HIV (M, N, O and P) each represent a single transmission event of SIVcpz to humans. Group M represents the pandemic form of HIV-1 accounting for the millions of infections worldwide. It contains 11 subtypes or clades (A1, A2, B, C, D, F1, F2, G, H, J and K). To investigate the early spread of HIV-1, all group M sequences in the HIV sequence database [17] (focussing on those encoding the Env C2V3 region) from countries in the Congo River basin were used together with sampling dates and geographical location in phylogenetic analyses to identify the Democratic Republic of the Congo (DRC) as the country from which group M HIV-1 spread [18]. Further phylogeographic analyses of sequences from different locations within the DRC as well as the neighbouring

Republic of Congo identified Kinshasa as the origin of the group M pandemic. The time of the most recent common ancestor of group M was estimated to be approximately 1920 [18]. Kinshasa was a convenient transport hub for roads, railways and rivers and entertained a growing sex trade around this time. The high population of migrants and sex trade might explain how HIV spread along these infrastructure routes, firstly to Brazzaville by 1937 and then onto Lubumbashi and Mbuji-Mayi respectively. The most prevalent HIV genetic forms are subtypes A, B, and C. Subtype A viruses are predominantly found in areas of central and Eastern Africa and Eastern Europe. Subtype B is the most geographically dispersed subtype and dominates Europe, Australia and the US. Subtype C is the most dominant HIV strain currently accounting for almost 50% of all HIV infection worldwide [19]. It is mainly located in southern and eastern Africa as well as in India.

2.3 Epidemiology of HIV infection in women

As of 2015 there were approximately 17.8 million women aged 15 years and older living with HIV; making up almost 48.5% of the people living with HIV worldwide and 80% residing in Sub-Saharan Africa. Here, women are disproportionately impacted by the HIV epidemic accounting for 58% of the total number of people living with HIV. There are almost 390 000 new HIV infections among adolescent girls and young women (15–24 years old) around the world every year. In Sub-Saharan Africa women acquire HIV infection at least 5–7 years earlier than men and young women (15–24 years old) are twice as likely to be living with HIV than men [1]. Women are particularly vulnerable to HIV infection for a variety of biological and socio-cultural reasons.

2.3.1 Socio-cultural factors associated with HIV infection in women

The disproportionately high HIV incidence amongst women (especially young women) is determined by sexual behaviour and patterning. Whilst women, when compared to men, share similar ages of sexual debut in Sub-Saharan Africa it has been shown that young women generally engage in sexual relationships with older men [20, 21]. This difference in age between partners maximises the risk of HIV acquisition by the younger partner since older individuals are more likely to be infected with HIV [21]. Additionally, women may struggle to negotiate condom use with their male counterpart. HIV rates can be high within young women reporting only a single lifetime partner and very limited sexual intercourse [20]. Other

behavioural factors such as douching and intra-vaginal practices may alter the vaginal flora [22, 23] which can potentially lead to inflammation, increasing the risk of HIV acquisition.

2.3.2 Biological factors associated with HIV infection in women

High HIV incidence per-coital act in young women [24] indicates that behavioural factors are unlikely to be solely responsible for increased susceptibility to infection [25]. An important factor that increases susceptibility to HIV infection is the much larger mucosal surface area of the female genital tract (FGT), the site of initial HIV exposure in women, compared with that of the penis and foreskin. Women may also be exposed for a longer duration to HIV as semen can remain within the FGT for up to three days post-coitus [26]. The mucosal immune environment is another important factor that may be responsible for increased vulnerability to infection. Cervical-associated $CD4^+$ T cells express higher levels, compared to blood-derived $CD4^+$ T cells, of the HIV co-receptor CCR5 and the $\alpha4\beta7$ integrin that not only mediates lymphocyte homing to mucosal lamina propria but also binds to HIV gp120 and may facilitate virus attachment [20]. Similar findings have been reported for foreskin-derived $CD4^+$ T cells [27, 28]. The increased expression of HIV co-receptors may further facilitate HIV infection. Finally, young women are more at risk to HIV infection compared to older women as the morphology within areas of the FGT gradually changes with age, particularly in the first pregnancy. The ectocervix transitions from a simple columnar and stratified squamous epithelium to a more mature predominantly squamous epithelium, a process known as squamous metaplasia. This simple columnar physiology of the ectocervix of a younger woman is more vulnerable to microabrasions during coitus [29, 30] which therefore provides a portal for HIV entry as well as entry for sexually transmitted infections (STI's) that contribute to HIV susceptibility, such as *Chlamydia trachomatis* and *Neisseria gonorrhoea* [31-33].

2.4 Targeting the viral lifecycle of HIV

2.4.1 HIV structure

The HIV-1 virion is approximately 150nm in diameter and like all retroviruses, possesses an inner core (Figure 2.2). This inner core contains two identical copies of 9.2kb single-stranded (sense) RNA molecules that are associated with the

nucleocapsid (NC) protein or p7. The inner core, the viral enzymes crucial for virus infection and replication (protease (PR), reverse transcriptase (RT), integrase (IN)) and the regulatory proteins tat, rev, nef, vif, vpr, and vpu are enclosed within the capsid (CA) protein p24. The capsid itself is surrounded by a lipid bilayer that derives from the infected host cell lipid membrane. The inner surface of this envelope is coated by the matrix (MA) protein p17, whereas the external surface exposes the Env glycoproteins gp120 and gp41 which are embedded within the lipid bilayer and responsible for binding and fusion of the virus to the host cell membrane. Cryo-electron tomography has shown that the late budding stage of a mature virion from the lipid bilayer represents an almost completely closed sphere whilst the inner HIV CA exhibits a tubular and coned morphology [34].

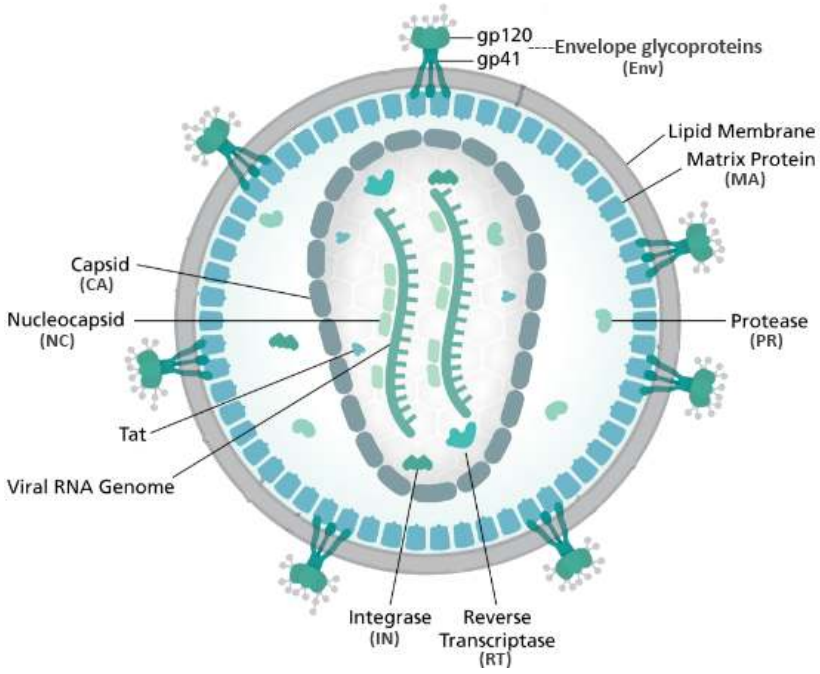

Figure 2.2 Basic diagram of a mature HIV-1 virion. HIV forms a spherical structure with the Env proteins gp120 and gp41 projecting through the lipid membrane. The inner surface of the bilayer is coated by the MA protein. The inner viral CA bilayer surrounds crucial proteins (PR, IN, RT and Tat) necessary for virus maturation. The cone shaped CA also houses the viral RNA genome that is associated with the NC proteins.

2.4.2 HIV-1 lifecycle

The HIV-1 lifecycle involves multiple stages. These included HIV-1 binding, fusion, reverse transcription, integration, transcription and translation, assembly, release and maturation and are described further below.

2.4.2.1 HIV-1 binding, fusion and reverse transcription

HIV infection of target cells requires fusion of the viral membrane and host cell membrane which is initiated by binding of the CD4 receptor and one of two chemokine receptor molecules CXCR4 or CCR5 with the virus envelope glycoprotein 120 (gp120). Primary infection involves exclusively binding of gp120 to the CCR5 [35, 36] receptor in both mucosal and intravenous transmission of HIV infection. Conversely, viruses that bind to the CXCR4 receptor are more commonly found in later stages of infection as the disease progresses to AIDS [37]. Once bound to CD4, a conformational change in gp120 is triggered which leads to the exposure of the co-receptor binding site. Binding of gp120 (through the V3 loop) to the co-receptor further triggers a conformational change in gp41 that leads to exposure of the N-terminal hydrophobic fusion peptide of gp41 that can penetrate into the host cell membrane. Further conformational changes in gp41 lead to shedding of gp120 and formation of a 6 α-helical bundle structure that promotes fusion of viral and host cell membranes. The HIV-1 capsid is then released and uncoats discharging the viral core into the host cell cytosol where reverse transcription is initiated. Recent experimental evidence suggests that three sequential mechanisms are involved in the uncoating process namely, immediate uncoating, cytoplasmic uncoating and nuclear pore complex (NPC) uncoating [38]. RT has two enzymatic activities; a DNA polymerase that synthesises the complementary DNA strand from the tRNA primer carried within the virus particle associated with the RNA genome, and an RNAse H that cleaves RNA that is part of an RNA/DNA duplex only. These two enzymatic processes convert viral RNA to double stranded viral cDNA [39].

2.4.2.2 HIV-1 integration, transcription and translation

Full length double stranded HIV cDNA is translocated into the host nucleus catalysed by the viral enzyme IN which interacts with cellular co-factors. The viral DNA is part of a large nucleoprotein complex known as the Pre-integration Complex (PIC), which derives from the viral core [40]. The PIC travels towards the nuclear envelope via a microtubule network [41] and subsequently enters the nucleus through the nuclear pore complex. A series of DNA breaking and joining reactions, along with the catalytic activity of IN, efficiently mediates the integration of the viral DNA within the PIC into the target DNA. Once integrated, short completely spliced mRNAs (produced by HIV-1) encoding the viral regulatory proteins Tat and Rev are

produced. Incompletely spliced mRNAs are also produced as the infection progresses; these encode the Env protein gp160 and the accessory genes Vif, Vpr, and Vpu. Full length unspliced transcripts are also synthesised and act both as the virion genomic RNA and the mRNA for the Gag-Pol polyprotein (discussed below). Tat and Rev promote transcription of the integrated HIV genome and nuclear export of intron-containing viral RNAs, respectively (reviewed in [42]).

2.4.2.3 HIV-1 assembly, release and maturation

The viral envelope glycoprotein Env is transported to the plasma membrane in vesicles via a secretory pathway during which it is cleaved by furin or furin-like proteases to produce gp120 and gp41 which remain non-covalently complexed. The viral polyproteins Gag and Gag-Pol are synthesised following Rev-mediated export from the nucleus of the intron-containing viral RNAs. Gag, a 55kDa precursor protein that is myristoylated at the N-terminus contains the MA, CA, NC, p6 proteins as well as two spacer peptides (SP1 and SP2) (Figure 2.3). The MA domain directs Gag to the plasma membrane promoting the incorporation of the viral Env glycoproteins into the newly produced virions. Gag molecules anchor in the plasma membrane by inserting the amino-terminal myristoyl group into the lipid bilayer and by direct interactions with acidic phospholipids [43, 44]. The CA domain mediates assembly of the Gag multimers and the p6 domain recruits the cellular endosomal sorting complex required for transport (ESCRT) apparatus which is important for completing the budding process of the virus [45]. Gag-Pol is a 165kDa polyprotein precursor which comprises Gag as well as the viral enzymes PR, RT and IN. After release of the immature virion, the viral PR is activated and cleaves the Gag precursor in a highly ordered, stepwise processing cascade [46] to form functional mature virions (as reviewed in [47]).

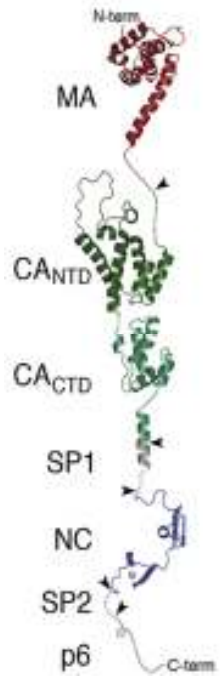

Figure 2.3 Structural model of the Gag polypeptide. Derived from high-resolution structures and models of isolated domains. Arrowheads indicate PR cleavage sites [48].

2.4.3 Structure of HIV-1 reverse transcriptase and protease

2.4.3.1 HIV reverse transcriptase

HIV RT is an asymmetric heterodimer comprising two related subunits p66 and p51. The p66 subunit is 560 amino acids in length and the p51 subunit, formed by proteolysis of p66 is 440 amino acids in length. Both subunits share four common amino terminal domains. These domains are referred to as “fingers”, “palm”, “thumb” and “connection” [49] (Figure 2.4). The larger p66 subunit of the RT heterodimer possesses both DNA polymerase and RNAse H activity. The smaller p51 subunit plays a more structural role and is important for stabilising the p66 subunit. The reverse transcription reaction starts with the binding of RT to the nucleic acid substrate leading to a conformational change of the p66 thumb from a “closed” to “open” state [39]. Requiring a primer (provided by the tRNA- Lys 3) and template, RT binds double stranded nucleic acid in the correct pairing orientation 5’-3’ at the priming site (P site) which is adjacent to the polymerase active site [50, 51]. Nucleotide incorporation involves binding of the incoming deoxynucleotide triphosphate (dNTP) to the nucleotide binding site (N site) forming a ternary complex [51]. The polymerisation reaction is a conformational change in which a

portion of the fingers of the p66 subdomain close down on the dNTP which helps to align the 3'-OH of the viral RNA strand, the α-phosphate of the dNTP, and the polymerase active site to form the phosphodiester bond linking the nucleotide to the growing DNA strand [52]. Once the new nucleotide has been incorporated the fingers open and the substrate is released permitting the arrival of the next incoming dNTP. This process continues until single stranded viral RNA is transcribed into a viral hybrid RNA/DNA double helix. RNAse H then breaks down the RNA and the polymerase completes the remaining DNA strand to form DNA/DNA double helix, producing proviral DNA containing the genetic material for HIV-1.

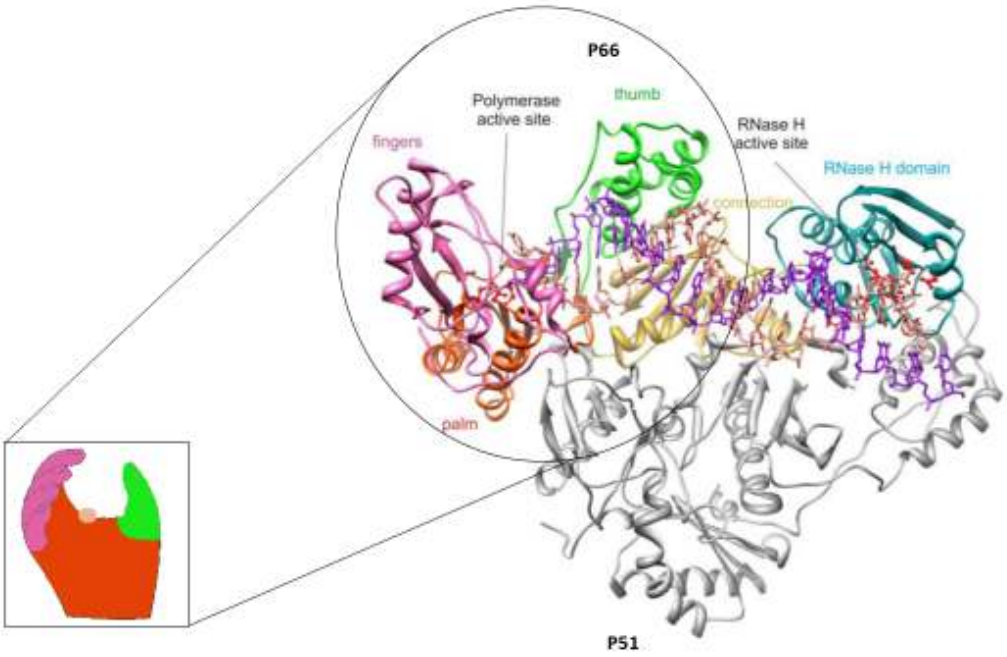

Figure 2.4 The structure of p66 and p51 asymmetric heterodimeric HIV RT in complex with nucleic acid representing a hand like structure.
The fingers (pink), palm (orange), thumb (green), connection (yellow), RNAse H domain (turquoise), polymerase active site (cream) and RNAse H active site subdomains of the p66 RT subunit are shown. The p51 subunit is in grey and RNA in purple. Figure adapted from [53].

2.4.3.2 HIV protease

The HIV protease is essential for virus maturation. The enzyme cleaves the viral Gag and Gag-Pol polyproteins in the immature virus particle that buds off from host cells, at 9 different processing sites to produce active forms of the proteins required for infection [54]. The protease (molecular weight 21.6 kDa) is formed by packing

together of two identical subunits (99 amino acid residues each) to form a flattened dome-like structure. More than 700 structures of the protease have been deposited in the protein data bank [55].

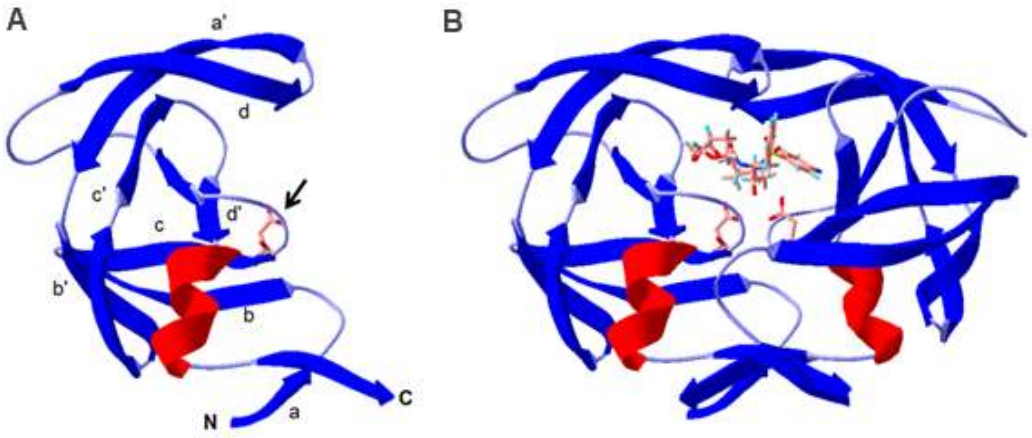

Figure 2.5 Structure of HIV-1 protease. The structure is represented as a ribbon diagram derived from crystal structure determined at a resolution of 1.8Å [56]. Panel **(A)** shows the arrangement of 8 β-strands (blue) and the single α-helix (red) in each of the monomers that form the protease structure. The side-chain of the catalytic Asp 25 is shown (arrowed) and the N- and C-termini are indicated. Panel **(B)** shows the structure of the homodimer with bound substrate (DRV). Strands d and a′ from each monomer are pulled down towards the active site forming a lid-like structure. Structures were drawn using Swiss PDB viewer with coordinates from the Protein Data Bank (PDB ID 5E5K).

The structure of the protease shown in Figure 2.5 by a ribbon diagram was determined at a resolution of 1.8Å [57]. Each monomer folds as a series of 8 β-strands with hairpin loops and a single α-helix. The β-strands show two fold pseudosymmetry and are labelled a,b,c,d and a′, b′,c′,d′ , respectively. Strands c and d′ and strands c′ and d form two pairs of parallel strands while strands b and c and strands b′ and c′ form anti-parallel sheets. The two monomers fold together to form the protease with a single catalytic site where the conserved Asp (or Asn) residues (position 25) from each monomer are in proximity. Strands d and a′ form flexible flap structures that in the liganded structure (panel b) move downwards towards the active site (closed state), as shown in (Figure 2.6A). In the absence of substrate, the flaps shift to a semi-open state (Figure 2.6B) that allow substrates to access the active site [58].

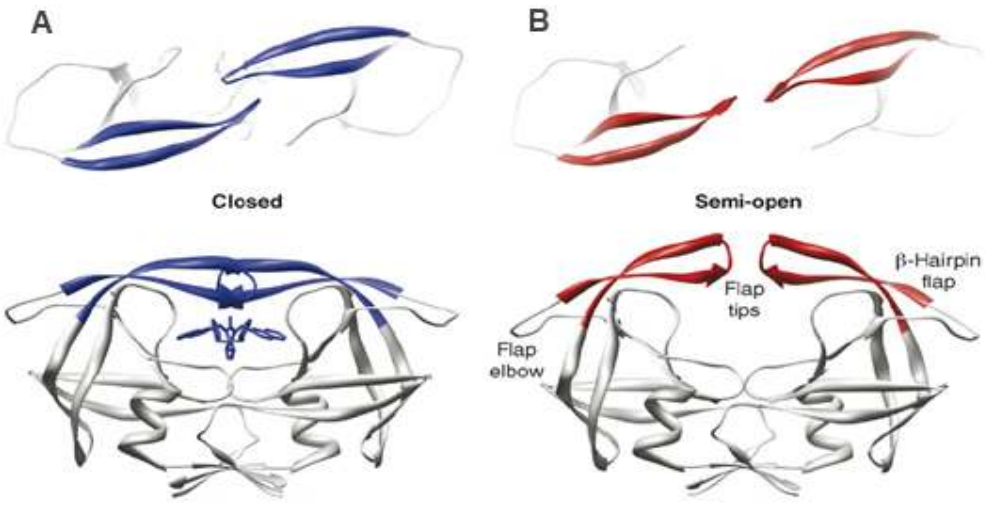

Figure 2.6 The two conformations of HIV-1 protease (top and side view). (A) The β-hairpin flaps in their "closed" conformation with a substrate bound to the active site (crystal structure from PDB code 1HVR is shown at a resolution of 1.8Å) **(B)** The "open" conformation of the flaps following an unbound substrate at the active site allowing it to become accessible (crystal structure from PDB 1HHP is shown at a resolution of 1.8Å).The two top views highlight the change in flap structure when in "open" and "closed" states. Illustration adapted from [58].

2.4.4 Prevention of HIV-1 infection

Recommendations for HIV prevention involve the use of condoms, sexual abstinence, and male circumcision [59, 60]. Compliance with the first two approaches is low. Voluntary male medical circumcision (VMMC) is partially effective [61] and programmes to expand the provision of VMMC are in progress in 14 countries in Africa with the aim of achieving 80% coverage in men [62]. Alternative methods of prevention are urgently needed.

An alternate prophylactic approach under investigation is the development of antiretroviral (ARV) agents that are designed for topical application at the vaginal or rectal mucosae to prevent infection. These products are known as microbicides and several different formulations in various delivery systems have been investigated including gels, capsules, tablets, films and intra-vaginal rings (IVR) [2, 63-66]. Microbicides are designed to be applied either at the time of coitus or on a daily basis and provide women with the opportunity to discreetly protect themselves. These dosage forms provide the ability to self-administer directly at the site of infection and limit systemic drug delivery. Requirements for an ideal vaginal microbicide are that it should:

- retain anti-HIV activity in the presence of semen and over a pH range that includes the low pH of the vagina
- not disrupt the normal vaginal microbiota
- not induce inflammation or impair barrier properties of the vaginal epithelium
- be amenable to formulation that are compatible with condom use
- have potential for topical or sustained release formulation
- deliver the active pharmaceutical ingredient to target tissues in sufficient concentrations to prevent infection
- have potential for large-scale production at an affordable cost [67-69].

2.5 Microbicides and their mechanisms as a preventative measure against vaginal HIV infection

Initial development of microbicides focused on a class of agents targeting the earlier stages of the HIV lifecycle by disrupting HIV virions or preventing virion fusion and cell entry [70]. Such compounds included surfactants, polyanions and acid buffering agents. One of the early attempts to prevent HIV was by using the surfactant nonoxynol-9, however, in a phase 3 clinical trial involving female sex workers , an increase in infection in the treatment group was observed when compared to the placebo group [71]. Nonoxynol-9 displayed the capabilities of mediating epithelial toxicity as increasing frequency of lesions correlated with escalating doses of nonoxynol-9 in the vaginal and cervical epithelium of women [72]. Additionally, epithelial toxicity was shown to compromise the integrity of the murine vaginal epithelium [73].

Other early generation compounds considered were long chain polyanionic molecules that could prevent HIV infection *in vitro* as they were able to prevent infection by binding to the gp120 envelope protein [74] on the virion surface, thereby restricting the viral binding to target cells [75]. Clinical trials of vaginal gel formulations of polyanions such as cellulose sulphate, polynaphthalene sulphonate (PRO-2000) and a specific form of the sulphated polysaccharide carrageenan (Carraguard) showed no protection against HIV infection [76].

With these early generation microbicides failing to demonstrate efficacy in clinical trials, the focus of microbicide development shifted to specific highly active ARV drugs. ARVs target post-fusion stages of the HIV cycle by preventing the replication

of viral genetic material, preventing the insertion of viral genetic material into human DNA and preventing the processing of viral proteins (Figure 2.7). ARVs are under investigation as potential microbicides from the following classes: nucleotide/nucleoside reverse transcriptase inhibitors (Nt/NRTIs), non-nucleotide reverse transcriptase inhibitors (NNRTIs), integrase inhibitors and protease inhibitors (PIs).

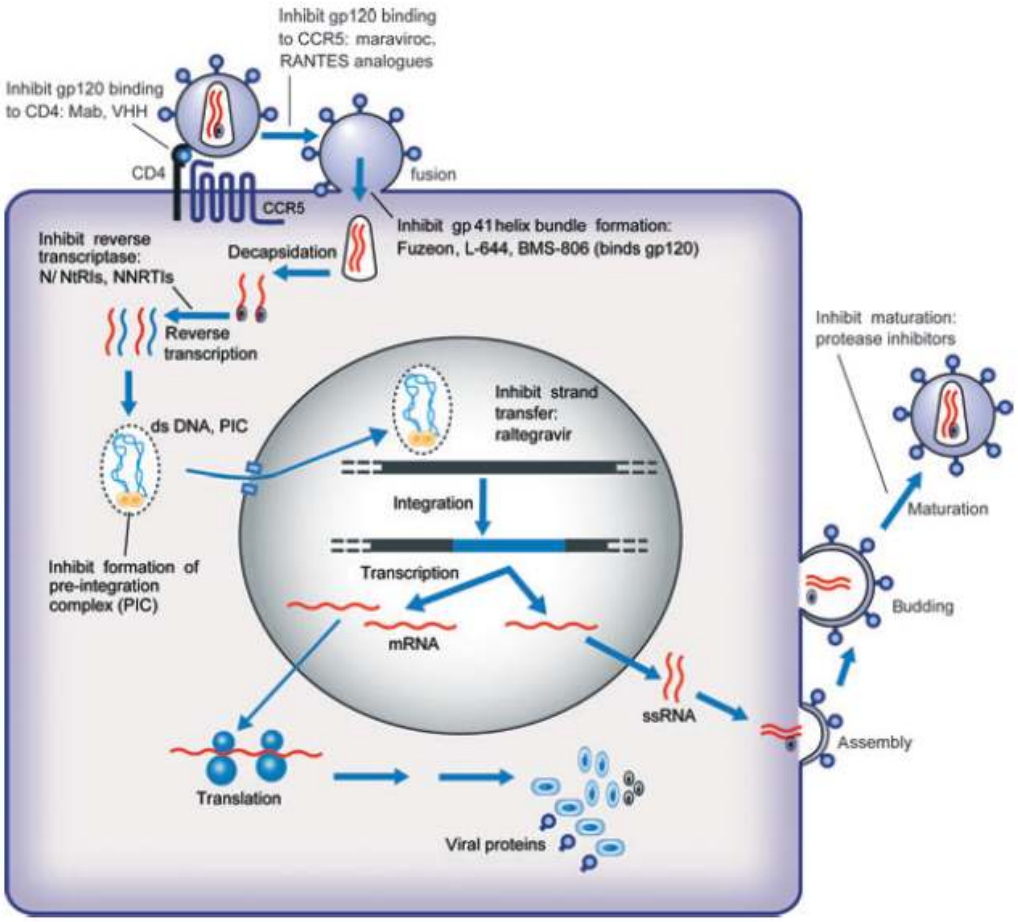

Figure 2.7 HIV lifecycle and targets for intervention with microbicides. Microbicides products that have been developed to target various stages of the HIV-1 lifecycle [70].

2.5.1 NRTIs/NtRTIs

NRTIs were the first class of drugs developed for HIV therapy [77]. They were also shown to be effective in post-exposure prophylaxis (PEP) and in prevention of mother-to-child transmission (PMTCT) [78]. This class of drug is able to block reverse transcription (Figure 2.8) by mimicking endogenous intracellular nucleoside

triphosphates for incorporation into the growing HIV DNA strand. These nucleoside/nucleotide analogues lack the 3' OH group found in normal dNTPs and therefore cannot form 3'-5' phosphodiester bonds with adjacent dNTPs, resulting in the formation of a dead end complex (DEC) that prevents production of viral cDNA [79]. Activation of NRTIs requires three consecutive phosphorylation reactions by intracellular kinases, whereas NtRTIs carry a phosphonate group and require only two consecutive phosphorylation reactions for activation [70, 80]. TFV, a small water-soluble NtRTI is currently the most advanced candidate in microbicide development. In a pivotal NHP (non-human primate) vaginal challenge study, 1% TFV gel showed full protection against SIV infection [81]. This provided a rationale for further development leading to a double-blinded, randomised, placebo controlled phase IIb clinical trial in South Africa [2]. The CAPRISA 004 trial demonstrated for the first time that an ARV-based microbicide could reduce HIV infection in women by 39% over a 30-month period, compared to hydroxyethycellulose (HEC) placebo gel. Furthermore, at 1 year, protection was 50% and amongst women who used the gel efficiently (>80% compliance), the overall reduction was 53% [2].

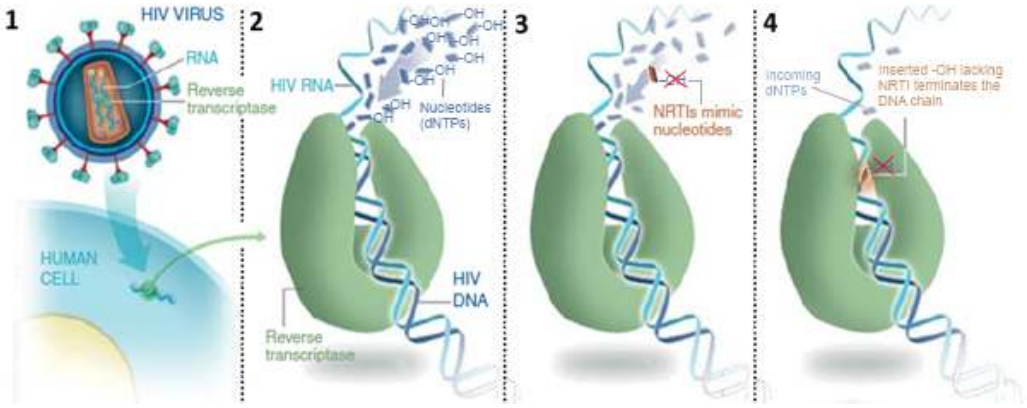

Figure 2.8 The action of NRTI such as TVF. (1) HIV virus releases its viral core into the host cell. This includes the viral protein RT which is responsible for creating HIV DNA for insertion into the host cell's DNA. (2) Normally, using nucleotides (dNTPs) RT converts single stranded HIV RNA into HIV DNA. (3) NRTIs such as TFV lack the 3' OH groups found in normal dNTPs but mimic the remaining nucleotide structure and are inserted into the new HIV DNA chain. (4) The next incoming nucleotide is unable to bind to the already incorporated hydroxyl lacking nucleotide which leads to the development of a DEC, resulting in the termination of the growing viral DNA chain. Illustration adapted from [68].

Nonetheless, replicating such data has proven more difficult than expected. A phase IIb trial, VOICE (MTN-003), designed to test the efficacy of an oral dosage form of TFV (Truvada) as well as TFV vaginal gel showed no significant protection [82]. Adherence to use of the gel product, estimated by measurement of drug in blood

samples from trial participants, was determined to be approximately 29% and likely contributed to the observed lack of protection. In subgroup analyses of women using the vaginal gel and who had detectable drug in blood samples, significant protection was observed (66%). Similar lack of compliance was reported in a phase III trial of a vaginal TFV gel (FACTS 001 trial) which followed on from the CAPRISA 004 trial. Again, the trial demonstrated no overall protection. Adherence was estimated by measurement of drug levels in vaginal fluid in a subgroup of participants. Findings indicated low adherence with women using the product on average in 50-60% sex acts [4]. Subgroup analyses of women with detectable TFV in vaginal fluid in this trial, however, showed significant protection against HIV infection of approximately 52% [3]. These trials demonstrate that vaginal microbicides have the potential to protect against HIV infection but emphasise the need to develop approaches to administration of the microbicide that will improve adherence. One such approach is discussed in the next section.

2.5.2 NNRTIs

The second class of reverse transcriptase inhibitors are NNRTIs. These non-competitive inhibitors bind to an induced allosteric hydrophobic pocket located in the palm subdomain of p66 that is 10Å from the polymerase active site of the reverse transcriptase enzyme [83]. NNRTIs (Figure 2.9) induce the p66 thumb to adopt an open and extended position blocking the conformational flexibility of this region on the RT enzyme [84]. These movements by RT are necessary for the catalytic cycle of the enzyme as only a closed position allows transcription of RNA. This conformational change to the structure of the RT enzyme prevents incoming dNTPs from binding to the HIV RNA, thereby preventing the formation of HIV dsDNA. A number of NNRTIs are currently being investigated as potential microbicides.

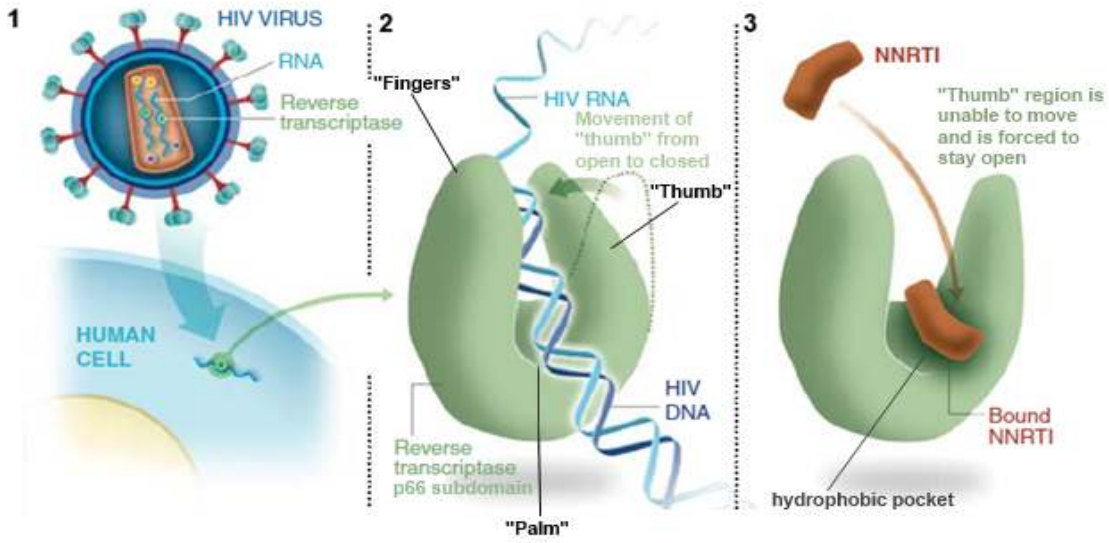

Figure 2.9 The action of NNRTI such as DPV. (1) HIV virus releases its viral core into the host cell. This includes the viral protein RT which is responsible for creating HIV DNA for insertion into the host cell's DNA. (2) The "fingers" region of the RT p66 subdomain close in order to align the HIV RNA strand and the dNTP. Once the new nucleoside has been incorporated the fingers open and the substrate is released permitting the arrival of the next incoming dNTP. (3) NNRTIs like DPV bind to a hydrophobic pocket located in the palm subdomain inducing the p66 thumb into an open and extended position blocking the conformational flexibility of this region on the RT enzyme. This conformational change to the structure of the RT enzyme prevents incoming dNTP's from binding to the HIV RNA, thereby preventing the further formation of HIV DNA. Illustration adapted from [68].

Current NNRTIs being developed as microbicides include Dapivirine, (TMC120), UC781, MIV-150, MIV-160, MIV-170, MC1220, and IQP-0528. Of these, Dapivirine (DPV) is the most advanced along the development pathway (Figure 2.9). In pre-clinical studies, intravaginal administration of a radiolabelled [^{14}C]DPV gel formulation showed high levels of drug accumulation in tissue 1hour after the final dose, and remained detectable at 24 hours in rabbits (mean, ≥2.5 ng/g) and 48 hours in macaques (mean, >80 g/ng) [85]. Minimal radioactivity levels were detected in the plasma and were undetectable in the draining lymph nodes of macaques. Moreover, drug related material (DRM) was detected by microautoradiography on the surfaces of vaginal and cervical tissues of both rabbits and macaques. In macaques DRM was shown to concentrate in the keratinised epithelial layer and penetrate deep into the germinal layer of vaginal epithelia [85]. The hydrophobic nature of DPV may be advantageous for topical application resulting in high concentrations locally with minimal systemic exposure. DPV has undergone phase I and phase II PK trials in both gel and intravaginal ring (IVR) formulations. More recently the IVR formulation has been tested in two phase III

clinical trials (IPM027, RING study and MTN020, ASPIRE study). These trials demonstrated reductions in HIV infections of 31% (RING) and 27% (ASPIRE), respectively when compared to placebo [5, 6]. Furthermore, in both studies, in women aged >21 higher levels of protection were observed with 37% in the RING study and 56% in the ASPIRE study. Further analyses confirmed higher levels of adherence in this age group compared with women aged 18-21. In the younger age group, little or no protection was observed in women. The relative success of these trials suggests that a sustained release formulation of vaginal microbicides may be more attractive to users than the gel applicators used in trials of TFV gel.

2.5.3 Integrase inhibitors

While very important for the treatment of HIV, microbicides containing integrase inhibitors are yet to be as extensively studied in comparison to the other ARV microbicides. In a two-step reaction, HIV-1 integrase is able to integrate proviral reverse-transcribed DNA into the host genome. However, oral raltegravir and elitegravir are two inhibitors that are able to specifically inhibit this proviral DNA-strand transfer, resulting in potent *in vitro* activity against HIV-1. Raltegravir is used for treatment of HIV infection and is approved for twice-daily oral administration [86, 87]. Long acting injectable formulations of integrase inhibitors to be administered by the intramuscular route are also being developed. This may be a means of improving adherence. The integrase strand transfer inhibitor (INSTI) GSK 1265744 has recently showed promising potent antiviral activity when given as an 800 mg intramuscular dose [88]. Similarly, a long lasting injectable formulation of rilpivirine is under investigation for prophylaxis against infection [89].

2.5.4 Protease Inhibitors

Virus maturation mediated by HIV protease have become a major target for anti-HIV drugs, leading to the development of PIs [90]. PIs inhibit HIV maturation by blocking the active site of the HIV-1 PR enzyme [54]. This interaction keeps the active site covered as the flaps of the enzyme are in the closed conformation, preventing binding of the viral protein substrates thus inactivating the enzyme. Of 26 anti-HIV compounds approved by the FDA 10 are PIs, these include saquinavir, indinavir, ritonavir, nelfinavir, amprenavir, fosamprenavir, lopinavir, atazanavir, tipranavir, and DRV. Most of these inhibitors are associated with serious side effects such as dyslipidaemia, insulin-resistance, lipodystrophy/lipoatrophy, cardiovascular and

cerebrovascular diseases when used long term [91-94]. DRV shows high *in vitro* and *in vivo* potency against a broad range of HIV-1 strains, including wild type and multidrug-resistant (MDR) clinical strains [95, 96]. DRV was effective against PI-resistant recombinant viruses (1,401 strains) derived from clinical samples [95]. DRV binds with high affinity to the protease active site forming hydrogen bonds directly or via water molecules with residues in both the catalytic site and the flap regions (Figure 2.10). Ritonavir boosted DRV (DRV 800 mg plus ritonavir 100 mg) is a current first-line antiretroviral regimen associated with minor side effects.

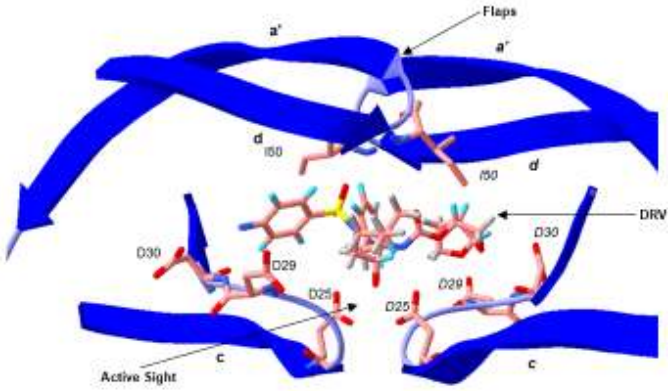

Figure 2.10 Darunavir in the HIV-1 protease binding site. Close up view of substrate binding with strands labelled as in Figure 2.5. Residues that form H-bonds with DRV are shown. H-bonding of the backbone nitrogen atoms of Ile 50 at the C-terminal of strand d from both subunits to DRV is via a highly conserved tetrahedrally coordinated water molecule. In the catalytic site, Asp 25 and Asp 29 from both subunits form H-bonds with DRV as does the backbone nitrogen of Asp 30. Structure was drawn using Swiss PDB viewer with coordinates from the Protein Data Bank (PDB ID 5E5K).

2.5.5 Combination-based microbicides

To improve the efficacy of microbicides, approaches such as formulations containing combinations of drugs has been considered. These combination-based microbicides provide improved efficacy by providing protection against the transmission of resistant viral strains [97] and targeting different stages of the lifecycle providing greater protection [68]. Additionally, combination-based microbicides may allow exploitation of useful drug–drug interactions either as additive or synergistic inhibitors or as a potential means of increasing drug uptake and retention in local tissues by effects on drug transporters for drug metabolism [70]. Such interactions may allow for lower initial drug doses and thereby minimise

the systemic exposure and adverse effects. While successful double combination regimens are currently used for orally administered HIV treatment (as described above), combination gel-based products are under investigation. Macaques administered with 3ml 1% TFV gel with 5% emtricitabine showed 100% protection against SHIV infection with less than 0.05% of both drug detected in the blood plasma after 30 minutes exposure [98]. More recently a DRV and DPV gel has been tested in a phase 1 clinical trial, showing no adverse effects. Additionally, a combination of DPV and the CCR5 inhibitor maraviroc (MVC) vaginal ring demonstrated concentration-dependent inhibition of HIV-1 infection in cervical tissue by DPV, however MVC concentrations were consistently detectable only in cervical vaginal fluid (CVF) and not in plasma indicating an improved drug release of MVC rings is needed [99]. Polyvinyl alcohol-based films have been used to co-formulate MVC and TFV as well as MVC and DPV [70]. DPV has also been co-formulated with TFV [100].

2.6 The vagina as a barrier to infection and vaginal HIV-1 transmission

2.6.1 The vaginal epithelial environment

The female genital tract consists of two different types of mucosal surfaces. The upper genital tract includes the endometrium and endocervix and represents the type I mucosal surface comprising of simple columnar epithelial cells. In contrast, the lower genital tract including the vagina and ectocervix represents the type II mucosal surface that is lined by 20-45 cell thick, multi-layered non-keratinising, stratified, squamous epithelium. The transition area from type I to type II mucosa is known as the cervical transformation zone (Figure 2.11). Forming the most superficial layer, these epithelial sheets are seeded with immune response cells such as $CD4^+$ T cells, macrophages and Langerhans cells (LCs). Resting on an indistinct lamina propria- an underlying vascular submucosa, vaginal epithelial cells are interconnected by desmosomes, adherens junctions and tight junctions. The sub-epithelium of the lamina propria is made up chiefly of connective tissue intertwined with a dense network of blood vessels as well as numerous elastic fibres, leukocytes, lymphocytes and occasional lymph nodules with varying densities among different tissue sites [101]. This epithelial layer acts as a first line of defence to infections and plays a critical role in the immunological response to pathogens by immune cell recruitment through TLR signalling cascades triggered by

PAMPS. At menarche, the production of oestrogen stimulates the vaginal epithelium to fill with glycogen. An enriched vaginal microbiota therefore maintains a physiological pH of 3.5-4.5 by the bacterial conversion of glycogen to lactic acid [102] which prevents the proliferation of pathogenic bacteria and yeast. Along with pH, vaginal secretions play an important role in protecting the vagina against infection by the production of proteins such as mucins [102, 103]. Mucins such as MUC1 mediate immunoregulatory mechanisms such as immune activation through cell-cell interactions and transmembrane signal transduction events [104]. The epithelial environment of the FGT can be modulated by processes of the female menstrual cycle which has two phases: the follicular phase (mature follicles produce estradiol that induces endometrial growth) and the luteal phase (the corpus luteum secretes progesterone to stabilise the lining of the endometrium and prepare it for the implantation of the fertilised egg) [105]. Immunomodulatory effects of estradiol and progesterone result in suppression of some innate, humoral and cell mediated immune responses in the first 7-10 days of the luteal phase providing a window of vulnerability, in which HIV may be enhanced (as reviewed in 'A new strategy to understand how HIV infects women: identification of a window of vulnerability during the menstrual cycle').

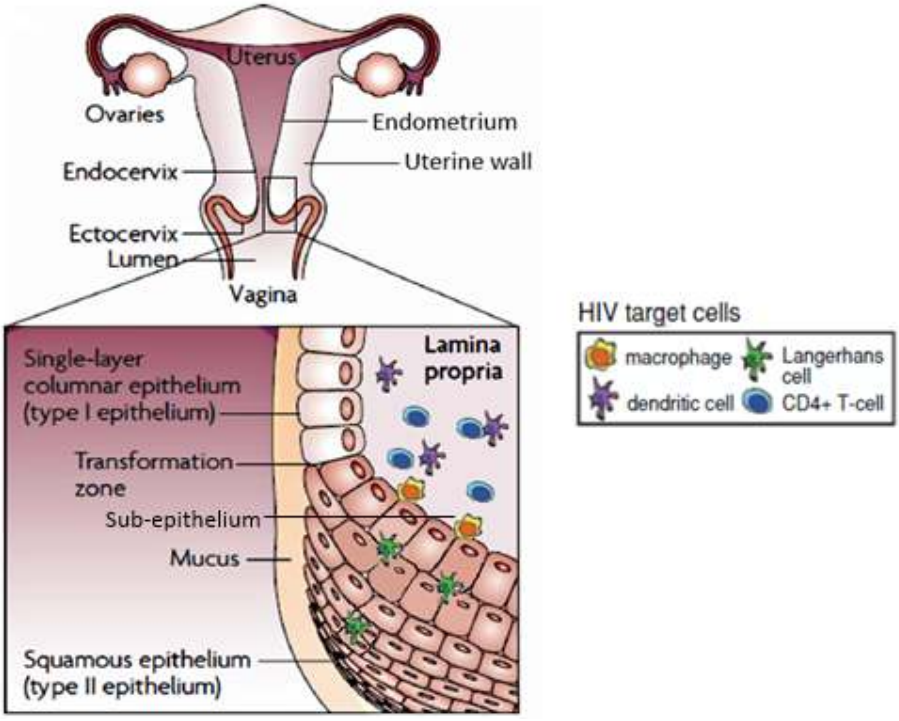

Figure 2.11 Anatomy of the female genital tract. The upper genital tract represents the type I mucosal surface comprising simple columnar epithelial cells and the lower genital tract represents the type II mucosal surface that is lined multi-layered non-keratinising, stratified, squamous epithelium. The transition area from type I to type II mucosa is known as the cervical transformation zone. Immune cells are densely located in the sub-epithelium.

2.6.2 HIV-1 transmission through the vaginal epithelium

The specific mechanisms involved in HIV transmission across the mucosal layer remain to be fully identified. In most cases HIV infection may be established by a single isolate as determined by single-genome amplification of the HIV-1 Env glycoprotein or of whole viral genome sequencing in HIV infected individuals [106, 107]. In a study of rectal challenge in the rhesus macaque model, low dose virus stocks containing on average 48 different SIV Env sequences were administered. DNA sequence analyses of virus from the 13 (out of 18) animals infected showed that productive infection was either due to a single virus or a very low number of viruses (median 1; range 1-5) [108].

SIV challenge experiments in NHP models identified small foci of sub-epithelial mucosal cells that were infected at 72 hours after vaginal exposure [109]. Furthermore, an *ex vivo* human vaginal model indicated that HIV targets $CD4^+$ T cells early in the infection process, suggesting that these cells are the initial site of infection [31, 110, 111].

Proposed HIV transmission mechanisms across the vaginal epithelium include; endocytosis by dendritic projections of LC [111] that are thought to extend to, or near, the luminal surface [101] or by the disruption of the integrity of the vaginal mucosa as a result of trauma, bacterial vaginosis, or inflammatory or ulcerative disease in the vagina [112] as shown in Figure 2.12. Using an *ex vivo* tissue model of human vaginal epithelium challenged with HIV followed by electron microscopy analyses of infected tissue, intact virions were readily observed in the cytoplasmic compartment of vaginal LCs up to 3 days post infection, suggesting that the persistent endocytosed virions remained accessible for trans infection of susceptible neighbouring $CD4^+$ T cells [111]. However, LCs are not readily infected and do not appear to be critical for initial infection but may contribute to the formation of the self-sustaining foci of infected $CD4^+$ T cells [113]. Other proposed mechanisms include HIV entry through transfer by direct cell-cell contact or via viral transcytosis across the epithelial cell [114, 115], via receptor mediated transport across M cells

[116] or by direct disruption of epithelial barrier integrity, opening tight junctions and increasing permeability to the virus [117].

Retroviral transmission has been shown to occur through the vaginal mucosa, as demonstrated by infections in a woman born without a uterus [118] and in macaques after surgical extirpation of the uterus [119]. Studies using macaque and human tissue also concluded that the less robust single layered columnar morphology of the type 1 mucosal surface and the differing epithelial cell types transitioning at the transformation zone are areas for primary portals for virus entry through the vaginal epithelium [109, 120]. More recently viral transmission sites have also been identified throughout the entire FGT in rhesus macaque models by using an SIV-based gene delivery vector modified into a dual reporter system containing the mCherry fluorescent protein and enhanced firefly luciferase. Monitoring of luciferase expression identified sites of infection within the intact FGT and fluorescent protein mCherry permitted the visualisation of single infected cells by spectral imaging and fluorescence microscopy. While high doses of this single round non-replicating SIV-based dual reporter system determined that the entire FGT including the vagina, ectocervix, endocervix, ovaries and draining lymph nodes contained infected cells 48hrs post inoculation, the primary site of infection was shown to occur at the squamous mucosal vaginal and ectocervical barriers of the vaginal vault [121].

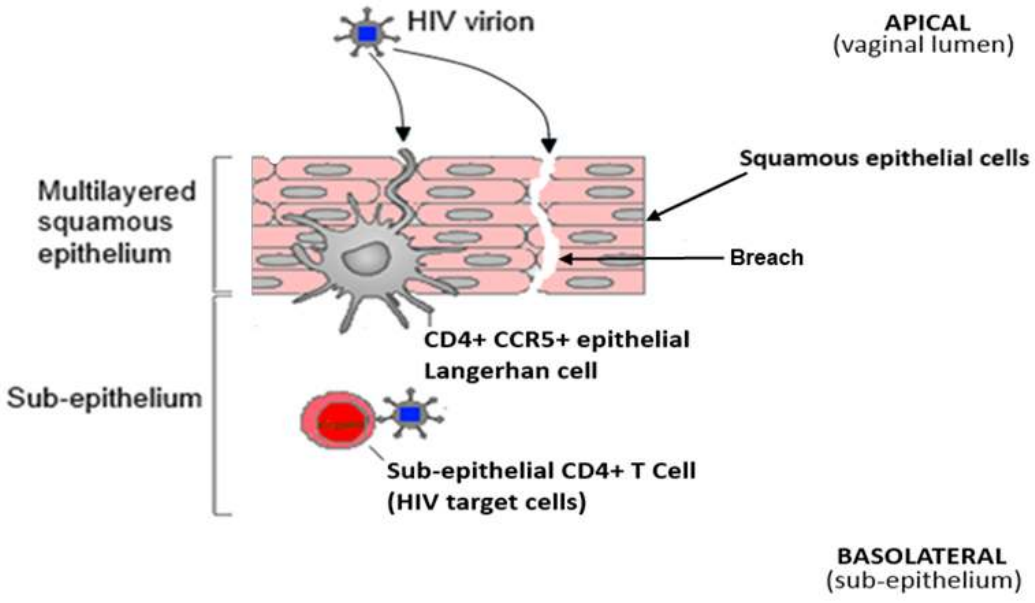

Figure 2.12 Transmission of HIV virions through the vaginal epithelium. Located within the multi-layered squamous epithelium, dendritic processes from LCs extend towards the lumen. Cell free virions are able to bind to the LC via epithelial surface receptors $CD4^+$ and $CCR5^+$. Though tears in the vaginal mucosa promote viral access to the $CD4^+$ T cells in the sub-epithelium, it is likely that virions crossing the mucous layer can directly reach these cells via the dendritic projections of LC.

2.7 The vagina- a site for drug administration

2.7.1 Vaginal drug permeability

The vagina has been extensively used as a site for drug delivery with traditional delivery systems formulated as solutions, gels, suppositories, foams, tablets and vaginal rings. These vaginal products have been developed for various purposes including; contraception, anti-fungal, anti-bacterial, hormone therapy and induction of labour [122]. With the development of vaginal microbicides, the vaginal route of administration is a growing area of interest for these products. Drug absorption through the vaginal epithelium can provide greater bioavailability of localised drug when compared with the oral route as well as limiting systemic drug exposure. Increased bioavailability was observed with TFV gel when administered to healthy women, when compared to oral TFV (Truvada). Genital tissue concentrations of active drug were approximately 100 fold greater after local administration compared with those in genital tissue from women who had taken TVF (Truvada) orally. In contrast, serum concentrations of TFV were considerably lower following vaginal application when compared with oral dosing [123]. The transport of a drug molecule across the vaginal epithelial barrier may occur by several routes, as represented schematically in Figure 2.13 and described below.

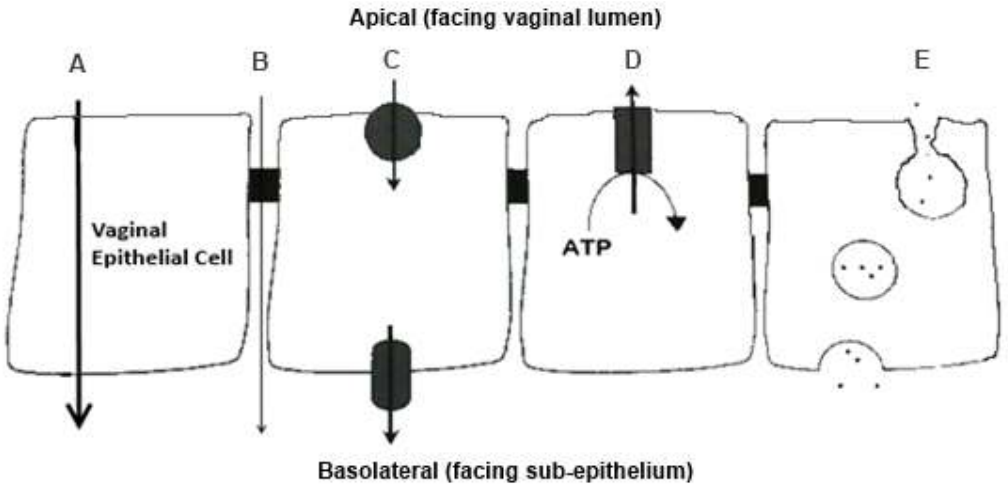

Figure 2.13 Drug transport routes across the vaginal epithelia. (A) Passive transcellular diffusion; **(B)** paracellular diffusion; **(C)** transporter-mediated absorption; **(D)** transporter-mediated secretion; **(E)** transcytosis.

2.7.1.1 Passive transcellular pathway

The passive transcellular pathway requires permeation of solute through the apical and basolateral cell membranes. These membranes are composed of phospholipids assembled into bilayers that are packed with membrane proteins. This is the route for many lipophilic drugs that are in general well absorbed. This permeation does not require adenosine triphosphate (ATP) hydrolysis but involves partition of (uncharged) drug particles into the membrane by diffusion along a concentration gradient (Figure 2.13A). The drug diffuses to areas of low drug concentrations (e.g. from the vaginal lumen to the blood). However, in epithelial cells, drugs can become trapped in the apical membranes if they are too lipophilic as was observed in intestinal epithelial cell with the anti-HIV agent Cosalane resulting in poor bioavailability [124].

2.7.1.2 Paracellular pathway

Paracellular permeation occurs through the gaps between adjacent epithelial cells and is restricted to polar drugs of low molecular weight which are generally poorly absorbed. The rate-limiting process in paracellular transport is diffusion through the barrier formed by tight junctions (Figure 2.13B) at the apical part of the intercellular space. Tight junctions show charge and size selectivity in their permeability, and ion transport across tight junctions is discriminative showing preference for anion selectivity as found in the rabbit colon and frog skin [125].

2.7.1.3 Transporter-mediated absorption

Solute transporter proteins are transmembrane proteins that act as gate keepers for cells and organelles. Their roles involve regulating the uptake and efflux of crucial endogenous substrates such as peptides, amino acids, sugars, nucleotides and inorganic ions. For uptake proteins acting in the absorptive direction, the apical cell membrane is able to actively shunt such nutrients across the phospholipid bilayer into the cell. Various substances display specific structural characteristics and are substrates for specific membrane bound transporters (Figure 2.13C). In order to use this pathway, a drug must represent some structural similarity with the normal

substrate. Most uptake transporters are classified as members of the solute carrier (SLC) transporter family, discussed further in section 2.7.3.

2.7.1.4 Transporter-mediated secretion

For transporter-mediated secretion, efflux proteins are able to secrete a variety of drugs. Efflux proteins actively remove toxic solutes that show substrate specificity (Figure 2.13D). The degree to which a drug accumulates within a tissue is often limited not so much by its ability to enter cells but by its tendency to leave. Such tendencies may arise from the activity of efflux proteins present in the cell membrane. These efflux mechanisms play a critical role in limiting the absorption and accumulation of potentially toxic substances [126]. Most efflux transporters are members of the ATP binding cassette (ABC) superfamily, discussed further in section 2.7.3.

2.7.1.5 Transcytosis

This mode of transport is a process by which a drug molecule gains entry into the cells without passing the phospholipid membrane bilayer but instead transport is within a membrane-bounded carrier formed by endocytosis (Figure 2.13E). Macromolecular solutes are transported from one side of a cell to the other. Strategies have been developed to take advantage of this mechanism for targeted drug delivery. Transport studies showed that permeability via the receptor-mediated transcytosis pathway increased the bi-directional bioavailability of insulin-Tf (conjugated with transferrin) by 5- to 15-fold, when compared to free insulin transport across Caco-2 cell monolayers [127].

2.7.2 Other determinants of microbicide effectiveness

Local drug delivery occurs in two main steps: drug dissolution in the vaginal fluid and a hydrodynamic layer on the walls of the vagina, followed by penetration into the epithelium based on a transport process with or without a concentration gradient. Drug stability and absorption are affected not only by the lipophilicity of the drug molecules but also by compatibility with properties of vaginal fluid, especially pH, enzymes, and microflora. Variation in pH, following menses or coitus activity could influence the solubility, uptake, and release profile of pH sensitive substances within the FGT [128]. Increases in vaginal fluid volume due to estrogens and sexual

stimulants may improve the absorption of poorly soluble drugs; alternatively, a greater presence of mucus could slow down the interaction between drug and epithelium [129] .Additionally, vaginal fluids can remove and wash away formulations. Microbicide effectiveness may also be hindered by vaginal washing, in turn reintroducing the risk of HIV infection. The effects of microbicides on the vaginal microbiome has yet to be studied in detail, however modifications that lead to increased inflammation or activation of potential HIV host cells may enhance transmission [130].

Topical vaginal application of ARV based microbicides delivers the active component to the site of transmission. However, the barrier formed by the mucus layer is often underestimated in drug delivery to the mucosa. This barrier relies on a thin sheet of mucus that lines the mucosal epithelial surface and is a hydrogel made up of mainly water that also contains mucin, glycoprotein, plasma proteins, enzymes, amino acids, cholesterol, lipids, and a range of inorganic ions. Mucins are high molecular weight glycoproteins with a mass range of 1-40 x 10^6 kDa and mucins can be classified into either secreted or cell bound forms [131]. The mucus barrier consequently forms a steric barrier due to its negative charge and hydrophobic domains [132]. However, the overall charge is hydrophilic and the mucus presents an interactive barrier that limits the free diffusion of drugs within and through the mucus [133]. The mucin protein backbone is rich in repeats of serine, threonine and proline and these domains are heavily glycosylated with fucose, galactose, sialic acids, N-acetylglucosamine and N-acetylgalactosamine. The glycosylated regions of mucins are hydrophilic whereas the non-glycosylated protein domains are hydrophobic. Such properties of the vaginal mucosa may present a barrier and impact drug delivery in the vagina. The presence of mucus can result in product dilution and can alter drug dissolution, affecting the efficacy of the drug by changing its concentration. Additionally, the hydrophilicity and viscosity of the mucus does not favour dissolution of hydrophobic drugs such as DPV and DRV, limiting drug diffusion across the epithelial barrier. Various ARV drugs behave differently in their ability to penetrate mucosal tissue, generally high protein-bound compounds do not gain access to the secondary layers because of their affinity for plasma proteins such as albumin and a_1-acid glycoprotein [134]. PIs that have shown high binding affinities to plasma proteins (95-99%), achieve lower FGT concentrations when compared to NRTIs that present lower protein binding affinities

(<0.7-49%) but achieve higher drug concentrations in the mucosal tissue rather than in plasma [135].

To bypass the mucus barrier, permeability enhancement techniques are often implemented within drug formulations. This includes the general use of inactive excipients/surfactants that may be added externally to a drug formulation to enhance (due to their physiochemical properties) the permeation of the pharmacologically active pharmaceutical ingredient (API) to improve its bioavailability. Furthermore, hydrophobic microbicides such as DPV and DRV can be developed in aqueous based gels using such techniques. HEC gel formulations containing the solubilisation excipient cyclodextrin was shown to improve the permeability profile of DPV when tested *in vitro*. However, when using such excipients care should be taken to maintain equilibrium between solubility and permeability in order to obtain optimal flux [136].

2.7.3 Drug transporters and expression in the FGT

Drug transporters continuously protect the body from dietary and environmental toxins. However, the broad substrate specificity of these transporters do not restrict their activity to physiological substrates only, but are also capable of transporting drugs that resemble these physiological substrates [137]. Numerous ARV drugs have been identified as substrates for efflux and/or uptake transporters and may modulate transporter activity [138]. Tissue distribution of drugs may also be affected by activity of the cytochrome P450 (CYP) enzyme.

Drug transporters are situated throughout the human body and patterns of expression vary in different tissues and cell types. Expression occurs highest mainly in tissues with barrier functions including the small intestine [139] which is involved in the absorption of dietary constituents into the bloodstream and the brain [140] which provides a protective function by modulating access of drugs and toxic substances into the central nervous system. Other tissues with barrier functions that express drug transporters include the kidney [141], liver [142] and placenta [143]. More recently expression has also been detected in the tissue of the FGT physical barrier [144-152]. The epithelial cells that border such barriers are polarised, as are the enterocytes of the intestine, proximal tubule cells of the kidney and the brain capillary endothelial cells of the blood-brain-barrier (BBB), forming apical and basolateral domains. Similarly, the epithelial cells that that form the FGT mucosal

surfaces are polarised with the apical domain facing the vaginal lumen and the basolateral domain facing the sub-epithelium (Figure 2.14B). This polarisation is reflected by the asymmetric distribution of drug transporters e.g. in epithelial cells of the small intestine the efflux and uptake transporters P-gp, BCRP, MRP2, MRP4, CNT1-3, OCT3, OATP1A2, OATP2B1 are expressed at the luminal surface while MRP1, MRP3, MRP5, OCT1, OAT2, ENT1-2 are expressed at the basolateral surface [138] (Figure 2.14A). While most drug transporters are polarised some are shown to be expressed on both the apical and basolateral surfaces [153], for example, ENT2 has been shown to be expressed on both surfaces of the choroid plexus [138].

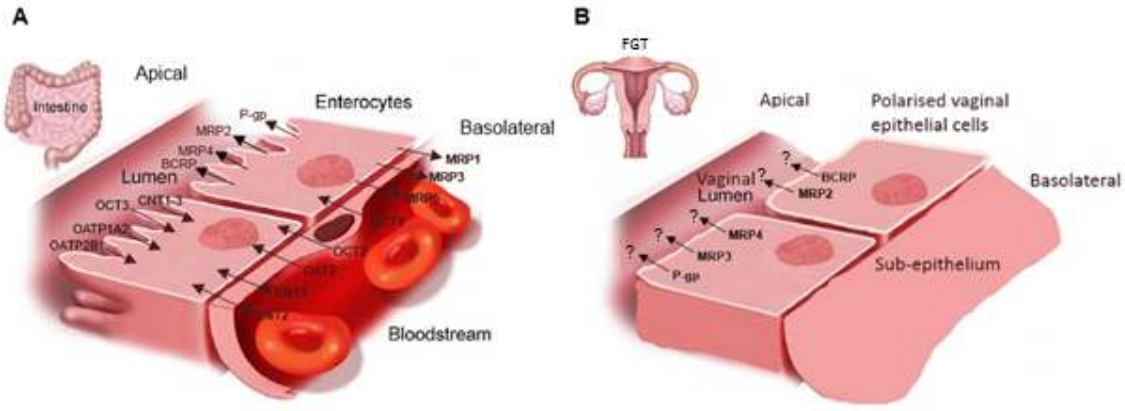

Figure 2.14 Tissues with barrier functions and expression of drug transporters. (A) The intestinal barrier is split into an apical side (lumen) and the basolateral side (bloodstream). Epithelial cells located here are polarised and express a variety of efflux transporters. **(B)** The FGT can also be split into an apical side (vaginal lumen) and the basolateral side (sub-epithelium). More recently, only drug efflux transporter protein expression have been detected throughout the FGT, these include; P-gp, MRP2, MRP3, MRP4 and BCRP [146, 147, 149-151]. Orientation of the transporters indicated in the FGT is by analogy with those expressed in the intestine but has not been confirmed experimentally. Expression in the FGT may enhance or limit the absorption of drugs applied at the vaginal lumen, thus potentially playing a pivotal role in determining the bioavailability of topically applied drugs. Black arrows pointing inwards represent uptake transporters; arrows pointing outwards represent efflux transporters.

To date more than 400 genes that encode transporter proteins have been identified in humans. There are two major superfamilies of transporters- the ABC efflux transporters and the SLC uptake transporter proteins [154]. While nomenclature of solute transporters has been standardised with different SLC families designated by numbers e.g. SLC1 and SLC2 etc and ABC transporter subfamilies designated by letters e.g. ABCA, ABCB etc, previous more descriptive names are often used as in the following section where both names are used. Additionally, the polarised

expression of drug transporters is important for mediating vectorial transport of drugs across epithelia. SLC and ABC transporter families show relatively broad and in some cases overlapping substrate specificities within their respective families as well as with different members from the two families. The latter has been demonstrated by the antiviral drug Adefovir, a substrate for SLC22A6 and ABCC4 respectively [155, 156] suggesting that Adefovir may be taken into cells by SLC22A6 and then effluxed by ABCC4.

2.7.3.1 Solute carrier transporters: structure and mechanisms of transport

2.7.3.1.1 Introduction

The SLC transporter family consists of 52 distinct subfamilies, including proton-dependent oligopeptide transporters (POT, SLC15A), organic anion transporters (OAT, SLC21A), organic anion-transporting polypeptides (OATP, SLCO), organic cation transporters (OCT, SLC22A), concentrative nucleoside transporters (CNT, SLC28A), equilibrative nucleoside transporters (ENT, SLC29A), the monocarboxylate transporters (MCT, SLC16A) and peptide transporters (PEPT, SLC15). Those shown to be involved in the transport of antiretroviral drugs include the (OATP, subfamily SLCO), (OAT, SLC22), (OCT, SLC22), (CNT, SLC28), (ENT, SLC29) and (PEPT, SLC15) [138, 157]. The OATP subfamily are especially important in the uptake of ARV drugs in the intestine and the protease inhibitors DRV and SQV as well as the reverse transcriptase inhibitor TFV have been identified as substrates [158-160]. Additionally, the NRTIs lamivudine and zalcitabine are substrates for OCT1 and OCT2. Some SLCs mediate bi-directional transport e.g. the equilibrative transporter ENT1 is involved in the uptake and efflux of the anticancer drug cladribine [161, 162].

2.7.3.1.2 Structure of SLC transporters

Unlike the ABC transporters, the SLC's display highly diverse structures that comprise a variety of folds which are unique to this superfamily. The two structural folds predicted to be the most common in the human SLCs are the structurally dissimilar major facilitator superfamily (MFS) and the Leucine transporter (LeuT)-like folds. The more common of the two structural folds is that of the MFS which is shared between numerous family members of human SLCs. The MFS fold contains 12 transmembrane α-helices (TMH) [163] arranged in two inverted structural

pseudo-repeats of 6 TMHs [164] that are interconnected by multiple intracellular and extracellular short and long loops. The N and C-termini of the transporter are both intracellular. The N-terminal extracellular loop joining TMH 1 and TMH 2 contains sites for N-linked glycosylation while the extended intracellular loop joining TMH 6 and TMH 7 possesses potential sites for protein kinase C-mediated phosphorylation [165]. Figure 2.15 is a representation of the secondary structure elements of MFS fold exemplified by the organic anion transporters (OATs, SLC 22 family). Mutagenesis studies indicate that residues in TMH 7 and TMH 8 that are highly conserved within SLC families are critical for substrate recognition and transport. More recently, these observations have been confirmed by determination of the crystal structure of the human glucose transporter GLUT1 (SLC2 family) at a resolution of 3.2 Å [166]. GLUT1 adopts the MFS fold in which TMH 1-6 form part of a pore structure that is completed by TMH 7-12 (Figure 2.16). Unlike the MFS fold the core of a LeuT-like fold possesses 10 TMHs, with two five TMHs inverted pseudo-repeats, where the first two TMHs in each of the two repeats are tilted relative to the three remaining TMHs of the repeat. This fold is adopted by multiple biomedically important families such as the SLC5 family of Na^+/glucose transporters and the SLC6 family of Na^+/Cl^- dependent neurotransmitter transporters [164].

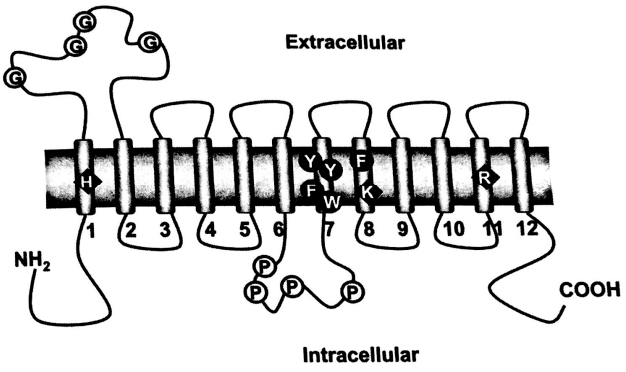

Figure 2.15 Transmembrane arrangement of SLC uptake proteins. SLCs comprise 12 TMHs (numbered) linked by extracellular and intracellular loops with intracellular amino (NH_2) and carboxy (COOH) termini. A large extracellular loop between TMDs 1 and 2 includes sites for N-linked glycosylation (G) while the extended intracellular loop between TMDs 6 and 7 includes sites for phosphorylation (P) by protein kinase C. Basic and aromatic residues conserved in the OATs are shown in TMHs 7 and 8.

The large extracellular loop linking TMH 1 and TMH 2 adopts an α-helical conformation. The long intra-cellular loop that connects TMH 1 and TMH 7 comprised 4 short α-helices and may be unique to sugar transporters since it has

not been described in other MFS structures. Substrate binding involves H-bonding principally with residues in TMHs 7, 8 and 10.

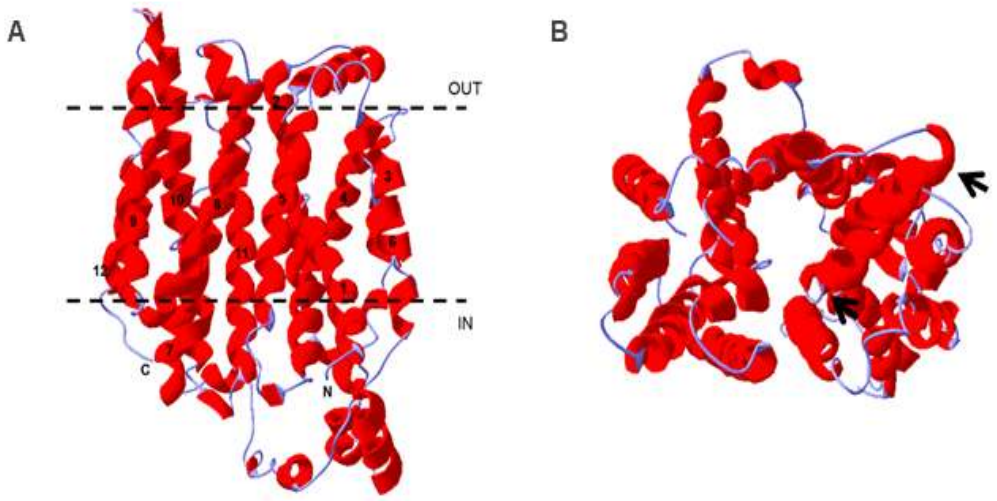

Figure 2.16 Crystal structure of the human GLUT1 glucose transporter. The arrangement of the 12 TMHs are shown in panel **(A)** with the approximate boundaries of the cell membrane indicated by dashed lines. TMHs 1-6 cluster to the right and 7-12 on the left. An extended intracellular domain comprising 4 short α-helices links TMHs 6 and 7 on the intracellular side of the membrane. Panel **(B)** shows the view looking down on the extracellular side where the pore structure is evident. The extracellular α-helix linking TMHs 1 and 2 is arrowed at each end. Structures were drawn using Swiss PDB viewer with coordinates from the Protein Data Bank (PDB ID 4GCO).

2.7.3.1.3 Mechanisms of SLC-mediated transport

Two major types of alternating access mechanisms have been described for SLC transporters displaying the MFS and LeutT folds. The first includes the “rocker-switch” mechanism; this involves the oscillating back and forth locomotion of the N- and C-terminal halves of the transporter to form alternately outward and an inward facing states along the symmetry axis perpendicular to the transmembrane. The characterisation of the “rocker-switch” mechanism was defined by analyses of the *Escherichia coli* Lactose Permease LacY an SLC37 homolog (Figure 2.17A and 2.17B) [167]. The second is the “gated pore” mechanism; this involves the enclosure of the binding site by two gates. Binding of the substrate occurs when the outward-facing gate permits the binding of the substrate, leading to the opening of the second gate that is facing the cytosol which releases the substrate into the cell.

The “gated pore” mechanism was determined in *Aquifex aeolicus* LeuT, an SLC6 homolog (Figure 2.17C and 2.17D) [168] .

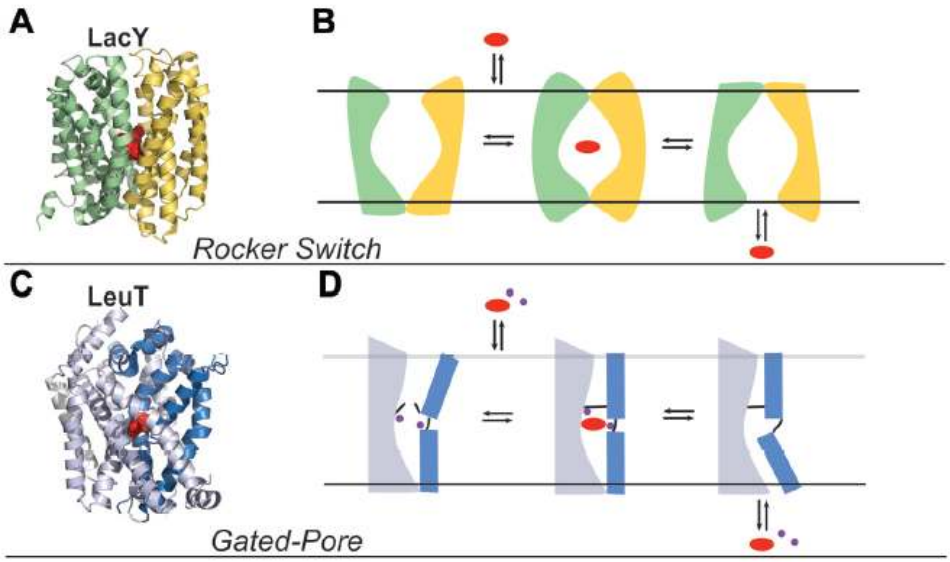

Figure 2.17 Models of the rocker switch and gated pore mechanisms. Rocker switch. **(A)** The outward-open bound structural conformation of the *E. coli* Lactose Permease LacY (PDB ID 40AA) with a cartoon depicting the N- and C-terminal halves in green and yellow, respectively, and the substrate in red. **(B)** Binding of substrate occurs within the V like conformation of the membrane that faces the extracellular membrane. The intermediate occluded state is triggered and the substrate is released from the inverted V-shape which orientates to an inward open conformation. Gated pore. **(C)** The outward-open bound structural conformation of LeuT (PDB ID 4FXZ) with a cartoon depicting the scaffold and bundle domains in grey and blue, with the substrate and ions in red and purple, respectively. **(D)** The scaffold maintains a static position, while the bundle domain undergoes conformational changes involved in binding and releasing of the substrate. The binding site is shielded by a thin gate on the extracellular side and a thicker gate on the intracellular side (ie. TMH1). Figure adapted from [164].

2.7.3.2 ATP-binding cassette (ABC) transporters: structure and mechanisms of transport

2.7.3.2.1 Introduction

The ABC drug transporters are primary active transporters that couple transport to ATP hydrolysis. The 49 ABC transporters identified in humans [169], are grouped into 5 families ABC A-G. ABC transporters are distributed in the small and large intestine, liver, kidney, brain, lymphatic system, placenta, and FGT [138, 170, 171].

The majority of ARV drugs are substrates, inhibitors and/or inducers of ABC transporters [172]. Intracellular concentrations of ARVs may therefore be profoundly affected potentially with adverse effects on antiviral activity. P-glycoprotein (P-gp, ABCB1) is a widely distributed drug transporter with high expression levels. All HIV PIs are high affinity substrates for P-gp (ABCB1) [138], MDR1a/b-knockout mice display enhanced brain accumulation of nelfinavir (40-fold), indinavir and saquinavir (8-10-fold), while systemic availability of these PIs is enhanced by 2.5-fold [173]. P-gp also mediates the transport of NRTIs such as tenofovir disoproxil fumarate (TDF) [174, 175]. P-gp substrates are typically lipophilic and accumulate within the lipid bilayer. The MRPs mediate the efflux of many NRTIs *in vitro* as MRP4 (ABCC4) and MRP5 (ABCC5) are substrates for TFV [176, 177]. Furthermore, the NRTIs zidovudine, lamivudine, didanosine, and stavudine have shown to be substrates for breast cancer resistance protein (BCRP, ABCG2) expressed by human $CD4^+$ T cells [178]. Similar to the SLCs, while most ABC drug transporters are polarised some have also shown to be expressed on both the apical and basolateral surfaces, for example, is has been reported that in mice the subcellular localisation of MRP4 (ABCC4) within the BBB was basolateral and apical, respectively [179].

2.7.3.2.2 Structure of ABC transporters

ABC transporters contain a pair of conserved cytoplasmic domains termed nucleotide binding domains (NBDs). The roles of NBDs are to hydrolyse ATP and trigger conformational changes in the attached transmembrane domains (TMD1 and TMD2), thus permitting substrates to cross the membrane lipid bilayer to either be taken up (uptake) into or effluxed out of the cytoplasm. The core functional units shared by all ABC family members' transporters comprise four functional domains: two TMDs typically made up of six TMHs each forming the substrate binding region and two cytosolic nucleotide binding domains (NBD1 and NBD2). These NBDs contain Walker A (G/AxxxxGKT/S, where x is any amino acid) and B (zzzzD or zzzzDE, where z is a hydrophobic amino acid) motifs as well as a C motif (LSGGQ) which are essential for ATP binding and hydrolysis [180, 181]. Most commonly a single polypeptide generally encodes all four of the functional units, including the 12 TMHs regions and the ATPase motifs (Figure 2.18). However, there are a number of exceptions as MRP1 (ABCC1), MRP2 (ABCC2), MRP3 (ABCC3), MRP6 (ABCC6) and MRP7(ABCC7) for example have an additional five TMHs whereas

BCRP has only 1 NBD with 6 TMHs (termed a “half transporter”) and forms homodimers [126, 182].

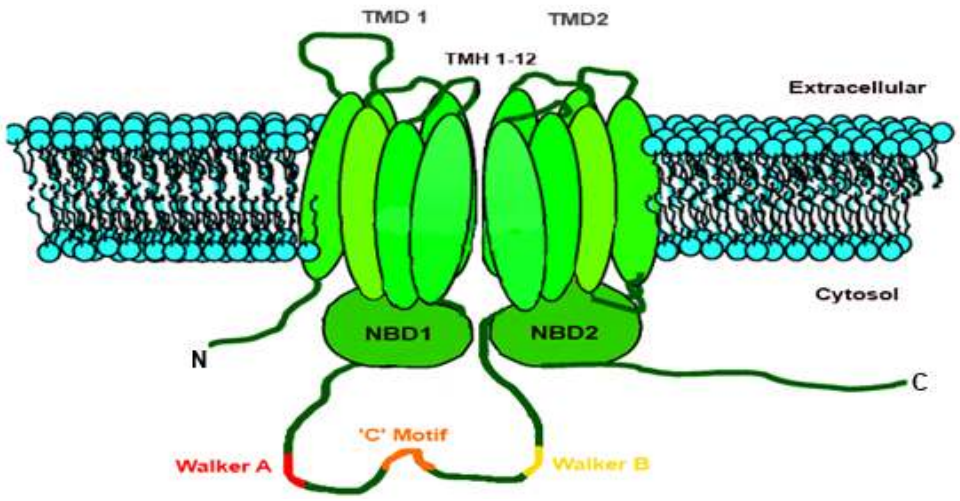

Figure 2.18 Transmembrane organisation of ABC transporter proteins. The domain arrangement of ABC transporters comprises NBD dimers, each with six TMHs and part of ATPase motifs (Walker A motif, Walker B motif and ‘C’ Motif) located on the cytosolic side. Modified from [183].

The structure of murine P-gp (ABCB1, 87% amino acid sequence identity with Human P-gp) in the nucleotide-free and substrate-free form has been determined at 3.8 Å [184] and subsequently refined [185] (Figure 2.19A). In this structure, the TMHs adopt an inward facing confirmation formed of two bundles of 6 TMHs that result in a large internal cavity opening to both the cytosol and the inner leaflet of the cell membrane with the NBDs separated by approximately 30 Å. In contrast to this inward facing conformation, crystal structure analyses of a prokaryotic ABC transporter (Sav 1866 from *Staphylococcus aureus*) in substrate-free and ADP-bound form reveals an outward facing conformation [186] (2.19B). In this conformation, the large internal cavity is closed to the cytosol but accessible to the outer leaflet of the cell membrane and the extracellular space presumably allowing substrate release. Sav 1866 although a homodimeric “half transporter” shows significant amino acid sequence homology to murine and human P-gp and adopts a similar fold.

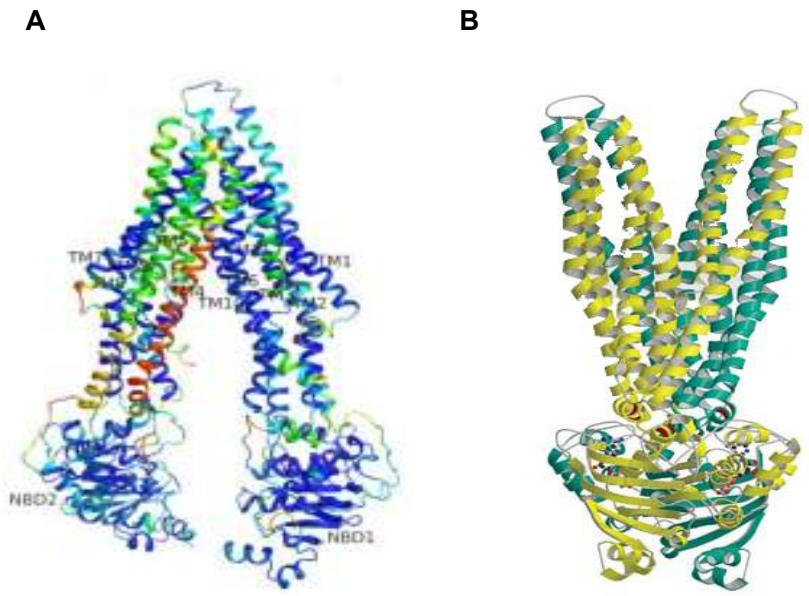

Figure 2.19 Ribbon structures of murine and prokaryotic P-gp transporters. (A) Murine P-gp structural TMHs adopt an inward facing conformation with the internal cavity opening to both the cytosol and the inner leaflet of the cell membrane [185]. **(B)** In contrast, crystal structure analysis of prokaryotic ABC transporter (Sav 1866) in substrate-free and ADP-bound form reveals an outward facing conformation. The large internal cavity is closed to the cytosol but accessible to the outer leaflet of the cell membrane and the extracellular space. Structural image adapted from [186].

2.7.3.2.3 Mechanisms of ABC transporter-mediated substrate efflux

ABC transporter-mediated substrate efflux likely involves major conformational changes in the TMHs as described above. High resolution X-ray structures of the NBDs from prokaryotic ABC transporters indicate that in the ATP-bound conformation the NBDs associate as dimers in which 2 molecules of ATP are bound in equivalent sites at the dimer interface, termed a “sandwich dimer”. The ATP binding sites are formed by the phosphate binding loop (P loop) that includes the Walker A motif of one NBD and the C motif of the other [180, 181]. Dimerisation presumably induces further conformational changes in the TMHs to adopt the outward open (inward closed) structure. An important feature of these structural studies is that in both the outward and inward open structures, portals that allow substrate access from or to the inner leaflet and outer leaflet of the cell membrane respectively were identified. The major drug efflux transporters such as P-gp (ABCB1), BCRP (ABCG2) and MRP1 (ABCC1) mediate efflux of a large range of

hydrophobic substrates. A number of studies (as reviewed in [187]) indicate that such substrates may be taken up directly from the plasmamembrane and effluxed before accessing the intracellular compartment – termed the hydrophobic vacuum cleaner model as shown in Figure 2.20A [188]. A variety of ABC transporters have been shown to possess phospholipid translocase activity mediating movement of phospholipids from the inner to the outer leaflet of the cell membrane (termed "flippase" activity), reviewed in [189]. Such flippase activity may also be involved in efflux of hydrophobic drugs (Figure 2.20B). Although this has been proposed as a mechanism for efflux mediated by P-gp [190], the recent refined structure for murine P-gp [185] describes a pore structure for drug translocation that is lined by highly-conserved (between mouse and human) hydrophobic residues including several with aromatic side chains. This is unlikely to be compatible with flippase activity but could provide an environment with strong affinity for hydrophobic substrates with lower constraints and therefore broader specificity than those required by electrostatic bonding.

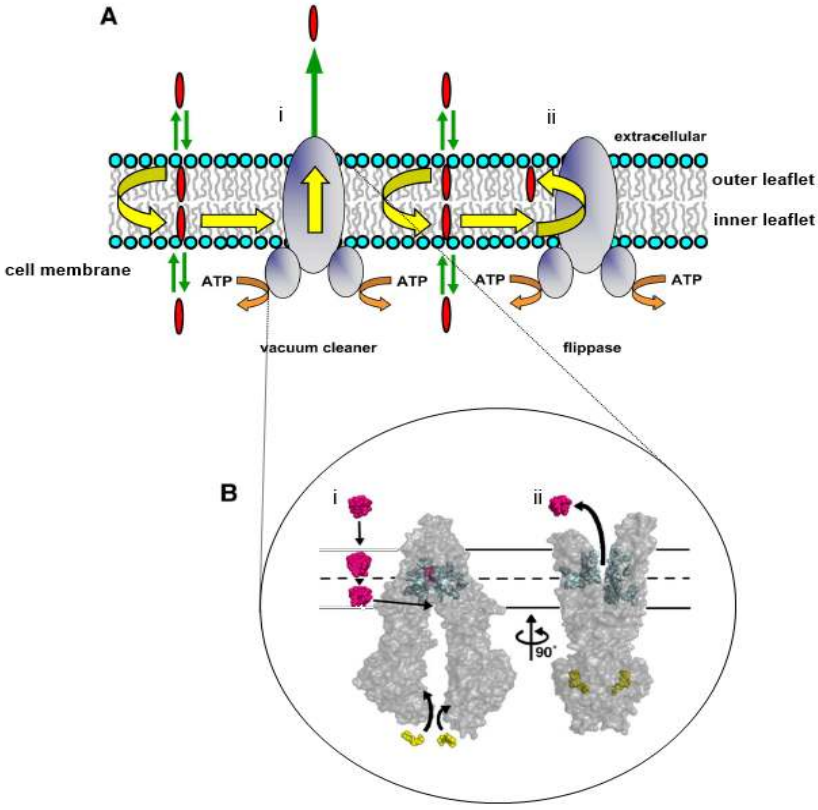

Figure 2.20 The hydrophobic vacuum cleaner model and drug flippase model of ABC transporters and the crystal structure of the drug vacuum cleaner model. (A) i. Vacuum cleaner model. Drugs partition into the lipid membrane and translocate to the inner

leaflet gaining access to the substrate-binding pocket located within the bilayer interior. Drugs are subsequently effluxed into the extracellular space before they are able to reach the inner cell membrane leaflet to enter the cell. **ii.** Flippase model. Drugs partition into the lipid membrane and translocate to the inner leaflet where they interact with the substrate binding pocket and are consequently flipped out to the outer membrane leaflet. Higher drug concentrations accumulate within the outer leaflet compared to the inner leaflet generating a concentration gradient, eventually drugs will rapidly partition from the two membrane leaflets into the extracellular aqueous phase **(B)** Structural view of the P-gp vacuum cleaner model **i.** External substrate (magenta) interacts with the substrate-binding pocket within the bilayer interior. **ii.** ATP (yellow) develops bonds with the NB domains forming a "sandwich dimer" which is the stimulus for initiating the power stroke necessary for the driving out of the substrate (magenta) in the form of the tweezer like conformation. Horizontal lines represent lipid bilayer and dashed horizontal lines separate the inner and outer bilayer leaflets. Figure adapted from [188] and [184], respectively.

2.7.4 ABC and SLC transporter expression in the vaginal epithelium

ABC drug transporter expression has been demonstrated throughout out the FGT [171]. Eight efflux transporters for ARVs (P-gp, BCRP and MRP1, MRP2, MRP4, MRP5 and MRP7) [138] were shown to be expressed in the uterus, ectocervix, endocervix and vagina [171]. In an oligonucleotide microarray study, 11 ABC transporters were shown to be moderately to highly expressed among all genes expressed in the cervix and RNA analysis confirmed similar findings in the lower genital tract as well as expression in various vaginal epithelial cell lines [144, 148, 191]. More recently expression of P-gp, BCRP and MRP4 has been analysed at the protein level by immunohistochemistry and Western blot [145, 146, 149]. Moderate to high expression of each transporter was demonstrated in ectocervix, endocervix and vaginal tissue of humans and macaques [145]. Additionally, immunohistochemistry confirmed expression of MRP2 and MRP3 [149, 150] and Western blotting confirmed expression of P-gp, BCRP, MRP2 and MRP4 in human cervicovaginal tissue [145-147, 149, 150, 192, 193]. The variation in expression of transporters along the FGT suggest that the pharmacokinetics of ARV drugs may vary at different areas of the FGT. Results from mRNA analyses and direct protein determination do not always correlate. MRP3 mRNA was not detected in vaginal tissue [144, 148] but expression was demonstrated by immunohistochemistry [149].

Expression of SLC drug transporters in the FGT has been reported primarily from analysis of mRNA by quantitative-PCR. Ten uptake transporters (SLC2A1, SLC6A9, SLC1683, SLC16A12, SLC22A18, SLC24A3, SLC35E1, SLC35E4, SLC38A10 and SLC44A1) for which ARVs are substrates were highly expressed in the human vaginal tract [149] and, in a microarray study mRNAs encoding 36 uptake transporters were expressed in the cervix [191]. Furthermore, RT-PCR analysis of

SLC transporters in human vaginal and ectoxervix tissue indicated that OAT2, OCT2, OCT3, ENT1, OATP-D, and OATP-E are the most highly expressed uptake transporters compared to their expression in liver [144]. Of the above transporters reported as expressed in the cervicovaginal epithelium, the SLC22 (OCT2 and OCT3), SLC28 (CNT) and SLC29 (ENT1) families have been associated with the transport of several nucleoside analogue ARV drugs [194]. Additionally, a study comparing 37 uptake transporter expression profiles between vaginal epithelial cells and tissue from various areas of the FGT further demonstrated expression of SLC transporters in vaginal tissue and epithelial cells at mRNA level [148]. SLC protein expression has yet to be detected by Western blot or immunohistochemistry in the FGT.

2.8 Antiretroviral drugs that form the focus for this study

2.8.1 Tenofovir

2.8.1.1 Physiochemical properties

TFV, (R)-9-(2-Phosphonomethoxypropyl)adenine, is an acyclic nucleotide analog of 2'-deoxyadenosine monophosphate (dAMP) (Figure 2.21) and is a small anionic molecule with a molecular weight of 287 kDa. The active form of TFV is a deoxy ATP analogue that can be incorporated into the growing DNA strand synthesised by HIV reverse transcriptase but cannot form a phosphodiester bond with the next nucleotide resulting in the termination of the viral DNA chain. It comprises an aromatic fused pyrimidine-imidazole ring system, a phosphate group, and a methyl group. As TFV is a monophosphate, it undergoes intracellular diphosphorylation to form tenofovir diphosphate (TFV-DP), the active form, which has a long tissue half-life of 164 hours [195, 196]. TFV is hydrophilic with aqueous solubility of 13.4 mg/ml in water and a Log P value of -1.6. TFV shows neutralising activity against HIV in both lymphocytes and macrophages [197], with *in vitro* IC_{50} (50% inhibitory concentration) and EC_{50} (concentration that gives 50% response) values in ranges from 0.2-8.5 μM against wild type laboratory strains of HIV [195, 198-200].

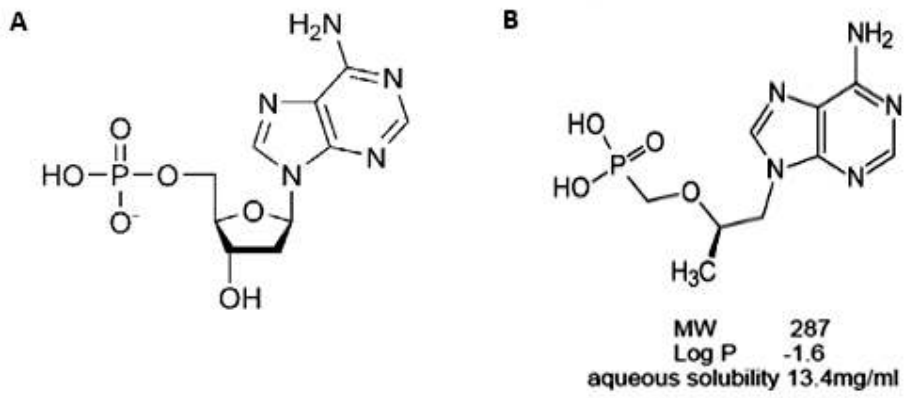

Figure 2.21 Similarity in structures between the nucleotide dAMP and the NRTI TFV with physiochemical propertis. (A) dAMP contains a deoxyribose sugar group **(B)** TFV lacks a sugar group and is replaced by a methyl group, an important alteration required for its function in terminating the viral DNA chain.

2.8.1.2 Pharmacology

As described above TFV is phosphorylated intracellularly to its active metabolite TFV-DP which competitively inhibits the activity of HIV reverse transcriptase, preventing further HIV replication. An orally bioavailable form of TFV (TDF) is used as a treatment for HIV-1 due to TFV's efficient intracellular activation, prolonged intracellular half-life and high barrier to resistance. Following a single dose of oral TDF 300 mg to HIV infected patients, maximum serum concentrations (C_{max}) were achieved in 1.0 ± 0.4 hrs. C_{max} and area under the curve (AUC) values were 0.30 ± 0.09 µg/ml and 2.29 ± 0.69 µg·hr/µl, respectively [201]. At steady state, following intravenous administration at 1.0 mg/kg and 3.0 mg/kg, the volume of distribution is 1.3 ± 0.6 l/kg and 1.2 ± 0.4 l/kg, with 7.2% of the drug binding to plasma protein. TFV is not a substrate for cytochrome P450 enzymes and 70-80% of intravenous TFV is recovered unchanged in the urine within 72 hours of dosing [201]. Following a single TDF oral dose of 300 mg, the elimination half-life of tenofovir is approximately 17 hours and intracellular half-life is >60 hours [202]. With multiple oral doses (under fed conditions), 32 ± 10% of the initial administered dose is recovered in the urine over a 24 hour period. TFV is eliminated by a combination of glomerular filtration and active tubular secretion [201].

Phase 1 and PK studies have provided significant data regarding TFV concentrations in the genital tract and in rectal tissue. Following oral TDF administration, TFV concentrations within the cervicovaginal fluid of the FGT relative

to blood plasma at first dose achieved a median of 135%, and 75% of that of blood plasma at steady state. Furthermore, TFV concentrations in genital secretions are 2.5 times greater than in plasma [135]. At the end of 24 hour dosing the median cervicovaginal fluid concentrations of TFV at a steady state were 68ng/ml. Vaginal tissue concentrations of TFV at the end of a 24hr dosing interval were 6.8 ng/g and 50 ng/g, respectively. TFV concentrations in rectal tissue following oral dosing with TVF-DP are 100 fold higher than that detected in vaginal and cervical tissue [203].

Following the use of topically applied 1% TFV gel, TFV exposure was low in blood plasma after single-dose and multi-dose with median C_{max} values of 4.0 and 3.4 ng/ml, respectively. In cervicovaginal fluid the median C_{max} was 1.9×10^6 ng/ml (range: 1.2×10^4 - 9.9×10^6 ng/ml) after single-dose and 1.4×10^6 ng/ml (range: 8.4×10^4 – 5.8×10^6 ng/ml) after multi-dose. From the same PK study, vaginal tissue TFV concentrations from biopsies (assessed by pooling of samples over a 24 hour period) demonstrated TFV concentrations ranging from 2.1×10^2 – 1.4×10^6 ng/ml with an average C_{max} of 2.2×10^5 ng/ml. Vaginal tissue concentrations of the active metaboloite TDP were 100 fold higher following vaginal application compared with oral dosing [123].

While orally administered TFV achieves effective blood plasma levels, this systemic exposure may lead to increased risk of adverse effects. Topically applied TFV not only provides effective levels directly to the site of infection, but also reduces the possibility of adverse effects as drug administered by this route leads to minimal blood plasma exposure. Additionally, data from the CAPRISA 004 study indicated that HIV incidence was considerably lower in women with TFV cervicovaginal concentrations of ≥1000 ng/ml when compared to placebo or drug concentrations ≤1000ng/ml [204]. TFV gel demonstrates 1000-fold higher concentration in vaginal tissues compared to oral TDF, suggesting that repeated application may maintain effective levels of drug. More recently TAF (tenofovir alafenamide) has been developed and has shown to be an effective prodrug of tenofovir diphosphate (TFV-DP) [205]. TAF provides significantly higher intracellular tenofovir concentrations in blood cells and lower serum levels. However, unlike the prodrugs TDF and TAF, TFV is not a substrate for P-gp (Table 2.1).

Antiretroviral drug	ABC transporters			SLC transporters		
	Substrate	Inhibitor	Inducer	Substrate	Inhibitor	Inducer
TFV	MRP2 MRP4 MRP7		MRP2	OAT1 OAT3		
TFV-DF (Prodrug)	P-gp					
TAF (Prodrug)	P-gp BCRP OATP					
DRV	P-gp MRP1	P-gp	MRP1 MRP5 MRP7	OATPD OATPE OATPC OATP1A2 OATP1B1		CNT3 OCT3 OATPE
DPV			MRP1 MRP3 MRP4 MRP5 MRP7			OCT3 CNT3

Table 2.1 Drug transporters for which Tenofovir, Darunavir or Dapivirine are substrates, inhibitors or inducers [171, 201, 206].

2.8.2 Dapivirine

2.8.2.1 Physiochemical properties

DPV, is the prototype of diarylpyrimidines (DAPY), formerly known as TMC120 or DAPY R147681 (IUPAC name: 4-[[4-(2,4,6- trimethylphenyl)amino]-2-pyrimidinyl]amino]-benzonitrile) of molecular weight 329.4 kDa. DPV comprises a pyrimidine ring covalently bound by a benzene ring on one side and a benzonitrile ring on the other, forming a “horseshoe” structure (2.22). This drug binds with high affinity in the induced hydrophobic pocket of the p66 subunit of HIV RT. DPV is highly hydrophobic with Log P of 5.3. Permeation of DPV may be via the passive transcellular pathway in which DPV partitions into cell membranes. DPV has shown potent neutralising activity in cell based models and human explants with IC_{50} values in the low (0.2-10) nM range [207, 208] and an EC_{50} of 1 nM *in vitro* [209].

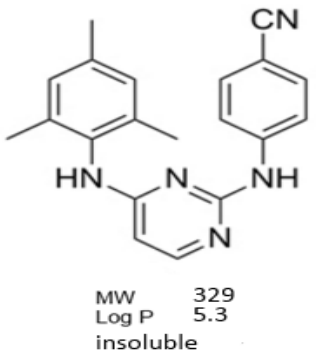

Figure 2.22 Horseshoe structure of DPV with its physiochemical properties. A central pyrimidine bound by benzene ring on one side (left) and benzonitrile ring on the other (right). This structural formation has been successful in binding to the hydrophobic pocket of the p66 subunit of HIV RT.

2.8.2.2 Pharmacology

Studies using rhesus macaques and rabbits [85] showed that intravaginal administration of [^{14}C]DPV gel (0.1 mg/ml to rabbits and 1 ml/day to macaques) over a 7 day period resulted in high DPV levels associated with vaginal and cervical tissue samples 1 hour after the final dose. In rabbits, high levels of DPV (246-16,241 dpm/ml corresponding to >3,000 ng/g) were measured in plasma and vaginal/cervical tissue samples, respectively. Furthermore, levels in tissue remained detectable (>2.5 ng/g) 24 hours after the final dose. In macaques, plasma radioactivity and DPV levels were lower (≤83 dpm/ml and ≤0.226 ng/ml, respectively). Due to the hydrophobic properties of DPV [210], it is plausible that the drug may partition into the cellular membrane with only a small amount of drug entering blood.

In humans, the PK of DPV was assessed in a randomised, placebo-controlled phase 3 DPV ring trial [211]. Healthy, sexually active women, 18-40 years of age were administered a vaginal ring containing 25 mg of DPV or placebo (in a 3:1 ratio) over a 56-57 day period. Multiple rings were used within this timeframe, with a 3-day washout period between selected ring changes. DPV concentrations were quantified in plasma, vaginal fluid and cervical tissue. Quantifiable DPV plasma concentrations were detected at the earliest scheduled time point (after 4 hours from insertion of the first ring) for all participants indicating the rapid release of DPV from the ring. Generally, plasma concentrations of DPV were low with maximal individual concentrations no higher than 553 pg/ml. Mean DPV plasma

concentrations over the ring use period were generally similar, at approximately 260-270 pg/ml. However, there was a 60% decrease in plasma concentration during a 3-day washout period between the first and second ring use periods. 1 month prior to removal of the final ring, DPV plasma concentrations were very low for the majority of participants at 3.38-8.89 pg/ml. DPV was detected in vaginal fluid 4 hours after insertion of the first ring with values ranging between 4,222-8,133 ng/g which were at least 1200-fold above the DPV concentration required *in vitro* for 99% inhibition (IC99) of provirus integration into cervical tissue following challenges with HIV-1BAL [207]. Within 24 hours, maximal DPV concentrations were rapidly reached following ring insertion with highest concentrations near the ring. In 7 participants, menses appeared to result in temporarily lower vaginal fluid concentrations of DPV with or without the use of a tampon, nonetheless no difference was observed in DPV plasma concentrations [211]. Tampons may reduce drug levels in vaginal fluid due to either adsorption to the tampon or increased blood levels in the vagina, or both. During the menses cycle, the lowest vaginal fluid concentration of DPV was 490 ng/g, 100-fold higher than the *in vitro* IC99. In cervical tissue biopsies from all DPV users, the DPV concentrations ranged between 46-4770 ng/g, approximately 14 to 1000 times higher than IC99. This also reflected inter-participant variability of DPV concentrations within cervical tissue.

2.8.3 Darunavir

2.8.3.1 Physiochemical properties

DRV, (3-[(4-amino-benzenesulfonyl)-isobutyl-amino]-1-benzyl-2-hydroxypropyl)-carbamic acid hexahydrofuro-[2,3-b]furan-3-yl ester or TMC114 has a molecular weight of 548 kDa. This PI contains cyclic ether bonds with a central phenylalanine amino acid bound to a bis-Tetrahydrofuran (THF) ligand to one side and a p-aminobenzenesulfonamide on the other; the drug is administered as its ethanoate salt (Figure 2.23). DRV binds with high affinity to the active site of the HIV-1 protease [212] and selectively blocks the cleavage of the HIV Gag-Pol polyprotein to prevent maturation of viral particles into infectious virions. The IC_{50} and EC_{50} values of DRV both range from 1 to 8.5 nM [95]. DRV exhibits lipophilic properties with a predicted Log P of 1.89 and with aqueous solubility of 0.15 mg/ml. DRV is metabolised almost exclusively by the hepatic CYP3A4 enzyme. The absolute bioavailability of oral DRV is 37% but increases to 82% when co-administered with

ritonavir. Ritonavir is an inhibitor of the CYP3A4 enzyme as well as the efflux transporter P-gp [213] of which DRV is a substrate [214].

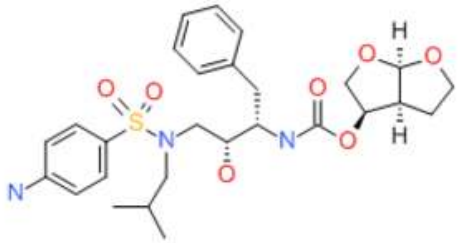

Figure 2.23 Structure of DRV with its physiochemical properties. DRV contains a central phenylalanine amino acid bound to a bis-Tetrahydrofuran (THF) ligand to one side (left) and a p-aminobenzenesulfonamide on the other (right). These features provide high-affinity binding to the pocket of the HIV-1 protease.

2.8.3.2 Pharmacology

In Caco-2 monolayers DRV shows intermediate to high levels of absorption [213]. Saturation of the active transport process occurs with increased DRV concentration, this may occur by the saturation of the P-gp efflux pump indicating an interaction between DRV and P-gp (Table 2.1). *In vitro* equilibrium dialyses of plasma samples demonstrate high (95%) binding of DRV to human plasma proteins [215]. DRV primarily undergoes oxidative metabolism [216] and is extensively metabolised by cytochrome P450 (CYP450) enzymes, largely by CYP3A [217]. DRV also inhibits CYP3A, however, it is not as potent as ritonavir (RTV) which increased DRV plasma concentrations. In a study of HIV-negative, healthy individuals, (100 mg) increased the absolute bioavailability of DRV (600 mg once daily) from 37% (DRV only) to 82% (DRV+RTV) [218]. A pharmacokinetic enhancement, such as the activity of RTV, indicates that the first pass elimination of DRV can almost be completely inhibited.. With this elimination taken into account, there was a 14-fold overall increase in the AUC for DRV when taken with RTV 100 mg twice daily versus DRV when taken alone. It has been shown however that increasing the dose of RTV to 200 mg twice daily with DRV 600 mg does not result in any significant increase in DRV plasma concentration, indicating that the maximal pharmacokinetic inhibitory effect was achieved with the lower RTV dose [216, 219].

In a DRV mass balance study where healthy volunteers were given a single dose of radiolabelled [^{14}C]DRV (400 mg) + low dose RTV (100 mg), metabolism after 48 hrs was found to be extensive when DRV only was administered but was significantly reduced when DRV was co-administered with RTV. In the absence of RTV the proportion of uncharged drug eliminated was 8% (6.8% in the faeces and 1.2% in urine) compared to 49% (41.2% faeces and 7.7% in urine) the presence of RTV [216, 217]. After a period of 168 hrs post administration [^{14}C]DRV or metabolites of [^{14}C]DRV were excreted mainly in the faeces (80%) and to a lesser extent in the urine (14%) [217].

A combination microbicide vaginal ring containing DRV (300 mg) and DPV (100 mg) was tested in macaques. Serum concentrations of both drugs were maintained between 10 - 100 pg/ml. Vaginal fluid levels ranged between 10^3 and 10^4 ng/ml and between 10^4 and 10^5 ng/g for DPV and DRV, respectively. In each tissue type, DPV and DRV showed very similar concentration levels: vagina ($1.8x10^3$ – $2.8x10^3$ ng/g), cervix ($9.4x10^1$-$3.9x10^2$) ng/g, uterus (0-108 ng/g), rectum (0-40 ng/g). In this study, IC_{50} values obtained were <2 ng/ml for both drugs [220].

2.9 Conclusions

This review has demonstrated that there is ample data concerning the mechanisms of HIV infection and a surge in recent research that addresses the methods for prevention of HIV. Such methods include advances in the development of vaginally and rectally applied ARV based microbicides. The permeability of the drugs that serve as the active agents of these products are yet to be extensively studied, especially with regards to interactions with membrane bound drug transporters. This provides scope for the further investigation into determining their precise transport kinetics. In addition, the relevance of these transporters, especially at the vaginal mucosal surface remains unknown.

Chapter 3 Materials and Methods

3.1 Cell Culture Methods

All cell culture methods were undertaken under a laminar flow hood along with the necessary aseptic conditions. All experiments involved the use of the vaginal epithelial cell line HEC-1A. This cell line was isolated in 1968 by H. Kuramoto and associates from a 71 year old woman with stage IA endometrial cancer [221]. The cell line was kindly provided by collaborators at Imperial College London and the University of Aberdeen. This is the only vaginal epithelial cell line that is reported to form tight junctions [222], a crucial characteristic for dual chamber- based drug transport kinetic studies.

3.1.1 Cultivation of HEC-1A (human endometrial adenocarcinoma 1a)

HEC-1A cells were maintained in McCoys 5A modified cell culture medium (Invitrogen, Paisley, UK) containing L-glutamine 0.21915g/L, glutathione 0.0005g/L, peptone 0.6g/L, phenol red 0.011g/L and D-Glucose 3g/L. A 500ml bottle of medium was supplemented with 10% (v/v) FBS (Fetal Bovine Serum, Invitrogen, Paisley, UK) and 2% of penicillin 5000 units.ml-1/streptomycin 5000µg.ml-1 solution (Sigma-Aldrich, Cambridge, UK). Cells were cultured at 37°C with 5% CO_2 in a humidified air incubator (Binder, New York, USA) and passaged every 2-4 days. Once confluent, cells were washed with 10 ml PBS (Phosphate Buffered Saline, PAA, Yeovil, UK) and incubated for 5-10 minutes with 5 ml 0.25% Trypsin-EDTA solution (PAA, Yeovil, UK) at 37°C with 5% CO_2. Detached cells were re-suspended in 7-10 ml of fresh cell culture medium and counted (see below). The desired number of cells was pipetted into a new flask.

3.1.2 Cell Counting

Trypsinised cells were re-suspended in 5-10 ml cell culture medium. Suspended cells (100 µl) were mixed with an equal volume of trypan blue (Sigma-Aldrich, Cambridge, UK) in a bijou (Greiner Bio-One, Stonehouse, UK). This cell suspension solution was then pipetted into a haemocytometer (Hawksley, Sussex, UK), enough to cover the counting grid in order to count viable cells. The 4 outer squares were counted and the following equation was used to calculate the cell number per ml of medium:

(counted cells ÷ 4) x 2 (dilution factor) x 10^4 = cells/ml in cell suspension

3.1.3 Thawing of cryopreserved cells

Prior to thawing, cryovials (Fisher Scientific, Loughborough, UK) containing HEC-1A cells were transferred from liquid nitrogen to a water bath (Grant Instruments, Cambridge, UK) at 37°C. Once thawed, cells were then transferred from the cryovials into 19 ml of pre-warmed (37°C) cell culture medium to allow dilution of the cryoprotector dimethyl sulfoxide (DMSO). The suspension was then centrifuged at 177 x g (Sanyo Mistral MSE 3000, U.K) at 25°C for 5 minutes. The supernatant was removed and the cell pellet was re-suspended in fresh cell culture medium. Cells were then transferred to a 25 cm^2 cell culture flask (Greiner Bio-One, Stonehouse, UK) and 7ml of medium was added. To increase cell density, confluent cells were then transferred to a larger 75 cm^2 flask and 175 cm^2 respectively.

3.1.4 Freezing of HEC-1A cells

Prior to storage in liquid nitrogen, the HEC-1A cells were split from a confluent cell layer grown in cell culture flask and detached from the flask using trypsinisation process as described and re-suspended in growth medium. Cells were counted as described and a cell suspension was produced with $1x10^6$ cells in 500 µl of cell culture medium and prepared in a 5ml bijou. An equal volume of 10% (v/v) DMSO (Dimethyl Sulfoxide, Sigma-Aldrich, Cambridge, U.K) in cell culture medium was then carefully droplet pipetted to mix with the 500 µl of HEC-1A cell suspension to make a final suspension solution of $1x10^6$ cells/ml of culture medium containing 5% DMSO. DMSO was used as a cryoprotective protective agent as gradual freezing leads to optimal viability of cryopreserved cells by minimising the formation of ice crystals both within and outside the cells undergoing cryopreservation. The suspensions were kept in cryovials marked for date and passage number and stored overnight at - 80°C freezer for slow cooling. On the following day, the cryovials were transferred to a liquid nitrogen tank at a temperature of -170°C.

3.2 Transwells®

3.2.1 Culturing Epithelial Cells on Transwells®

The apical chambers of 12-well polycarbonate (PC) and polyester (PE) systems (Corning Costar Corp, Cambridge, UK) seeded with different densities of HEC-1A cells in 500 µl of medium. Following addition of 1500 µl culture medium to the basolateral chamber, cells were cultured for the desired number of days. The medium in the apical and basolateral chambers was changed every 48-72 hours. Table 3.1 shows the properties of the Transwells® used throughout this study.

Membrane material	Pore size (µm)	Pore density (pores/cm^2)	Surface area (cm^2)	Optical properties
PC	0.4	1x10^8	1.12	Translucent
PC	3.0	2x10^6	1.12	Translucent
PE	0.4	4x10^6	1.12	Clear

Table 3.1 Properties of the Transwells® used in this study.

3.2.2 Coating of semi-pearmeable Supports

12-well Transwells® were coated with the major extracellular matrix membrane protein Laminin (Sigma-Aldrich, Cambridge, UK) or reconstituted basement membrane preparation Matrigel® (Corning Costar Corp, Cambridge, UK). Matrigel® is extracted from the Engelbreth-Holm-Swarm (EHS) mouse sarcoma, a tumor rich in extracellular matrix proteins. This material, once isolated, is approximately 60% laminin, 30% collagen IV, and 8% entactin. Human Laminin, Mouse Laminin and Matrigel® were compared to investigate any effects on cell attachment and TEER. Various concentrations were prepared as recommended by the manufacturer's instructions. All laminin and Matrigel® solutions were diluted in PBS or ice cold serum free cell culture media, respectively. Once coated, Transwell® permeable supports were left to air dry (lid off) for 16-24 hours in a laminar flow hood. Any remaining solution was aspirated from the inserts which were then washed once with either PBS or cell culture medium.

3.3 Measurement of Transepithelial Electrical Resistance (TEER)

The TEER of HEC-1A cell monolayers grown on permeable supports was measured with an Epithelial Voltohmmeter (EVOM^2), (World Precicion Instruments, Sarasota, FL) which measured cell resistance. TEER reflects the ionic conductance of the

paracellular pathway in the epithelial monolayer. The STX2/"chopstick" electrode (WPI, Sarasota, FL) pair that are connected to the EVOM^2 voltohmmeter were rinsed in 70% ethanol for sterilisation prior to taking measurements. Each stick of the electrode pair (4 mm wide and 1 mm thick) contains a silver/silver chloride pellet for measuring voltage and a silver electrode for passing current. All TEER measurements were made in a laminar flow hood and were made within approximately 3 minutes of removal of Transwells® from the incubator as TEER can fluctuate with temperature. For electrical measurements, two electrodes are used, with the shorter electrode immersed in the apical (upper) compartment and the longer electrode in the basolateral (lower) compartment and the electrodes are separated by the cellular layer. It was important to make sure the shorter tip did not contact cells growing on the membrane, with the longer tip gently touching the bottom of the basolateral chamber (Fig. 9).

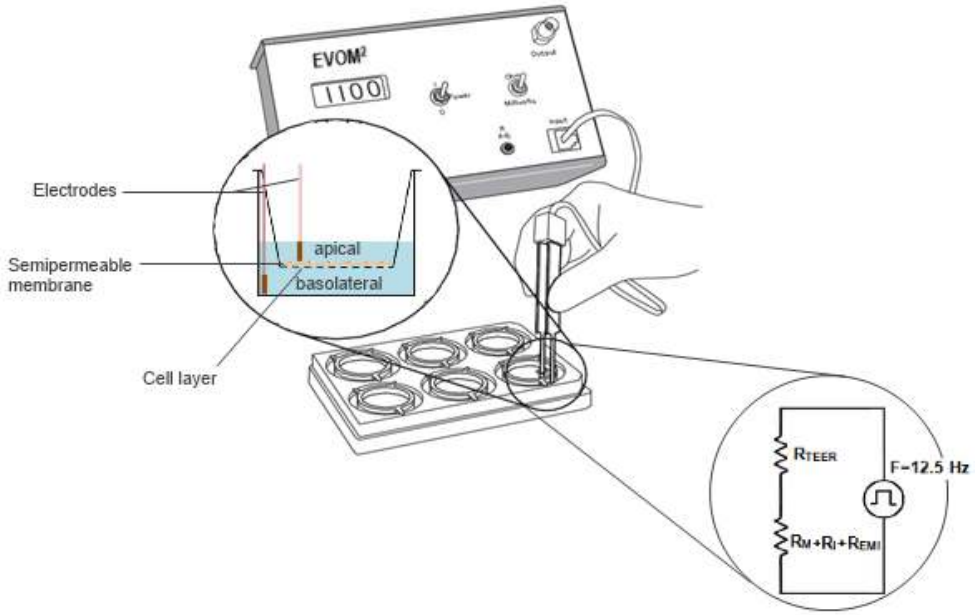

Figure 3.1 Measurement of TEER of HEC-1A cells using the EVOM^2 voltohmmeter and STX2 electrodes. Electrodes are immersed into the medium of apical and basolateral compartments. The ionic conductance of the paracellular pathway in the epithelial monolayer is measured. Total electrical resistance includes; resistance of the cell layer (R_{TEER}), resistance of the cell culture medium (R_M), resistance of the semipermeable membrane insert (R_I) and the resistance pf the electrode medium interface (R_{EMI}). Application of AC with a square waveform.

The ohmic resistance is calculated based on Ohm's law as the ratio of the voltage and current. However, as direct current (DC) can damage both cells and the electrode tips, an alternating current (AC) with a square waveform is therefore

applied. An AC square wave at a frequency of 12.5 Hz is used to avoid any detrimental effects on the electrodes and the cell layer. The EVOM system has a measurement range of 1-9,999 Ω with a 1 Ω resolution [223].

The measurement procedure includes measuring the blank resistance (R_{blank}) of the semipermeable membrane only (without cells) and measuring the resistance across the cell layer on the semipermeable membrane (R_{sample}). The cell specific resistance (R_{net}) is the corrected TEER value of the cell monolayer multiplied by the surface area of the permeable support to give a value in ohms(Ω) x cm^2, can be calculated using the following equation:

$$(R_{sample}(\Omega) - R_{blank}A = R_{net}$$

TEER was also used as method to determine cell viability in all assays. Toxicity would be indicated by a rapid and significant decrease in TEER reading.

3.4 Disrupting tight junctions using the calcium chelator EDTA

HEC-1A cells were cultured on transwells as described as described above. The Ca^{2+} chelator EDTA (Sigma-Aldrich, Cambridge, UK) was diluted in cell culture medium. After removal of medium, 500 µl of medium containing 2.5 mM EDTA was added to the apical chamber and 1500 µl of EDTA-free cell culture medium was added to the basolateral chamber. Cells were incubated at 37°C. TEER was monitored at various time points over a 90 minute period. At T=90, HEC-1A cell layers were then washed twice with HBSS and the medium in both chambers was replaced with fresh EDTA-free cell culture medium. HEC-1A cell layer recovery was allowed to proceed and TEER was measured at 150 minutes and 1440 minutes.

3.5 Immunofluorescence

3.5.1 Glass slides

HEC-1A cells were seeded on 0.69 cm^2 glass slides (BD Biosciences, Oxford, England) with a removable plastic chamber separator (8 chambers) and cultured in 500µl of culture medium which was replaced every 2-3 days. Slides were washed with 2X with 100µl HBSS and cells were fixed with 100 µl of fixing agent 4% paraformaldehyde (Sigma-Aldrich, Cambridge, UK), (PFA- 4% v/v in 10X PBS) for 15 minutes at 37 °C in 5% CO_2. Fixed cells were washed 3X with 100 µl HBSS then

permeabilised by adding 100 µl Triton X-100 (Sigma-Aldrich, Cambridge, U.K), (0.2%, v/v for 15 minutes at 37 °C in 5% CO_2). Triton X-100 was removed by washing 2X with HBSS, and any non-specific binding sites were blocked by adding 100 µl of blocking agent (1X TBS Tris Buffered Saline, Severn Biotech, Kidderminster, UK) and Tween 20 (Sigma-Aldrich, Cambridge, UK)) supplemented with 3% BSA (Bovine Serum Albumin, Sigma-Aldrich, Cambridge, UK) for 30 minutes at 37 °C in 5% CO_2. Blocking solution was removed and cells were then incubated for 90 minutes with 100 µl of 2.5 µg/ml anti-ZO-1 monoclonal primary antibody (clone 1, BD Bioscience, Oxford, England) diluted in TBS-T/BSA. Omission of the primary antibody served as negative control as did an isotype-matched control anti-gp41 secondary antibody diluted 1:500. Cells were washed 3X with 100 µl HBSS and incubated with FITC goat anti-mouse IgG conjugated secondary (Sigma-Aldrich, Cambridge, UK) 100 µl diluted 1:100 in TBS-T/BSA for 2 hours at room temperature in the dark. Slides were washed 3X with HBSS and the plastic separating chamber was removed. To each well 8 µl of Vectashield mounting medium (Vector Laboratories, Burlingame, USA) containing Dapi was then added and a microscope cover slip (Fisher Scientific, Loughborough, UK) was gently applied. Slides were analysed using an Olympus BX61 microscope that was equipped with an Olympus XM10 digital monochrome camera and images were observed by the Olympus Cell F imaging software.

3.5.2 Transwell® membrane

HEC-1A cells were seeded on insert membranes of clear PE Transwells® and cultured as described in above. After 7 days in culture HEC-1A cell layers were washed 2X with HBSS and cells were fixed with 150 µl of fixing agent 4% paraformaldehyde (Sigma-Aldrich, Cambridge, UK), (PFA- 4% v/v in 10X PBS) for 15 minutes at 37 °C in 5% CO^2. Fixed cells were washed 3X with 150µl HBSS then permeabilised by adding 150 µl Triton X-100 (Sigma-Aldrich, Cambridge, U.K), (0.2%, v/v for 15 minutes at 37 °C in 5% CO^2). Triton X-100 was removed by washing 2X with HBSS, any non-specific binding sites were blocked by adding 150 µl of blocking agent (1X TBS Tris Buffered Saline, Severn Biotech, Kidderminster, UK) and Tween 20 (Sigma-Aldrich, Cambridge, UK) supplemented with 3% Bovine Serum Albumin (BSA) (Sigma-Aldrich, Cambridge, UK) for 30 minutes at 37 °C in 5% CO^2. Blocking solution was removed and cells were washed 3X with 100µl PBS. Cells were then incubated for 90 minutes with 150 µl of 2.5 µg/ml anti-ZO-1

monoclonal primary antibody (clone 1, BD Bioscience, Oxford, England) diluted in TBS-T/BSA. Omission of the second antibody served as negative control. Cells were washed with 3X 150 µl HBSS and incubated with FITC goat anti-mouse IgG conjugated secondary (Sigma-Aldrich, Cambridge, UK) 150 µl diluted 1:100 in TBS-T/BSA for 2 hours at room temperature in the dark. Slides were washed 3X with HBSS and the plastic separating chamber was removed. The membranes of the Transwell inserts were cut out with a scalpel (Sigma-Aldrich, Cambridge, UK) and placed on a glass microscope slide (Sigma-Aldrich, Cambridge, UK). To each membrane 10 µl of Vectashield mounting medium (Vector Laboratories, Burlingame, USA) containing Dapi was then added and a microscope cover slip (Fisher Scientific, Loughborough, UK) was gently applied. A round cover glass was gently placed on top of the membrane and the edges were sealed with nail varnish. Slides were analysed using an Olympus BX61 microscope that was equipped with an Olympus XM10 digital monochrome camera and images were observed by the Olympus Cell F imaging software.

3.6 Protein assays

3.6.1 Protein extraction from cells

$1x10^6$ HEC-1A cells were seeded in 6-well plates to obtain overnight confluency of 70-80%, at 37 °C in 5% CO^2. All sample lysis steps were carried out outside of the laminar hood and on ice unless otherwise stated. Following overnight incubation, the 6-well plate was placed on ice and the media was aspirated. Plate was washed 2X with 500 µl ice-cold PBS and removed by aspiration. 250 µl ice-cold 0.5% NP40 lysis buffer (Tris 2M, NP40, dH_2O, NaCl), (Sigma-Aldrich, Cambridge, UK) with the addition of 1:100 protease inhibitor was added to each well. The wells were scraped with a cell scraper (Fisher Scientific, Loughborough, UK) and the lysate was transferred to a pre-chilled 1.5 ml Eppendorf tube. Lysates were incubated on ice for 30 minutes then spun at full speed (~14,000 × g) in a microcentrifuge for 10 minutes at 4°C. Supernatant was transferred to a new tube and the pellet was discarded. The supernatant was aliquoted and stored at −80°C for long term storage and -20°C for short term storage prior to further analysis. Repeated freeze thaw cycles were avoided.

3.6.2 Protein extraction from tissue

Human (provided by Imperial College London whom ethically obtained from the NIH repository [224]) and rat tissues (already sacrificed rats by qualified staff) were obtained. Tissue was washed with ice cold PBS to remove any blood and then cut and weighed. Tissue was placed into an Eppendorf tube containing 1.4mm lysing matrix beads (MP Biomedical, UK). 1% NP40 lysis buffer (500ul/10mg tissue) containing 1:100 protease inhibitor was added to each tube. Tissue was homogenised by Fastprep-24 (MP Biomedical, UK) with functions set to 4 m/s and ran for 40 seconds, this was repeated 3-4X. Lysate was transferred to an Eppendorf tube which was then spun down (~14,000 × g) in a microcentrifuge for 10 minutes at 4°C. Supernatant was transferred to a new Eppendorf tube.

3.6.3 Bicinchoninic (BCA) assay

Total protein concentrations were determined using a BCA kit (Thermo Scientific). This biochemical assay is based on a reduction of Cu^{2+} ions from the copper sulphate to Cu^{+} in the BCA reagent. The amount of Cu^{2+} reduced is proportional to the amount of protein present. Two molecules of the bicinchoninic acid chelate with each Cu^{+} ion and is depicted by a colour change of the sample solution from green to purple, measurable at a wavelength of 562 nm. The amount of protein present is quantified by comparing the absorption with a protein solution of known concentration, which serves as the standard.

For this assay, samples were diluted 1:12 in PBS and Bovine Serum Albumin (BSA) was used as the standard, with concentrations ranging between 31.25 and 2000 µg/ml prepared. 25 µl of each standard and sample were mixed with 200 µl of BCA reagent. The absorbance of the plate was measured at 562 nm and the protein concentration in individual samples calculating using a standard curve. From this, proteins could be prepared to the appropriate amount for further studies.3.6.4 SDS-PAGE (sodium dodecylsulphate polyacrylamide gel electrophoresis)

This type of gel electrophoresis is used to analyse proteins. Proteins are denatured by an anionic detergent SDS and separated by size on a polyacrylamide gel. An electric current is applied; smaller proteins migrate faster through the gel matrix than larger proteins.

For Western blots described in this thesis, the NuPAGE® Novex Bis-Tris electrophoresis system (Invitrogen, Paisley, UK) was used. This is a neutral pH, discontinuous SDS-PAGE, pre-casted polyacrylamide [Bis-(2-hydroxethyl) imino-tris (hydroxymethyl) methane-HCL) mini-gel system made with a separating gel acrylamide concentration of 4-12% and a stacking gel acrylamide concentration of 4% at a thickness of 1.0mm. Prior to running of the gel, denatured protein concentrations were prepared and 40 µg/ml of protein was prepared for each sample. Each sample contained NuPAGE® LDS sample buffer (lithium dodecyl sulfate pH 8.4, coomasie G250 and phenol red), NuPAGE® reducing agent (500mM dithiotreitol (DTT)) and added at volumes according to the manufacturer's instructions. Once samples were prepared and added to Eppendorf tubes, tubes were spun and mixed by turning upside down. Samples were then boiled in a pre-heated waterbath (Grant Instruments, Cambridge, UK) for 10 minutes at 70°C. Samples were then spun again for 2 minutes and placed on ice. The pre-casted gel was placed into a gel electrophoresis tank (BioRad, CA, USA) in the correct orientation and filled with 1X running buffer (NuPAGE MOPS, SDS Running Buffer, ddH_20). 10-25µl of protein sample was then loaded into the wells of the pre casted gel in addition with 5µl of the ColorBurst™ (myosin-violet, BSA-red, GDH-blue, ADH-red, Carbonic Anhydrase-orange, Trypsin Inhibitor-blue, Lysozyme-red, Aprotinin-blue, 200 mM Tris, SDS and, formamide) electrophoresis marker. Gel was set to run for 2 hours at 100V.

3.6.5 Western blot analysis

Proteins that are separated on SDS can be transferred onto nitrocellulose membrane where they are detected by specific antibodies. The primary antibody directly binds to the protein of interest on the membrane and the secondary antibody is species-specific (e.g. mouse or rabbit) and detects the bound primary antibody. The secondary antibody is linked to a reporter enzyme, which catalyses the conversation of a peroxidase substrate contained in the enhanced chemiluminescence (ECL) solution. X-ray films are used to capture the light emitted during this reaction, creating an image on the film of the bound antibodies.

Upon completion of gel electrophoresis, the gel was gently removed from the tank and placed on top of the nitrocellulose membrane (GE Healthcare Life Sciences, Bucks, UK) within a "sandwich" cassette (sponge>3x filter paper>gel>membrane>3x filter paper>sponge). The cassette was closed and placed into a transfer tank

(BioRad, CA, USA) which was filled with transfer buffer (running buffer, ddH_20, methanol). A magnetic stirrer (Velp Scientifica, IT) and an ice pack were also added into the tank which was connected to a basic power supply (BioRad PowerPac). A constant of 400 mAmp and a voltage of 90V was set for 90 minutes.

Once transfer was completed, the membrane was gently removed from the cassette and washed by incubating with washing solution (5% milk PBS/Tween20) for 30 minutes on an orbital shaker at 60 revolutions per minute (RPM), (Astra Zeneca, DE, USA). Washing buffer was then removed and primary antibody was added at the required concentration (diluted in 3% milk PBS/Tween20) and incubated overnight at 4°C at 60 RPM. The membrane was then washed 3x with washing solution, 10 minutes each, at 60 RPM at room temperature. Secondary antibody conjugated to HRP (horseradish peroxidase) was diluted in 3% milk PBS/Tween20 was added and left to incubate for 1 hour at room temperature. 3X washes were repeated and the membrane was placed inside a film developing cassette containing a clear plastic A4 cover sheet. 5 ml of Luminata Crescendo Substrate (Millipore, MA, USA) was added to the membrane a left to incubate for 2 minutes at room temperature. Excess substrate was removed, the cover sheet was applied over the membrane and the cassette was closed. In a dark room, X-ray film (SLS, Yorkshire, UK) was then exposed to the membrane for various time points to detect a chemiluminescent signal.

3.6.5.1 Antibody concentrations for Western blot analysis

All primary and secondary antibodies were used at the following concentrations:

Primary antibody	Abcam antibody code	Species/Isotype	Dilution ratio
Anti-MRP1 (ABCC1)	ab24102	Mouse monoclonal IgG2a Isotype	1:1000
Anti-MRP2 (ABCC2)	ab3376	Mouse monoclonal IgG2a Isotype	1:500
Anti-MRP3 (ABCC3)	ab3376	Mouse monoclonal IgG2b Isotype	1:500
Anti-MRP4 (ABCC4)	ab15602	Rat monoclonal IgG2a Isotype	1:1000
Anti-MRP5 (ABCC5)	ab180724	Rat monoclonal IgG2a Isotype	1:1000
Anti-ENT1 (SLC29A4)	ab135756	Rabbit Polyclonal IgG	1:1000
Anti-P-gp (ABCB1)	ab168337	Rabbit monoclonal IgG	1:100
OATP1B3 (SLCO1B3)	ab122123	Rabbit polyclonal IgG	1:1000
OATP4A1 (SLCO4A1)	ab122123	Rabbit polyclonal IgG	1:100
Anti-β-actin	ab8226	Mouse monoclonal IgG2a	1:5000

Table 3.2 Primary antibody information and their working concentrations. All primary antibodies were purchased from Abcam, Cambridge, USA.

Secondary antibody	Thermo antibody code	Species/Isotype	Dilution ratio
Anti-Rat	31470	Goat anti-Rat IgG2a polyclonal- HRP conjugated	1:20000
Anti-Rabbit	65-6120	Goat anti-Rabbit IgG polyclonal- HRP conjugated	1:20000
Anti-Mouse	31450	Rabbit anti-mouse IgG polyclonal-HRP conjugated	1:2500

Table 3.3 Secondary antibody information and their working concentrations. Anti-Rat secondary was purchased from (Thermo Fisher Scientific, PA, USA), Anti-Rabbit and Anti-Mouse secondary antibodies were purchased from Sigma-Aldrich, Cambridge, UK.

3.7 mRNA analysis

3.7.1 SYBRgreen® drug transporter primers

Using the expression profiles of the cell lines, obtained using the TaqMan® 96-well Drug Transporter Array plates, and cervicovaginal tissue data, a panel of 2 endogenous controls, 9 ABC efflux transporters and 11 SLC uptake transporters were selected as a focus for validation of expression and for stimulation experiments.

3.7.1.1 Design and reconstitution of primers

The first goal to generating this new condensed panel of primers for targeting the two endogenous controls and 20 drug transporters was to ensure proper design that were specific to the target of interest. All primer sets were designed in that at least one of each pair of primers would span an exon-exon boundary to prevent the amplification of genomic DNA. The Roche universal probe library assay design centre software was used to design all primer pairs (https://lifescience.roche.com/). The software generated a list of potential primer sets for each target that were all designed to generate primers with optimal annealing temperatures ≈ 60˚C. All primer sets were then checked for specificity to their target gene, including all transcript variants, using the NCBI nucleotide BLAST software (http://blast.ncbi.nlm.nih.gov/Blast.cgi). All primer sets had to pass these three main criteria (exon-exon spanning, annealing temperature ≈ 60˚C, specific to target gene and transcript variants).

Drug Transporter	Forward Sequence 5'>3'	Reverse Sequence 5'>3'
HPRT1	TGACCTTGATTTATTTTGCATACC	CGAGCAAGACGTTCAGTCCT
RPLP0	TCCAGGCTTTAGGTATCACCAC	TTGATCAGCTGCACATCACTC
P-gp	CTTCATCGAGTCACTGCCTAATAA	GCTATGGCAATGCGTTGTT
BCRP	TGGCTTAGACTCAAGCACAGC	TCGTCCCTGCTTAGACATCC
MRP1	CCTGTTCAACGTCATTGGTG	AGGAAGCCACGTAGAACCTCT
MRP2	CTGGATCACCTCCAACAGGT	AGAAGACAGTCAGGTTCCCAAC
MRP3	AATGTCGACCCTAACCCCTAC	GGGTCAGGGTTTAGCAGCTT
MRP4	GCGCCTGGAATCTACAACTC	CTTTGTATGCCCGGATGGT
MRP5	CAGCGACCTGACGGAGAT	GGGCAAGGCTGATCCTCT
MRP6	CGGGAAGGATTGCATCAC	GGCACCGTGAGGTTTATTCT
MRP7	GCCCTCAATGATGACCTCAG	CCTCCGCTAAGGGTGACA
ENT1	TCACCAGCCTCAGGACAGAT	GAGTGGCCGTCATGAAAAA
ENT2	GCTGAGCTCCTCCAGTCTGA	GGCTCATCTGGCTCTGATTC
CNT3	CTGAACTCCACGCCATCA	CAAGTGGGAGGATGGAACC
OCT1	CTCGCCCAACTACATGTCC	CGAGCCAACAAATTCTGTGAT
OCT3	CACCATCGTCAGCGAGTTT	CAGGATGGCTTGGGTGAG
OATPD	TGTTCCCTATGGAAACAGCA	CAGGTAGGTGATGCCATCTG
OATPE	AGCTGCCACCTTGTTTGG	GCCTGAGCTTGTTCACAAAGA
OATP8	TCAAGTGGTATTAAAAAGCATACAGTG	TTCACCCAAGTGTGCTGAGT

Table 3.4 Primer sequences for use with SYBRgreen® RT-qPCR experiments. Primer sets were optimised to find the ideal dilutions using the same cycling conditions.

3.7.1.2 Optimisation of primers

The optimal primer concentration for each target was investigated until acceptable assay efficiencies of 90-110% were obtained. To determine primer efficiencies standard curves were generated for each primer set by performing a series of 1/10 dilutions of cervicovaginal cell line cDNA template from 50 ng down to 5 pg. Due to the lack of P-gp expression within the four cervicovaginal cell lines, cDNA obtained from Caco-2 cells, which express P-gp, was used to optimise this primer set. A value of -3.32 generated from the slope of the standard curve signifies 100% efficiency from the primer set, with slopes between -3.1 and -3.6 signifying acceptable primer efficiencies of 90-110%. All primers sets were originally tested at a concentration of 10 pmol/µl, however many of the primer sets did not generate acceptable efficiencies (90-110%) with this concentration, mainly due to primer-dimer formation, confirmed by the generation of a second peak detected at a lower temperature than the melting temperature (T_m) of the amplified product. A major cause of primer dimer formation is excessive primer concentration which leads to hybridisation of the primer pairs and unwanted amplification. Therefore a range of reduced primer pair concentrations were investigated down to 4 pmol/µl until acceptable efficiencies were obtained for each primer pair. These ranged between 4-10 pmol/µl with efficiencies between 94.54-107.57% obtained. Dissociation curves were also performed to ensure no, or minimal, primer-dimer and non-specific amplification was generated from the primer pairs at their optimised concentrations. Primer sets were validated by comparing the expression levels with those generated by Taqman® Human Drug Transporter array plates.

Drug Transporter	Primer Concentration (pmol/µl)	Slope	Efficiency (%)
HPRT1	6	-3.24	103.63
RPLP0	6	-3.33	99.79
P-gp	10	-3.30	100.75
BCRP	6	-3.20	105.49
MRP1	10	-3.36	98.48
MRP2	10	-3.23	103.98
MRP3	4	-3.15	107.57
MRP4	10	-3.31	100.50
MRP5	6	-3.18	106.10
MRP6	4	-3.26	102.83
MRP7	4	-3.19	105.77
ENT1	10	-3.38	97.63
ENT2	10	-3.28	101.78
CNT3	4	-3.27	102.21
OCT1	4	-3.17	106.57
OCT3	4	-3.27	102.21
OATPD	4	-3.43	95.68
OATPE	10	-3.46	94.54
OATP8	6	-3.36	98.44
PEPT1	10	-3.25	99.01
PEPT2	6	-3.18	104.03
CNT3	4	--3.27	101.22

Table 3.5 The optimised primer concentrations for all individual assays designed for use with SYBRgreen®. Slope values are given, obtained from standard curve plots, in addition to the calculated efficiencies for all primer sets.

3.7.1.3 SYBRgreen® RT-qPCR

SYBRgreen® PrecisionTM 2X qPCR Mastermix with ROX quencher (Primer Design, Southampton, UK) was used for all individual assay RT-qPCR experiments.

Standard curves were generated to determine primers set efficiency using cDNA from our cell lines that was generated as described previously. The cDNA was

diluted to 10 ng/µl and then serially (1/10) using nuclease free water to give final cDNA template concentrations of $1x10^{-2}$-$1x10^{-6}$ µg/µl. To duplicate wells of 96-well MicroAmp® Fast Optical 96-Well Reaction Plates (Life Technologies, Paisley, UK) 5µl of diluted cDNA was plated to give final concentrations of $5x10^{-2}$-$5x10^{-6}$ µg. To these wells 15 µl of Master Mix consisting of SYBGgreen® and primers was added to give a final volume of 20µl per well. Primers were diluted to workable concentrations (10 pmol/µl) from stock concentrations using nuclease-free water.

Material	**Volume (µl)**
SYBRgreen® Precision™ Mastermix	10
Forward Primer (10pmol/µl)	1
Reverse Primer (10pmol/µl)	1
Nuclease-free Water	3
Total Volume	**15**

Table 3.6 Mastermix for SYBGgreen® RT-qPCR

The plate was then covered using MicroAmp® Optical Adhesive Film and centrifuged at 1000 RPM for 1 minute to ensure that the reaction mix was pooled at the bottom of the wells. The plate was then transferred to the Applied Biosystems® 7900HT Fast Real-Time PCR system and the PCR run using SDS 2.4 software. The cycling conditions used were an enzyme activation step at 95˚C for 5 minutes, followed by 40 cycles of denaturation at 95˚C for 10 seconds, annealing at 60˚C for 10 seconds and extension at 72˚C for 10 seconds. A melting curve was also performed to detect the presence of primer-dimers and non-specific binding. R_2 values were generated from the standard curves generated. The optimal R_2 value that indicates 100% efficiency is -3.32, however values of -3.1-3.6 (80-110%) are widely accepted. To generate the optimal primer set efficiency (80-110%), the primer concentrations were reduced, where necessary, in a stepwise fashion from 10 pmol/µl to 8, 6 and 4 pmol/µl until primer-dimers and non-specific binding were eliminated, if present, to improve primer set efficiency.

3.7.2 Gene expression calculations

Target gene ratios were generated by calculating the combined mean Ct value of the triplicate repeats of the three selected housekeeper genes and dividing by the mean Ct value of each drug transporter from the triplicate repeats, as shown;

Housekeeper (HK) 1 = (Ct repeat 1 + Ct repeat 2 + Ct repeat 3)/3 = $HK1_{mean}$

Housekeeper (HK) 2 = (Ct repeat 1 + Ct repeat 2 + Ct repeat 3) /3 = $HK2_{mean}$

Housekeeper (HK) 3 = (Ct repeat 1 + Ct repeat 2 + Ct repeat 3) /3 = $HK3_{mean}$

$HK_{combined} = (HK1_{mean} + HK2_{mean} + HK3_{mean})/3$

$Target\ Gene\ (TG)_{combined} = (Ct\ repeat\ 1 + Ct\ repeat\ 2 + Ct\ repeat\ 3)/3$

$Ratio\ (TG\ expression) = HK_{combined}/TG_{combined}$

3.8. P-gp cDNA production and transfection into HEC-1A

3.8.1 Production of P-gp expression plasmid

Plasmid pcDNA3.1 Zeo was digested with EcoR5 and the linearised vector was purified by preparative agarose gel electrophoresis. Linearised vector was combined with 5'-phosphorylated amplification products (P-gp) at 3-fold molar excess and ligated by incubation with T4 DNA ligase for 2h at 25°C. Ligation mixture was desalted and used to transform E. coli XL1Blue electrocompetent cells.

Plasmids DNA obtained from transformants were used as template for PCR amplification using primers flanking the site of insertion of DNA encoding the P-gp sequence (Table 3.7). Amplification products were analysed by agarose gel electrophoresis. Transformants that showed DNA bands corresponding to the expected size of the inserted DNA were sent for sequencing. The following procedures described below were undertaken for the production of the P-gp expressing plasmid.

	P-gp primers
PGP amp F	[Phos]GACATGGATGGATCTTGAAGGGGACCGCAATGGA
PGP amp R	[Phos]TCACTGGCGCTTTGTTCCAGCCTGGAC

Table 3.7 Forward and reverse oligonucleotides used for amplification of P-gp.

3.8.1.1 Polymerase Chain Reaction (PCR)

Polymerase Chain Reaction (PCR) was carried out using 10ng of plasmid DNA, in 50 µl of PCR mixture {dNTPs (deoxyribonucleotides: dATP, dCTP, dGTP and dTTP each at 0.2 mM); 2.5 mM MgCl2 (Promega, Southampton, UK); 10X reaction buffer [200 mM Tris-HCl (pH 8.8 at 25°C), 100 mM (NH4)2SO4, 100 mM KCl, 1% (v/v) Triton X-100, 1 mg/mL BSA]; 2.5U PfuUltra™ HF DNA polymerase (Stratagene, La Jolla, CA, USA); 10 pmol of 5' phosphorylated sense and antisense oligonucleotide (Sigma-Aldrich, Dorset, UK)}. Following initial template denaturation (2 min at 95°C), PCR proceed through 12-30 denaturation-annealing-extension cycles. Finally, reactions were incubated for 1 min at the annealing temperature and for 5 min at 72 °C for final annealing and extension. Extension time was evaluated according to the DNA polymerase speed as well as the target length. Annealing conditions were optimized based on the oligonucleotide sequences.

3.8.1.2 Digestion of DNA

Restriction enzymes were all from New England Biolabs and were used according to the manufacturer's instructions. Generally 10-20 U of restriction enzyme were used to digest 1 µg of plasmid DNA in the presence of the buffer supplied. Mixtures were incubated at 37 °C for a minimum of 60 minutes. Enzyme inactivation, when necessary, was carried out after digestion by heating the reaction for the time and temperature required for each enzyme according to the manufacturer's instructions. DNA digestion was verified by agarose gel electrophoresis.

3.8.1.3 Preparative agarose gel electrophoresis for purification of DNA fragments

3.8.1.3.1 DNA agarose gel electrophoresis

DNA plasmids/fragments were analysed by agarose gel electrophoresis. Gels were prepared by dissolving electrophoresis grade agarose [(0.8-2% w/v) Sigma-Aldrich, Dorset, UK] in TAE buffer (0.004 M Tris-acetate, pH 8.0; 1 mM EDTA). 6-10 µl of GelRed (Biotium, Hayward, CA, USA) were added to the solution after it was cooled down to 55-60 °C. Solution pouring into a gel cast containing combs followed. GelRed is an intercalating nucleic acid stain structurally closely related to ethidium

bromide consisting of two ethidium subunits bridged by a linear spacer. It is noncytotoxic, nonmutagenic and non-hazardous at concentrations well above the working concentrations used in gel staining and more sensitive than ethidium bromide. DNA samples were mixed with loading buffer [0.04% (w/v) bromophenol blue; 0.04% (w/v) xylene cyanol; 5% glycerol] and loaded into wells at the end of the gel closer to the cathode. A voltage of 80-120 V was applied allowing for DNA migration to the positive terminal (anode). Bromophenol blue and xylene cyanol served ad as tracking dyes migrating at about the same rate as a 500 and 4000 base pair DNA fragment respectively. DNA molecular weight markers (1 kb DNA ladder, 100 bp DNA ladder; New England Biolabs, Ispwich, MA, USA) were run in parallel with the DNA samples as a reference for DNA fragment size. DNA fragments were visualised by UV light exposure. Pictures were taken by using a gel documentation system (Syngene).

3.8.1.3.2 Purification of DNA fragments

To maximise the efficiency of ligation into vectors, digested plasmid and inserts werere solved on agarose gel and bands of interests were excised and purified. Agarose gels were prepared as described in Section 3.8.1.3.1, using autoclaved 1 x TAE buffer. With the exception of the chamber lid, all the equipment used for electrophoresis (chamber, gel cast and combs) was pre-washed with 10% SDS and rinsed with autoclaved distilled water in order to minimise nuclease activity. DNA (1-5 µg) in 20-60 µl was applied to the gel wells. Electrophoresis was run at 80 volts for 4-5 hours for optimal separation. DNA was visualised by brief (5-10 seconds) exposure to long wavelength UV to reduce the likelihood of phosphodiester bond cleavage (DNA nicking). DNA bands corresponding to inserts and linearised vectors were excised with sterile blades and purified using the QIAquick Gel Extraction Kit (QIAGEN) following the manufacturer's instructions. This system is based on DNA selective absorption by a silica membrane. Agarose gel slices were solubilized using a guanidine thiocyanate-containing buffer which also provided the high-salt concentration conditions required for DNA binding to the silica membrane. Following adsorption to silica and washing with 70% ethanol, DNA was eluted in 15-30 µl of deionized water or TE buffer (10 mM Tris pH 8.0, 1 mM EDTA).

3.8.1.4 Determination of DNA concentration

The concentration of DNA was determined using the Nanodrop 2000 (LabtechInternational Ltd, East Sussex, UK). DNA preparations with an OD 260/OD 280 ratio in the range 1.8-2.0 were suitable for further use.

3.8.1.5 Ligation of DNA

Purified linearised vectors (approximately 100 ng) were combined with a 3-fold molar excess of insert DNA in the presence of the supplied ATP-containing ligase buffer (30 mM TRIS-HCl pH 7.8, 10 mM MgCl2, 10 mM DTT and 1 mM ATP) and 10 U (1 µl) of the T4 DNA ligase. The reaction was incubated for 2 hours at 25 °C, temperature at which the enzyme has optimal activity. Control reactions in which i) no insert was added, ii) no polymerase was added; were also set to check for false positives. ATP (Adenosine triphosphate) is a nucleoside triphosphate composed of an adenine ring, a ribose sugar and three phosphate groups. This molecule is crucial for DNA ligation as once it is hydrolysed to Adenosine monophosphate (AMP) the DNA ligase transfers it to the 5' phosphate (pyrophosphate bond). Then, the AMP-phosphate bond is attached by the 3'-OH, forming the covalent bond and releasing AMP. The formula used to calculate the 3-fold molar excess of insert DNA is shown below: 3 x {[amount of vector (ng) x length of insert (bp)]/ length of vector (bp)}

3.8.1.6 Transformation of *E.coli* by Electroporation

DNA was desalted to reduce the likelihood of sample arcing using the QIAquick PCR purification Kit (QIAGEN) according to the manufacturer's instructions and was eluted in deionized water. Electrocompetent *E.coli* cells were thawed on ice 15 min before transformation. Cells (45 µl) were transferred to an ice-cold electroporation cuvette (gap width 0.1 cm) (Biorad CA, USA) and gently mixed with the desalted DNA (1-10 ng in a maximum of 10 µl). Electroporation was carried out using the Gene-Pulser (Biorad) set to discharge a 25 µF capacitor, charged to 2.5 kV in parallel with a 200 Ω resistor giving time constants ranging between 4.5 and 5 ms. SOC medium (950 µl) was added immediately after electroporation. The cell suspension was then incubated for 60 min at 37 °C with shaking at 250 rpm to allow

for expression of the antibiotic resistance gene. Cells were then plated on LB agarose plates supplemented with carbenicillin (50 µg/ml).

3.8.1.7 Sequencing of DNA

DNA sequencing analysis was carried out by Eurofins MWG Operon (Ebersberg, Germany). The DNA of interest (1.3 µg) was mixed in aqueous solution of a final volume of 50 µl with a primer (13 ρmol) annealing at least 50 bp upstream the fragment. Samples were run on a DNA sequencer and high quality sequence data on 500-700 bp fragments was generally obtained.

	P-gp primers
PGP F1 seq	TCCAAGTCTTCCACCCCATTG
PGP F2 seq	TGCCTATGGAGACAACAGCC

Table 3.8 Oligonucleotides used for P-gp DNA sequencing.

3.9 PAMP stimulation of cells

Toll-like receptors (TLRs) are pattern recognition receptors that recognise various microbial and viral molecules known as pathogen-associated molecular patterns (PAMPs). When cells are stimulated with various PAMPS, immune responses are activated to protect the host from infection and intracellular signalling proteins (cytokines) are released.

Cells were stimulated with different PAMPS (Pam $_3$CSK$_4$, LTA, Poly I:C, *E. coli* LPS, FSL-1, Flagellin, Imiquimoid, Zymosan), (InvivoGen, CA, USA) diluted in serum free cell culture media and left to incubate at 37°C in 5% CO^2 for 24 hours. Blank samples contained media only. After 24 hours, supernatant was collected and transferred to Eppendorf tubes for cytokine detection assay (R&D Systems Inc, Minneapolis, USA).

Agonist	Recognition Receptor	Stock Conc (mg/ml)	Woking Conc (µg/ml)	Dilution
LPS *E.coli*	TLR4	5	5	1:1000
Poly I:C	TLR3	1	25	1:40
Pam $_3$CSK$_4$	TLR1/2	1	1	1:1000
Zymosan	TLR2/4	10	50	1:200
LTA	TLR2	1	10	1:100
FSL-1	TLR2/6	0.1	1	1:100
Flagellin	TLR5	0.1	5	1:20
Imiquimoid	TLR7/8	1	5	1:200

Table 3.9 PAMP properties. Including stock concentrations and recognition receptors.

3.9.1 Cytokine detection assay

Cytokine levels were determined using a Magnetic Luminex® Performance Assay kit (R&D Systems, MN, USA) following the manufacturer's instructions. Analyte-specific antibodies were used, which were pre-coated onto colour-coded microparticles. All microparticles, standards were prepared. 50 µl of microparticle cocktail was added to each well of a 96-well plate. 50 µl of Standard and samples were then all pipetted into wells of the 96-well plate and left to incubate at room temperature on a plate shaker set at 800 RPM. The immobilised antibodies bind the analytes of interest. The plate is then placed on a magnetic platewasher and wells are washed with 100 µl washing buffer. After wash, any unbound substances are removed, and 50 µl of a biotinylated antibody cocktail specific to the analytes of interest is added to ach well. Following another wash, any unbound biotinylated antibody was removed. 50 µl of streptavidin-phycoerythrin conjugate is added to each well and left to incubate a room temperature for 30 minutes on a plate shaker set at 800 RPM, which binds to the biotinylated antibody. After a final wash, microparticles are resuspended in 100 µl of washing buffer and left to shake for 2 minutes at 800 RPM. Measurements are made using a Luminex 100 machine according to the manufacturer's protocol. Lasers in the machine determine the magnitude of the phycoerythrin-derived signal, which is proportional to the amount of the analyte bound.

3.10 *In vitro* drug permeability studies

3.10.1 Drug permeability studies using the HEC-1A model

All transport experiments were undertaken over a 2 hour period (unless stated) at 37°C in HBSS supplemented with 1% HEPES buffer (Sigma-Aldrich, Cambridge,

UK) at pH 7.4 as reported [225]. HBSS was used to prevent drug from binding to albumin found in cell culture media. All solutions were warmed to 37 °C and experiments were performed on a heated orbital shaker set at 50 RPM. Two HBSS based transport solutions were prepared: a donor solution containing drugs generally solubilised in HBSS + 1% HEPES +/- DMSO (0.01-1 %) to final dug concentrations of 0.1-100 µM, depending on the drug being investigated, and a receiver solution containing HBSS + 1% HEPES +/- poloxamer 407 (0.2% w/v), (Sigma-Aldrich, Cambridge, UK). Prior to the initiation of the drug transport experiments TEER was measured. Cell layers were then washed twice with pre-warmed HBSS+1%HEPES transport buffer and equilibrated in the same solution for 30 minutes at 37 °C. In all permeability assays, donor solutions were spiked with approximately 4000 Becquerel (Bq) of either radioactive [^{14}C]mannitol or [^{3}H]mannitol. The experiment was initiated when either 520 µl or 1520 µl of donor solution was added to the donor compartment and either 520 µl or 1520 µl of receiver solution was added to the receiver compartment, subject to the direction of transport being measured. A timer was started as soon as the donor solution was added and 20 µl samples were taken from donor and receiver compartments, termed T=0 (for assessment of initial concentration and background radioactivity, respectively). Transwells® were then placed on an orbital shaker set at 50 RPM. Samples, either 200 µl or 600 µl depending on the receiver compartment, were taken from the receiver compartments at time points T=30, T=60, T=90 and T=120 (to obtain cumulative amount of drug in the receiver side versus time) and added to polyethylene liquid scintillation vials. Samples were taken in triplicate and replaced with equivalent volumes of the receiver solution. After final sampling, TEER was measured to confirm that there was no disruption to the epithelial barrier during the experimental procedure. Radioactive samples were mixed with 4 ml of scintillation fluid (Fisher Scientific, USA) prior to being analysed using a liquid scintillation counter (Beckman Coulter, CA, USA). Additionally, with the use of a scalpel, the semipermeable membranes of the Tanswell® inserts were cut and also placed into scintillation vials for mass balance measurements.

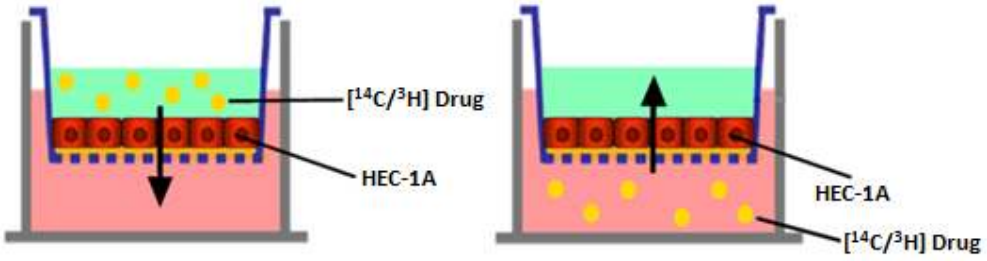

Figure 3.2 Schematic diagram representing the transport of [$^{14}C/^{3}H$]drug from apical-to-basolateral (A-B) and basolateral-to-apical (B-A) directions.

Apparent permeability (P_{app}) was calculated using the following equation:

$$P_{app}\,(cm/s) = (\Delta Q/\Delta t)/(AC_0V)$$

Where $\Delta q/\Delta t$ is the gradient of the (linear) slope of the cumulative amount of drug in the receiver given as disintegrations per minute (DPM) vs time, *A* is the surface area of the Transwell® membrane, C_o denotes the initial loading concentration in the donor chamber at T=0 and *V* is the volume of the initial receiver sample taken at T=0.

3.10.2 Drug permeability studies using the Epivaginal™ model

Upon receipt, EpiVaginal™ tissues were placed in a refrigerator (2-8°C) until assay medium (Mattek Corp, MA, USA) was warmed to 37°C. 900 µl pre-warmed assay medium was added to each well of a Nunc® 6-well plate (MatTek Corp, MA, USA). Under sterile conditions open, sterile forceps were used to remove the inserts containing the tissues from the agarose they were packaged in, making sure the plate was at refrigerator temperature allows smooth removal of the insert from the agarose. Each insert was placed into each well of the 6 well plates and incubated at 37°C 5% CO^2 overnight- allowing for tissue recovery.

On the following day, inserts were transferred to new Nunc® 24-well plates and transport experiments were undertaken at 37°C in HBSS supplemented with 1% HEPES buffer at pH 7.4. All solutions were warmed to 37°C and experiments were performed on a heated orbital shaker set at 50 RPM. Two HBSS based transport solutions were prepared: a donor solution containing drugs generally solubilised in HBSS + 1% HEPES +/- DMSO (0-0.01%) to final dug concentrations of 10 µM, and a receiver solution containing HBSS + 1% HEPES. Cell layers were then washed

twice with pre-warmed HBSS + 1% HEPES transport buffer and equilibrated in the same solution for 30 minutes at 37°C. In all permeability assays, donor solutions were spiked with approximately 4000 Becquerel (Bq) of either radioactive [^{14}C]mannitol or [^{3}H]mannitol. The experiment was initiated when either 270 µl or 320µl of donor solution was added to the donor compartment and either 270 µl or 320 µl of receiver solution was added to the receiver compartment, subject to the direction of transport being measured. A timer was started as soon as the donor solution was added and 20 µl samples were taken from donor and receiver compartments, termed T=0 (for assessment of initial concentration and background radioactivity, respectively). Transwells® were then placed on an orbital shaker set at 50 RPM. Samples, either 100 µl or 120 µl depending on the receiver compartment, were taken from the receiver compartments at time points T=30, T=60, T=90 and T=120 minutes and added to polyethylene liquid scintillation vials. Samples were taken in triplicate and replaced with equivalent volumes of the receiver solution. Radioactive samples were mixed with 4 ml of scintillation fluid prior to being analysed by a liquid scintillation counter. Additionally, with the use of a scalpel, the semipermeable membranes of the Nunc® inserts were cut out and also placed into scintillation vials for mass balance measurements.

3.10.3 Drugs used in this study

3.10.3.1 Radiolabelled Drugs and concentrations

Drug	Isotope location	Stock conc	Conc MBq/ml
DRV	carbonyl-^{14}C	2 mCi in 20 ml	3.7
DPV	pyrimidine-2-^{14}C	2 mCi in 20 ml	3.7
TFV	adenine-8-^{14}C	0.05 mCi in 0.5ml	3.7
Digoxin	[^{3}H(G)]	0.25 mCi in 0.25ml	3.7
D-mannitol	1-^{3}H(N)	1 mCi in 1ml	37
D-mannitol	1-^{14}C(N)	0.25 mCi in 2.5ml	37

Table 3.10 Properties of radioactive drugs. Including isotope location and concentrations.

DRV (carbonyl-^{14}C), 2 mCi in 20ml (Moravek Biochemicals Inc, CA, USA)

DPV (pyrimidine-2-^{14}C) 2 mCi in 20ml (Moravek Biochemicals Inc, CA, USA)

TFV (adenine-8-^{14}C) 50 µCi in 0.5ml (Moravek Biochemicals Inc, CA, USA)

*1 mCi = 37 MBq

Mannitol D-[1-^{3}H(N)] 37 MBq (Perkin-Elmer, MA, USA)

Mannitol D-[1-^{14}C (N)] 37 MBq (Perkin-Elmer, MA, USA)

Digoxin [^{3}H(G)] 9.25 MBq (Perkin-Elmer, MA, USA)

	Vol added in each well (µl)	number of wells	total vol required (µl)	excess prepared (µl)	activity required per well (Bq)	total activity required (Bq)	Stock activity (Bq/ml)	Vol of stock required for experiment (ml)	Vol of stock required for experiment (µl)
Apical									
^{14}C DRV	260	3	780	1000	4000	15384.62	3700000	0.00416	4.16
^{14}C TFV	260	3	780	1000	4000	15384.62	3700000	0.00416	4.16
^{14}C DPV	260	3	780	1000	4000	15384.62	3700000	0.00416	4.16
^{14}C Mannitol	260	3	780	1000	4000	15384.62	37000000	0.00042	0.42
^{3}H Mannitol	260	3	780	1000	4000	15384.62	37000000	0.00042	0.42
^{14}C Digoxin	260	3	780	1000	4000	15384.62	3700000	0.00416	4.16
Basolateral									
^{14}C DRV	760	3	2280	2500	4000	13157.89	3700000	0.00356	3.56
^{14}C TFV	760	3	2280	2500	4000	13157.89	3700000	0.00356	3.56
^{14}C DPV	760	3	2280	2500	4000	13157.89	3700000	0.00356	3.56
^{14}C Mannitol	760	3	2280	2500	4000	13157.89	37000000	0.00036	0.36
^{3}H Mannitol	760	3	2280	2500	4000	13157.89	37000000	0.00036	0.36
^{14}C Digoxin	760	3	2280	2500	4000	13157.89	3700000	0.00356	3.56

Table 3.11 Volumes of radiolabelled drug prepared for each drug for a permeability assay. As each condition was generally undertaken in triplicate, calculations were based on the volumes of 3 wells. A maximum of 2 drugs were used in one experiment and 1 of the 2 drugs was always mannitol.

3.10.3.2 Unlabelled drugs and concentrations

Drugs were weighed on a µg scale and transferred to a bijou. Solubilising solution was added and drug solution was vortexed. TFV (Johnson and Johns, NJ, USA) solubilised freely in HBSS.

DRV and DPV (Gilead Sci, CA, USA), DPV (Selleckchem, Stractech Sci, Suffolk, UK) and Digoxin (Sigma-Aldrich, Cambridge, UK) required pre-warmed (37 °C) solubilising solutions and extended vortex periods prior to becoming completely solubilised. Stock and working concentrations of each of the drugs are shown below:

TFV

- 0.01 gm + 3.48ml HBSS = 10000 µM (Stock)
  → 100 µl + 9900 µl = 100 µM
  → 1000 µl + 9000µl = 10 µM

DPV

- 0.015 gm + 5 ml DMSO = 9000 µM @ 100 % DMSO (Stock)
  → 50µl + 9950µl HBSS = 45 µM @ 0.5 % DMSO
  → 2222µl + 90 µl DMSO + 7690 µl HBSS = 10 µM @ 1 % DMSO

DRV

- 0.02 gm + 0.5ml DMSO = 70000 µM @ 100% DMSO (Stock)
  → 25 µl + 9975 µl HBSS = 175 µM @ 0.25 % DMSO
  → 571 µl + 9429µl HBSS = 10µM @ 0.01% DMSO

- 0.02 gm + 0.5ml DMSO = 70000 µM @ 100% DMSO (Stock)
  → 14.3µl + 9985.7 µl 1X Krebs = 100 µM @ 0.14% DMSO

Digoxin

- 1 gm in 12.8 ml DMSO = 100000µM @ 100% DMSO (Stock)
  →1 0 µl + 9990 µl HBSS = 100 µM @ 0.1% DMSO
  → 1000 µl + 9000 µl = 10 µM @ 0.01% DMSO

3.11 *Ex vivo* drug permeability studies

3.11.1 Rat cervicovaginal tissue preparation

Excised tissue segments were from adult female Wistar rats that had been sacrificed as part of separate studies. Tissue from the genital tract was carefully washed with cold Krebs solution containing NaCl, $NaHCO_3$, $MgSO_4$, KCL, NaH_2PO_4, HEPES, ddH_2O (Sigma-Aldrich, Cambridge, UK) solution and transferred to a beaker with oxygenated (95%O_2/ 5%CO_2) ice cold Kreb's buffer. All segments were cut along their mesenteric border and the muscularis externa was removed using blunt dissection. The stripped cervicovaginal mucosa was mounted in modified Ussing Chambers containing oxygenated 37˚C transport buffer solutions and tissue was allowed to recover for 30 minutes. The effective exposed area of the tissues was 0.2 cm^2.

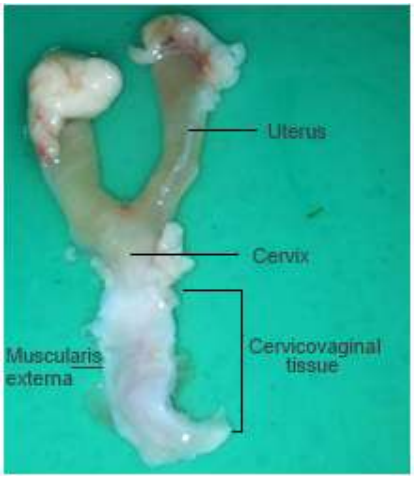

Figure 3.3 Excised rat genital tract. Uterus, cervix, cervicovaginal tissue and muscularis externa are labelled.

2.11.2 Macaque tissue preparation

Excised tissue segments from adult female NHP *M. fascicularis* were used. Excision of vaginal tissue was performed by scientists at the CEA. On receipt, tissue was washed with cold Krebs solution and transferred to a beaker with oxygenated 95% O_2/ 5% CO_2) ice cold Kreb's buffer. All cervicovaginal segments were cut along their mesenteric border and the muscularis externa was removed using blunt dissection. The stripped cervicovaginal mucosa was mounted in modified Ussing Chambers

containing oxygenated 37˚C transport buffer solutions and tissue was allowed to recover for 30 minutes. The effective exposed area of the tissues was 0.2 cm^2.

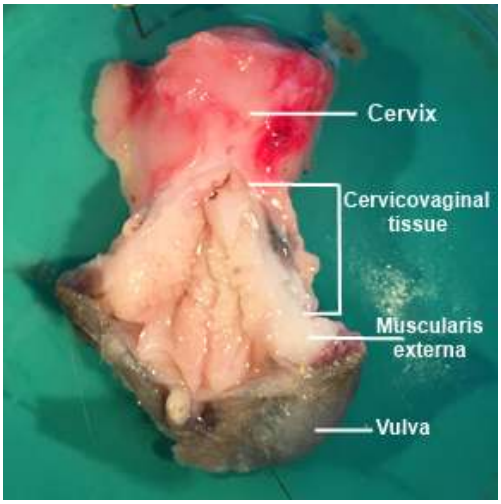

Figure 3.4 Excised macaque cericovaginal tissue. Cervix, cervicovaginal tissue, muscularis externa and vulva are labelled.

3.11.3 Drug permeability studies using animal cervicovaginal tissue

Before an experiment Ussing Chambers (Harvard Apparatus, Cambridge, UK) were assembled. Were possible, the low permeability compound [^{3}H]mannitol was included in every chamber as an integrity marker. The diffusion cells were composed of two glass chambers (apical and basolateral) and separated by the mounted tissue. For mammalian physiological buffers, the gas is carbogen (95% O_2 and 5% CO^2) which oxygenates solutions to high levels was necessary to overcome the lack of haemoglobin delivery by the blood. A flow through system was used to continuously supply tissue via tubing that leads to each half of the chamber. Once the tissue is mounted and relevant tubes are connected, drug test solutions to each chamber half depending on the direction of permeability were ready for the experimental procedure. The entire system was maintained at vaginal temperature of approximately 37°C and was achieved by the continuous circulation of pre-warmed water pumped through a heat block. The P_{app} for all compounds was determined in three independent studies. The tissue was allowed to recover for 30 minutes, bathed bilaterally with 0.35 ml of Krebs at pH 7.4 and continuously gassed (95% CO_2 / 5% $O_{2)}$. Two Krebs based transport solutions were prepared: a donor

solution containing 100μM DRV +/- [^{14}C]DRV solubilised in Krebs + 0.1% DMSO and a receiver solution containing Krebs solution only.

The experiments were initiated by removal of Krebs buffer solution from both sides (donor and receiver chambers). Donor solution containing drug was then applied to the donor side and receiver solution was added to the receiver side. 20 μl samples from both donor and receiver side of each chamber were taken and termed as time zero (T=0), (for assessment of initial concentration and background radioactivity, respectively). At 15 minute intervals over a 1 hour period, 100 μl samples were taken from the receiver side and replaced with fresh receiver solution over a 60 minute period. At the end of the experiment, 100 μl samples were again taken from both the donor and receiver chambers. All samples were collected in labelled scintillation vials, mixed with 4 ml of scintillation fluid and analysed a Beckman Coulter LS6000TA (Beckman Coulter™, Bucks, UK). Additionally, if no radiolabelled drug was used, samples were collected in labelled Eppendorf tubes for drug analysis by liquid chromatography mass spectrometry (LC-MS) carried out at the institute of pharmaceutical sciences (King's College London, UK).

3.12 Liquid scintillation counting

Liquid scintillation counting is an analytical technique which is defined by the incorporation of the radiolabeled analyte into uniform distribution with a liquid chemical medium capable of converting the kinetic energy of nuclear emissions into light energy. Beta particles are emitted in a radioactive decay. To assure efficient transfer of energy between the beta particle and the solution, the solution is a solvent for the sample material. A beta particle will take only a few nanoseconds to dissipate all its kinetic energy. The energy is absorbed by the liquid scintillation counter in 3 forms: heat, ionization and excitation. Some of the beta energy is absorbed by solvent molecules making them excited (not ionized). Energy of the excited solvent is emitted as UV light and the solvent molecule returns to ground state. The excited solvent molecules can transfer energy to each other and to the solute. The solute is a fluor- an excited solvent molecule which passes its energy to a solute molecule disturbing the orbital electron cloud of the solute, raising it to a state of excitation. As the excited orbital electrons of the solute molecule return to the ground state, a radiation results, in this case a photon of UV light. The UV light is absorbed by fluor molecules which emit blue light flashes upon return to ground

state. This is subsequently detected by the scintillation counter and read out as DPM (disintegrations per minute).

3.13 Statistical analysis

Where statistical data is given for analysis of three or more datasets, one-way ANOVA tests were performed and post-hoc comparisons were conducted according to the Tukey method. For datasets comparing two samples, an unpaired two-tailed t-test was performed. All values are represented as means ± SD. Differences were considered statistically significant when $P < 0.05$. Statistical analyses were conducted using the GraphPad Prism 6 software.

>Chapter 4 Optimisation of an *in vitro* model for drug transport studies

4.1 Aim

To optimise an *in vitro* model of the vaginal epithelium for measurement of drug permeability. To develop a model of *in vitro* inflammation and assess effects on drug permeability.

4.2 Introduction

The aim of work described in this chapter was to optimise an *in vitro* model of the vaginal epithelium for measurement of drug permeability. Previous studies have described formation of an *in vitro* barrier epithelium by the human endometrial adenocarcinoma cell line HEC-1A [199, 226-230] and use of this model to measure drug permeability in the apical to basolateral (A-B) direction [136]. However, this model was designed also to investigate HIV transmission through vaginal epithelium using both cell-associated and cell free virus and therefore cells were cultured on membranes with pore sizes (3 μm, 6 μm) that allowed transmigration of cells in the dual chamber Transwell® culture system [222]. In addition, no studies of bi-directional drug transport were reported.

The findings that HEC-1A cells form a barrier epithelium when cultured in the dual chamber system (Figure 4.1) [177, 185-189] provided the basis for the studies described in this chapter. Microbicides against HIV that are based on the reverse transcription inhibitors DPV and TFV or the protease inhibitor DRV target intracellular events in HIV replication. *In vitro* models of barrier epithelium provide a means of investigating factors that influence permeability of such ARVs across the epithelium - an essential requirement for the ARVs to access the sub-mucosal T cells that form the initial targets for infection. Models based on culture of continuous cell lines such as the Caco-2 model of gastrointestinal epithelium [231-233] and the 16HBE14o [234] model of the respiratory epithelium has provided invaluable data on drug transport in other systems. The Caco-2 system is considered as the “gold standard” of *in vitro* models and has been extensively used for high throughput drug screening for drug permeability analysis. Caco-2 cells cultured for approximately 21-

28 days [233, 235] in Transwells® differentiate to form a confluent epithelial cell monolayer consisting of columnar and polarised cells interconnected by tight junctions. As well as developing microvilli on their apical membranes, Caco-2 cells naturally express a variety of drug transporters (i.e. P-gp) and metabolising enzymes. Such characteristics are typical of the human jejunum. In contrast, Calu-3 cells are primarily used for assessing the permeability of nasal/inhaled and pulmonary drug delivery and can be air-liquid interphase cultured or liquid-covered cultured depending on the drug delivery route being tested. After 2-3 weeks in culture these cells form monolayers that express drug transporters and efficiently secrete mucus, typical characteristics of the human lung epithelia [236]. Key requirements for such models is the formation of tight junctions, resulting in both polarisation of the cell and barrier function, and adherence of cells to the semi-permeable membrane of the Transwell® insert. A further desirable property is that the profile of drug transporter expression resembles that of the corresponding human tissue. When cultured in inserts, epithelial cell layers separate two liquid compartments. The polarisation of these cells differentiates the apical (donor) and basolateral (receiver) liquid compartments, which are in direct contact with the respective domain of the cells. The drug concentration, when sampled from the receiver compartment, must be lower than that of the donor compartment drug concentration per time interval. This maintenance is defined as the “sink condition” of the receiver. Additionally, impaired “sink conditions” can be avoided by applying suitable liquid volumes in each of the compartments or by using bio-enhancers to improve hydrophilic drug permeability.

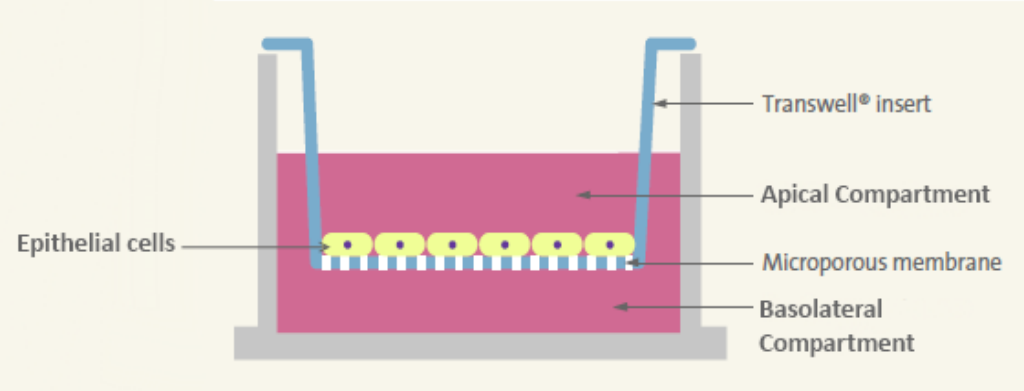

Figure 4.1 A schematic representation of a Transwell® chamber. The microporous membrane of the Transwell® insert is used for culturing epithelial cells suitable for drug

transport studies and separates the well into two compartments (apical and basolateral). Image adapted from [237].

Movement of a paracellular tracer (mannitol) between the two compartments is a result of paracellular diffusion and is a quantitative routine control to assess barrier integrity. The flux of such tracers (expressed as permeability coefficient) indicates the paracellular water flow, as well as the pore size of the tight junctions [238]. Typically, this mode of transport displays a linear cumulative rate of transport as well as symmetry between the rate of transport in the apical-to-basolateral (A-B) and basolateral-to-apical (B-A) direction. Rate of transport can be calculated by the apparent permeability coefficient (P_{app}, unit: cm/s) and is determined from the amount of compound that is transported per time (as described in chapter 3). An additional control to monitor barrier formation and integrity, involves the qualitative measurement of TEER.

4.2.1 Expression of drug transporters in HEC-1A cells

Comparative analyses of drug transporter expression in human vaginal and cervical tissue and in HEC-1A cells have been reported. The mRNA profile of efflux transporters in HEC-1A and human tissue showed reasonable correlation [206]. BCRP was not expressed and expression of P-gp was lower in HEC-1A cells compared with human tissue where expression of both was high. In contrast, MRP3 and MRP4 were highly expressed in HEC-1A cells but at lower levels in human tissue. Expression of uptake transporters showed some overlap but in contrast to human tissue, OCT3, CNT2 and CNT3 were not expressed in HEC-1A cells. Additionally, transporters OAT1-3 have also shown no expression in HEC-1A cells but the less well-characterised OAT4 and OAT6 showed low to moderate expression, respectively [214]. Protein expression of P-gp, BCRP and MRP2 was also undetected in HEC-1A cells when compared to positive expression from vaginal and endocervical tissue of premenopausal women [134]

4.2.2 Tight junctions

Epithelial and endothelial cells form morphologically distinct seals connecting the membranes of adjacent cells. These apically located junctional complexes of the lateral membrane consist of three components: tight junctions, adherens junctions and desmosomes [156] and have been identified throughout the cervicovaginal

epithelium [215]. Tight junctions contribute to the formation of polarised epithelial barriers by forming a paracellular diffusion barrier, or gate, that regulates epithelial permeability, and an intra-membrane diffusion barrier, or fence, which restricts the apical-to-basolateral diffusion of membrane components [216]. These junctions are composed of transmembrane and cytosolic proteins that interact with each other as well as with components of the cytoskeleton. Tight junctions are formed by association of tetra spanning membrane proteins occludin, tricellulin and the claudins as well as the single-pass membrane proteins, the junctional adhesion molecules (JAMs), (Fig. 4.2).

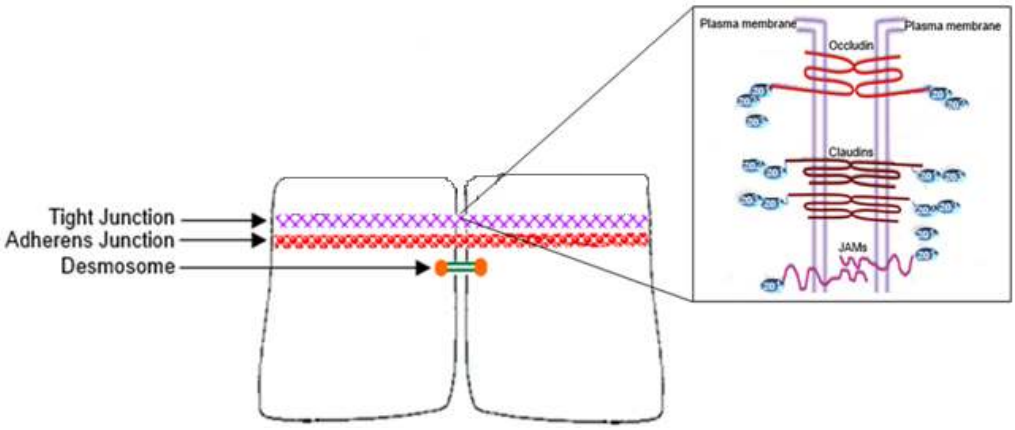

Figure 4.2 Schematic representation of the tight junction, adherens junction and desmosome of between epithelial cells. Magnification of the tight junction protein and its physiological components.

Occludin was the first trans-membrane tight junction protein discovered [239] and its function in the tight junction remains to be fully understood. It is, however, an important structural element to the complex as over expression has shown to increase electrical resistance, phenotypically implying a tight apical-basolateral intra-membrane lipid diffusion barrier [240]. The occludin-related protein tricellulin is involved in tight junction composition and shares a conserved domain with occludin mediating the binding to zona occludens-1 (ZO-1) [241]. It is concentrated at regions where three cells form a contact or at the tricellular tight junction, hence the name tricellulin. Like occludin [242, 243], tricellulin knockdown interferes with tight junction assembly and enhances solute diffusion across cultured epithelial monolayers [244], while tricellulin overexpression enhances barrier function [245]. The claudin composition of a junction determines the ion selectivity of the

paracellular pathway. All claudins (except claudin-12) end in a carboxyl terminal (PSD59-D1gA-ZO-1) PDZ binding motif [246] and interact with several PDZ domains of the tight junction scaffolding proteins. Claudin interaction involves binding with the first three PDZ domains ZO-1, ZO-2 and ZO-3 [246] of the tight junction proteins. Claudin interaction with the other PDZ domain-containing proteins has also been reported, these include MPDZ (MUPP1, Multi PDZ domain protein 1) [247] and Pat J (protein associated with tight junctions) [248], however they remain to be fully investigated. The ZO's appear to be fundamental for tight junction formation, particularly ZO-1 and ZO-2 as these scaffolding proteins are required to create claudin-based junctional strands in the mouse breast epithelial cell line Eph4 [249]. The cytoplasmic C-terminus of occludins also binds to the tight junction associated proteins ZO-1, ZO-2 and ZO-3 via PDZ binding motifs and therefore provides a link between the extracellular domains. Removal of claudin proteins have shown disrupted barrier-specific phenotypes as deletion of claudin-1 in mice compromises the epidermal barrier causing wrinkled skin and is lethal within 1 day of birth due to excessive water loss [239].

The JAMs are a group of proteins that are sub-divided as JAM-A, JAM-B, JAM-C. Of these JAM family members, several studies have implicated JAM-A in the regulation of barrier function and the inflammatory response. This single-pass transmembrane protein is expressed in several cell types but is particularly abundant in epithelial and endothelial cells, where it accumulates at tight junctions. JAM-A has been reported to influence various cellular processes, including regulation of paracellular permeability, cell polarity, cell adhesion, cell migration, angiogenesis, and leukocyte migration [250-254]. JAM-A knockout mice display increased polymorphonuclear leukocyte infiltration increasing mucosal permeability [255] which is consistent with an *in vitro* study that showed that JAM-A is crucial for epithelial cell polarity [250].

Linkage of the cytoplasmic domain of tight junctions to the actin cytoskeleton is mediated by the ZO proteins which bind actin directly and interact with actin binding proteins (reviewed in [246]). Extracellular Ca^{2+} has shown importance in the physiology and maintenance of tight junctions [256-258] . Depletion of Ca^{2+} in cell cultures resulting in a decrease in TEER that is reversible on replacement of Ca^{2+} has been used as an indication of tight junction formation [256, 257, 259]. The

mechanisms of tight junction disassembly are complex and involve differential inhibition of protein kinase c isoforms [258] as well as actin remodelling with clathrin-mediated endocytosis of junctional proteins [260] and a variety of intracellular signalling pathways [261].

The tight junction is composed of at least two functionally distinct pathways, this includes a high-capacity, charge selective pore pathway that mediates the movement of small ions and uncharged molecules, and a low-capacity leak pathway that allows the free movement of larger ions and macromolecules, regardless of charge. TEER measures the flux of all ions across confluent monolayers (measured with AC current), and is indicative of transepithelial ionic permeability as electrical currents are carried by ions in aqueous solution using Ohms law to calculate the resistance to current flow [262]. The most common ions in physiological solutions are Na^+ and Cl^- which carry the electrical currents; TEER therefore reflects tight junction permeability depending on the conductance of these ions. If ion conductance across the tight junction is far greater than across the apical and basolateral domains, then this is indicated by low TEER readings and signifies 'leaky' epithelia. If ion conductance across the tight junction is far less than across the apical and basolateral domains then this is indicated by higher TEER readings and signifies 'tight' epithelia [263].

4.2.3 Cell attachment to dual chamber porous membrane

Physiologically, the basolateral surface of the epithelium is associated with an extracellular matrix protein complex termed the basement membrane as reviewed in [264]. Major components of the basement membrane include type IV collagen and laminin, that self-assemble to form a polymeric scaffold, as well as entactin which interacts with both components. To model extracellular matrix and promote cell attachment, several studies including those using HEC-1A cells have reported coating of the chamber surface with laminin [222, 229, 230] or Matrigel® [265], a reconstituted murine basement membrane preparation that is approximately 60% laminin, 30% collagen IV, and 8% entactin [265-267]. While this may be beneficial for some cell lines, others such as the intestinal cell lines Caco-2/15, HT29 and T84 synthesise and secrete their own extracellular basement matrix [268-270].

In the study described in this chapter, a variety of conditions including nature of the support membrane, seeding cell density, length of culture and requirement for coating with extracellular matrix proteins were investigated for optimising the barrier properties of HEC-1A cells in dual chamber cultures. Formation of tight junctions was monitored by measurement of TEER and the permeability of the paracellular marker mannitol as well as by immunofluorescent staining. In addition, expression of selected drug transporters at the protein level was investigated by Western blotting.

4.3 Results

4.3.1 Determination of optimal culture protocols

Optimal conditions for establishing a permeability barrier in HEC-1A cell cultures using the Transwell® dual chamber system were investigated in a step by step process by comparison with the procedures published previously [222, 230]. Barrier properties were estimated by measurement of TEER.

4.3.1.1 Effect of pore size

In previous studies where HEC-1A model epithelial barriers were used to model HIV transmission by cell-free and cell-associated virus, a pore size of 3.0 μm in the semi-permeable membrane of the Transwell® insert was used to allow transmigration of cells [222]. Since transmigration is not required in drug permeability assays, the barrier properties of HEC-1A cells cultured on membranes containing pore sizes of 3.0 μm or 0.4 μm were compared using the Transwell® culture system. $1x10^5$ cells were seeded in Transwell® inserts and cultured for 10 days. TEER values were measured in the cultures daily. As shown in Figure 4.3, TEER values reached a plateau on day 6 of culture in inserts containing 0.4 μm pore size membranes and day 8 for inserts containing the 3.0 μm pore size membranes. No significant difference ($P \geq 0.05$, two-tailed t test) was evident in the maximal TEER values of 90±20 $\Omega x cm^2$ (0.4 μm pore size) and 100±20 $\Omega x cm^2$ (3.0 μm pore size).

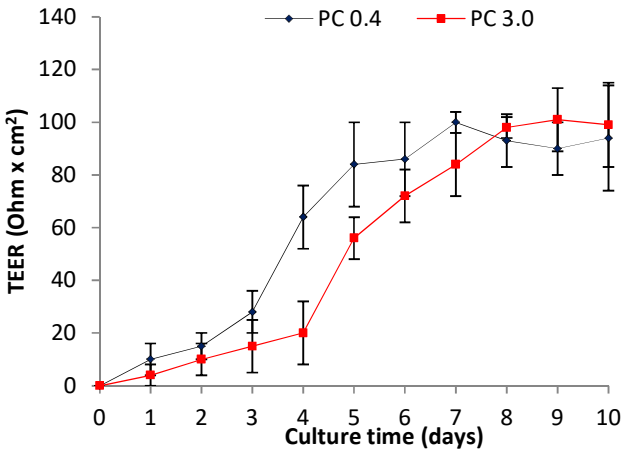

Figure 4.3 Effect of pore size on TEER. The time-course of increasing TEER of HEC-1A cells cultured in inserts with 3.0 µm and 0.4 µm filter pore sizes is shown. TEER values were measured daily over 10 days and corrected by subtracting the blank value (115 Ω) obtained from inserts containing culture media only and expressed as ohms Ω×cm^2. Cells were seeded at a density of 1x10^5/1.12cm^2 in each Transwell® insert. Data represent mean ± S.D., n = 2 (6 technical repeats).

4.3.1.2 Effect of seeding cell density

The effect of seeding the Transwell® inserts at cell densities/insert surface area (1.12cm^2) of 1x10^5, 2x10^5 and 4x10^5 on development of TEER was investigated over the period of culture. For these experiments, inserts with the larger pore size were also included. As shown in Figure 4.4, in the inserts with the 0.4 µm pore size membrane, the size of the seeding density did not affect the maximum TEER value but at higher seeding density the maximum value was reached more quickly.

A

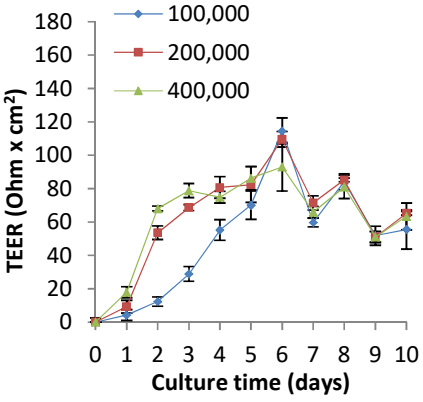

B

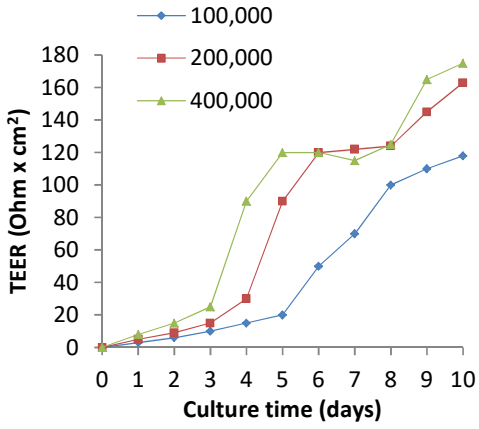

Figure 4.4 Effect of seeding cell density on TEER. The time-courses are shown of TEER increase in HEC-1A cell cultures in inserts containing 0.4 µm **(A)** and 3.0 µm **(B)** membrane pore sizes at three different seeding densities. Data represent mean ± S.D., n = 2 (6 technical repeats).

For the inserts containing 3.0 µm pore size membranes, TEER increased with cell density. At the higher densities, values between days 4 and 7 plateaued but then appeared to increase. For the lower densities, TEER values increased more slowly beginning to plateau between days 8 to 10. In these Transwells®, partial passage or migration of cells through the larger pores may contribute to the apparent increase in TEER following the initial plateau. The inserts containing 3.0 µm pore size membranes were not considered further for culture of a HEC-1A cell-based model epithelium for drug permeability studies.

4.3.1.3 Comparison of Polycarbonate (PC) and Polyester (PE) Semi-Permeable Membranes

Transwell® inserts containing a polyester (PE) supporting semi-permeable membranes have the advantage of being optically transparent compared with the translucent polycarbonate (PC) membranes used in the experiments described above. Cells cultured in PE Transwells® can therefore be visualised directly by microscopy.

Barrier properties of HEC-1A cell cultures on both surfaces were compared as before by measuring TEER development over time. For these experiments, inserts were seeded with $2x10^5$ cells/1.12cm^2 each. As shown in Figure 4.5, TEER values for the cultures in PE Transwells® were significantly higher ($P < 0.05$, ANOVA) than those in PC Transwells® with maximum values of 228±20 Ωxcm^2 and 91 Ωxcm^2 ($p \leq 0.05$, two-tailed t test), respectively. As before, blank values (TEER for membrane alone) were subtracted. Thus PE semi-permeable membranes may provide an improved surface for adherence of HEC-1A cells and development of a permeability barrier.

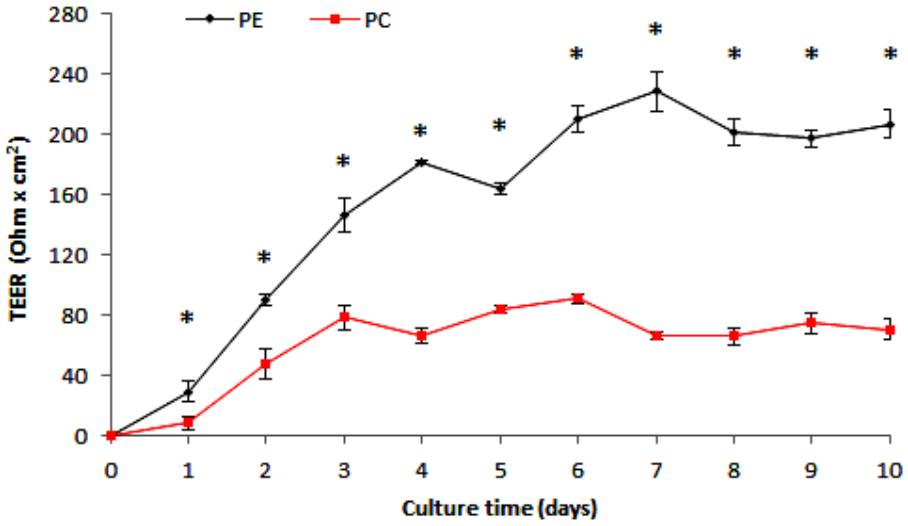

Figure 4.5 Effect of chemical nature of semi-permeable membrane. The time-course of increasing TEER in HEC-1A cells cultures on PC and PE Transwells® (0.4 µm pore size) is shown. Cells were seeded at a density of $2x10^5$/1.12 cm^2 on each Transwell®. (*, $P < 0.05$). Data represent mean ± S.D., n = 2 (6 technical repeats).

4.3.1.4 Effect of coating Transwell® insert membrane with extracellular matrix proteins

As described above, prior coating of the Transwell® insert membrane with extracellular matrix proteins that form the basal membrane may improve adherence and barrier formation by some cell types. Individual Transwell® insert membranes (both PE and PC) were coated with human or mouse laminin by applying 0.25ml of solutions at different concentration and left to air-dry overnight in a laminar flow hood. In these experiments, PC inserts were seeded with $2x10^5$ cells. As shown in Figure 4.6A and Figure 4.6B, coating with the higher concentrations of (5 µg/cm^2 or 10 µg/cm^2) of human or mouse laminin resulted in small but significant ($P \leq 0.05$, ANOVA) increases in the maximum TEER value. In PC Transwell® cultures increased TEER readings of 110-120 Ωxcm^2 were observed compared with 70-80 Ωxcm^2 in cultures with no coating. Coating of PE Transwells® with mouse or human laminin at 5µg/cm^2 also resulted in a minor increase in the plateau TEER value (Figure 4.6C).

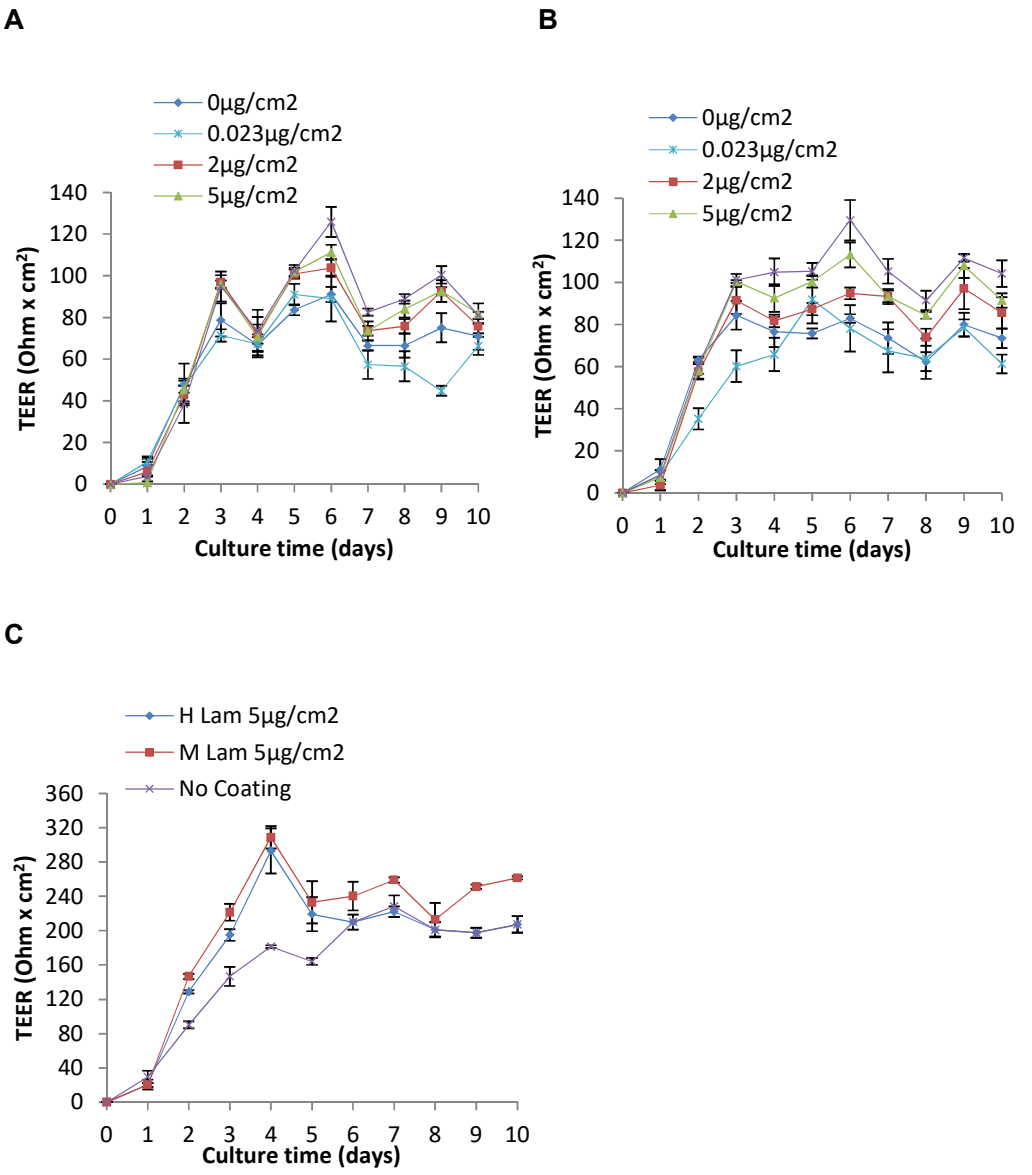

Figure 4.6 Time-dependent development of TEER by HEC-1A cells cultured in Transwells® coated with Human or Mouse laminin. (A) 2x10^5 HEC-1A cells cultured on PC insert membranes coated with varying concentrations of human laminin. **(B)** 2x10^5 HEC-1A cells cultured on PC insert membranes coated with varying concentrations of mouse laminin. **(C)** 2x10^5 HEC-1A cells cultured on PE membranes inserts coated with either mouse or human laminin at a concentration of 5 µg/ml. Uncoated Transwells® were used as a control. Data represent mean ± S.D., n = 2 (6 technical repeats).

The effect of coating with Matrigel® was investigated in PE Transwells® only as shown in Figure 4.7. There was no difference in the plateau TEER values between uncoated membranes of the Transwell® inserts and any of the Matrigel® coated membranes of the Transwell® inserts.

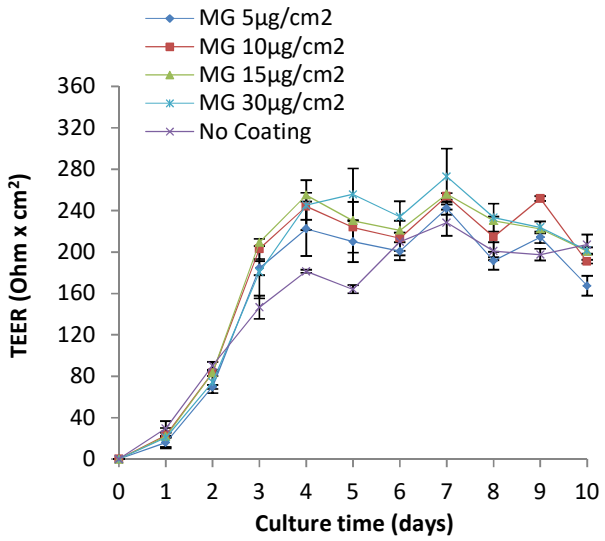

Figure 4.7 Time-dependent development of TEER by HEC-1A cells cultured in Transwells® coated with Matrigel®. $2x10^5$ HEC-1A cells were cultured on PE inserts coated with varying concentrations of Matrigel®. Uncoated inserts were used as a control. Data represent mean ± S.D., n = 2 (6 technical repeats).

Overall, these results indicate that optimum conditions for culture of HEC-1A cells in the dual chamber system to produce a barrier epithelium for drug transport assays is to seed 0.4 µm PE Transwell® with $2x10^5$ cells and to culture for 6-10 days. The effect of coating with either laminin or Matrigel® is relatively minor.

4.3.1.5 Extended assessment of barrier properties of HEC-1A culture over 21 days

The time to reach plateau values of TEER in HEC-1A cultures is considerably shorter than that required for some other cell lines, notably the human colon-derived cell line Caco-2 that is approved by the FDA as a model for measuring drug transport [233, 271]. To confirm the time frame of when HEC-1A cell layers are at their most stable in regards to barrier integrity, HEC-1A cells were cultured in Transwells® over a 21 day period. Barrier properties were assessed by both; measurement of TEER and by measurement of permeability of radiolabelled [^{14}C]mannitol which is used a bi-directional marker for paracellular transport.

As shown in Figure 4.8 TEER values increased to a maximum value of 250 Ωxcm^2 while P_{app} values decreased to a minimum of $1.50x10^{-6}$ cm/s on day 6. TEER values remained high and P_{app} values remained low until day 10 after which TEER declined

and P_{app} increased more rapidly. These data confirm the window between days 6 and 10 of culture as optimum for drug transport assays. Paracellular [^{14}C]mannitol fluxes across the HEC-1A cells displayed bi-directional permeation as calculated absorptive A-B permeability and secretory B-A. Maximum TEER values (in excess of 190 Ωxcm^2) were achieved between days 6 and 10 by cells seeded at 2x10^5 cells per Transwell®, after which the TEER value decreased from day 10 onwards. Measurement of bi-directional P_{app} of [^{14}C]mannitol through cells cultured under the optimised culture conditions indicated that mannitol permeability declined with time in culture as the cell layers developed a concomitant increase in TEER (Figure 4.8). From day 6 the bi-directional P_{app} of [^{14}C]mannitol was reduced to 1-3x10^{-6} cm/s and remained in this region until day 10.

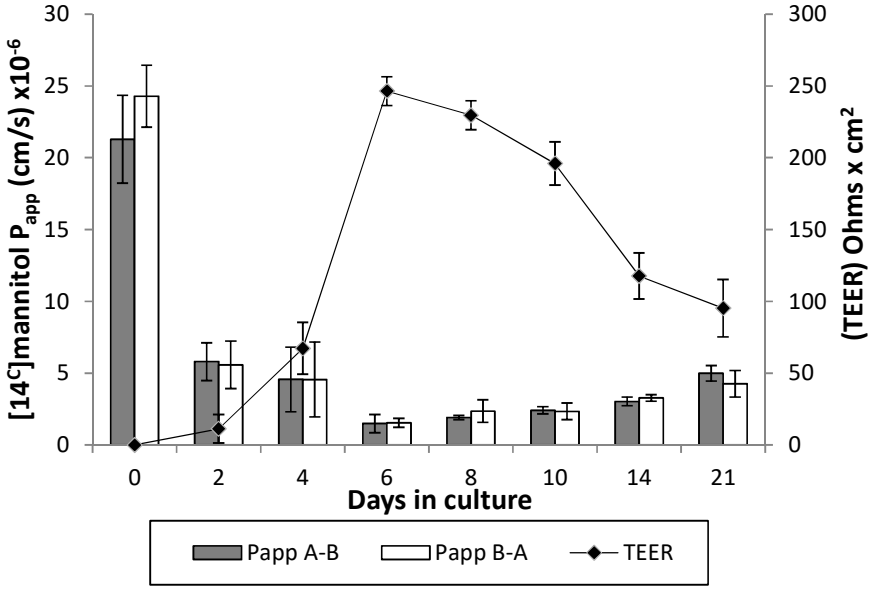

Figure 4.8 Stability of HEC-1A model barrier epithelium over time. 2×10^5 HEC-1A cells were seeded and cultured on uncoated 0.4 µm PE transwells over a 21 day period. Data represent mean ± S.D., n = 3-6 (9-18 technical repeats).

4.3.2 Investigation of tight junction formation

Formation of tight junctions by HEC-1A cells was investigated by measuring the effect of calcium depletion on TEER values in the Transwell® system and by immunofluorescent staining of confluent cells cultured on glass slides.

4.3.2.1 Calcium depletion

The Ca^{2+} chelator EDTA disrupts tight junctions [256] by a process that modulates activity of protein kinase c family members and involves actin remodelling with clathrin-mediated endocytosis of junctional proteins [258, 260]. The effect is reversible and tight junctions reform when re-exposed to a solution containing Ca^{2+} [256]. The effect of EDTA on Transwell® cultures was investigated by measurement of TEER during and after 90 minutes exposure to cell culture medium containing 5 mM EDTA. Following the addition of 5 mM EDTA TEER values decreased by 45% at 90 minutes (Fig. 4.9). Cell culture medium containing EDTA was removed and replaced with EDTA -free cell culture medium. After 2 hours TEER values were 82% of pre-exposure levels and by 24 hours culture in EDTA-free media, TEER values returned to pre-exposure levels. In control cells maintained in EDTA-free cell culture media there was no decrease in TEER.

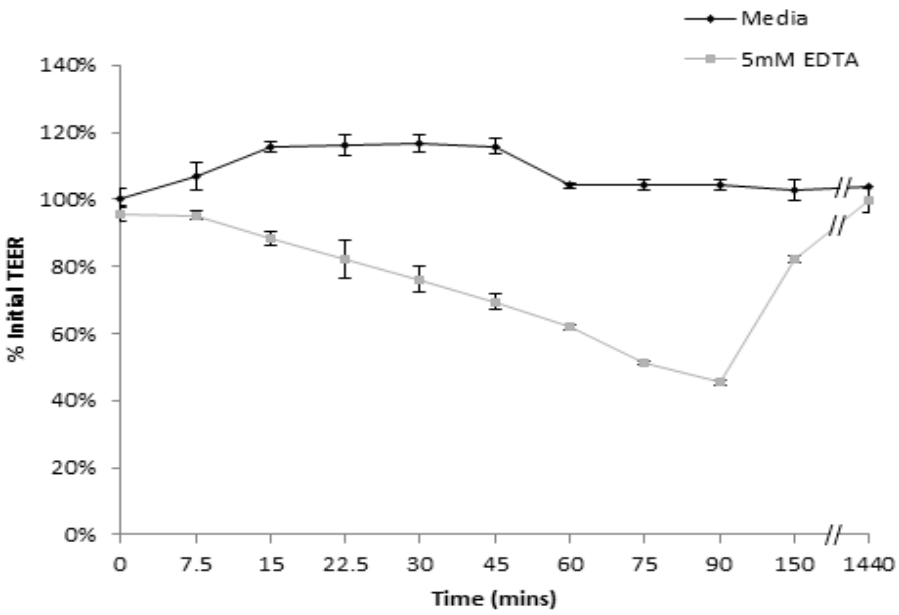

Figure 4.9 Disruption of tight junction functions by EDTA. HEC-1A cells were exposed to 5 mM EDTA diluted in normal cell culture media. HEC-1A cells were cultured on 0.4 µm PE Transwells® at a seeding density of $2x10^5$. TEER measurements gradually decreased over a 90 minute period when exposed to the Ca^{2+} chelator EDTA. TEER values returned to pre-exposure levels on re-incubation in EDTA-free cell culture medium. Data represent mean ± S.D. from one experiment. n = 2 (6 technical repeats).

4.3.2.2 Immunofluorescent analyses of tight junctions in HEC-1A cultures

To further investigate the formation of tight junctions, HEC-1A cells were cultured on glass slides and stained for the cytoplasmic adaptor protein ZO-1 using an FITC-conjugated anti-ZO-1 monoclonal antibody which was visualised by fluorescence microscopy. Intense bands of fluorescence surrounding the periphery appeared as a series of apparent fusions or “kissing points” between HEC-1A cells confirming the expression and localisation of ZO-1 (Fig. 4.10, panel 2B). In contrast, no fluorescence was detected in cell layers exposed to the isotype-matched control anti-gp41 monoclonal antibody produced no fluorescence (Fig. 4.10, panel 1B).

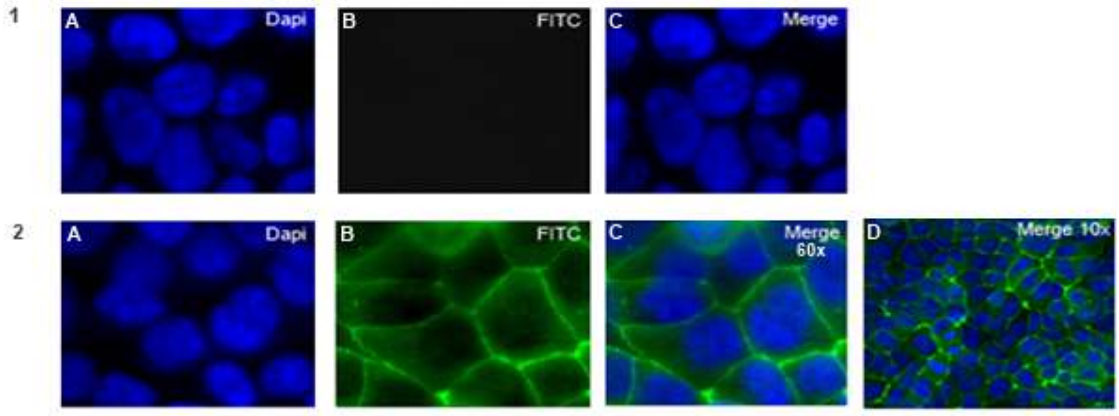

Figure 4.10 Immunofluorescence staining of ZO-1 expression in HEC-1A cells five days after seeding on small glass culture slides. ZO-1 expression was visualised using a mouse IgG1 FITC-conjugated monoclonal antibody to the ZO-1 tight junction protein (green), panel **(2B)**. In contrast no ZO-1 expression was visualised when using a control mouse IgG1 anti-gp41 monoclonal antibody, panel **(1B)**. In both cases cell nuclei were stained with Dapi (blue), panels **(1A)** and **(2A)**. A merge image was produced of cell nuclei and tight junction staining at 10X and 60X magnifications, panels **(2C)** and **(2D)**.

Tight junction formation was also determined in cultures of HEC-1A cells on the transparent membrane of a PE Transwell®. In agreement with results from cells cultured on glass slides, intense bands of fluorescence were detected surrounding the periphery of the cells (Figure 4.11A). Confocal microscopy also indicated that the confluent barrier, was not formed by a simple monolayer but that several multi-layered ‘cell clumps’ were formed (Figure 4.11A). The Z-stack image of the PE Transwell® (Figure 4.11B) confirmed that HEC-1A cells formed an irregular 1-4 cell thick multilayer. This multi-layered structure is in agreement with previously reported

imaging of HEC-1A on Transwells® [222]. Green fluorescence ZO-1 staining can also be observed at areas of cell to cell contact.

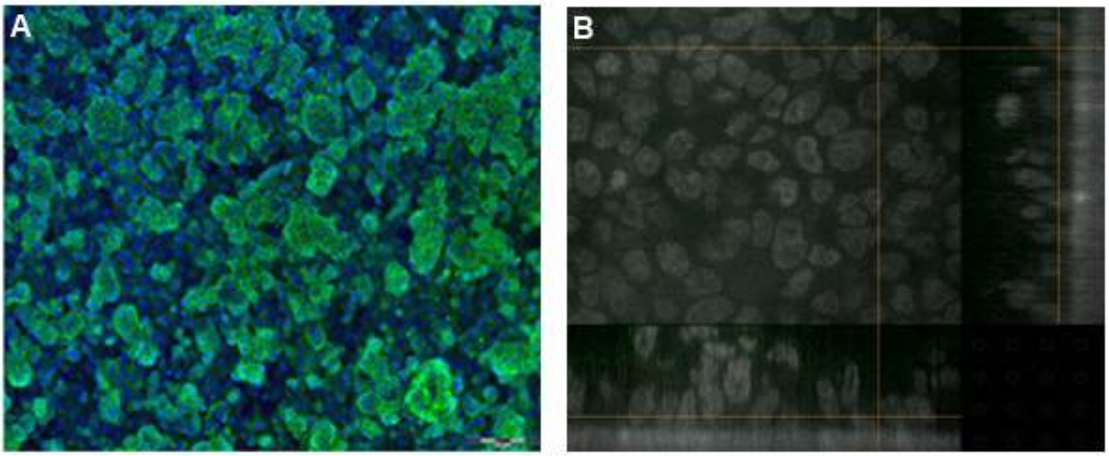

Figure 4.11 Confocal microscopy of HEC-1A cell layers cultured for 7 days on PE Transwells®. (A) HEC-1 cells exhibit areas of clump-like formations as they grow on top of each other. ZO-1 expression was visualised using a mouse IgG1 FITC-conjugated monoclonal antibody to the ZO-1 tight junction protein (green). Cell nuclei were stained with Dapi (blue). **(B)** Z-stack image produced a sliced view of HEC-1A cells attached to the PE transwell. Cell multilayers ranged from a 1-4 cell thickness, and maintained tight junction formation (green) at cell to cell contact.

4.3.3 Expression of drug transporters in HEC-1A cells

Expression of drug transporters in HEC-1A cells lines and in human cervico-vaginal tissues has been investigated by quantitative analyses of mRNA using PCR arrays [206]. Efflux transporters, which affect the uptake of ARVs including DRV and TFV, including MRP1 (ABCC1), MRP3 (ABCC3), MRP4 (ABCC4) and MRP5 (ABCC5) were reported to be highly expressed in HEC-1A cells while P-gp (ABCB1) and MRP2 (ABCC2) showed lower expression. Some differences were noted with expression of efflux transporters in vaginal tissue where P-gp, MRP1 and MRP5 were highly expressed while no expression of MRP2, MRP3 or MRP4 was evident. Uptake transporters including organic anion transporters and nucleotide transporters that may also influence ARV uptake were also identified. To investigate the correlation between these findings and protein expression of transporters, lysates of HEC-1A cells were resolved by SDS-PAGE and transferred to nitrocellulose membranes for Western blot analyses of specific transporters (Figure 4.12). In parallel, human vaginal tissue lysates were prepared and also analysed by

Western blotting (Figure 4.13). Lysates were also prepared from the well characterised human colon cell line Caco-2 and used as controls for expression of some transporters.

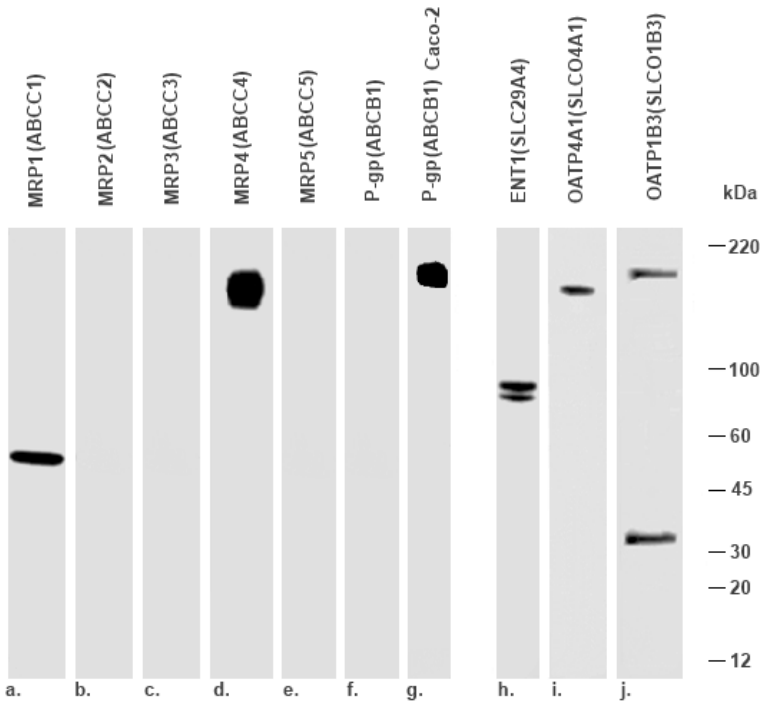

Figure 4.12 Expression of ABC and SLC transporters in HEC-1A cells and Caco-2 cells. Cell lysates were prepared, samples (40 µg total protein in each well) were loaded and separated by SDS-PAGE. Proteins were transferred electrophoretically to nitrocellulose membranes and probed with specific antibodies to individual drug transporters. Lane's **a-f** and **h-j**: Western blotting of HEC-1A lysates for ABC and SLC transporter expression respectively. Lanel **g**: Western blotting of Caco-2 lysate as a control.

Probing blotted lysates with anti-MRP4 antibody showed a diffuse band corresponding to the expected molecular weight of 159kDa (Figure 4.12, lane d). MRP4 has 7 sites for N-linked glycosylation and the diffuse nature of the band may reflect the presence of differentially glycosylated isoforms. Expression of MRP1 (Figure 4.12, lane a) was indicated by a single band of approximate molecular weight 55 kDa, much lower than the expected value of approximately 172 kDa, and assumed to represent a product of proteolysis. No bands were observed on probing with antibodies recognising MRP2, MRP3 or P-gp (Figure 4.12, lanes b, c and f) consistent with lack of expression of these transporters. Additionally, MRP5 was undetected at protein level (Figure 4.12, lane e) but has reported to show relatively high expression at mRNA level [206]. Expression of the uptake transporters

OATP1B3 (SLCO1B3) and OATP4A1 (SLC4OA1) was indicated by bands albeit of higher molecular weight than expected value of 77 kDa for each (Figure 4.12, lanes i and j). Bands of higher molecular weight (approximately 200 kDa) may represent oligomers formed by association of the extensive hydrophobic regions in the multi-membrane spanning molecules that are not disrupted by heating in SDS prior to electrophoresis. In contrast, the additional band of lower molecular weight observed for OATP1B3 may be a proteolytic product. Similarly the bands evident on probing with antibody against ENT1 (SLC29A4), (Figure 4.12, lane h) are considerably higher than the expected value of 55 kDa and likely to be oligomers. The doublet may be the result of proteolysis or differential glycosylation or both. These blots were repeated 2-3 times and similar patterns of bands were observed on each occasion. For each experiment, control blots where the first antibody was omitted, no bands were visible.

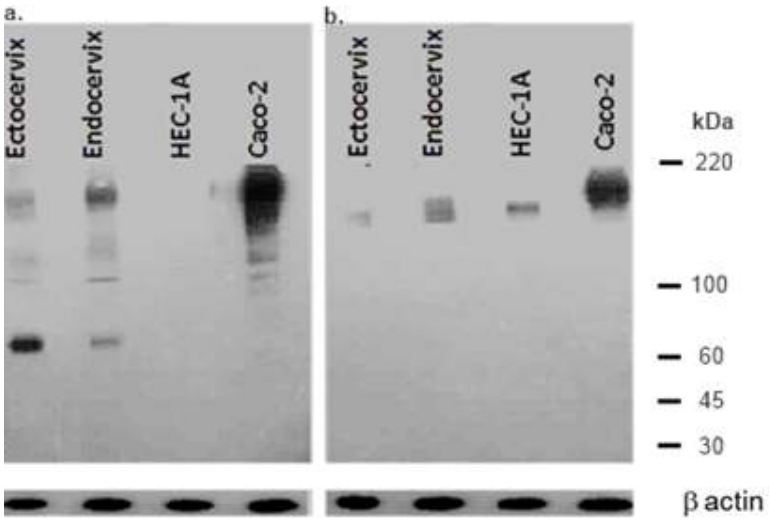

Figure 4.13 Expression of P-gp and MRP4 transporters in human endocervix and ectocervix tissue, HEC-1A cells and Caco-2 cells. Tissue and cell lysates were prepared, samples (40 ug total protein in each well) were loaded and separated by SDS-PAGE. Proteins were transferred electrophoretically to nitrocellulose membranes and probed with specific antibodies to individual drug transporters. Panel **a**: Western blotting of tissue and cell lysates for P-gp expression. Panel **b**: Western blotting of tissue and cell lysates for MRP4 expression.

Blotted ectocervical and endocervical tissue lysates probed with anti-P-gp antibody showed bands corresponding to a molecular weight of approximately 141 kDa (Figure 4.13, Panel a), also with some diffuse bands. Expression of MRP4 was also detected in these tissue lysates (Figure 4.13, panel b) and was indicated by bands

presenting expected molecular weights of approximately 159 kDa. HEC-1A and Caco-2 cell lysates were used as controls, additionally the housekeeping gene anti-β actin was used as a protein concentration loading control and produced bands at 42kDa (Figure 4.13).

4.3.4 Modelling of inflammation

In many cases, particularly when users of topical microbicides suffer from bacterial vaginosis or sexually transmitted diseases, topical microbicides may be administered to inflamed genital mucosae. To develop an *in vitro* model of vaginal inflammation, HEC-1A cells were screened against a panel of 8 PAMPs that stimulate different TLRs to identify those that most potently stimulated production of pro-inflammatory cytokines. Cytokine production was measured by Multiplex bead based immunoassay. Consistent with reports that TLR3 is expressed by this cell line, the TLR3 agonist Poly I:C was the most potent stimulator of TNF-α, GM-CSF, IL-1α, IL-6 and IL-8 (Figure 4.14).

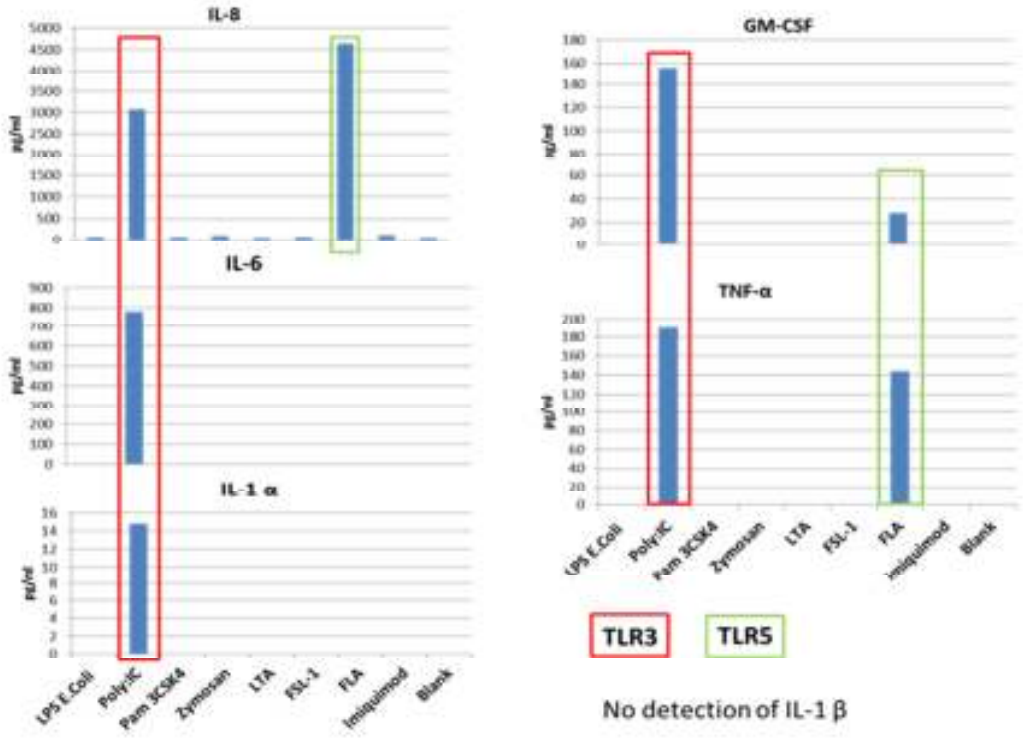

Figure 4.14 PAMP stimulation of pro-inflammatory cytokines in HEC-1A cells. Cultures of HEC-1A cells were stimulated with each PAMP at a single concentration (50 µg/ml) and

production of selected cytokines was determined by Multiplex bead immunoassay. n=1 (2 technical repeats).

Dose response analyses indicated that Poly I:C stimulation was most potent at a concentration of 25 µg/ml (Figure 4.15). Poly I:C stimulation at 25 µg/ml produced the highest concentrations for all cytokines apart from IL-6, where 50 µg/ml marginally produced the highest concentration. Based on the effects on the stimulation of the other cytokines as well as the effect on IL-6, 25 µg/ml was selected as the final dose concentration for the permeability studies (discussed in chapter 5).

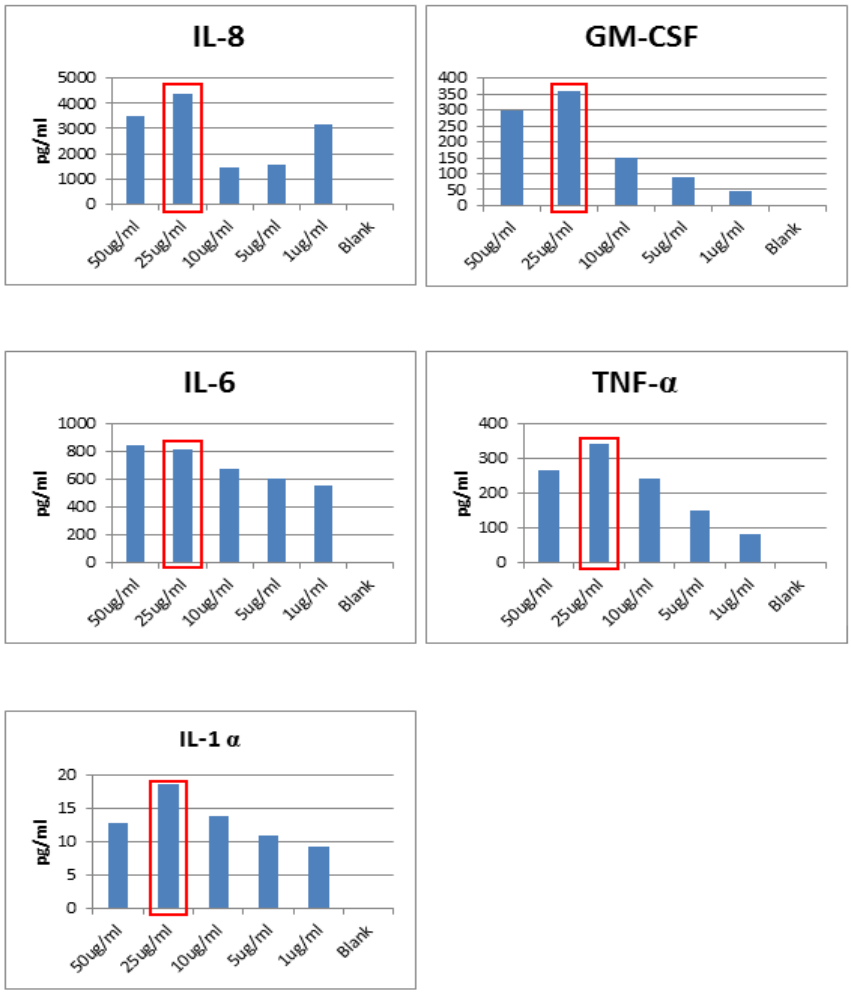

Figure 4.15 Dose-response of pro-inflammatory cytokines in HEC-1A cells with different concentrations of Poly I:C. Cultures of HEC-1A cells were stimulated with different concentrations of Poly I:C in the ranges of 0-50 µg/ml and production of selected

cytokines was determined by Multiplex bead immunoassay. The dose that stimulated the highest concentrations of cytokines was selected the final dose concentration. n=1 (2 technical repeats).

4.4 Discussion

The results presented above confirm findings reported previously [222] that HEC-1A cells form a permeability barrier when cultured in the dual chamber system. Barrier properties of this model epithelium were demonstrated by measurement of TEER and by restricted permeability of mannitol, a low molecular weight polar compound that is excluded from the cell and penetrates by the paracellular route. In repeated experiments, TEER reached a maximum value around day 6 of culture and remained at that level until around day 10. Consistent with these findings, permeability of mannitol reached a minimum and remained low within the same timeframe. These conditions provide a convenient window for drug permeability assays. The maximum TEER values of HEC-1A cultures were approximately 10-fold lower than those of Caco-2 cells cultured in parallel and reported previously, although for the latter, a longer period of culture (21-28 days) is required to reach maximum TEER [233]. These differences may reflect different physiological requirements for the corresponding epithelia. Caco-2 TEER readings of 1500-2000 Ωxcm^2 and P_{app} values for mannitol of $1\text{-}2\times10^{-7}$ cm/s [233] reflect a 'tight' barrier formation. In contrast, HEC-1A TEER readings of 150-250 Ωxcm^2 and P_{app} values for mannitol of $1\text{-}2x10^{-6}$ cm/s reflect an 'intermediate' barrier. Tight epithelia have a deep complex network of junctional strands, while 'leaky' epithelia have shallower junctions composed of fewer junctional strands. Epithelia with 'intermediate' permeability generally have junctional strands with intermediate or variable morphology. The 10 fold increase in TEER between Caco-2 and HEC-1A cells is proportional to the 10 fold difference in mannitol permeability.

Increases in TEER readings over time provided evidence of tight junction and barrier formation. Nonetheless, to confirm tight junction formation, abundant expression of the tight junction protein ZO-1 at contact regions of cells cultured on glass slides or in PE Transwells® was demonstrated by immunofluorescence. Confocal microscopy also indicated that HEC-1A cells in culture formed an irregular multilayer possibly more reflective of the multi-layered epithelium of the vaginal and ectocervix surfaces of the FGT. The abrupt decrease in TEER following removal of Ca^{2+} from HEC-1A cultures as well as the recovery in TEER after replacement of

Ca^{2+} provided further evidence for formation of tight junctions. Moreover, scanning electron microscopy (SEM) shows apical and basolateral polarised phenotype displayed by HEC-1A [272].

Topical microbicides may be administered under conditions of vaginal inflammation that result from conditions such as bacterial vaginosis or sexually transmitted diseases (STDs). Pro-inflammatory cytokines have been shown to increase epithelial permeability in a variety of systems by reducing tight junction activity (reviewed in [273]). Mechanisms of tight junction inhibition include downregulation and relocalisation of tight junction proteins. In this chapter, the potential for modelling inflammation was investigated by stimulation of HEC-1A cells with ligands for TLR-3 and TLR-5. Induction of TNF-α and IL-6, as reported here, reduce tight junction activity by downregulation and relocalisation of ZO-1, respectively [274]. Levels of IL-8 were higher than those reported previously to be associated with occludin redistribution and corresponding tight junction inhibition [275].

Expression of selected drug transporters was investigated in HEC-1A cells and in human endocervix and ectocervix tissue by Western blotting. Expression of 3 uptake transporters (ENT1, SLCO1B3, SLCO4A1) and two efflux drug transporters (MRP1, MRP4) was demonstrated in HEC-1A cells. MRP4 and P-gp expression was detected in human ectocevrix and endocervix tissue. ENT1, MRP1 and MRP4 protein expression validates our findings with recently published HEC-1A mRNA expression data for these drug transporters. The ARV drugs Atazunauvir, Ritonavir, Lopinavir, Saquinavir and Emtricitabine have been identified as substrates for MRP1 and TFV and Zidovudine are substrates for MRP4 [138]. No expression of P-gp, MRP2, MRP3 or MRP5 was detected by Western blotting. These findings were not consistent with quantitative analyses of mRNA encoding these transporters [148]. Lack of correlation between mRNA concentrations and protein expression may be due to several factors such as instability and turnover of mRNA or because levels of endogenous proteins were too low to be detected by Western blotting. Patterns of drug transporter expression vary along the FGT [151] and the endometrial epithelium-derived HEC-1A cell line may not reflect the pattern of expression of some transporters in vaginal or cervical epithelia. Expression of specific transporters by transfection of HEC-1A cells to improve the physiological relevance is investigated in Chapter 5 of this thesis.

The finding that pre-coating with either laminin or Matrigel® had little effect on barrier formation in HEC-1A cultures as determined by measurement of TEER has also been reported in other models [276, 277] and may reflect intrinsic production of extracellular matrix proteins [268]. Direct culture of HEC-1A cells on PE membranes with no addition of such proteins may provide a more standardised system to measure drug transport.

The findings reported here that, HEC-1A cells in dual chamber cultures consistently form tight junctions to provide a barrier epithelium in a relatively short time (compared with the Caco-2 model), provide a rationale for its use as a model for bi-directional drug transport studies. The ability to induce secretion of pro-inflammatory cytokines by TLR ligands and the pattern of transporter expression that approximates to that of the FGT further support the physiological relevance of this model.

4.4.1 Limitations

Interpretation of data from western blotting analyses of drug transporter expression was limited by the lack of positive controls. While the presence of bands in HEC-1A lysates probed with specific anti-drug transporter antibodies together with data from quantitative mRNA analyses is indicative of expression, absence of bands does not exclude expression. For P-gp, Caco-2 cell lysates provided a positive control and the lack of detectable protein in the HEC-1A lysate together with the lack of associated transporter function (described in Chapter 5) suggests strongly that P-gp is not expressed at significant levels in HEC-1A cells. Cells transfected with MRP2, MRP3 or MRP5 and lysates or membrane preparations are commercially available and would be appropriate controls for this study.

The PAMP stimulation assays undertaken in this chapter provided preliminary data. While pro-inflammatory cytokines by TLR ligands were activated, further biological replicates would need to be completed to confirm the reliability of this particular dataset. Levels of cytokines that were induced in these studies, with the exception of IL-8 and IL-6, were significantly lower than those measured in vaginal fluid from women with bacterial vaginosis [278].

Chapter 5 Determination of Tenofovir (TFV), Darunavir (DRV) and Dapivirine (DPV) transport across HEC-1A cell layers

5.1 Aim

To investigate the permeability properties of three ARV drugs in the HEC-1A dual chamber models described in Chapter 4.

5.2 Introduction

This chapter describes an investigation of the permeability properties of three ARV drugs in the HEC-1A dual chamber model described in Chapter 4. The study was performed as part of a collaborative project aimed at developing topically applied microbicides against HIV. Specific objectives of the project were to correlate *in vitro* and *in vivo* studies of drug distribution at vaginal and rectal mucosae and to develop formulations to optimise drug uptake at mucosal surfaces. The ARVs chosen for study in this project were those which had been most advanced along the development pathway as topical microbicides. TFV was selected because, at the time, it was the only ARV to have demonstrated efficacy in a clinical trial (as reviewed in Chapter 2). DPV had been extensively tested in both gel and intravaginal ring formulations in several phase I trials and plans for testing in phase III efficacy trials were well advanced. DPV has since shown significant efficacy in the ASPIRE and RING trials (also reviewed in Chapter 2). Protease inhibitors have not been investigated as extensively as other ARV classes for use as microbicides, in part, because they act post-integration. However macaque transmission studies have suggested that establishment of infection is dependent upon “broadcasting” of initial isolated mucosal foci of infection to disseminating lymph nodes and beyond [111]. Protease inhibitors may be ideally suited to prevent such secondary “broadcasting” leading to an aborted infection. DRV is a potent protease inhibitor with a high genetic barrier to resistance [279] and has recently been tested in a vaginal gel co-formulation with DPV in a phase I trial.

In vitro drug permeability assays are useful methods to determine the PK properties of drugs. The assays can be optimised for the routine assessment of interactions

with drug transporters as well as barrier penetration. To measure the bi-directional permeability of the various ARV drugs, the optimised HEC-1A dual chamber model was used. The distribution of drug between the two compartments of the Transwell® system is a result of passive transcellular diffusion, paracellular diffusion, transporter-mediated absorption or transporter mediated secretion. While paracellular diffusion displays a linear rate of transport and symmetrical A-B/B-A permeability, transporter mediated transport is detected by asymmetry between the rate of transport in the A-B and B-A direction.

Bi-directional drug transport assays across polarised epithelial cells are useful for detecting drug transporter activity, especially drug efflux. Drug efflux transporter activity can be identified by the detection of bi-directional differences in drug permeability. This method also provides drug accumulation analysis for each of the tested drugs. Based on data obtained in Chapter 4 and the general FDA/nature protocol guidelines [7, 233], the conditions shown in Table 5.1 were adopted for all drug permeability assays in this study.

	A-B/B-A
Minimum TEER value ($\Omega \times cm^2$)	150*
TEER value as % deviation of initial	100±20**
Cumulative flux linearity (r^2)	> 0.980**
Mannitol P_{app} (cm/s)	$< 4x10^{-6}$*
Solute recovery (%)	100 ± 15**

Table 5.1 Experimental data acceptance criteria.
*Conditions based on our findings
**FDA and Nature protocol [7, 233]

HEC-1A seeded Transwells® with TEER values below 150 $\Omega x cm^2$ were not used for experiments. All drug transport experiments were undertaken with mannitol, this paracellular tracer molecule serves as a routine control for paracellular diffusion as well as a quantitative routine marker to assess barrier integrity (as described in Chapter 4). Therefore, Transwell® inserts in which mannitol permeability values exceeded $4x10^{-6}$ cm/s were not considered in any data analysis. Similarly, analyses were considered invalid if post TEER values deviated by more than 20% from pre

experiment value, flux linearity was less than an r^2 value of 0.98 and total drug recovered was outside the range of 90-110% of the original quantity added to the donor chamber. All transport experiments were undertaken when HEC-1A cell layers had been cultured for a period of 6-10 days. All drug concentrations used in this study were within or above the EC^{50} values of each drug and did not exert a cytotoxic effect *in vitro*.

5.2.1 Tenofovir, Darunavir and Dapivirine drug permeability across HEC-1A cell layers

Previous drug formulation studies have used the HEC-1A model to measure the permeability and trans-cellular accumulation of TFV, DRV and DPV in the absorptive A-B direction only [136]. The permeation profiles of each drug were determined after 1 hour incubation when formulated in acidified HBSS (pH 4.2) diluted with vaginal fluid simulant (VFS) as the solvent in the apical compartment. DPV showed highest permeation with 20.8% detected in the receiver compartment, followed by permeation fractions of 10.1% for DRV and 1.85% for TFV suggesting that the more lipophilic drugs (DRV and DPV) permeated faster than the hydrophilic drug (TFV). Additionally, intracellular fractions were measured at <1% TFV, 3% DRV and 56% for DPV.

5.2.2 Tenofovir, Darunavir and Dapivirine drug interactions with transporters expressed by HEC-1A and P-gp

Of the three ARV drugs, analyses of drug transporter interactions with transporters expressed by HEC-1A have been reported only for TFV and DRV [177, 214]. Increased TFV accumulation was detected in MRP4-overexpressing MDCK cells in the presence of the MRP4 inhibitor MK571. TFV was selectively taken up by membrane vesicles prepared from insect cells transfected with MRP4. DRV was effluxed by the P-gp transporter when permeability was assessed across Caco-2 monolayers. After 6 hours, approximately 20% of DRV from the donor compartment in the A-B absorptive direction was present in the basolateral compartment while in the B-A direction, 43% of donor DRV was detected in the apical compartment. P-gp inhibitors enhanced the A-B transport of DRV in Caco-2 cells providing further evidence that P-gp mediates efflux transport of DRV in the apical membranes of Caco-2 cells.

5.2.3 Drug-drug interactions

As discussed in Chapter 2, development of microbicides combining more than one ARV may improve efficacy and present a higher barrier to the development of resistant strains of HIV. Drug interaction studies are fundamental for determining the PK of a particular drug when formulated as a combination or co-administered with other drugs. Drug-drug interactions can alter the PK properties of drugs or their metabolites. For the purpose of this study, which focuses on the pre-clinical assessment of topically applied microbicides that may include ARV co-formulations, it is essential to determine the PK interactions between each of the drugs. Alterations in metabolism or transport can completely change the safety and efficacy of a drug. Changes in parameters such as area under the curve (AUC), maximum blood plasma concentration (C_{max}) and minimum blood plasma concentration (C_{min}) can have detrimental effects on the body. Drug databases such as [280] provide useful information on HIV drug interactions. Currently no drug-drug interactions have been identified between TFV, DRV and DPV.

5.3 Results

5.3.1 Permeability of TFV in the dual chamber HEC-1A cell culture model

Permeability of the hydrophilic ARV drug TFV was assessed in the HEC-1A barrier epithelium model described in Chapter 4. All assays were performed between days 6-10 of culture corresponding to the period when TEER values remained at a maximum. TEER values were measured before and after each assay and [^{3}H]mannitol was included as a marker for the HEC-1A barrier integrity. Experiments were repeated at least 2 times and data represents all experiments. Bi-directional P_{app} values determined for [^{14}C]TFV concentrations ranging from 0.1-100 µM (prepared in HBBS+1%HEPES) across HEC-1A cell layers are shown in Figure 5.1A. No significant differences ($P \geq 0.05$, ANOVA) were evident in P_{app} values determined for A-B or B-A directions. In addition, P_{app} values (1-2x10^{-6} cm/s) were similar at each concentration of TFV. Furthermore, the low rate of [^{14}C]TFV movement across HEC-1A cell layers was similar to that measured for the paracellular tracer molecule [^{3}H]mannitol (Figure 5.1B).

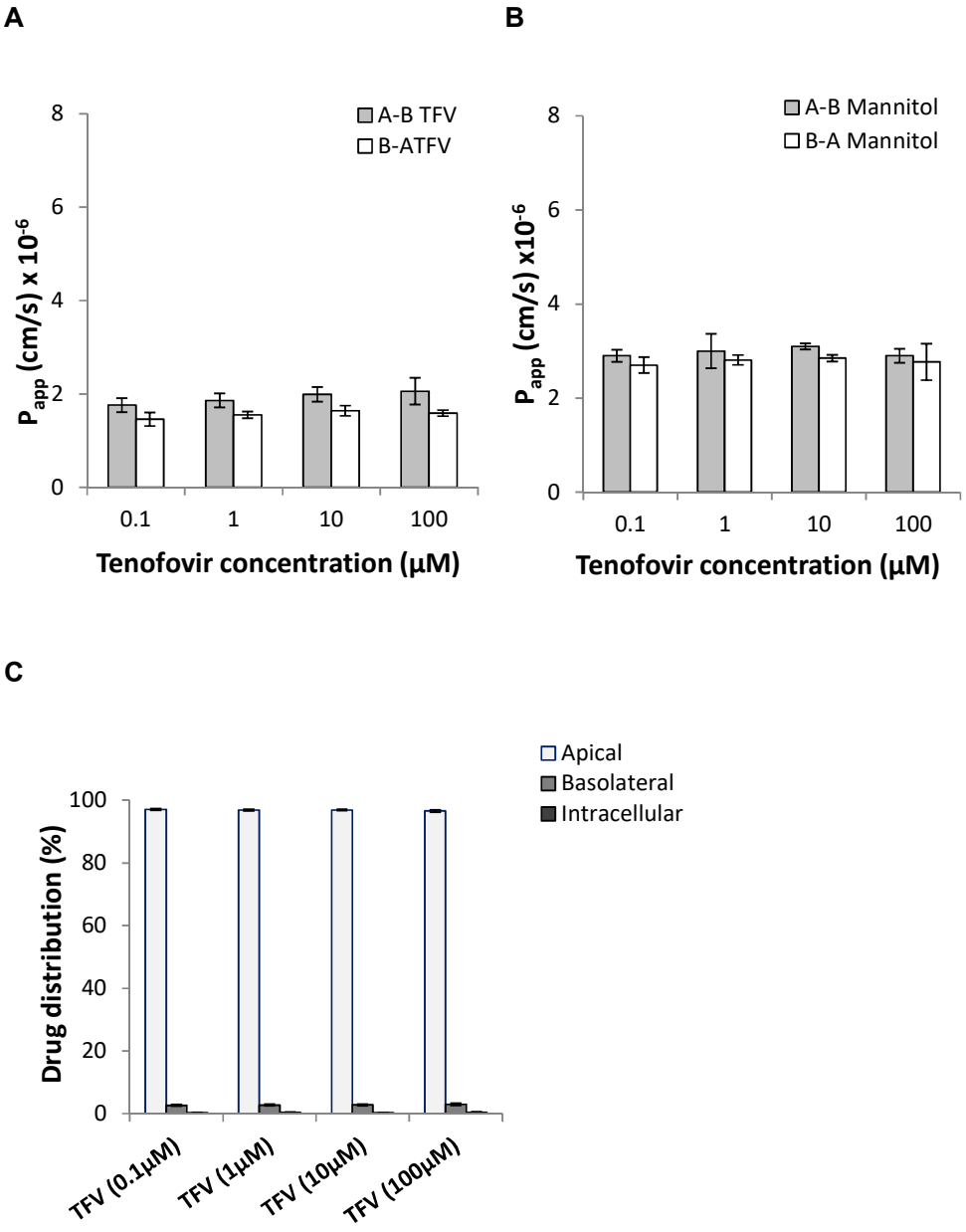

Figure 5.1 A-B/B-A permeability of different TFV concentrations and the percentage distribution of various TFV concentrations in the A-B direction. (A) A-B/B-A P_{app} TFV **(B)** A-B/B-A P_{app} mannitol **(C)** A-B TFV distribution in each compartment of the Transwell®. Data represent mean ± S.D., n = 2-3 (4-6 technical repeats).

The distribution of TFV at the end of the assay was determined in the absorptive (A-B) direction within the apical, basolateral and intracellular compartments of the Transwells® system and is depicted in Figure 5.1C. For each TFV concentration,

most drug was in the apical compartment (approximately 97%), 2-3% was detected in the basolateral compartment and less than 0.5% was detected intracellularly. The low permeability coefficient of 1-2x10^{-6} cm/s across the HEC-1A layers for TFV and extremely low intracellular accumulation is consistent with the transport characteristics of a molecule permeating via the paracellular pathway. Additionally, the efflux ratio value of approximately 0.8 for each concentration (shown in Table 5.2) confirmed the transporter-independent permeability of TFV through HEC-1A cell layers.

	P_{app} (x10^{-6} cm/s)		
	A-B	B-A	Efflux ratio $P_{app\ (B-A)}/P_{app\ (A-B)}$
TFV (0.1μM)	1.76 (0.15)	1.46 (0.15)	0.83
TFV (1μM)	1.86 (0.15)	1.55 (0.07)	0.83
TFV (10μM)	1.99 (0.16)	1.64 (0.11)	0.82
TFV (100μM)	2.09 (0.29)	1.59 (0.07)	0.77

Table 5.2 Efflux ratio for each TFV concentration. Data represent mean ± S.D., n = 2-3 (4-6 technical repeats).

5.3.2 Permeability of DRV through HEC-1A model epithelium

Permeability of DRV was also assessed in the HEC-1A model system. DRV is poorly soluble in aqueous buffer and 0.01% DMSO was included for solubilisation. Experiments were repeated at least 2 times and data represents all experiments. No effect of DMSO on TEER or permeability of mannitol was evident in these assays. Apparent permeability (P_{app}) values for [^{14}C]DRV (1-20 μM prepared in HBBS+1%HEPES+0.01% DMSO) are shown in Figure 5.2A. As for TFV, there were no significant differences ($P \geq 0.05$, ANOVA) in P_{app} values determined for A-B or B-A directions. P_{app} values (8-12x10^{-6} cm/s) were again independent of DRV concentration. However, the rate of [^{14}C]DRV permeation across HEC-1A cell layers was 9-10-fold higher than that measured for the paracellular tracer molecule [^{3}H]mannitol (Figure 5.2B) and correspondingly higher than that of TFV.

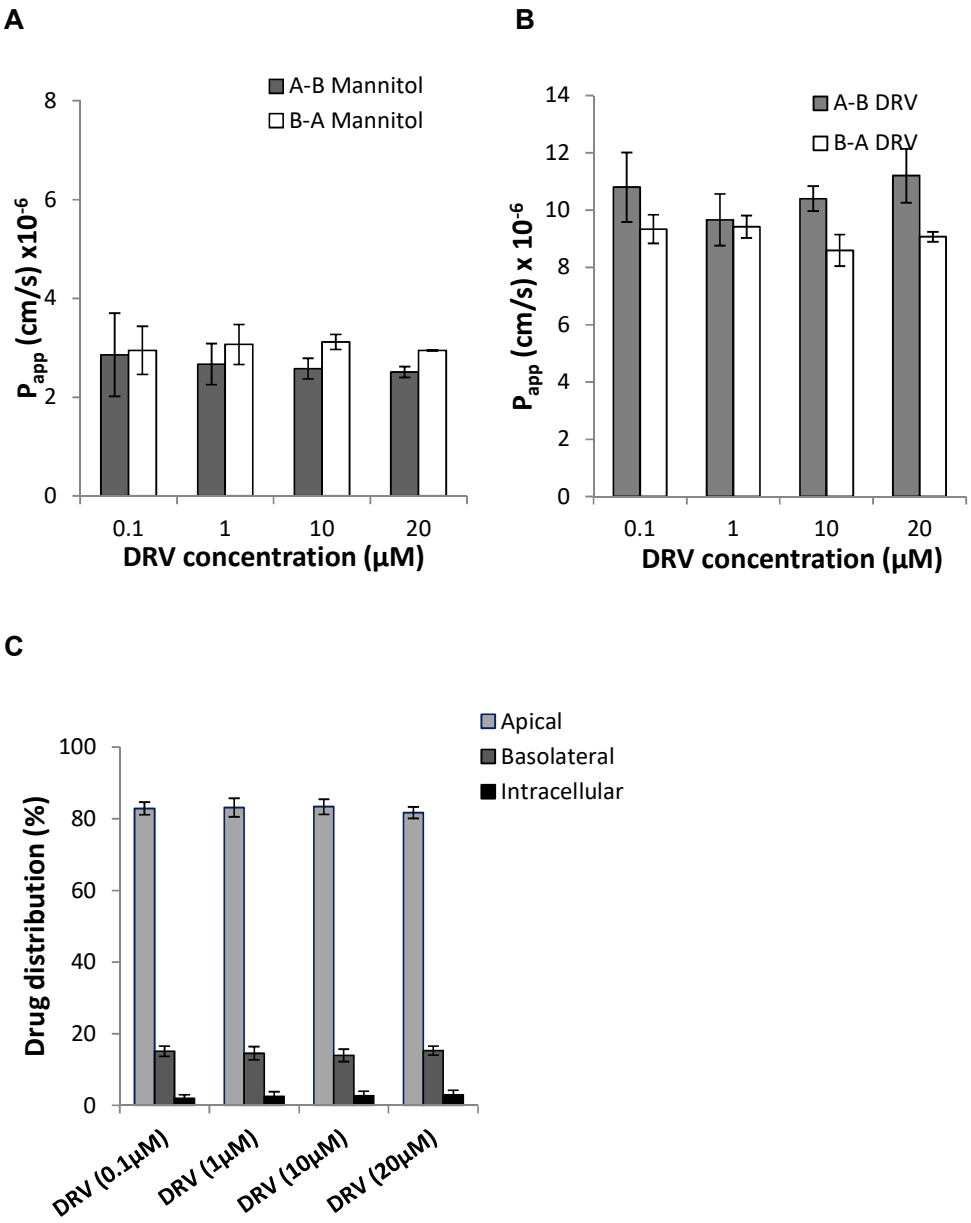

Figure 5.2 A-B/B-A permeability of different DRV concentrations and the percentage distribution of various DRV concentrations in the A-B direction. (A) A-B/B-A P_{app} DRV **(B)** A-B/B-A P_{app} mannitol **(C)** A-B DRV distribution in each compartment of the Transwell®. Data represent mean ± S.D., n = 2-3 (4-6 technical repeats).

The distribution of DRV at the end of the assay was determined in the absorptive (A-B) direction transport within the apical, basolateral and intracellular compartments of the Transwell® system as shown in Figure 5.2C. For each of the DRV concentrations, the level of drug was highest in the apical compartment (approximately 82%), 15% was detected in the basolateral compartment and 2-3%

was detected intracellularly. The higher permeability coefficient of 8-10x10^{-6} cm/s for DRV when compared to that of [^{14}C]mannitol and [^{14}C]TFV, and higher accumulation in the basolateral compartment is consistent with the transport characteristics of a molecule permeating via the passive transcellular pathway. Additionally, the efflux ratio value of approximately 0.8-1 for each concentration (Table 5.3.) confirmed the transporter-independent permeability of DRV through HEC-1A cell layers.

	P_{app} (x10^{-6} cm/s)		
	A-B	B-A	Efflux ratio $P_{app\ (B-A)}/P_{app\ (A-B)}$
DRV (1μM)	10.8 (1.21)	9.34 (0.50)	0.86
DRV (5μM)	9.66 (0.91)	9.42 (0.39)	0.98
DRV (10μM)	10.4 (0.43)	8.59 (0.55)	0.82
DRV (20μM)	11.2 (0.94)	9.07 (0.17)	0.80

Table 5.3 Efflux ratio for each DRV concentration. Data represent mean (± S.D), n = 2-3 (4-6 technical repeats).

5.3.3 Permeability of DPV through HEC-1A model epithelium

Permeability of the highly hydrophobic ARV drug DPV was also determined in the HEC-1A cell dual chamber model. Experiments were repeated at least 2 times and data represents all experiments. For solubilisation of DPV, DMSO (1% v/v) was included in the transport assay buffer. In preliminary experiments, the effect of DMSO on HEC-1A dual chamber cultures was investigated by determination of TEER and [^{3}H]mannitol permeability. DPV at concentrations ranging from 1-20μM was dissolved in HBBS+1% HEPES +1% DMSO for these experiments.

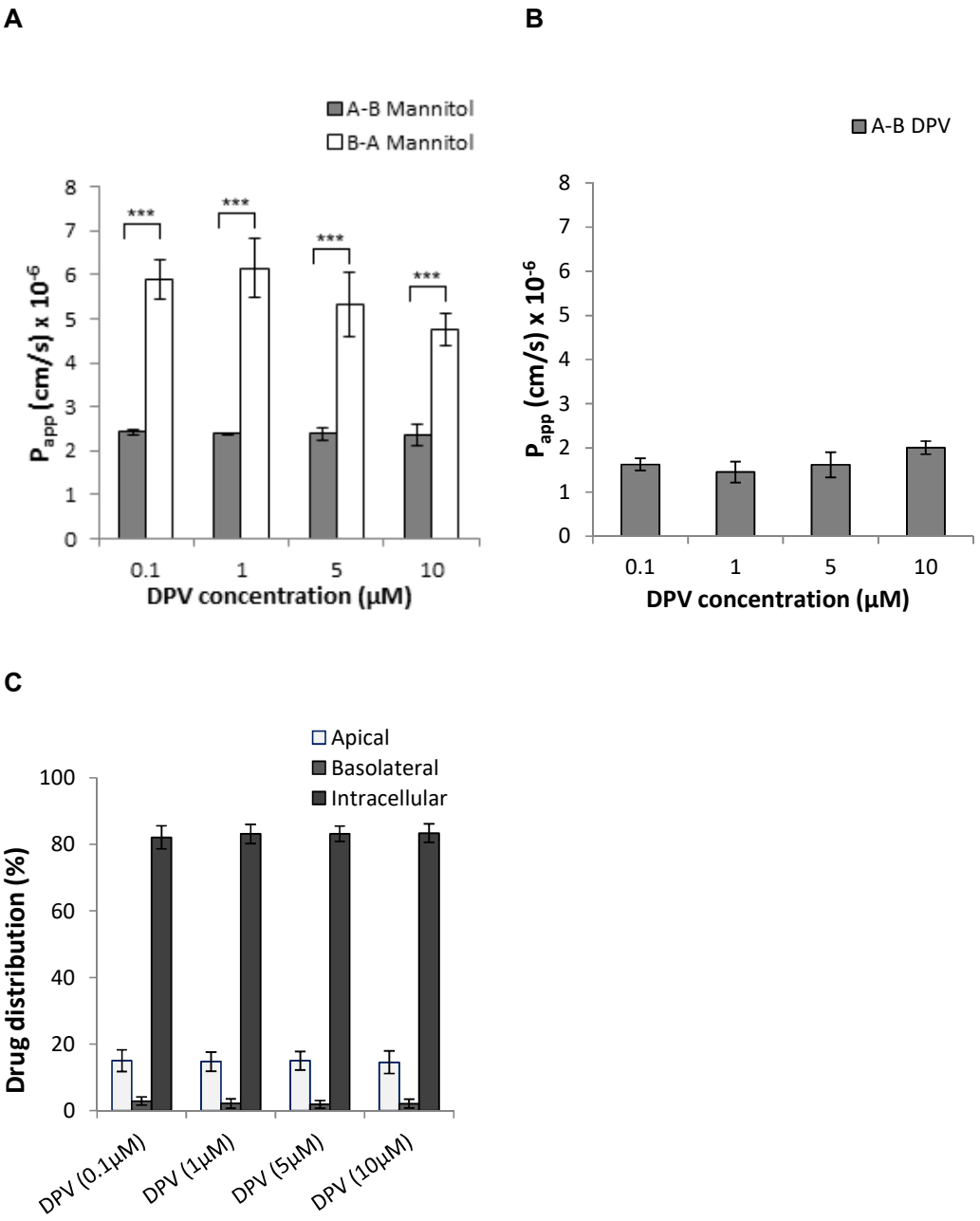

Figure 5.3 A-B/B-A permeability of different DPV concentrations and the percentage distribution of various DPV concentrations in the A-B direction. (A) A-B/B-A P_{app} DPV (***, $P < 0.05$) **(B)** A-B/B-A P_{app} mannitol **(C)** A-B DPV distribution in each compartment of the Transwell®. Data represent mean ± S.D., n = 2-3 (4-6 technical repeats).

Figure 5.3A shows the effect of the 1% DMSO + DPV test solutions on HEC-1A cell layer integrity, by the measurement of P_{app} [^{3}H]mannitol. Following application of DMSO/DPV solutions in the apical chamber, P_{app} values for [^{3}H]mannitol (approximately 2.38 x10^{-6} cm/s) were consistent with maintenance of a barrier

epithelium. In contrast, application of the same solutions to the basolateral chamber resulted in statistically significant ($P \leq 0.05$, ANOVA) increased secretory mannitol flux indicating some loss of barrier integrity. This was confirmed by the substantial decrease in post experimental TEER readings which showed a reduction of 60-70% when compared to the pre (initial) experimental TEER readings (Table 5.4).

Consistent with mannitol permeability, application of 1% DMSO in the apical compartment did not affect TEER values post-assay which remained within 100±15% of the initial TEER measurements. [^{14}C]DPV absorptive permeability (A-B) was determined with P_{app} of 1-2x10^{-6} cm/s irrespective of DPV concentration (Figure 5.3B). The distribution of [^{14}C]DPV in the absorptive direction was determined in each compartment. As shown in Figure 5.3C, for all concentrations, approximately 80% of [^{14}C]DPV was shown to accumulate intracellularly, while 15% remained in the apical compartment and 2% was in the basolateral compartment. This 2% accumulation in the basolateral compartment was similar to that detected for TFV, however unlike TFV, DPV partitions into the cell membranes. This is consistent with the characteristics of an extremely lipophilic molecule.

Test Solution	A-B Mannitol		B-A Mannitol	
	P_{app} (x10^{-6} cm/s)	TEER (% initial)	P_{app} (x10^{-6} cm/s)	TEER (% initial)
0.1µM DPV+HBSS+1%HEPES+1%DMSO	2.42±0.0	95-105	5.88±0.5	25-40
1µM DPV+HBSS+1%HEPES+1%DMSO	2.38±0.0	96-103	6.14±0.7	30-42
5µM DPV+HBSS+1%HEPES+1%DMSO	2.38±0.2	93-105	5.31±0.7	27-38
10µM DPV+HBSS+1%HEPES+1%DMSO	2.35±0.3	96-107	4.74±0.4	29-42

Table 5.4 A-B/B-A [^{3}H]mannitol P_{app} values and % of initial TEER in the presence of test solution containing various concentrations of 1% DMSO + DPV. In the A-B direction HEC-1A barrier integrity is stable. In contrast, loss of barrier integrity is detected in the B-A direction. Data represent mean ± S.D., n 2-3 (4-6 technical repeats).

Since DPV could not be dissolved in solutions containing <1% DMSO further analyses of secretory permeability of the drug were not performed. Addition of amphiphilic compounds such as the surfactant poloxamer 407 in the receiver compartment increases flux of lipophilic compounds across model epithelium [281].

Such compounds may partially mimic drug interactions with components on the basolateral side of the epithelium and improve transfer of lipophilic drugs.

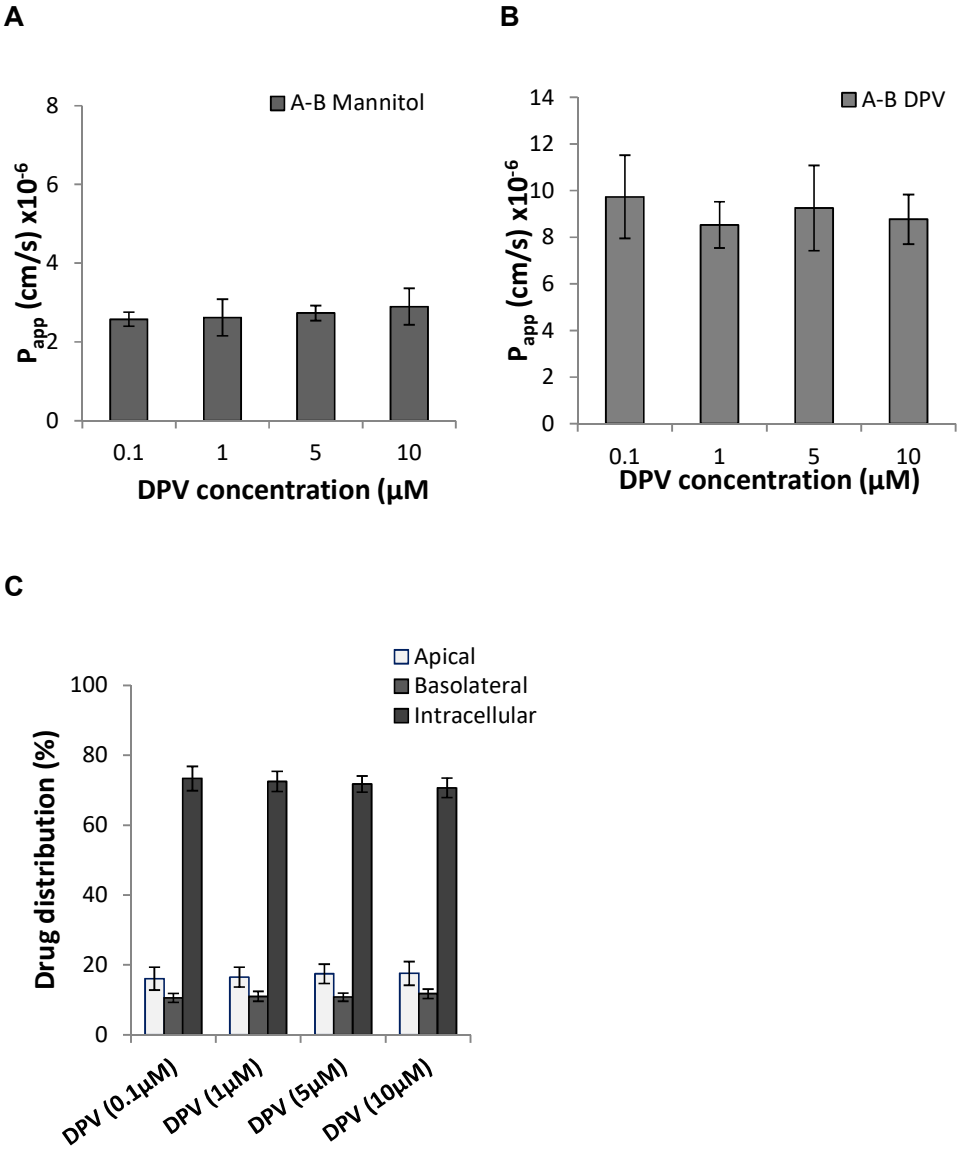

Figure 5.4 A-B permeability of different DPV concentrations and the percentage distribution of various DPV concentrations in the A-B direction. (A) A-B P_{app} DPV with poloxamer 407 in the receiver compartment **(B)** A-B P_{app} mannitol **(C)** A-B DPV distribution in each compartment of the Transwell®. Data represent mean ± S.D., n = 2-3 (4-6 technical repeats).

Poloxamer 407 (0.2% w/v) was added to the basal chamber and absorptive permeability (A-B) of [^{14}C]DPV was determined. Under these conditions, higher P_{app} values (8-12x10^{-6} cm/s) were observed compared with those in the absence of

poloxamer (Figure 5.4A). No significant difference ($P \geq 0.05$, ANOVA) in absorptive permeability was observed between the various DPV concentrations (addition of poloxamer 407 had no effect on permeability of the polar paracellular marker mannitol), (Figure 5.4B).

The increased P_{app} correlated with the data shown in Figure 5.4C as poloxamer 407 enhanced [^{14}C]DPV permeability by an additional 10% into the basolateral compartment, reducing the amount of DPV in the cells to approximately 70%. Residual [^{14}C]DPV in the apical (donor) chamber remained at 16%. Since DPV may absorb to the surfaces of the culture chambers, a series of permeability assays were performed with poloxamer 407 added to the basolateral compartment of Transwells® with and without HEC-1A cell cultures and the distribution of drug was determined as shown in Table 5.5.

A-B DPV (HBSS+1%HEPES+1%DMSO) PE Transwell®	Intracellular/Transwell® membrane DPV accumulation (%)
With cells - poloxamer 407 in basolateral compartment	80
With cells + poloxamer 407 in basolateral compartment	70
Without cells + poloxamer 407 in basolateral compartment	10-20

Table 5.5 Percentage of DPV that absorbs to the PE membrane material of the Transwell® insert. Data represent mean ± S.D., n = 2-3 (4-6 technical repeats).

Table 5.5 indicates that of the 70-80% of [^{14}C]DPV described as “intracellular” DPV accumulation, above, a significant proportion (10-20% of total) [^{14}C]DPV is absorbed to the PE membrane material of the Transwell® insert. Thus of the 70% “intracellular” [^{14}C]DPV recovered, approximately 50-60% is cell associated, presumably partitioned into cell membranes.

5.3.4 Permeability of double drug combinations in the HEC-1A model system

Microbicides comprising two or more ARVs may be more effective than those based on a single drug as discussed previously. An important requirement for combination microbicides is that there should be no detrimental binding competition between drugs to enter the cells ie. drug-drug interactions. The effects of drug combinations on permeability were therefore investigated. For all permeability experiments

described below, a fixed concentration of 10 μM was used in test solutions for each drug. Permeability coefficients were determined for the double combinations. For all TFV+DRV combinations A-B/B-A transport was assessed and for DRV+DPV and TFV+DPV combinations A-B transport was assessed only.

5.3.4.1 Permeability of 10μM [^{14}C]TFV and combinations with DRV or DPV in the HEC-1A model

To determine any drug-drug interactions between TFV and either DRV and DPV, the permeability of 10 μM [^{14}C]TFV in the presence of varying concentrations of DRV and DPV was evaluated. Drug transport assays were performed as described above but in the presence of unlabelled DRV or DPV (Figure 5.5A and 5.5B, respectively). Addionally, all combinations with DPV contained poloxamer 407 (0.2% w/v) in all receiver (basolateral) compartments.

The effect of the addition of DRV 0-10 μM or DPV 0-10 μM in double combinations with TFV was assessed. The double combinations of either [^{14}C]TFV+DRV or [^{14}C]TFV+DPV had no effect on [^{14}C]TFV transport as there were no significant differences ($P \geq 0.05$, ANOVA) in P_{app} coefficients (1-2x10^{-6} cm/s) between drug combinations and controls of TFV alone. Additionally, HEC-1A exposure to test solutions containing TFV+DRV and TFV+DPV combinations had no effect on the barrier integrity, as mannitol permeability was consistent with maintenance of a barrier epithelium (Figure 5.5C and 5.5D, respectively).

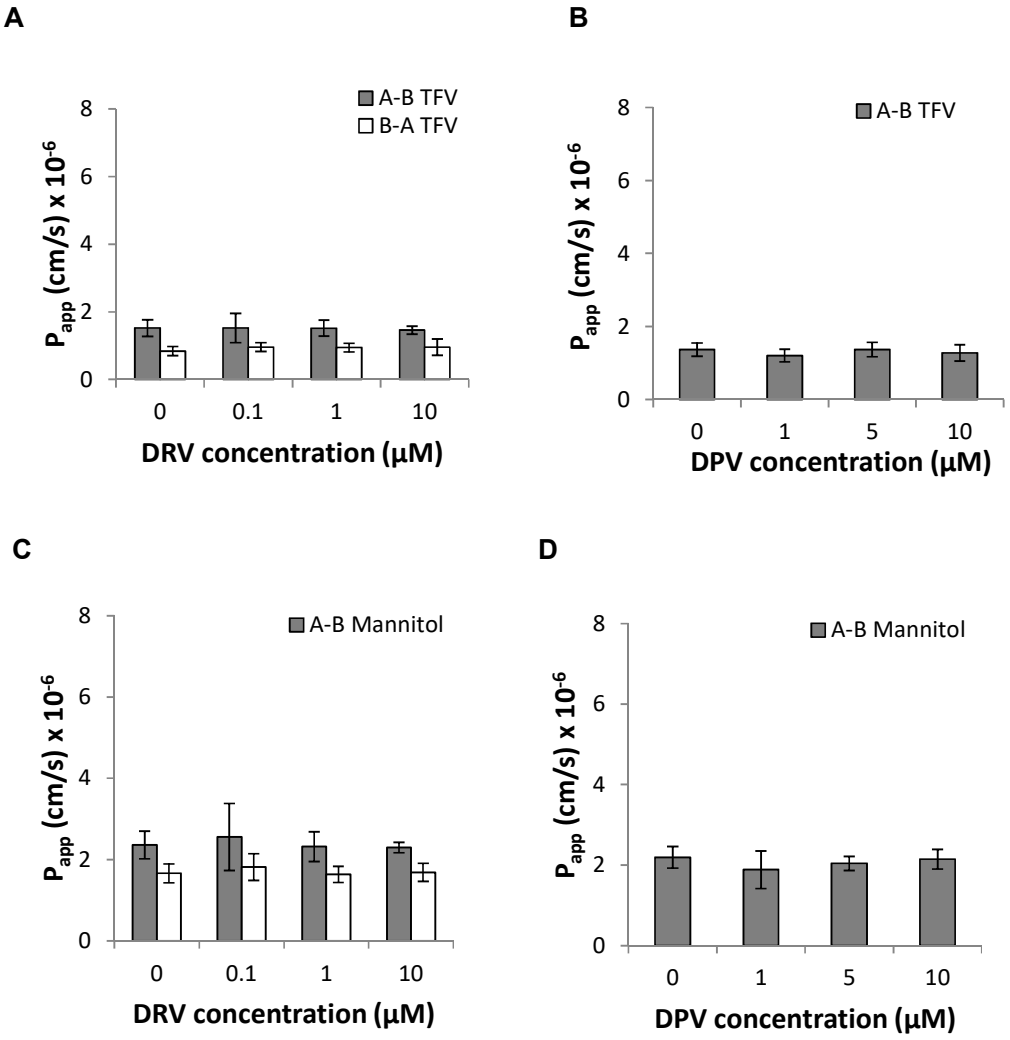

Figure 5.5 A-B and/or B-A permeability of 10µM [^{14}C]TFV in the presence of various DRV and DPV concentrations. (A) A-B/B-A P_{app} 10 µM [^{14}C]TFV in the presence of 0-10 µM DRV **(B)** A-B/B-A P_{app} [^{3}H]mannitol in the presence of 0-10 µM DRV **(C)** A-B/B-A P_{app} 10 µM [^{14}C]TFV in the presence of 0-10 µM DPV **(D)** A-B/B-A P_{app} [^{3}H]mannitol in the presence of 0-10 µM DPV. Data represent mean ± S.D., n = 2-3 (4-6 technical repeats).

5.3.4.2 Permeability of 10µM [^{14}C]DRV and combinations with TFV or DPV in the HEC-1A model

To determine drug-drug interactions between DRV and either TFV and DPV, the permeability of 10 µM [^{14}C]DRV in the presence of varying concentrations of unlabelled TFV or DPV was evaluated (Figures 5.6A and 5.6B). All combinations with DPV contained poloxamer 407 (0.2% w/v) in all receiver (basolateral) compartments

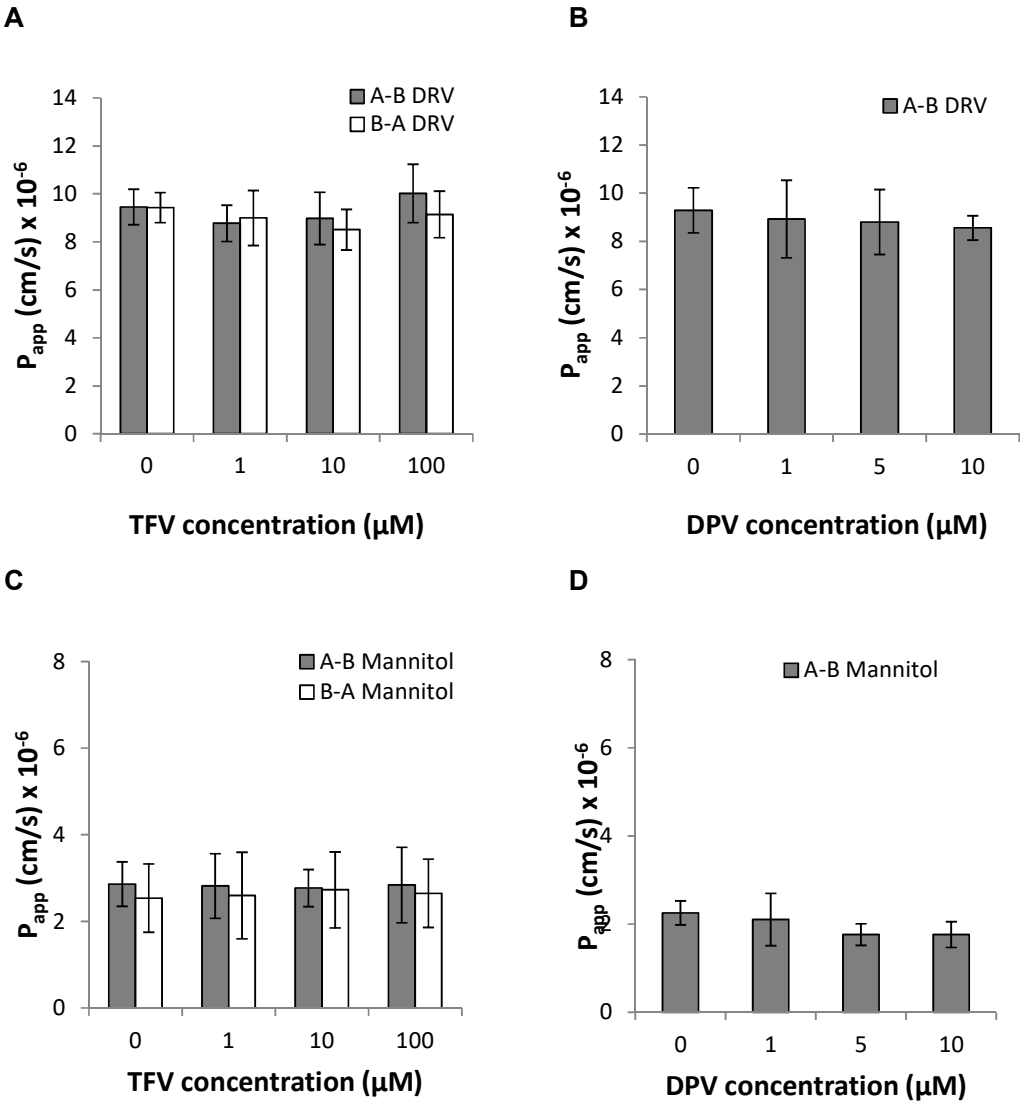

Figure 5.6 A-B and/or B-A permeability of 10µM [^{14}C]DRV in the presence of various TFV and DPV concentrations. (A) A-B/B-A P_{app} 10µM [^{14}C]DRV in the presence of 0-100 µM TFV **(B)** A-B/B-A P_{app} [^{3}H]mannitol in the presence of 0-100 µM TFV **(C)** A-B/B-A P_{app} 10 µM [^{14}C]DRV in the presence of 0-10 µM DPV **(D)** A-B/B-A P_{app} [^{3}H]mannitol in the presence of 0-10 µM DPV. Data represent mean ± S.D., n = 2-3 (4-6 technical repeats).

The effect of including TFV 0-100 µM or DPV 0-10 µM in double combinations with DRV was assessed. The double combinations of either [^{14}C]DRV+TFV or [^{14}C]DRV +DPV had no effect on [^{14}C]DRV transport as a P_{app} coefficients of 8-12x10^{-6} cm/s were not significantly different ($P \geq 0.05$, ANOVA) in all combinations and in the control test solutions in which TFV and DPV were not present. Mannitol permeability remained consistent in both combination test solutions (Figure 5.6C and 5.6D).

5.3.4.3 Permeability of 10 μM [^{14}C]DPV and combinations with DRV or TFV in the HEC-1A model

To evaluate drug-drug interactions between DPV and either TFV or DRV, the permeability of 10 μM [^{14}C]DPV in the presence of varying concentrations of unlabelled TFV and DRV was evaluated (Figures 5.7A and 5.7B).

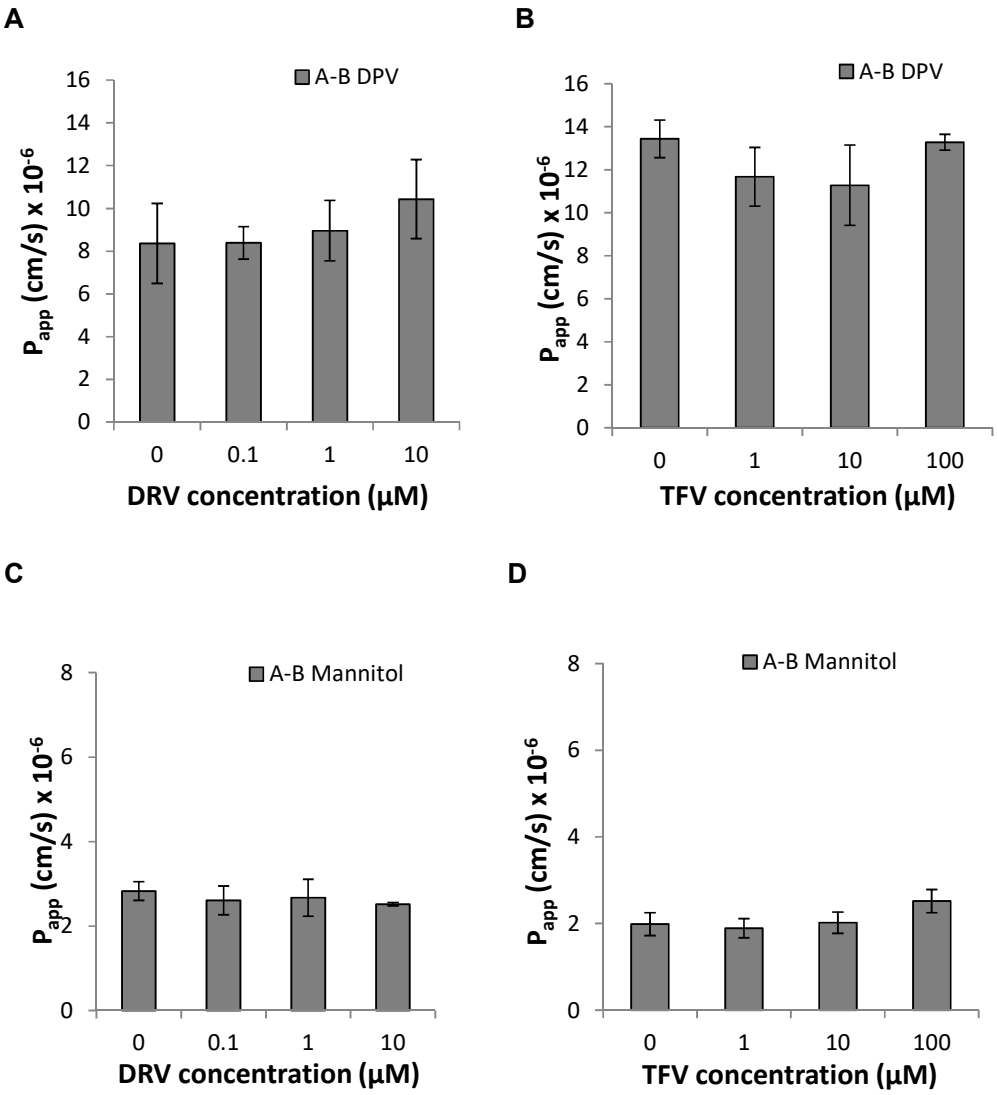

Figure 5.7 A-B permeability of 10μM [^{14}C]DPV in the presence of various TFV and DPV concentrations. (A) A-B P_{app} 10 μM [^{14}C]DPV in the presence of 0-100 μM TFV **(B)** A-B P_{app} [^{3}H]mannitol in the presence of 0-100 μM TFV **(C)** A-B P_{app} 10 μM [^{14}C]DPV in the presence of 0-10 μM DRV **(D)** A-B P_{app} [^{3}H]mannitol in the presence of 0-10 μM DRV. Data represent mean ± S.D., n = 2-3 (4-6 technical repeats).

The effect of including DRV (0-10 μM) or TFV (0-100 μM) in double combinations with DPV was assessed. The double combinations of either [^{14}C]DPV+DRV or [^{14}C]DPV+TFV had no effect on [^{14}C]DPV transport as a P_{app} coefficients of 10-14x10^{-6} cm/s were similar in all combinations as well as the control test solutions in which DRV and TFV were not present. Small increases in DPV P_{app} coefficients were obtained in these assays compared with those reported above, however, the values for the control test solutions were also raised confirming that this was not influenced by the presence of either DRV or TFV. Mannitol permeability again remained consistent in both combination test solutions with P_{app} values in the range of 2-3x10^{-6} cm/s.

5.3.5 Transfection and transient expression of P-gp in HEC-1A cells

DRV is a substrate for the P-gp efflux transporter [214] which is expressed in the FGT [145, 146, 149] although expression could not be detected in HEC-1A cells. To improve the physiological relevance of this model to assess permeability across cervicovaginal epithelium, transient expression of P-gp was investigated by transfection of HEC-1A cells with the plasmid pcDNA-Pgp encoding the entire P-gp protein. In preliminary experiments, HEC-1A cells were transfected, pooled and used to seed Transwell® cultures. After 6 days, when TEER values reached a maximum, cells were harvested and lysed for analysis of P-gp expression by Western blotting.

Lysates of HEC-1A cells (transfected and non-transfected) and from Caco-2 cells (which express P-gp constitutively) were resolved by SDS-PAGE, transferred to nitrocellulose filters and probed with anti-P-gp antibody. As shown in Figure 5.8, diffuse bands corresponding to the expected molecular weight of 141 KDa were evident in lysates from Caco-2 cells and transfected HEC-1A cells but not in lysates from non-transfected HEC-1A cells. The total protein loaded on the gel was equivalent for all lysates (40 μg) thus the level of P-gp expression in transfected HEC-1A cells appears to be similar to that in Caco-2 cells. P-gp has three glycosylated isoforms and so the diffuse nature of the band may reflect these. In control blots, where the first antibody was omitted, no bands were visible.

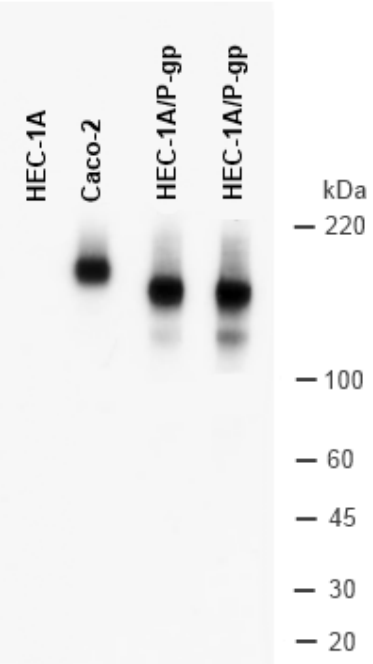

Figure 5.8 Expression of P-gp in transfected HEC-1A cells and Caco-2 cells. Cell lysates were prepared, samples (40 µg total protein in each well) were loaded and separated by SDS-PAGE. Proteins were transferred electrophoretically to nitrocellulose membranes and probed with an anti-P-gp specific antibody to the P-gp drug transporter. Diffuse bands were detected in two samples of transfected HEC-1A cells (HEC-1A/P-gp). Caco-2 cell lysates served as a positive control. In contrast, non-transfected HEC-1A cells served as a negative control.

5.3.6 Permeability of the P-gp substrate 10 µM [^{3}H]digoxin the HEC-1A/P-gp model

Activity of the P-gp transporter expressed in HEC-1A cells was investigated by performing permeability assays in parallel cultures with 10 µM digoxin, a well-characterised substrate for P-gp [214]. As shown in Figure 5.9A, P_{app} values for [^{3}H]digoxin were similar for both absorptive and efflux permeation and no effect of P-gp transport was evident. Formation of tight junctions was demonstrated both by TEER and the limited permeability to [^{14}C]mannitol (Figure 5.9B). Transport assays were performed with Caco-2 Transwell® cultures in parallel where P-gp activity was demonstrated by an increase in P_{app} in the B-A direction compared with A-B (data not shown).

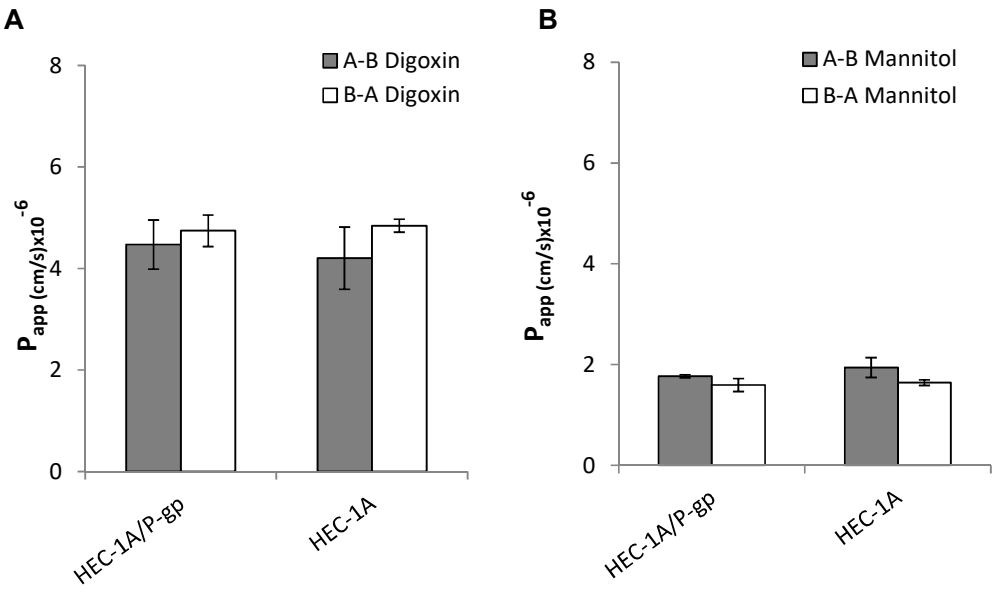

Figure 5.9 A-B/B-A permeability of the P-gp substrate 10 μM [^{3}H]digoxin across non-transfected and transfected HEC-1A cell layers. A-B/B-A permeability of [^{14}C]mannitol. No differece in digoxin permeability was determined between transfected and non-transfected HEC-1A cells. Data represent mean ± S.D., n=1 (3 technical repeats).

5.3.7 Modelling inflammation in HEC-1A Transwell® cultures and effect on TFV and DRV drug perembaility.

HEC-1A cells cultured in Transwells® were stimulated at the apical surface with the TLR 3 agonist Poly I:C for 18-24h as described in Chapter 4. Aliquots of culture media from both apical and basolateral compartments were analysed for production of inflammatory cytokines as also described in Chapter 4. As shown in Figure 5.10, high levels of IL-8 and IL-6 were secreted together with high concentrations of TNF-α and GM-CSF and lower concentrations of IL-1α. IL-1β was not detected. Levels of cytokines were consistent with those published previously in studies of *in vitro* cytokine production from immune cells [282]. Low levels of TNF-α and GM-CSF were measured in unstimulated HEC-1A cell cultures but no other cytokines were detected in these cultures. For all cytokines except IL-8, secretion appeared to be polarised to the apical surface.

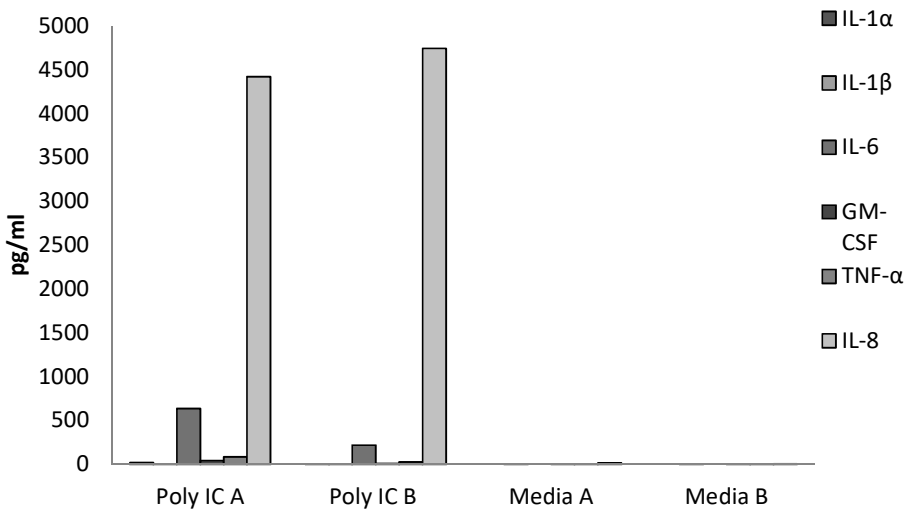

Figure 5.10 Stimulation of HEC-1A cultures in Transwells® by Poly I:C. Patterns of IL-1α, IL-1β, IL-6, GM-CSF, TNF-α and IL-8 release into A-apical and B-basolateral compartments containing culture supernatants of HEC-1A epithelial cells cultured in Transwell® inserts and treated for 24 hours with 25 µg/ml of Poly I:C. Cytokines were determined by Multiplex bead immunoassay. Mean secretion-blank are shown n=1 (3 technical repeats).

The effects of Poly I:C stimulation on permeability of TFV and DRV were assessed in the same cultures. Apparent pereability values for 10 µM [^{14}C]TFV and [^{14}C]10 µM DRV are shown. Figure 5.11A indicates that there were no significant differences ($P \geq 0.05$, ANOVA) in P_{app} values determined for A-B or B-A directions for TFV and DRV when compared to the permeability across unstimulated HEC-1A cell layers. The P_{app} values for TFV were approximately $1x10^{-6}$ cm/s when cells were unstimulated and $1.4x10^{-6}$ cm/s when cells were stimulated. Additionally DRV P_{app} was approximately $8x10^{-6}$ cm/s for both, when cells were stimulated and unstimulated. The paracellular tracer molecule mannitol further confirmed that there were no significant ($P \geq 0.05$, ANOVA) effects of Poly I:C stimulation on barrier integrity as [^{3}H]mannitol P_{app} values for stimulated cells were $1.5\text{-}1.9x10^{-6}$ cm/s and for simulated cells they were $2.2\text{-}2.4x10^{-6}$ cm/s (Figure 5.11B).

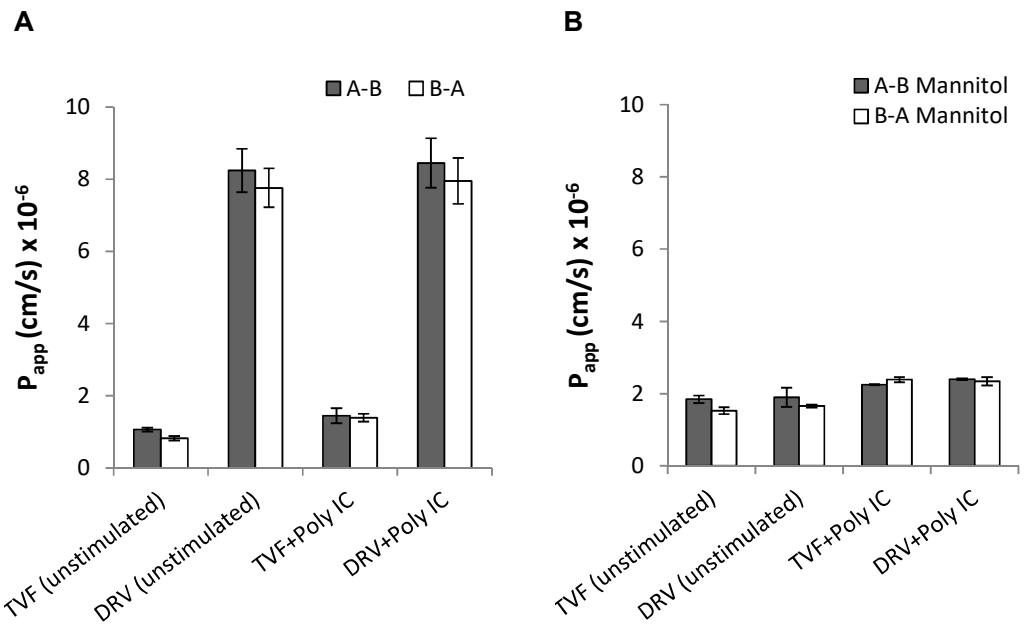

Figure 5.11 A-B/B-A [^{14}C]TFV, [^{14}C]DRV and [^{3}H]mannitol permeability across Poly I:C stimulated and unstimulated HEC-1A cell layers. (A) A-B/B-A [^{14}C]TFV and [^{14}C]DRV permeability across HEC-1A stimulated and unstimulated HEC-1A cell layers, with no significant differences ($P \geq 0.05$) of P_{app} values. **(B)** A-B/B-A [^{14}C]mannitol permeability across HEC-1A stimulated and unstimulated HEC-1A cell layers, again with no significant differences ($P \geq 0.05$, ANOVA) of P_{app} values. n=2, data represent mean ± S.D., from 1 experiment (3 technical repeats).

5.4 Discussion

The major findings from this part of the work are that permeation of each drug across the HEC-1A model epithelium is transporter-independent. TFV permeates across HEC-1A cell layers by paracellular diffusion, while DRV and DPV both permeate by diffusion across the transcellular route. Intracellular accumulation was highest for DPV as reported previously [136] whereas intracellular accumulation was substantially lower for DRV and TFV. Bi-directional permeability of single drugs was compared with double drug combinations and no drug-drug interactions were detected.

For the studies reported here, permeability was determined in both absorptive and secretory directions. Significant differences in P_{app} values for either direction may

indicate the effects of drug transporters. In contrast, previous studies have reported TFV permeability in the absorptive (A-B) direction only [136, 199, 283]. The P_{app} values for TFV in both directions determined in this study (1-2x10^{-6} cm/s) are in good agreement with those reported previously for TFV permeability through HEC-1A dual chamber cultures [136] and through human ectocervical explants [283] pointing to the consistency and physiological relevance of this model. Bi-directional permeability was also demonstrated in the human ectocervical polarised explant model by a functional assay in which basolateral application of TFV prevented infection of the tissue following apical challenge with HIV [199].

The distribution of TFV between donor, intracellular and receptor compartments reported here is also consistent with those reported previously [136] of approximately 2% in the basolateral (acceptor) compartment and negligible quantities in the intracellular compartment. Drug concentrations in tissue were not reported for permeability studies of 1% TFV gel formulations using ectocervical explants but TFV recovered in the basolateral compartment was estimated to be approximately 2-5% or 5-10% (with different formulations) of the input dose [199]. The TFV gel formulation that resulted in 2-5% permeation was that used in the CAPRISA 004 trial [2] but extrapolation to *in vivo* administration of TFV gel may also require estimation of drug loss due to discharge of vaginal fluid. Vaginal tissue concentrations of TFV 24 hours after dosing with the vaginal gel (total dose of 40 mg TFV) following the CAPRISA 004 trial regime, were reported to be in the range of 10^3 - 10^4 ng/g or approximately 3.5-35 μM [284] compared with the *in vitro* tissue EC_{50} of 0.2-8.5 μM [195, 198-200].

The efflux ratio for TFV was close to 1 and both absorptive and efflux P_{app} values for TFV were similar to those of the paracellular marker, mannitol, consistent with transfer across the epithelium by paracellular diffusion. No efflux of TFV mediated by MRP4 was evident. In a connected study, within the collaborative project, permeability of TFV was also assessed in the Caco-2 Transwell® system and again no effect of MRP4 was evident [Swedrowska et al, personal communication; manuscript submitted for publication). Additionally, activity of uptake and efflux transporters expressed in the cervicovaginal epithelium is yet to be reported.

DRV displays a bi-directional P_{app} coefficient in the range of 8-12x10^{-6} cm/s and an ER close to 1. Like TFV, this indicates that DRV permeability is transporter-

independent. While DRV has been reported to be a substrate for P-gp [214], HEC-1A cells do not naturally express P-gp (as identified in Chapter 4). DRV exhibits low A-B HEC-1A intracellular accumulation of 1-2% and basolateral accumulation of 15% of drug from the donor compartment. With a log P of 1.80, DRV has low solubility in aqueous buffers but does not show the properties of a highly lipophilic drug as evident from its low intracellular HEC-1A accumulation. The data here suggests that DRV freely permeates through HEC-1A cell layers via passive diffusion without binding to lipids within cell membranes. In areas of the vagina with low, inactive or no expression of P-gp, DRV may freely permeate into the sub-epithelium. In contrast, although DPV shares a similar basolateral accumulation value to DRV (in the presence of poloxamer 407), the much higher intracellular accumulation (50%) reflects the difference in lipophilicity between the two drugs. The low absorptive P_{app} of DPV is consistent with partition and accumulation of (uncharged drug) at high levels in the membrane compartment of epithelial cells. Such accumulation has also been shown in vaginal epithelial tissue following vaginal administration in rabbit and macaque models [100].

Drug permeability in this study was assessed at pH 7.4 whereas healthy vaginal pH is 3.5-4.5 [102]. Further work should include repeating the assays at lower pH. In preliminary experiments, exposure of the HEC-1A dual chamber cultures to low pH led to significant reductions in TEER (data not shown) and has also shown to reduce TEER in Caco-2 cells [146]. Furthermore the correspondence between the findings reported here and those described previously [136] where assays were performed at pH 4.2, indicate that the transporter-independent permeation shown by these drugs is not altered within this pH range. The more lipophilic drugs DRV and DPV are uncharged in this pH range. TFV is amphiprotic displaying both positively charged (NH_3^+) and negatively charged moieties (as a mixture of $H_2PO_3^-$ and HPO_3^{2-}) in this pH range.

When formulated in double combinations, TFV, DRV and DPV do not show evidence of incompatibility with regard to solubility although solubilising excipients such as DMSO are required for both DPV and DRV. The presence of the surfactant poloxamer 407 in all combination test solutions which contained DPV did not have an effect on TFV and DRV permeability. Additionally, no drug-drug interactions were

identified, as P_{app} coefficients for each of the drugs showed similar values when compared as single and double formulations.

To investigate the effects of inflammation on drug permeability, HEC-1A cell layers were stimulated with the TLR ligand Poly I:C. Levels of pro-inflammatory cytokines were comparable to those previously reported to reduce maintenance of tight junctions (as discussed in Chapter 4) although no reduction in TEER or increase in mannitol permeability was evident in these studies. In future work, longer term stimulation may be necessary. Studies of the effects of inflammation on expression of drug transporters generally focus on intestinal, hepatic, or placental transporters and data for the female reproductive tract are not available. In inflamed tissue of duodenal biopsies from patients with ulcerative colitis, the expression of P-gp and BCRP efflux transporters is reduced as compared to non-affected mucosa or normal controls [285]. In colon biopsies from patients with ulcerative colitis, mRNA levels of the nucleoside transporters ENT1, ENT2 (SLC29 family), and CNT2 (SLC28) were significantly increased as were mRNA levels of the organic anion transporters OATP2B1, OATPE (SLCO), and OCTN1 (SLC22) [286]. The net effect of these changes has not been determined although reduction in efflux transporters could lead to higher tissue levels of topically applied drugs.

In any case, inflammation may not have detrimental effects on uptake of the drugs studied here. Any reduction of tight junction function may lead to increased permeability of TFV. In addition, permeability of DPV and DRV requires partition into lipophilic compartments and may not be compromised in an inflammatory environment.

In studies involving heterologous overexpression of the efflux transporter MRP4 in mammalian or insect cell lines, TFV was identified as a substrate for MRP4 [177]. As above, no effect of MRP4 was evident either in the HEC-1A model or in Caco-2 Transwell® cultures. This may simply reflect low intracellular uptake of TFV since organic anion transporters OAT1 and OAT3 identified as uptake transporters for TFV [287] are not expressed in HEC-1A cells [206]. To model more closely transporter expression of the FGT, transient expression of P-gp in HEC-1A cells was investigated. Expression of P-gp in transfected HEC-1A cells was comparable to that in constitutively-expressing Caco-2 cells, however, in contrast to Caco-2, no P-gp transport activity could be detected in transfected HEC-1A cells. The simplest

explanation is that P-gp was not correctly folded, however, this result may also reflect differences in the nature of intestinal and cervicovaginal epithelial cells. Several tissue dependent post-translational modifications of transporter proteins may be critical for transporter activity [288]. Moreover, the vaginal epithelium, in contrast to the intestinal mucosa, is not regularly exposed to xenobiotics, especially in the form of ingested drugs. The continuous efflux activity of these transporters that prevent the absorption of foreign material into the bloodstream may result in a state of higher activation of transporters in intestinal derived cells such as Caco-2 and MDCK lines compared with HEC-1A.

The findings from the work described here have some implications for vaginal administration of ARV-based microbicides. TFV can readily access sub-epithelial cells by paracellular diffusion. Although the proportion that diffuses is relatively low (approximately 2% of total input in these studies), a higher sub-epithelium dose can be achieved simply by increasing the dose of TFV with no requirement to include inhibitors of specific efflux transporters. Moreover, potential “loss” of drug in the epithelium does not occur as the proportion of TFV that enters epithelial cells is very low. For DRV, transcellular diffusion is relatively efficient again with low levels of drug remaining in the intracellular compartment. For higher doses solubilising excipients may be required although inclusion of such excipients has been shown to decrease permeability by increasing the affinity of the drug for the donor compartment [136]. DPV is readily taken up by the model epithelium but remains cell associated. Physiologically, it may transfer to sub-epithelial cells that make close contact at the basolateral surface or be transferred as a complex with proteins or other solubilising moieties. DPV may also partition directly into the HIV membrane during transmission through the mucosal epithelium. The results of the RING and ASPIRE phase III trials of DPV formulated as intravaginal rings confirm that effective levels of drug permeate the epithelium to access sub-epithelial cells [6].

5.4.1 Limitations

Cytotoxicity assays were not undertaken to determine cell viability in the drug permeability assays although TEER values were recorded to assess the barrier properties of the cell cultures. Various studies have demonstrated strong correlation of TEER with cell viability [289-291] with some suggesting that TEER may be a

more sensitive measure of cell cytoxicity than conventional assays [292]. Nonetheless, in future work some determination of cellular cytotoxicity in parallel to TEER measurement should be performed.

No effect of PAMP stimulation of HEC-1A cells on drug permeability was evident. In view of the relatively low levels of inflammatory cytokines and chemokines (as discussed in Chapter 4), direct addition of cytokines and chemokines at higher concentrations should be considered in further work. In addition, since the effects of IL-8 may be indirect and mediated by activated macrophages or dendritic cells, co-culture with these cell types should be investigated.

Expression of P-gp following transfection of HEC-1A cells was demonstrated by western blotting, however, P-gp activity was not detected in transport studies. Transfection of other cells (both epithelial and non-epithelial) should be performed to investigate whether activity is influenced by the cellular environment.

Chapter 6 Investigation of alternative cellular and tissue-based models for drug permeability analysis

6.1 Aim

To compare drug permeability in different models including *ex vivo* epithelial tissue.

6.2 Introduction

HEC-1A cell layers provide a useful model to determine drug transport across the cervicovaginal epithelium as discussed in Chapters 4 and 5. Nonetheless, alternative approaches have been used to determine drug permeability across tissue. *In vitro* models have been developed that mimic the vaginal epithelium including three-dimensional (3D) organotypic tissue and *ex vivo* (animal or human) excised mucosae.

The work described in this chapter assesses drug permeability using one *in vitro* model and one *ex vivo* model. The EpiVaginal™ model developed by MatTek Corporation (Ashland, MA, USA), is an organotypic 3D vaginal tissue model formed by culture of primary epithelial cells with or without fibroblasts from women undergoing hysterectomy [293]. The second model is to use excised vaginal tissue from adult rats and macaques. Tissues are mounted on custom-made Ussing diffusion chambers (Figure 6.2).

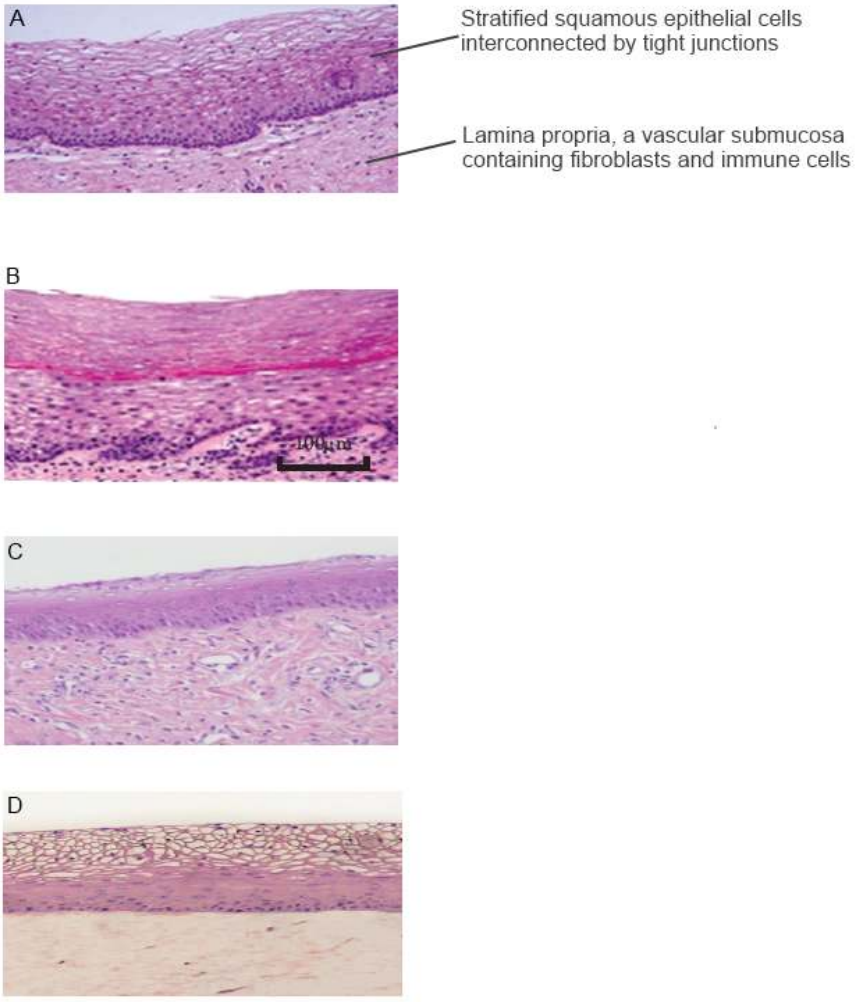

Figure 6.1 Histology of the vaginal epithelium. Comparison of the morphological characteristics of the vaginal epithelium between **(A)** Human **(B)** Macaque **(C)** Rat **(D)** MatTek Epivagina™. All tissue types represent an epithelial layer resting on a submucosal lamina propria. Images (A,B,D) [294] and image **(C)** [295].

6.2.1 The MatTek EpiVaginal™ tissue model

Although this primary cell-based model was initially developed for vaginal irritation assays and vaginal pathogen transmission assays such as HIV transmission, various reports have described the use of the EpiVaginal™ tissues for assessing drug permeability [296, 297]. The EpiVaginal™ models investigated in this study were the VEC-100-PT (partial thickness), containing epithelial cells only and the VEC-100-FT (full thickness) that also includes primary fibroblasts as well as the primary epithelial cells. Previous studies reported the use of the VEC model for

permeability studies [296, 297]), presumably due to the morphological similarities to the epithelial layer of the cervicovaginal epithelium. The VEC Epivaginal™ model is formed by culture of primary ectocervical epithelial cells in a process that involves exposure at the air-liquid interface to produce a non-keratinised, multi-layered epithelium that can be used in a dual chamber system [293, 298].

6.2.2 *Ex vivo* models and Ussing diffusion chambers

An alternative approach to determine drug permeability, involves the use of mucosal tissues excised from animals which may better represent *in vivo* tissue by preserving native tissue architecture and normal healthy tissue processes. Typical permeability experiments involve mounting of the excised cervicovaginal tissue between two Ussing chambers (Figure 6.2) which is especially designed to provide exposure to a small area of the animal tissue (0.2 cm^2). The rate of permeability will be directly correlated to the surface area of tissue exposed to media. The diffusion system is composed of two glass chambers (apical and basolateral) that are separated by the mounted tissue. A continuous supply of oxygen and carbon dioxide is supplied to the tissue. Drug test solutions are added to the donor chamber and samples are taken for both chambers subsequently. After the final time point sampling, the tissue can be collected to determine tissue accumulation of drug. Similar to the permeability studies in Chapter 5, the data acceptance criteria for these experiments were: flux linearity r^2 must be >0.98 and total drug recovery must be within the range of 80-120% of the original quantity added to the donor chamber.

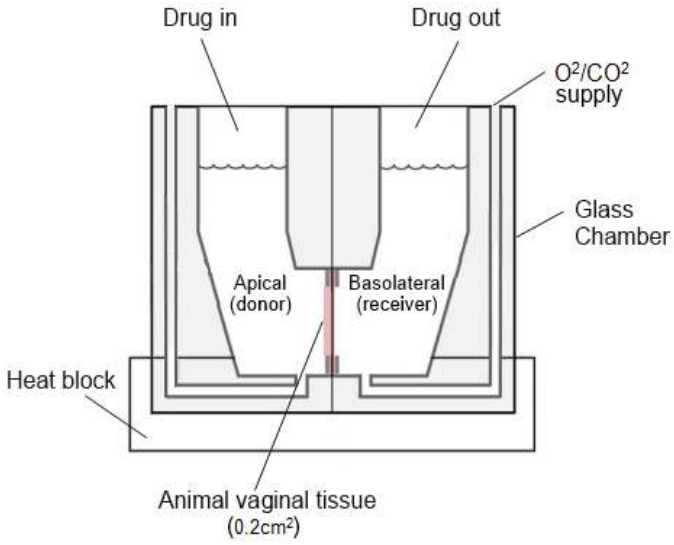

Figure 6.2 Schematic representation of a small piece of tissue mounted between Ussing chambers. The Ussing chamber system includes a heat block in which the chambers are mounted on as well as tubing connectors for the O_2 and CO_2 supply into the test solution and across the tissue.

6.2.3 Drug transporter expression in tissue-based models

Ideally, *in vitro* models for drug permeability should be well characterised with regard to expression of drug transporters. No studies that characterise drug transporters in the rat vagina appear to have been reported. In macaques, expression of the efflux transporters P-gp, MRP4 and BCRP has been demonstrated by quantitative PCR and by immunohistochemistry in endocervical, ectocervical and vaginal tissues [151]. A more systematic study of drug transporter expression in the macaque was performed as part of the collaborative MOTIF project and demonstrated a similar pattern of expression compared with human cervicovaginal tissue although some differences including expression of CNT2 and ENT2 in macaque but not human tissue (K. Hijazi, personal communication, unpublished data). Since the data from Chapter 5 demonstrate that permeability of the drugs investigated in this thesis, in vaginal tissue may be transporter-independent, full characterisation of transporters in the models used here may be of less importance. Nonetheless, characterisation of transporter expression in the Epivaginal™ models was performed as were permeability assays in rat and macaque tissue.

6.3 Results

6.3.1 Quantitative mRNA analyses of expression of transporters in the EpiVaginal™ model

Permeability of DRV and TFV was measured in the Epivaginal™ model. Before these studies, expression of drug transporters was investigated in the VEC-100-PT and VEC-100-FT primary cell-based models for comparison with expression profiles of HEC-1A cells and human vaginal tissue. Total RNA from each model was converted to cDNA and levels of mRNA encoding 9 ABC efflux transporters and 11 uptake drug transporters were assessed by quantitative PCR using the TaqMan PCR Array Human Drug Transporters system. The data presented in Table 6.1 are compared with data from previous studies of expression in HEC-1A cells and human vaginal tissue [206]. Expression profiles in VEC-100-PT and VEC-100-FT were similar apart from lower expression of OATP-D in the VEC-100-PT model. Expression of ABC and SLC transporters in both EpiVaginal™ models was also similar to that in HEC-1A cells [206] with 15 transporters in common. Three transporters (BCRP, PEPT1, and CNT3) were expressed in Epivaginal™ models but not in HEC-1A cells. Conversely, three transporters (MRP6, OATP8, and OCT1) were expressed only in HEC-1A cells.

Comparison with the data from human vaginal tissue indicates that for both models there are a few significant differences in transporter expression compared with human cervicovaginal tissue. Epivaginal™ cultures of primary cells more closely resemble human tissue with regard to expression of BCRP, PEPT1 and CNT3 and similar levels of expression of MRP3, MRP4 and MCT1. In contrast, the HEC-1A model is more suitable for assessing permeability of drugs that are substrates for MRP6, OATP8 and OCT1 transporters.

Transporter	Gene expression level					
	Cell-based models			Tissues		
	HEC-1A [206]	VEC-100-PT	VEC-100-FT	Ectocervix [206]	Endocervix [206]	Vagina [206]
P-gp	+	+	+	++	+	++
BCRP	-	+	+	++	+	++
MRP1	++	++	++	++	+	++
MRP2	+	+	+	+	-	-
MRP3	++	+	+	+	+	-
MRP4	++	+	+	+	+	-
MRP5	++	++	++	++	++	++
MRP6	+	-	-	+	-	-
MRP7	+	++	++	+	+	++
OATPD	+	+	++	+	+	++
OATPE	++	++	++	+	+	++
OATP8	+	-	-	+	+	-
ENT1	++	+	++	++	++	++
ENT2	++	+	+	+	-	-
OCT1	+	-	-	+	-	-
OCT3	+	+	+	++	+	++
PEPT1	-	++	++	+	+	++
PEPT2	+	++	++	+	++	-
CNT3	-	++	++	+	+	-
MCT1	+	++	++	++	+	+

Table 6.1 Expression of drug transporter genes. ABC and SLC drug transporters in VEC-100 partial (PT) and full thickness (FT) MatTek Epivaginal™ models and as reported previously [206] for the HEC-1A cell line and human vaginal tissue. Data were calculated as Ct(control gene)/Ct(target gene). Values obtained correspond to ratio ranges of <0.65 as -; 0.65-0.80 as +, 0.81-1 as ++ and >1 as +++. n=1 (3 technical repeats).

6.3.2 MatTek Epivaginal™ barrier properties

Drug permeability was measured in the EpiVaginal™ VEC-100-PT model of vaginal epithelium only. All assays were performed on the day after receiving the tissue, allowing for overnight recovery by incubation in recovery culture medium (supplied by MatTek) at 37°C. The barrier properties of the model epithelium were assessed by bi-directional permeability of the paracellular tracer [^{3}H]mannitol as described in Chapter 4. As shown in Figure 6.3. paracellular [^{3}H]mannitol fluxes across the

EpiVaginal™ were similar in both absorptive and secretory directions with P_{app} values of 3-5x10^{-6} cm/s. In control inserts with no cells, P_{app} values were 10.8x10^{-6} cm/s (data not shown). Thus the EpiVaginal™ model has some barrier function although the P_{app} values for mannitol in the A-B direction were 4-5x10^{-6} cm/s which were higher than those observed in the HEC-1A model (2-4x10^{-6}), (Chapter 4), indicating a more leaky barrier epithelium.

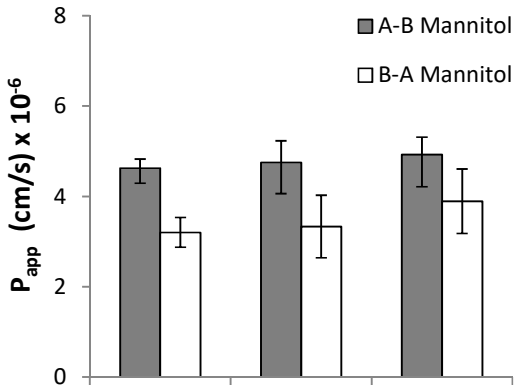

Figure 6.3 Bi-directional permeability of [^{3}H]mannitol across the MatTek Epivaginal™ primary cell-based model. Assays were conducted at 37°C over a 2 hour period. Data represent mean ± S.D. n=1 (3 technical repeats).

6.3.3 Effect of PAMP stimulation in the EpiVagina™ model

To investigate the potential for modelling inflammation in the EpiVaginal™ model, cultures were screened against a panel of 5 PAMPs that stimulate different TLRs to identify those that most potently stimulated production of pro-inflammatory cytokines. Medium from both apical and basolateral compartments was collected and analysed by Multiplex bead based immunoassay to determine the concentrations of 6 pro-inflammatory cytokines (Figure 6.4). Strikingly, in unstimulated Epivaginal™ cultures, high levels of IL-1α, IL-1β and IL-8 were measured in the culture medium. The concentration of IL-8 was comparable to that of Poly I:C stimulated HEC-1A cultures as reported in Chapter 5 while the concentrations of IL-1α and IL-1β were much higher than those of Poly I:C stimulated HEC-1A cultures. The high concentrations of these cytokines may account for reduced barrier function of the Epivaginal™ model compared with HEC-1A dual chamber cultures. Stimulation with the TLR5 agonist, flagellin (FLA) and the TLR2/6 agonist FSL-1 resulted in significantly increased secretion of GM-CSF and

TNF-α. A small increase in IL-6 production was also evident following stimulation with FSL-1 but these values are at least 10 fold lower than those of stimulated HEC-1A cultures. LPS, LTA and imiquimod were not screened; nonetheless when exposed to HEC-1A cell layers they did not stimulate any TLRs (Chapter 4.3.4).

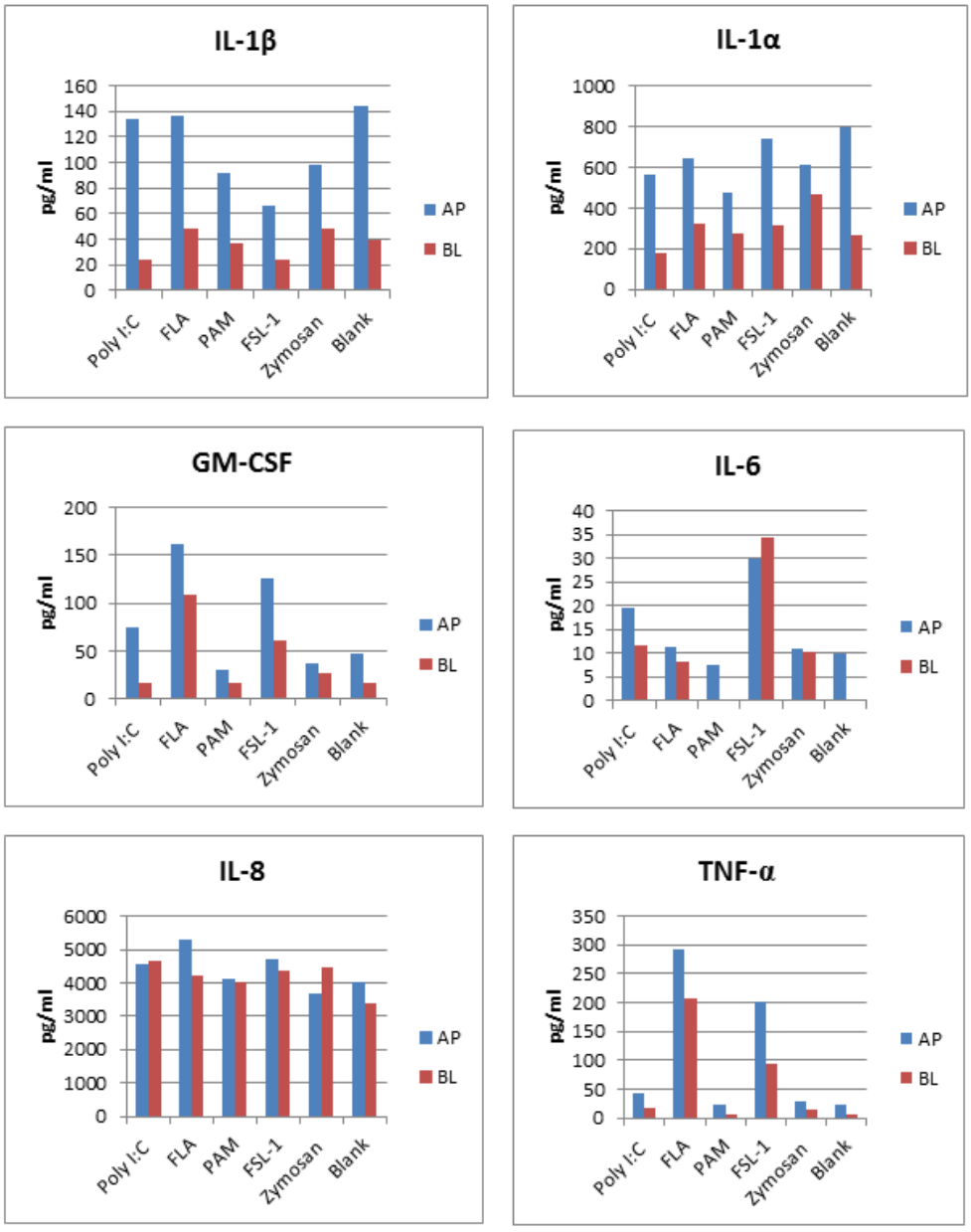

Figure 6.4 PAMP stimulation of pro-inflammatory cytokines in the Epivaginal™ model. Epivaginal™ tissues were stimulated with each PAMP at a single concentration (50 µg/ml) and production of selected cytokines was determined by Multiplex bead immunoassay. n=1. (2 technical repeats).

6.3.4 Bi-directional permeability of Tenofovir (TFV) through MatTek Epivaginal™ model epithelium

Permeability of the hydrophilic ARV drug TFV was assessed in the Epivaginal™ model over a 2 hour period. [^{3}H]mannitol was included as a marker for integrity of the epithelial barrier. Bi-directional apparent permeability (P_{app}) values determined for 10 µM [^{14}C]TFV across the EpiVagina™ are shown in Figure 6.5A. P_{app} values (2-4x10^{-6} cm/s) were similar in both A-B and B-A directions. The rate of [^{14}C]TFV flux across the EpiVaginal™ was slightly lower than that measured for the paracellular tracer molecule [^{3}H]mannitol 3-5x10^{-6} cm/s (Figure 6.3) which was measured in parallel in the same experiment.

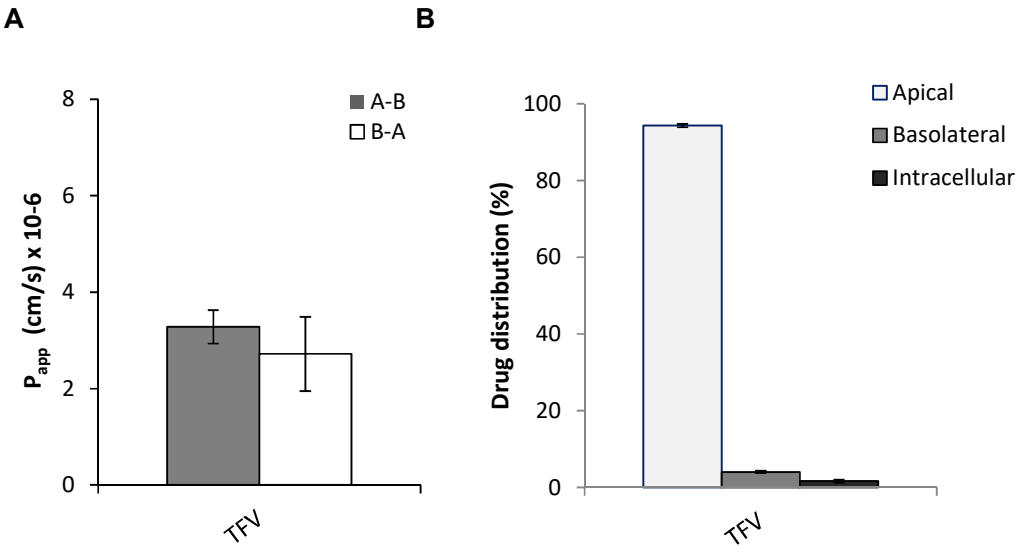

Figure 6.5 TFV permeability and distribution in the EpiVaginal™ model. (A) A-B and B-A apparent permeability (P_{app}) of TFV across the EpiVagina™. **(B)** % distribution of TFV in each compartment of the EpiVagina™ "transwell" system. Data represent mean ± S.D. n=1 (3 technical repeats).

The distribution of TFV at the end of the assay was determined in the A-B direction within the apical, basolateral and intracellular compartments of the "'transwell' and is shown in Figure 6.5B. The highest proportion of the drug was present in the apical compartment (approximately 94%), 4% was detected in the basolateral compartment and 1-2% was detected intracellularly. Additionally, the ER value of approximately 0.8 (Table 6.2) for TFV confirmed the transporter-independent permeability of TFV in this system.

	P_{app} ($x10^{-6}$ cm/s)		Efflux ratio
	A-B	B-A	$P_{app\ (B-A)}/P_{app\ (A-B)}$
TFV (10μM)	3.28 (1.21)	2.72 (0.50)	0.83

Table 6.2 Efflux ratio (ER) of TFV. Data represent mean ± (S.D.), n=1 (3 technical repeats).

6.3.5 Bi-directional permeability of Darunavir (DRV) through MatTek Epivaginal™ model epithelium

Permeability of DRV was also assessed in the EpiVaginal™ model. DRV was solubilised in the transport buffer containing 0.01% (v/v) DMSO. Apparent permeability (P_{app}) values for [^{14}C]DRV 10 μM are shown in Figure 6.6A. As for TFV, there were no significant (P ≥ 0.05, ANOVA) differences in P_{app} values determined for A-B and B-A directions. Average P_{app} values were in the range 2-4$x10^{-6}$ cm/s and were comparable to those for mannitol. These values were lower than those determined in the HEC-1A system as reported in Chapter 5. The P_{app} [^{3}H]mannitol (3-5$x10^{-6}$) was measured in parallel in the same experiment (Figure 6.3).

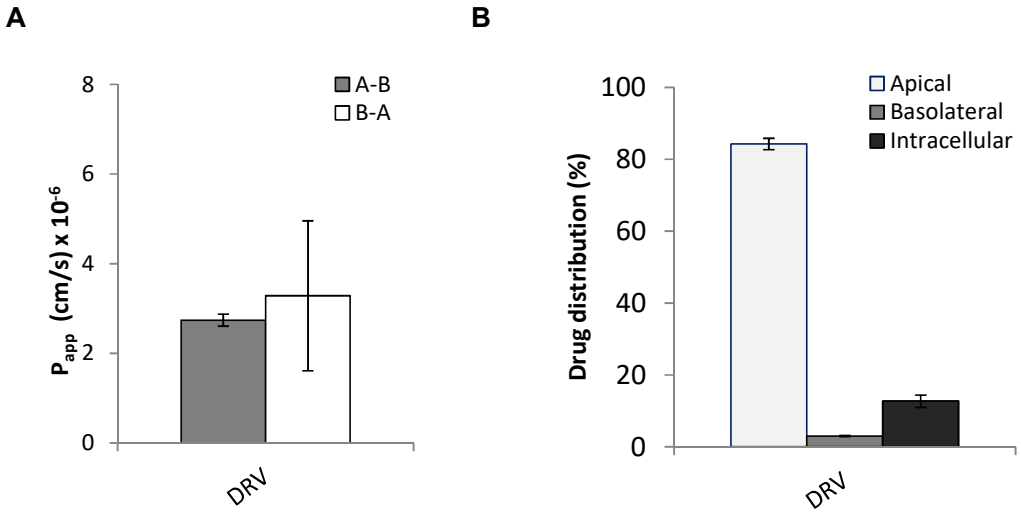

Figure 6.6 Figure 6.6 DRV permeability and distribution in the EpiVaginal™ model. (A) A-B and B-A apparent permeability (P_{app}) of DRV across the EpiVagina™. **(B)** % distribution of DRV in each compartment of the EpiVagina™ "transwell" system. Data represent mean ± S.D. n=1 (3 technical repeats).

The distribution of DRV was determined in the absorptive (A-B) direction of transport within the apical, basolateral and intracellular compartments of the

EpiVagina™ “transwell” system. The highest amount of DRV was in the apical (donor) compartment (approximately 84%), 3% was detected in the basolateral compartment and 13% was detected intracellularly.

	P_{app} ($x10^{-6}$ cm/s)		Efflux ratio
	A-B	B-A	$P_{app\ (B-A)}/P_{app\ (A-B)}$
DRV (10μM)	2.74 (0.14)	3.28 (1.67)	1.20

Table 6.3 Efflux ratio (ER) of DRV. Data represent mean ± (S.D.), n=1 (3 technical repeats).

Moreover, the efflux ratio value of approximately 1.20 (Table 6.3) for DRV also confirmed the transporter-independent permeability of DRV through EpiVaginal™ tissue.

6.3.6 Permeability of Darunavir (DRV) through Rat cervicovaginal tissue

Permeability of DRV was also assessed in *ex vivo* rat tissue. Because quantities of tissue were limited, these studies could be performed with one drug only. DRV was selected due to its reported affinity for the efflux transporter P-gp, as observed in the Caco-2 model (discussed in Chapter 5). Bi-directional permeability of DRV was assessed across rat cervicovaginal epithelium. Excised vaginal tissues from two adult female rats were used as tissue-based models to determine DRV permeability. Excised tissue was stripped of any muscle layers prior to placement between the apical (donor) and receiver glass chambers of the Ussing system. Tissue from a single rat was sufficient for 4 sets of chambers. This allowed analyses in duplicate of both A-B and B-permeability. Samples were taken over a 1 hour period at 37°C. Tables 6.4 and 6.5 show the A-B and B-A permeability of DRV through individual segments of cervicovaginal tissue from 2 rats.

There was considerable variability in the data. [^{3}H]mannitol P_{app} values ranged between 2-8$x10^{-6}$ cm/s (Tables 6.4 and 6.5) in tissues from the same or different animals. Results are shown as individual data rather than grouping and averaging data from each animal. Increased [^{3}H]mannitol P_{app} provided a correlation with

[^{14}C]DRV P_{app}, as [^{14}C]DRV P_{app} also increased. This was observed in rat 1 tissues 2 and 3 (Table 6.4) and rat 2 tissues 1, 3 and 4 (Table 6.5).

Rat 1	A-B			Drug distribution (%)	
	Tissue 1	Tissue 2		Tissue 1	Tissue 2
P_{app} Mannitol	3.80	7.95	Apical	97.40	94.15
			Basolateral	0.80	3.61
			Tissue	1.80	2.24
P_{app} DRV	2.14	10.01	Apical	91.76	88.89
			Basolateral	2.33	5.36
			Tissue	5.90	5.75
	Papp B-A			% Drug distribution	
	Tissue 3	Tissue 4		Tissue 3	Tissue 4
P_{app} Mannitol	7.63	-	Apical	3.05	-
			Basolateral	95.10	-
			Tissue	1.85	-
P_{app} DRV	8.10	-	Apical	3.37	-
			Basolateral	90.38	-
			Tissue	6.25	-

Table 6.4 DRV permeability across rat cervicovaginal tissue (Rat 1). A-B/B-A P_{app} for Mannitol and DRV as well as drug distribution is presented. Tissues 1 and 2 were used to assess A-B permeability and tissue 3 was used for B-A permeability. Tissue 4 data did not comply with data acceptance criteria as drug recovery was <80%. Assay conducted at 37°C over a 1 hour period. Data represent n=1 (2 technical repeats).

Rat 2	A-B			Drug distribution (%)	
	Tissue 1	Tissue 2		Tissue 1	Tissue 2
P_{app} Mannitol	5.54	2.19	Apical	95.59	98.45
			Basolateral	2.22	0.75
			Tissue	2.19	0.80
P_{app} DRV	6.34	1.86	Apical	92.16	96.49
			Basolateral	1.79	0.52
			Tissue	6.05	2.98
	B-A			% Drug distribution	
	Tissue 3	Tissue 4		Tissue 3	Tissue 4
P_{app} Mannitol	5.10	7.99	Apical	1.66	2.66
			Basolateral	97.68	96.68
			Tissue	0.66	0.66
P_{app} DRV	4.45	7.61	Apical	1.92	3.52
			Basolateral	95.03	94.03
			Tissue	3.05	2.45

Table 6.5 DRV permeability across rat cervicovaginal tissue (Rat 2). A-B/B-A P_{app} for [^{3}H]mannitol and [^{14}C]DRV as well as drug distribution is shown. Tissues 1 and 2 were used to assess A-B permeability and tissues 3 and 4 were used for B-A permeability. Assay conducted at 37°C over a 1 hour period. Data represent n=1 (2 technical repeats).

In these tissues the epithelia presented a leaky barrier as [^{3}H]mannitol P_{app} values were in the ranges of 5-7x10^{-6} cm/s and likely resulted in an increased rate of [^{14}C]DRV flux (4-10x10^{-6} cm/s). In rat 1 tissue 1 and rat 2 tissue 2 (Table 6.4), mannitol flux was more restricted as [^{3}H]mannitol P_{app} values ranged between 2-4x10^{-6} cm/s, and [^{14}C]DRV flux was slower with P_{app} values of 1-2x10^{-6} cm/s. The distribution of DRV in the A-B and B-A directions was determined in each of the compartments of the individual Ussing chambers (Tables 6.4 and 6.5). For the A-B direction approximately 88-92% of DRV remained in the apical side of the chamber, 0.5-5% permeated into the basolateral side and 3-6% accumulated within the tissue. For the B-A direction approximately 90-95% remained in the basolateral side, 1.5-3.5% permeated into the apical and 2-6% accumulated within the tissue. DRV tissue accumulation amongst all 7 tissue segments averaged 4.63±1.71%.

6.3.7 Darunavir (DRV) accumulation in Macaque cervicovaginal tissue

DRV permeability was also assessed in *ex vivo* macaque cervicovaginal epithelium using the Ussing system. This work was performed at the Commissariat à l'énergie atomique et aux énergies alternatives, Fontenay-aux-roses, France. Cervicovaginal tissue was separated, segmented and stripped of any muscle layers prior to placement between the apical and basolateral glass chambers of the Ussing system. Tissue from a single macaque was sufficient for 6 sets of chambers allowing triplicate determinations of both A-B and B-Apermeability. Two independent experiments were performed with tissues from 2 animals. Samples were taken at T=0 and T=1 hour from the donor compartments and at 15 minute intervals over 1 hour from the receiver compartments. Radiolabelled drug could not be used for these experiments and drug concentrations were determined by LC-MS. Levels of drug in the receiver compartments have yet to be quantified. The decrease (%) in total drug over the 1 hour period of the assay in the donor compartments is shown in Table 6.6 together with the level of drug (% of total) in tissue.

Experiment	A-B		B-A	
	*Donor Decrease (%)	**Tissue (%)	*Donor Decrease (%)	**Tissue (%)
1	7.1 ± 0.44	2.6 ± 0.3	17.0 ± 2.8	0.95 ± 0.35
2	16.6 ± 2.4	2.4 ± 0.4	35.6 ± 0.5	0.83 ± 0.5

Table 6.6 Permeability of DRV across macaque cervical vaginal tissue.
*Decrease in total drug (% ± SD) in donor chamber over 1 hour
**Total drug in tissue at 1 hour (% ± SD) n=1 (2 technical repeats).

Although there is considerable variation in the quantity of drug leaving the donor chamber between the experiments, in both experiments the quantity of drug transferred from the basal donor chamber is 2 fold higher than the quantity transferred from the apical donor chamber. Together with the differences between the level of tissue associated drug, these data suggest that DRV may be effluxed at the apical surface of macaque vaginal epithelium.

6.4 Discussion

The main findings from the experiments described above are that TFV and DRV permeate across the primary cell-based MatTek Epivaginal™ model in a

transporter-independent-manner, similar to observations in the HEC-1A model (as described in Chapter 5). TFV permeates across the EpiVagina™ via paracellular diffusion, while DRV permeates by transcellular diffusion. Quantitative mRNA analyses indicated that the expression profile of major drug transporters, including BCRP, in the Epivaginal™ model was similar to that of human cervicovaginal tissue. This model may therefore be of use in measuring permeability of drugs that are substrates for the transporters identified here. As discussed in Chapter 5, mRNA analyses may not correlate absolutely with functional protein expression and further experiments are required to confirm expression in the Epivaginal™ model.

P_{app} values for mannitol in the Epivaginal™ system were consistently higher than those observed in HEC-1A dual compartment cultures and at least in the A-B direction were higher than 4 x 10^{-6} cm/s. Similarly, permeability of TFV was slightly higher in this system than in the HEC-1A model and the proportion of drug in the receiver compartment following the assays was higher (4% compared with 2-3%). The geometry of the Epivaginal™ insert did not allow measurement of TEER with the available electrode. Nonetheless, these findings together with observations of cell detachment in some of the Epivaginal™ cultures suggest that the epithelial barrier in this model is leakier than that of the HEC-1A model. In contrast to the findings for TFV, the bi-directional P_{app} coefficient of 2-3.5x10^{-6} cm/s for DRV is 2-3 fold less than that observed in HEC-1A. However, A-B intracellular accumulation of DRV was higher (approximately 13%) and basolateral accumulation lower (3%) compared with HEC-1A cultures. Thus, DRV does not permeate as freely as in the HEC-1A model. The EpiVagina™ presents a thicker, multi-layered epithelial morphology (approximately 20 cells thick) compared to the HEC-1A cell layers (1-4 cells thick) as identified in chapter 4. Therefore, DRV may partition and accumulate within the thicker epithelial layer of the EpiVagina™.

Experiments to model inflammation in Epivaginal™ cultures, by stimulation with PAMPS, indicated that unstimulated cultures produced levels of IL-8 that were 10-fold higher than those reported to disrupt tight junctions in a human colonic cell line model [275]. This may be at least a partial explanation for the relatively high permeability of mannitol. Although other cytokines were also detected in the unstimulated cultures, the concentrations were significantly lower than those reported previously to be required for tight junction disruption [274, 299].

Permeability studies of DRV across rat vaginal tissue were performed to investigate correlation between cell-based models and tissue. P_{app} values for mannitol varied in the range 2-8x10^{-6} cm/s suggesting some disruption in barrier function. Out of 8 tissue segments excised from 2 different rats, 7 tissues provided acceptable drug recovery values and P_{app} values for mannitol were below 4x10^{-6} cm/s in 2 tissues. However, there are currently no reported P_{app} values for mannitol across vaginal tissue to compare with the results reported here. Accumulation of DRV within tissue is consistent with transcellular diffusion. Although the range is wide, the average P_{app} values for DRV lie between those determined in the HEC-1A and Epivaginal™ models. Further repeats with increased consistency of tissue handling are required to provide a more accurate measurement of permeability.

Similar permeability assays were performed with macaque vaginal tissue. In these experiments, radiolabelled DRV could not be used and analyses of drug concentrations in receiver chambers are incomplete. Differences in the levels of drug remaining in apical and basolateral chambers, however, suggest that DRV may be effluxed at the apical surface in these tissues.

The data presented in this chapter suggests that primary cell-based and tissue-based models can provide an alternative screening method for drug permeability. Preliminary analyses of the data from macaque tissue suggest that DRV may be effluxed at the apical surface. Similar activity in humans could potentially limit uptake of DRV. This activity was not evident in the Epivaginal™ and HEC-1A models. However, a clear drawback of this approach is the limited availability of tissue. Additionally, the stripping of the muscle layer from the animal tissue is both extremely challenging and time consuming, adding to the possibility of physically disrupting the tissue integrity when mounted on the Ussing chamber.

The attraction of the Epivaginal™ model is that primary cells are cultured which may more closely resemble normal epithelium. However, at least in the cultures examined in this study, the barrier properties of the epithelium appear to be sub-optimal. This together with the expense and inconvenience of relying on external providers, emphasises the advantages of the HEC-1A model.

6.4.1 Limitations

The main limitations here involve the low number of repeat experiments undertaken with rat and macaque tissue. While data presented here is preliminary, repeated permeability studies need to be undertaken. Lack of animal availability (especially Macaque) was the main reason for the low experimental repeats. However, although repeats with Macaques would be difficult, repeated experiments with rats would be achievable. Variability in TFV and DRV permeability data between rat vaginal tissue segments from the same animal under the same conditions was also observed when determining TFV and DRV permeability. This discrepancy in values may be due to the difficulty involved with stripping the muscle layer from epithelium, producing differing tissue thicknesses.

Chapter 7 Final Discussion

7.1 Study Outcomes

The main outcomes from this study were:

1. Development and optimisation of a reproducible *in vitro* model of vaginal barrier epithelium, using the HEC-1A cell line, to investigate drug permeability.
2. Determination of the drug transporter-independent permeability properties of 3 ARVs, namely, TFV, DRV and DPV.
3. Demonstration of the potential for *in vitro* modelling of inflammation in dual chamber cultures of HEC-1A cells.
4. Comparison of the HEC-1A model with the commercially available Epivaginal™ model epithelium and *ex vivo* tissue models.

7.1.2 The HEC-1A model of the vaginal epithelium

The study described in chapter 4 builds on previous work showing that HEC-1A, in contrast to several other cervicovaginal epithelial cell lines, forms a barrier epithelium in dual chamber cultures. The barrier results from the formation of intercellular tight junctions and is demonstrated by high TEER values [222]. Tight junction formation by epithelial cells is fundamental for drug permeability, as it discriminates the paracellular and transcellular diffusion pathways. HEC-1A cells reproducibly form a barrier epithelium after 6 days in culture that remains stable until day 10, providing a 4 day experimental window. The relatively short period to reach the maximum TEER compares favourably with the 21-28 day culture period necessary for the Caco-2 intestinal model epithelium [233]. The maximum TEER value for the HEC-1A model epithelium (approximately 250 $\Omega x cm^2$) is noticeably lower than the reported maximum for Caco-2 cells (1000 $\Omega x cm^2$) [236]. Additionally, the lowest mannitol apparent permeability coefficient for HEC-1A ($2x10^{-6}$ cm/s) is considerably higher (10-fold) compared to that reported for Caco-2 ($1.2 \pm 0.5x10^{-7}$ cm/s) [233], indicating that Caco-2 cells form a tighter epithelial cell layer. This tightness may reflect the functional differences in epithelia as the intestine is continuously involved in nutrient absorption and rigorously controls movement of

molecules across the intestine. Importantly, drug transporter expression in HEC-1A cultures resembles that of human vaginal tissue and therefore this model may be regarded as physiologically relevant for the investigation of drug permeability. The main difference from human tissue is the lack of expression of the efflux transporters P-gp and BCRP in HEC-1A cells. Although expression of P-gp was indicated by mRNA analyses [148], P-gp could not be detected by Western blotting and no effects were evident on the transport of the P-gp substrate digoxin across HEC-1A layers. Attempts were made by transfection to express P-gp in HEC-1A cells. Although P-gp expression was demonstrated in transfected cells by Western blotting, at a level similar to the endogenous expression in Caco-2 cells, no efflux activity was demonstrated by HEC-1A for the P-gp substrate digoxin. Lack of P-gp activity may again be related to the functional differences in epithelia as the cervicovaginal epithelia, in contrast to the intestinal epithelia, is not regularly exposed to xenobiotics. Cell lines such as Caco-2 that are derived from intestine may reflect the increased transporter activity of this tissue.

Further development of this model as a useful screening tool for vaginal drug permeability studies could include determination of the requirements for functional expression of P-gp. Culture conditions may be altered to increase P-gp activity. Thus *in vitro* studies with tumour cells show that P-gp activity was increased (more than 2-fold) at acidic pH (pH 6.6) with no increase in P-gp expression [300, 301]. P-gp activity was also increased in 3-dimensional cultures of a human prostate cancer cell line by incubation at elevated temperature (42 °C) by a mechanism that involves activation of p38 mitogen activated protein kinase [302]. Similarly, expression and activation of other transporters including BCRP warrants further investigation.

The permeability studies described in this thesis were performed at neutral pH initially, to determine the transporter activity of HEC-1A in the optimum culture conditions that they are maintained and cultured in. The healthy vaginal pH is 4.0 $\pm$ 0.5 due largely to production of lactic acid by lactobacilli [303]. Further permeability studies should therefore be performed at this pH in the apical compartment, however, low pH was shown to decrease HEC-1A TEER values in preliminary experiments.

7.1.3 Permeability properties of TFV, DRV and DPV

TFV, DRV and DPV showed transporter-independent permeability in the models used in this study (as described in Chapters 5 and 6). Apparent permeability values and drug intracellular accumulation for each drug reflected the physiochemical properties of each drug. TFV, a negatively charged hydrophilic molecule slowly permeates via the paracellular route through pores of the tight junctions with negligible intracellular accumulation. In contrast, DPV is a highly hydrophobic, lipophilic molecule that rapidly permeates via transcellular passive diffusion with high intracellular accumulation. DRV is less lipophilic and efficiently permeates via transcellular passive diffusion with low intracellular accumulation.

Further work to increase TFV permeability across HEC-1A cell layers may involve increasing initial loading concentrations. DRV permeability is generally efficient in the presence of cells that are either not expressing P-gp or contain inactivated P-gp. For DPV, solubilising excipients may be used in the basolateral compartment in attempts to further draw across intracellularly bound DPV. Excipients that increase solubility of DPV may however decrease permeability when present in the donor compartment by reducing partitioning of the drug into cell membrane compartments [136]. Although highly lipophilic drugs may be substrates for transporters, the effect may be limited as drug uptake or efflux is likely to be dominated by transcellular diffusion. Screening of other drugs in this model would be useful to determine if the drug transporters (described in Chapter 4) can influence drug disposition.

7.1.4 Modelling of vaginal inflammation

The stimulation of HEC-1A with PAMPS provided a model to investigate drug permeability under conditions reflective of an inflammatory response (as described in Chapter 5). The use of PAMPS here provided a “more physiological” representation compared to the direct application of inflammatory cytokines to HEC-1A cell layers. Stimulation by this method may better mimic the expression of inflammatory molecules in conditions such as bacterial vaginosis or STDs. Stimulation of HEC-1A with the TLR 3 ligand Poly I:C and the TLR 5 ligand Flagellin, induced production of some inflammatory cytokines. In particular, IL-8 and IL-6 were detected at concentrations comparable to those reported as sufficient for disruption of tight junctions. GM-CSF, IL-1 and TNF-α were also detected but at

concentrations lower than those required for tight junction disruption [274]. In this study, PAMP stimulation had no effect on TEER and P_{app} values for mannitol, TFV and DRV were unaffected. Further experiments should involve direct addition and titration of pro-inflammatory cytokines to investigate effects on TEER. Increasing the length of exposure to PAMPs may also provide a more pro-inflammatory environment.

7.1.5 Epivaginal™ model

Analyses of drug transporter expression in the Epivaginal™ primary cell-based model by mRNA quantitation indicated that the expression profile more closely resembled that of human tissue when compared with HEC-1A. A major difference in both models was lack of BCRP expression. TFV permeated across the EpiVaginal™ model with P_{app} values lower than mannitol and negligible intracellular drug accumulation. In comparison to HEC-1A, TFV and mannitol permeability was elevated, indicative of a leakier barrier. Nonetheless, the permeability was similar with regard to diffusion via the paracellular pathway and transporter-independency. In contrast, P_{app} values for DRV permeation across the EpiVaginal™ were lower and intracellular accumulation was elevated when compared to HEC-1A. The low P_{app} value for DRV was similar to that of TFV and mannitol, but may reflect higher DRV intracellular accumulation rather than paracellular diffusion. This may be due to the thicker cell layer of the EpiVaginal™ model compared to the thinner cell layer of the HEC-1A model. Nonetheless, to further determine the reliability of these results, the data reported should be repeated due to the limited number of replicates.

The main concern with the Epivaginal™ model is that the barrier properties of the culture were sub-optimal compared with the HEC-1A model as evidenced by increased P_{app} values for mannitol. Significant levels of IL-8 were also detected in unstimulated cultures which could compromise the integrity of the tight junctions. In contrast to the Epivaginal™ model, dual chamber cultures of HEC-1A cells provided a reproducible, convenient and relatively cost-effective alternative.

7.1.6 *Ex vivo* tissue models for drug permeability studies

Models involving mounted animal tissue in between Ussing chambers may mimic the vaginal tissue *in vivo* more closely. In these permeability studies using animal

vaginal tissue a few challenges were encountered. Removing the underlying rigid muscle layer prior to all experiments was difficult and time consuming. Tissue was maintained in ice cold Krebs solution however some proteolysis may still occur. Initial *ex vivo* experiments included the use of rat tissue; the limited availability of rat tissue allowed only preliminary studies to be performed. Permeability of DRV and mannitol only was investigated. DRV is a substrate for P-gp [214] and was therefore selected as a means of investigating activity of this transporter in tissue. DRV permeability was transporter-independent with fluctuating P_{app} values. This fluctuation was a result of unstable individual tissue barrier integrities reflected in variable and high mannitol P_{app} values. Low mannitol permeability resulted in low DRV permeability and high mannitol permeability resulted in high DRV permeability. DRV accumulation was also detected intracellularly. The lower permeability rate of DRV was similar to that observed in the EpiVagina™ and may be due to thicker tissue which restricts the permeability of drug to the basolateral compartment.

DRV permeability was also investigated using macaque vaginal tissues. The analyses of drug concentrations in the receiver compartment have not been completed but initial results suggest increased flow of drug in the basolateral to apical direction compared to the flow in the apical to basolateral direction. This may indicate efflux of DRV at the apical surface. The limitation of this work is that macaque tissue is less available than rat.

Ex vivo animal tissues are significantly different in anatomy and physiology from human tissues. The rat vaginal epithelium is constituted by pluristratified squamous cells which undergo prominent changes throughout the estrous cycle which results in the regular transitioning of thin and thick epithelial layers. These morphological changes have shown to impair the hydrophilic drug absorption during ovulation [304, 305]. Additionally, the pH of the rat vaginal epithelium is neutral [306]. Macaque vaginal physiology is more similar to human exhibiting epithelial thickness within the same ranges mentioned previously. One notable difference is that the vaginal pH in macaques is also near neutral, and may be due to the smaller colonization of lactobacilli [307]. Due to the physiological differences and limitations encountered by each of these models, the drug permeability assessments described here have not been as informative as those obtained from the HEC-1A

model. Further optimisation is needed with the drug transport studies described here.

7.2 Conclusions

The most significant finding from this study is that the HEC-1A cell line can be used as a model epithelium for the pre-clinical screening of drugs developed for vaginal application. Optimal culture conditions results in maximal TEER measurements and efficiently restricts mannitol permeability. After a short time of 6-10 days in culture on PE permeable supports, barrier integrity of HEC-1A reaches a stable plateau producing a 4 day experimental window. Furthermore, drug transporter expression as determined by mRNA and protein analyses shows significant similarity to that in human vaginal tissue.

To further determine the usefulness of this model, the permeability of 3 ARV drugs were investigated and their permeability properties assessed. While all three drugs show transporter-independent permeability, TFV permeates via paracellular diffusion and DRV and DPV permeate via transcellular diffusion. Additionally, intracellular drug accumulation analysis provided a further insight into the transport kinetics of the drugs. Intracellular accumulation was negligible for TFV, low for DRV and high for DPV, reflecting the physiochemical properties of these drugs. Investigation of double drug combinations shows no drug-drug interactions. The vaginal inflammation model, although limited, suggested some resistance to tight junction disruption as TEER values were no reduced, mannitol permeability remained stable and TFV and DRV permeability were unaffected. Lack of transporters present in HEC-1A compared to human tissue such as P-gp and BCRP may present limitations but use of plasmid or viral vectors may allow expression of selected transporters [160].

The second part of the thesis focused on the use of other *in vitro/ex vivo* systems to determine their suitability as alternative drug transport models. With many challenges and limitations, permeability properties for TFV and DRV were assessed in the primary cell-based MatTek EpiVaginal™ model while DRV permeability was assessed in the tissue-based *ex vivo* rat and macaque models. Permeability of TFV was similar to that detected in the HEC-1A model but differences in permeability for DRV in the EpiVagina™, rat and macaque were observed, although there was

varying DRV accumulation within all models. As discussed, this may due to the varying thicknesses between tissue and cell based models, requiring further optimisation. Additionally, high and fluctuating mannitol permeability identified in these systems suggest barrier properties are unstable.

7.2.1 Overall conclusions

Overall, the limitations for each chapter have been identified and acknowledged with solutions suggested for future experiments. In Chapter 4, improved experimental control measures and increases in experimental replicates were recognised. In Chapter 5, the need to include cytotoxicity studies as well as TEER is necessary to confirm cell viability, and P-gp transfections using other cell lines are appropriate to investigate the effect of P-gp activity by the cellular environment. Similar to Chapter 4, Chapter 6 also acknowledges the low repeat experiments that involved the use of animal tissue, with future focus on increasing experimental numbers especially with rat tissue. Additionally, the difficulty of individual tissue preparation is taken into consideration for these experiments.

Bibliography

1. UNAIDS, *Gap Report 2015.* http://www.unaids.org/sites/default/files/media_asset/UNAIDS_FactSheet_en.pdf, 2015. (Accessed 18/May/2017).

2. Abdool Karim, Q., et al., *Effectiveness and safety of tenofovir gel, an antiretroviral microbicide, for the prevention of HIV infection in women.* Science, 2010. **329**(5996): p. 1168-74.

3. Rees H, D.-M.S., Lombard C, et al., *FACTS 001 phase III trial of pericoital tenofovir 1% gel for HIV prevention in women CROI 2015: Presented at the Conference on Retroviruses and Opportunistic Infections* Abstract, 2015. (Accessed 18/May/2017).

4. CONRAD. *http://www.conrad.org/news-pressreleases-107.html* 2015. (Accessed 18/May/2017).

5. Palanee-Phillips, T., et al., *Characteristics of Women Enrolled into a Randomized Clinical Trial of Dapivirine Vaginal Ring for HIV-1 Prevention.* PLoS One, 2015. **10**(6): p. e0128857.

6. Baeten, J.M., et al., *Use of a Vaginal Ring Containing Dapivirine for HIV-1 Prevention in Women.* N Engl J Med, 2016. **375**(22): p2121-2132.

7. FDA, *US Department of Health and Human Services, Food and Drug Administration, Center for Drug Evaluation and Research (CDER). Guidance for Industry. Waiver of In Vivo Bioavailability and Bioequivalence Studies for Immediate- Release Solid Oral Dosage Forms Based on a Biopharmaceutics Classification System. US FDA website 2000:http://www.fda.gov/downloads/Drugs/GuidanceComplianceRegulatoryInformation/Guidances/UCM070246.pdf.* (Accessed 18/May/2017).

8. Gallo, R.C., et al., *Isolation of human T-cell leukemia virus in acquired immune deficiency syndrome (AIDS).* Science, 1983. **220**(4599): p. 865-7.

9. Broder, S. and R.C. Gallo, *A pathogenic retrovirus (HTLV-III) linked to AIDS.* N Engl J Med, 1984. **311**(20): p. 1292-7.

10. Barre-Sinoussi, F., et al., *Isolation of a T-lymphotropic retrovirus from a patient at risk for acquired immune deficiency syndrome (AIDS).* Science, 1983. **220**(4599): p. 868-71.

11. *aidsinfo.unaids.org/* (Accessed 18/May/2017).

12. Sharp, P.M., D.L. Robertson, and B.H. Hahn, *Cross-species transmission and recombination of 'AIDS' viruses.* Philos Trans R Soc Lond B Biol Sci, 1995. **349**(1327): p. 41-7.

13. Huet, T., et al., *Genetic organization of a chimpanzee lentivirus related to HIV-1.* Nature, 1990. **345**(6273): p. 356-9.

14. Gao, F., et al., *Origin of HIV-1 in the chimpanzee Pan troglodytes troglodytes.* Nature, 1999. **397**(6718): p. 436-41.

15. Bailes, E., et al., *Hybrid origin of SIV in chimpanzees.* Science, 2003. **300**(5626): p. 1713.

16. Hahn, B.H., et al., *AIDS as a zoonosis: scientific and public health implications.* Science, 2000. **287**(5453): p. 607-14.

17. *HIV Database* http://www.hiv.lanl.gov/content/index. (Accessed 18/May/2017).

18. Faria, N.R., et al., *HIV epidemiology. The early spread and epidemic ignition of HIV-1 in human populations.* Science, 2014. **346**(6205): p. 56-61.

19. Buonaguro, L., M.L. Tornesello, and F.M. Buonaguro, *Human immunodeficiency virus type 1 subtype distribution in the worldwide epidemic: pathogenetic and therapeutic implications.* J Virol, 2007. **81**(19): p. 10209-19.

20. Glynn, J.R., et al., *Why do young women have a much higher prevalence of HIV than young men? A study in Kisumu, Kenya and Ndola, Zambia.* AIDS, 2001. **15 Suppl 4**: p. S51-60.

21. Kelly, R.J., et al., *Age differences in sexual partners and risk of HIV-1 infection in rural Uganda.* J Acquir Immune Defic Syndr, 2003. **32**(4): p. 446-51.

22. McClelland, R.S., et al., *Vaginal washing and increased risk of HIV-1 acquisition among African women: a 10-year prospective study.* AIDS, 2006. **20**(2): p. 269-73.

23. Low, N., et al., *Intravaginal practices, bacterial vaginosis, and HIV infection in women: individual participant data meta-analysis.* PLoS Med, 2011. **8**(2): p. e1000416.

24. Pettifor, A.E., et al., *Highly efficient HIV transmission to young women in South Africa.* AIDS, 2007. **21**(7): p. 861-5.

25. Dellar, R.C., S. Dlamini, and Q.A. Karim, *Adolescent girls and young women: key populations for HIV epidemic control.* J Int AIDS Soc, 2015. **18**(2 Suppl 1): p. 19408.

26. Jain, R. and S. Muralidhar, *Contraceptive methods: needs, options and utilization.* J Obstet Gynaecol India, 2011. **61**(6): p. 626-34.

27. McKinnon, L.R., et al., *Characterization of a human cervical CD4+ T cell subset coexpressing multiple markers of HIV susceptibility.* J Immunol, 2011. **187**(11): p. 6032-42.

28. Prodger, J.L., et al., *Foreskin T-cell subsets differ substantially from blood with respect to HIV co-receptor expression, inflammatory profile, and memory status.* Mucosal Immunol, 2012. **5**(2): p. 121-8.

29. Stanley, M., *Early age of sexual debut: a risky experience.* J Fam Plann Reprod Health Care, 2009. **35**(2): p. 118-20.

30. Hladik, F. and T.J. Hope, *HIV infection of the genital mucosa in women.* Curr HIV/AIDS Rep, 2009. **6**(1): p. 20-8.

31. Haase, A.T., *Targeting early infection to prevent HIV-1 mucosal transmission.* Nature, 2010. **464**(7286): p. 217-223.

32. Gray-Swain, M.R. and J.F. Peipert, *Pelvic inflammatory disease in adolescents.* Curr Opin Obstet Gynecol, 2006. **18**(5): p. 503-10.

33. Galvin, S.R. and M.S. Cohen, *The role of sexually transmitted diseases in HIV transmission.* Nat Rev Microbiol, 2004. **2**(1): p. 33-42.

34. Briggs, J.A. and H.G. Krausslich, *The molecular architecture of HIV.* J Mol Biol, 2011. **410**(4): p. 491-500.

35. Margolis, L. and R. Shattock, *Selective transmission of CCR5-utilizing HIV-1: the 'gatekeeper' problem resolved?* Nat Rev Microbiol, 2006. **4**(4): p. 312-7.

36. Kuhmann, S.E. and O. Hartley, *Targeting chemokine receptors in HIV: a status report.* Annu Rev Pharmacol Toxicol, 2008. **48**: p. 425-61.

37. Scarlatti, G., et al., *In vivo evolution of HIV-1 co-receptor usage and sensitivity to chemokine-mediated suppression.* Nature Medicine, 1997. **3**(11): p. 1259-1265.

38. Campbell, E.M. and T.J. Hope, *HIV-1 capsid: the multifaceted key player in HIV-1 infection.* Nat Rev Microbiol, 2015. **13**(8): p. 471-83.

39. Sarafianos, S.G., et al., *Structure and Function of HIV-1 Reverse Transcriptase: Molecular Mechanisms of Polymerization and Inhibition.* Journal of Molecular Biology, 2009. **385**(3): p. 693-713.

40. Bowerman, B., et al., *A Nucleoprotein Complex Mediates the Integration of Retroviral DNA.* Genes & Development, 1989. **3**(4): p. 469-478.

41. McDonald, D., et al., *Visualization of the intracellular behavior of HIV in living cells.* Journal of Cell Biology, 2002. **159**(3): p. 441-452.

42. Karn, J. and C.M. Stoltzfus, *Transcriptional and Posttranscriptional Regulation of HIV-1 Gene Expression.* Cold Spring Harbor Perspectives in Medicine, 2012. **2**(2): a006916

43. Gottlinger, H.G., J.G. Sodroski, and W.A. Haseltine, *Role of Capsid Precursor Processing and Myristoylation in Morphogenesis and Infectivity of Human Immunodeficiency Virus Type-1.* Proceedings of the National Academy of Sciences of the United States of America, 1989. **86**(15): p. 5781-5785.

44. Zhou, W.J., et al., *Identification of a Membrane-Binding Domain within the Amino-Terminal Region of Human-Immunodeficiency-Virus Type-1 Gag Protein Which Interacts with Acidic Phospholipids.* Journal of Virology, 1994. **68**(4): p. 2556-2569.

45. Votteler, J. and W.I. Sundquist, *Virus budding and the ESCRT pathway.* Cell Host Microbe, 2013. **14**(3): p. 232-41.

46. Viread, *VIREAD® (tenofovir disoproxil fumarate) datasheet. http://rsc.tech-res.com/docs/default-source/pi-list doc/pi_tenofovirdisoproxilfumarate(viread)pi_feb2016.pdf?Status=Master&sfvrsn=0.* (Accessed 18/May/2017).

47. Freed, E.O., *HIV-1 assembly, release and maturation.* Nat Rev Microbiol, 2015. **13**(8): p. 484-96.

48. Ganser-Pornillos, B.K., M. Yeager, and W.I. Sundquist, *The structural biology of HIV assembly.* Curr Opin Struct Biol, 2008. **18**(2): p. 203-17.

49. Steitz, T.A., *Hot Papers - Biochemistry - Crystal-Structure at 3.5 Angstrom Resolution of Hiv-1 Reverse-Transcriptase Complexed with an Inhibitor by Kohlstaedt,L.A., Wang,J., Friedman,J.M., Et-Al.* Scientist, 1993. **7**(17): p. 16-16.

50. Meyer, P.R., et al., *Stable complexes formed by HIV-1 reverse transcriptase at distinct positions on the primer-template controlled by binding deoxynucleoside triphosphates or foscarnet.* Journal of Molecular Biology, 2007. **369**(1): p. 41-54.

51. Huang, H.F., et al., *Structure of a covalently trapped catalytic complex of HIV-I reverse transcriptase: Implications for drug resistance.* Science, 1998. **282**(5394): p. 1669-1675.

52. Reardon, J.E., *Human immunodeficiency virus reverse transcriptase: steady-state and pre-steady-state kinetics of nucleotide incorporation.* Biochemistry, 1992. **31**(18): p. 4473-9.

53. Ilina, T., et al., *Inhibitors of HIV-1 Reverse Transcriptase-Associated Ribonuclease H Activity.* Biology (Basel), 2012. **1**(3): p. 521-41.

54. Lv, Z., Y. Chu, and Y. Wang, *HIV protease inhibitors: a review of molecular selectivity and toxicity.* HIV AIDS (Auckl), 2015. **7**: p. 95-104.

55. *Protein Data Bank (www.pdb.org).* (Accessed 18/May/2017).

56. Nakashima, M., et al., *Unique Flap Conformation in an HIV-1 Protease with High-Level Darunavir Resistance.* Front Microbiol, 2016. **7**: p. 61.

57. King, N.M., et al., *Structural and thermodynamic basis for the binding of TMC114, a next-generation human immunodeficiency virus type 1 protease inhibitor.* J Virol, 2004. **78**(21): p. 12012-21.

58. Hornak, V. and C. Simmerling, *Targeting structural flexibility in HIV-1 protease inhibitor binding.* Drug Discov Today, 2007. **12**(3-4): p. 132-8.

59. Pinkerton, S.D. and P.R. Abramson, *Effectiveness of condoms in preventing HIV transmission.* Soc Sci Med, 1997. **44**(9): p. 1303-12.

60. Cottrell, M.L. and A.D.M. Kashuba, *Topical Microbicides and HIV Prevention in the Female Genital Tract.* Journal of Clinical Pharmacology, 2014. **54**(6): p. 603-615.

61. Auvert, B., et al., *Randomized, controlled intervention trial of male circumcision for reduction of HIV infection risk: the ANRS 1265 Trial.* PLoS Med, 2005. **2**(11): p. e298.

62. http://www.avert.org/professionals/hiv-programming/prevention/voluntary-medical-male-circumcision. (Accessed 18/May/2017).

63. Garg, S., et al., *Advances in development, scale-up and manufacturing of microbicide gels, films, and tablets.* Antiviral Research, 2010. **88**: p. S19-S29.

64. Malcolm, R.K., et al., *Advances in microbicide vaginal rings.* Antiviral Research, 2010. **88**: p. S30-S39.

65. Akil, A., et al., *Development and Characterization of a Vaginal Film Containing Dapivirine, a Non- nucleoside Reverse Transcriptase Inhibitor (NNRTI), for prevention of HIV-1 sexual transmission.* Drug Deliv Transl Res, 2011. **1**(3): p. 209-222.

66. Poelvoorde, N., et al., *In vivo evaluation of the vaginal distribution and retention of a multi-particulate pellet formulation.* Eur J Pharm Biopharm, 2009. **73**(2): p. 280-4.

67. Klasse, P.J., R.J. Shattock, and J.P. Moore, *Which topical microbicides for blocking HIV-1 transmission will work in the real world?* PLoS Med, 2006. **3**(9): p. e351.

68. Shattock, R.J. and Z. Rosenberg, *Microbicides: topical prevention against HIV.* Cold Spring Harb Perspect Med, 2012. **2**(2): p. a007385.

69. Ndesendo, V.M., et al., *A review of current intravaginal drug delivery approaches employed for the prophylaxis of HIV/AIDS and prevention of sexually transmitted infections.* AAPS PharmSciTech, 2008. **9**(2): p. 505-20.

70. Kelly, C.G. and R.J. Shattock, *Specific microbicides in the prevention of HIV infection.* J Intern Med, 2011. **270**(6): p. 509-19.

71. Van Damme, L., et al., *Effectiveness of COL-1492, a nonoxynol-9 vaginal gel, on HIV-1 transmission in female sex workers: a randomised controlled trial.* Lancet, 2002. **360**(9338): p. 971-977.

72. Roddy, R.E., et al., *A dosing study of nonoxynol-9 and genital irritation.* Int J STD AIDS, 1993. **4**(3): p. 165-70.

73. Galen, B.T., et al., *A comprehensive murine model to evaluate topical vaginal microbicides: mucosal inflammation and susceptibility to genital herpes as surrogate markers of safety.* J Infect Dis, 2007. **195**(9): p. 1332-9.

74. Esser, M.T., et al., *Cyanovirin-N binds to gp120 to interfere with CD4-dependent human immunodeficiency virus type 1 virion binding, fusion, and infectivity but does not affect the CD4 binding site on gp120 or soluble CD4-induced conformational changes in gp120.* J Virol, 1999. **73**(5): p. 4360-71.

75. Fletcher, P.S. and R.J. Shattock, *PRO-2000, an antimicrobial gel for the potential prevention of HIV infection.* Current Opinion in Investigational Drugs, 2008. **9**(2): p. 189-200.

76. Ramjee, G., A. Kamali, and S. McCormack, *The last decade of microbicide clinical trials in Africa: from hypothesis to facts.* Aids, 2010. **24**: p. S40-S49.

77. Broder, S., *Twenty-Five Years of Translational Medicine in Antiretroviral Therapy: Promises to Keep.* Science Translational Medicine, 2010. **2**(39): ps33.

78. Wiznia, A.A., et al., *Zidovudine use to reduce perinatal HIV type 1 transmission in an urban medical center.* Jama-Journal of the American Medical Association, 1996. **275**(19): p. 1504-1506.

79. Boyer, P.L., et al., *Nucleoside analog resistance caused by insertions in the fingers of human immunodeficiency virus type 1 reverse transcriptase involves ATP-mediated excision.* J Virol, 2002. **76**(18): p. 9143-51.

80. Mehellou, Y. and E. De Clercq, *Twenty-Six Years of Anti-HIV Drug Discovery: Where Do We Stand and Where Do We Go?* Journal of Medicinal Chemistry, 2010. **53**(2): p. 521-538.

81. Parikh, U.M., et al., *Complete Protection from Repeated Vaginal Simian-Human Immunodeficiency Virus Exposures in Macaques by a Topical Gel Containing Tenofovir Alone or with Emtricitabine.* Journal of Virology, 2009. **83**(20): p. 10358-10365.

82. Amico, K.R. and M.J. Stirratt, *Adherence to preexposure prophylaxis: current, emerging, and anticipated bases of evidence.* Clin Infect Dis, 2014. **59 Suppl 1**: p. S55-60.

83. Hsiou, Y., et al., *Structure of unliganded HIV-1 reverse transcriptase at 2.7 A resolution: implications of conformational changes for polymerization and inhibition mechanisms.* Structure, 1996. **4**(7): p. 853-60.

84. Schauer, G.D., et al., *Mechanism of allosteric inhibition of HIV-1 reverse transcriptase revealed by single-molecule and ensemble fluorescence.* Nucleic Acids Res, 2014. **42**(18): p. 11687-96.

85. Nuttall, J.P., et al., *Concentrations of dapivirine in the rhesus macaque and rabbit following once daily intravaginal administration of a gel formulation of [C-14]dapivirine for 7 days.* Antimicrobial Agents and Chemotherapy, 2008. **52**(3): p. 909-914.

86. Steigbigel, R.T., et al., *Raltegravir with optimized background therapy for resistant HIV-1 infection.* New England Journal of Medicine, 2008. **359**(4): p. 339-354.

87. Eron, J.J., et al., *Efficacy and safety of raltegravir for treatment of HIV for 5 years in the BENCHMRK studies: final results of two randomised, placebo-controlled trials.* Lancet Infectious Diseases, 2013. **13**(7): p. 587-596.

88. Nicol, M.R., J.L. Adams, and A.D. Kashuba, *HIV PrEP Trials: The Road to Success.* Clin Investig (Lond), 2013. **3**(3): 10.4155/cli.12.155.

89. Jackson, A. and I. McGowan, *Long-acting rilpivirine for HIV prevention.* Curr Opin HIV AIDS, 2015. **10**(4): p. 253-7.

90. Saskova, K.G., et al., *Molecular Characterization of Clinical Isolates of Human Immunodeficiency Virus Resistant to the Protease Inhibitor Darunavir.* Journal of Virology, 2009. **83**(17): p. 8810-8818.

91. Bozzette, S.A., et al., *Cardiovascular and cerebrovascular events in patients treated for human immunodeficiency virus infection.* N Engl J Med, 2003. **348**(8): p. 702-10.

92. Hruz, P.W., *HIV protease inhibitors and insulin resistance: lessons from in-vitro, rodent and healthy human volunteer models.* Curr Opin HIV AIDS, 2008. **3**(6): p. 660-5.

93. Kotler, D.P., *HIV and antiretroviral therapy: lipid abnormalities and associated cardiovascular risk in HIV-infected patients.* J Acquir Immune Defic Syndr, 2008. **49 Suppl 2**: p. S79-85.

94. Soontornniyomkij, V., et al., *HIV protease inhibitor exposure predicts cerebral small vessel disease.* AIDS, 2014. **28**(9): p. 1297-306.

95. De Meyer, S., et al., *TMC114, a novel human immunodeficiency virus type 1 protease inhibitor active against protease inhibitor-resistant viruses, including a broad range of clinical isolates.* Antimicrob Agents Chemother, 2005. **49**(6): p. 2314-21.

96. Boffito, M., D. Miralles, and A. Hill, *Pharmacokinetics, efficacy, and safety of darunavir/ritonavir 800/100 mg once-daily in treatment-naive and -experienced patients.* HIV Clin Trials, 2008. **9**(6): p. 418-27.

97. Adams, J.L. and A.D. Kashuba, *Formulation, pharmacokinetics and pharmacodynamics of topical microbicides.* Best Pract Res Clin Obstet Gynaecol, 2012. **26**(4): p. 451-62.

98. Parikh, U.M., et al., *Complete protection from repeated vaginal simian-human immunodeficiency virus exposures in macaques by a topical gel containing tenofovir alone or with emtricitabine.* J Virol, 2009. **83**(20): p. 10358-65.

99. Chen, B.A., et al., *Phase 1 Safety, Pharmacokinetics, and Pharmacodynamics of Dapivirine and Maraviroc Vaginal Rings: a Double-Blind Randomized Trial.* J Acquir Immune Defic Syndr, 2015. **70**(3): p242-249.

100. Akil, A., et al., *Increased Dapivirine Tissue Accumulation through Vaginal Film Codelivery of Dapivirine and Tenofovir.* Molecular Pharmaceutics, 2014. **11**(5): p. 1533-1541.

101. Edwards, J.N. and H.B. Morris, *Langerhans' cells and lymphocyte subsets in the female genital tract.* Br J Obstet Gynaecol, 1985. **92**(9): p. 974-82.

102. Iwasaki, A., *Antiviral immune responses in the genital tract: clues for vaccines.* Nat Rev Immunol, 2010. **10**(10): p. 699-711.

103. Gipson, I.K., et al., *Mucin genes expressed by human female reproductive tract epithelia.* Biol Reprod, 1997. **56**(4): p. 999-1011.

104. Agrawal, B., et al., *Expression of MUC1 mucin on activated human T cells: implications for a role of MUC1 in normal immune regulation.* Cancer Res, 1998. **58**(18): p. 4079-81.

105. Stringer, E. and E. Antonsen, *Hormonal contraception and HIV disease progression.* Clin Infect Dis, 2008. **47**(7): p. 945-51.

106. Keele, B.F., et al., *Identification and characterization of transmitted and early founder virus envelopes in primary HIV-1 infection.* Proc Natl Acad Sci U S A, 2008. **105**(21): p. 7552-7.

107. Salazar-Gonzalez, J.F., et al., *Genetic identity, biological phenotype, and evolutionary pathways of transmitted/founder viruses in acute and early HIV-1 infection.* J Exp Med, 2009. **206**(6): p. 1273-89.

108. Keele, B.F., et al., *Low-dose rectal inoculation of rhesus macaques by SIVsmE660 or SIVmac251 recapitulates human mucosal infection by HIV-1.* J Exp Med, 2009. **206**(5): p. 1117-34.

109. Miller, C.J., et al., *Propagation and dissemination of infection after vaginal transmission of simian immunodeficiency virus.* J Virol, 2005. **79**(14): p. 9217-27.

110. Zhang, Z., et al., *Sexual transmission and propagation of SIV and HIV in resting and activated CD4+ T cells.* Science, 1999. **286**(5443): p. 1353-7.

111. Hladik, F., et al., *Initial events in establishing vaginal entry and infection by human immunodeficiency virus type-1.* Immunity, 2007. **26**(2): p. 257-70.

112. Lederman, M.M., R.E. Offord, and O. Hartley, *Microbicides and other topical strategies to prevent vaginal transmission of HIV.* Nat Rev Immunol, 2006. **6**(5): p. 371-82.

113. Keele, B.F. and J.D. Estes, *Barriers to mucosal transmission of immunodeficiency viruses.* Blood, 2011. **118**(4): p. 839-46.

114. Kohli, A., et al., *Oral and vaginal epithelial cell lines bind and transfer cell-free infectious HIV-1 to permissive cells but are not productively infected.* PLoS One, 2014. **9**(5): p. e98077.

115. Bomsel, M., *Transcytosis of infectious human immunodeficiency virus across a tight human epithelial cell line barrier.* Nat Med, 1997. **3**(1): p. 42-7.

116. Fotopoulos, G., et al., *Transepithelial transport of HIV-1 by M cells is receptor-mediated.* Proceedings of the National Academy of Sciences of the United States of America, 2002. **99**(14): p. 9410-9414.

117. Nazli, A., et al., *Exposure to HIV-1 directly impairs mucosal epithelial barrier integrity allowing microbial translocation.* PLoS Pathog, 2010. **6**(4): p. e1000852.

118. Kell, P.D., et al., *Hiv-Infection in a Patient with Meyer-Rokitansky-Kuster-Hauser Syndrome.* Journal of the Royal Society of Medicine, 1992. **85**(11): p. 706-707.

119. Miller, C.J., et al., *Mechanism of Genital Transmission of Siv - a Hypothesis Based on Transmission Studies and the Location of Siv in the Genital-Tract of Chronically Infected Female Rhesus Macaques.* Journal of Medical Primatology, 1992. **21**(2-3): p. 64-68.

120. Pudney, J., A.J. Quayle, and D.J. Anderson, *Immunological microenvironments in the human vagina and cervix: Mediators of cellular immunity are concentrated in the cervical transformation zone.* Biology of Reproduction, 2005. **73**(6): p. 1253-1263.

121. Stieh, D.J., et al., *Vaginal challenge with an SIV-based dual reporter system reveals that infection can occur throughout the upper and lower female reproductive tract.* PLoS Pathog, 2014. **10**(10): p. e1004440.

122. Hussain, A. and F. Ahsan, *The vagina as a route for systemic drug delivery.* J Control Release, 2005. **103**(2): p. 301-13.

123. Hendrix, C.W., et al., *MTN-001: Randomized Pharmacokinetic Cross-Over Study Comparing Tenofovir Vaginal Gel and Oral Tablets in Vaginal Tissue and Other Compartments.* Plos One, 2013. **8**(1): e55013.

124. Wils, P., et al., *High lipophilicity decreases drug transport across intestinal epithelial cells.* J Pharmacol Exp Ther, 1994. **269**(2): p. 654-8.

125. Powell, D.W., *Barrier Function of Epithelia.* American Journal of Physiology, 1981. **241**(4): p. G275-G288.

126. Chan, L.M.S., S. Lowes, and B.H. Hirst, *The ABCs of drug transport in intestine and liver: efflux proteins limiting drug absorption and bioavailability.* European Journal of Pharmaceutical Sciences, 2004. **21**(1): p. 25-51.

127. Shah, D. and W.C. Shen, *Transcellular delivery of an insulin-transferrin conjugate in enterocyte-like Caco-2 cells.* J Pharm Sci, 1996. **85**(12): p. 1306-11.

128. Woolfson, A.D., R.K. Malcolm, and R. Gallagher, *Drug delivery by the intravaginal route.* Crit Rev Ther Drug Carrier Syst, 2000. **17**(5): p. 509-55.

129. R. Karl Malcolm, et al., *Enhancement in drug delivery: Vagina and Uterus as Drug-Absorbing Organs.* 2006. **21**: p. 395-431.

130. Saxena, D., et al., *Human microbiome and HIV/AIDS.* Curr HIV/AIDS Rep, 2012. **9**(1): p. 44-51.

131. Shakya, P., et al., *Palatal mucosa as a route for systemic drug delivery: A review.* Journal of Controlled Release, 2011. **151**(1): p. 2-9.

132. Wang, Y.Y., et al., *The microstructure and bulk rheology of human cervicovaginal mucus are remarkably resistant to changes in pH.* Biomacromolecules, 2013. **14**(12): p. 4429-35.

133. Boegh, M. and H.M. Nielsen, *Mucus as a barrier to drug delivery - understanding and mimicking the barrier properties.* Basic Clin Pharmacol Toxicol, 2015. **116**(3): p. 179-86.

134. Cohen, M.S., et al., *Narrative review: Antiretroviral therapy to prevent the sexual transmission of HIV-1.* Annals of Internal Medicine, 2007. **146**(8): p. 591-U63.

135. Dumond, J.B., et al., *Antiretroviral drug exposure in the female genital tract: implications for oral pre- and post-exposure prophylaxis.* AIDS, 2007. **21**(14): p. 1899-907.

136. Grammen, C., P. Augustijns, and J. Brouwers, *In vitro profiling of the vaginal permeation potential of anti-HIV microbicides and the influence of formulation excipients.* Antiviral Res, 2012. **96**(2): p. 226-33.

137. Roth, M., A. Obaidat, and B. Hagenbuch, *OATPs, OATs and OCTs: the organic anion and cation transporters of the SLCO and SLC22A gene superfamilies.* Br J Pharmacol, 2012. **165**(5): p. 1260-87.

138. Kis, O., et al., *The complexities of antiretroviral drug-drug interactions: role of ABC and SLC transporters.* Trends Pharmacol Sci, 2010. **31**(1): p. 22-35.

139. Taipalensuu, J., et al., *Correlation of gene expression of ten drug efflux proteins of the ATP-binding cassette transporter family in normal human jejunum and in human intestinal epithelial Caco-2 cell monolayers.* Journal of Pharmacology and Experimental Therapeutics, 2001. **299**(1): p. 164-170.

140. Ohtsuki, S., et al., *Quantitative targeted absolute proteomics-based ADME research as a new path to drug discovery and development: methodology, advantages, strategy, and prospects.* J Pharm Sci, 2011. **100**(9): p. 3547-59.

141. Sun, W., et al., *Isolation of a family of organic anion transporters from human liver and kidney.* Biochem Biophys Res Commun, 2001. **283**(2): p. 417-22.

142. Shitara, Y., H. Sato, and Y. Sugiyama, *Evaluation of drug-drug interaction in the hepatobiliary and renal transport of drugs.* Annu Rev Pharmacol Toxicol, 2005. **45**: p. 689-723.

143. Iqbal, M., et al., *Placental drug transporters and their role in fetal protection.* Placenta, 2012. **33**(3): p. 137-42.

144. Zhou, T., et al., *Short Communication: Expression of Transporters and Metabolizing Enzymes in the Female Lower Genital Tract: Implications for Microbicide Research.* Aids Research and Human Retroviruses, 2013. **29**(11): p. 1496-1503.

145. Zhou, T., et al., *Expression and Localization of P-Glycoprotein, Multidrug Resistance Protein 4, and Breast Cancer Resistance Protein in the Female Lower Genital Tract of Human and Pigtailed Macaque.* Aids Research and Human Retroviruses, 2014. **30**(11): p. 1106-1116.

146. Grammen, C., et al., *Vaginal Expression of Efflux Transporters and the Potential Impact on the Disposition of Microbicides in Vitro and in Rabbits.* Molecular Pharmaceutics, 2014. **11**(12): p. 4405-4414.

147. Finstad, C.L., et al., *Immunohistochemical localization of P-glycoprotein in adult human ovary and female genital tract of patients with benign gynecological conditions.* J Histochem Cytochem, 1990. **38**(11): p. 1677-81.

148. Hijazi, K., et al., *Expression of Genes for Drug Transporters in the Human Female Genital Tract and Modulatory Effect of Antiretroviral Drugs.* Plos One, 2015. **10**(6): e0131405.

149. Gunawardana, M., et al., *Global expression of molecular transporters in the human vaginal tract: implications for HIV chemoprophylaxis.* PLoS One, 2013. **8**(10): p. e77340.

150. Nicol, M.R., et al., *Expression of Six Drug Transporters in Vaginal, Cervical, and Colorectal Tissues: Implications for Drug Disposition in HIV Prevention.* Journal of Clinical Pharmacology, 2014. **54**(5): p. 574-583.

151. Zhou, T., et al., *Expression and localization of p-glycoprotein, multidrug resistance protein 4, and breast cancer resistance protein in the female lower genital tract of human and pigtailed macaque.* AIDS Res Hum Retroviruses, 2014. **30**(11): p. 1106-16.

152. Langmann, T., et al., *Real-time reverse transcription-PCR expression profiling of the complete human ATP-binding cassette transporter superfamily in various tissues.* Clin Chem, 2003. **49**(2): p. 230-8.

153. Ito, K., et al., *Apical/basolateral surface expression of drug transporters and its role in vectorial drug transport.* Pharm Res, 2005. **22**(10): p. 1559-77.

154. Venter, J.C., et al., *The sequence of the human genome.* Science, 2001. **291**(5507): p. 1304-51.

155. Cihlar, T., et al., *The antiviral nucleotide analogs cidofovir and adefovir are novel substrates for human and rat renal organic anion transporter 1.* Mol Pharmacol, 1999. **56**(3): p. 570-80.

156. Imaoka, T., et al., *Functional involvement of multidrug resistance-associated protein 4 (MRP4/ABCC4) in the renal elimination of the antiviral drugs adefovir and tenofovir.* Mol Pharmacol, 2007. **71**(2): p. 619-27.

157. Zakeri-Milani, P. and H. Valizadeh, *Intestinal transporters: enhanced absorption through P-glycoprotein-related drug interactions.* Expert Opin Drug Metab Toxicol, 2014. **10**(6): p859-871.

158. Minuesa, G., et al., *Drug uptake transporters in antiretroviral therapy.* Pharmacol Ther, 2011. **132**(3): p. 268-79.

159. Kohler, J.J., et al., *Tenofovir renal proximal tubular toxicity is regulated by OAT1 and MRP4 transporters.* Lab Invest, 2011. **91**(6): p. 852-8.

160. Taneva, E., et al., *Differential Mechanisms of Tenofovir and Tenofovir Disoproxil Fumarate Cellular Transport and Implications for Topical Preexposure Prophylaxis.* Antimicrob Agents Chemother, 2016. **60**(3): p. 1667-75.

161. Baldwin, S.A., et al., *The equilibrative nucleoside transporter family, SLC29.* Pflugers Arch, 2004. **447**(5): p. 735-43.

162. Wright, A.M., W.P. Gati, and A.R. Paterson, *Enhancement of retention and cytotoxicity of 2-chlorodeoxyadenosine in cultured human leukemic lymphoblasts by nitrobenzylthioinosine, an inhibitor of equilibrative nucleoside transport.* Leukemia, 2000. **14**(1): p. 52-60.

163. You, G.F., *Structure, function, and regulation of renal organic anion transporters.* Medicinal Research Reviews, 2002. **22**(6): p. 602-616.

164. Colas, C., P.M.-U. Ung, and A. Schlessinger, *SLC transporters: structure, function, and drug discovery.* MedChemComm, 2016. **7**(6): p.1069-1081.

165. Eraly, S.A., et al., *The molecular pharmacology of organic anion transporters: from DNA to FDA?* Mol Pharmacol, 2004. **65**(3): p. 479-87.

166. Deng, D., et al., *Crystal structure of the human glucose transporter GLUT1.* Nature, 2014. **510**(7503): p. 121-5.

167. Radestock, S. and L.R. Forrest, *The alternating-access mechanism of MFS transporters arises from inverted-topology repeats.* J Mol Biol, 2011. **407**(5): p. 698-715.

168. Singh, S.K., et al., *A competitive inhibitor traps LeuT in an open-to-out conformation.* Science, 2008. **322**(5908): p. 1655-61.

169. Vasiliou, V., K. Vasiliou, and D.W. Nebert, *Human ATP-binding cassette (ABC) transporter family.* Hum Genomics, 2009. **3**(3): p. 281-90.

170. Leschziner, G.D., et al., *ABCB1 genotype and PGP expression, function and therapeutic drug response: a critical review and recommendations for future research.* Pharmacogenomics J, 2007. **7**(3): p. 154-79.

171. Hu, M., et al., *Drug transporters in tissues and cells relevant to sexual transmission of HIV: Implications for drug delivery.* J Control Release, 2015. **219**: p. 681-96.

172. Kis, O., et al., *Role of Drug Efflux and Uptake Transporters in Atazanavir Intestinal Permeability and Drug-Drug Interactions.* Pharmaceutical Research, 2013. **30**(4): p. 1050-1064.

173. Kim, R.B., et al., *The drug transporter P-glycoprotein limits oral absorption and brain entry of HIV-1 protease inhibitors.* J Clin Invest, 1998. **101**(2): p. 289-94.

174. van Gelder, J., et al., *Intestinal Absorption Enhancement of the Ester Prodrug Tenofovir Disoproxil Fumarate through Modulation of the Biochemical Barrier by Defined Ester Mixtures.* Drug Metabolism and Disposition, 2002. **30**(8): p. 924-930.

175. Mallants, R., et al., *Multidrug resistance-associated protein 2 (MRP2) affects hepatobiliary elimination but not the intestinal disposition of tenofovir disoproxil fumarate and its metabolites.* Xenobiotica, 2005. **35**(10-11): p. 1055-66.

176. Reid, G., et al., *Characterization of the transport of nucleoside analog drugs by the human multidrug resistance proteins MRP4 and MRP5.* Mol Pharmacol, 2003. **63**(5): p. 1094-103.

177. Ray, A.S., et al., *Mechanism of active renal tubular efflux of tenofovir.* Antimicrobial Agents and Chemotherapy, 2006. **50**(10): p. 3297-3304.

178. Wang, X., et al., *Breast cancer resistance protein (BCRP/ABCG2) induces cellular resistance to HIV-1 nucleoside reverse transcriptase inhibitors.* Mol Pharmacol, 2003. **63**(1): p. 65-72.

179. Leggas, M., et al., *Mrp4 confers resistance to topotecan and protects the brain from chemotherapy.* Mol Cell Biol, 2004. **24**(17): p. 7612-21.

180. Sharom, F.J., *Multidrug Resistance Protein: P-Glycoprotein*, in *Drug Transporters*. 2006, John Wiley & Sons, Inc. p. 223-262. (Accesed 22/May/2017)

181. Higgins, C.F., et al., *A family of related ATP-binding subunits coupled to many distinct biological processes in bacteria.* Nature, 1986. **323**(6087): p. 448-50.

182. Deeley, R.G., C. Westlake, and S.P. Cole, *Transmembrane transport of endo- and xenobiotics by mammalian ATP-binding cassette multidrug resistance proteins.* Physiol Rev, 2006. **86**(3): p. 849-99.

183. Lugo, M.R. and F.J. Sharom, *Interaction of LDS-751 with P-glycoprotein and mapping of the location of the R drug binding site.* Biochemistry, 2005. **44**(2): p. 643-55.

184. Aller, S.G., et al., *Structure of P-glycoprotein reveals a molecular basis for poly-specific drug binding.* Science, 2009. **323**(5922): p. 1718-22.

185. Li, J., K.F. Jaimes, and S.G. Aller, *Refined structures of mouse P-glycoprotein.* Protein Sci, 2014. **23**(1): p. 34-46.

186. Dawson, R.J. and K.P. Locher, *Structure of a bacterial multidrug ABC transporter.* Nature, 2006. **443**(7108): p. 180-5.

187. Sharom, F.J., *ABC multidrug transporters: structure, function and role in chemoresistance.* Pharmacogenomics, 2008. **9**(1): p. 105-27.

188. Sharom, F.J., *Complex Interplay between the P-Glycoprotein Multidrug Efflux Pump and the Membrane: Its Role in Modulating Protein Function.* Front Oncol, 2014. **4**: p. 41.

189. Coleman, J.A., F. Quazi, and R.S. Molday, *Mammalian P4-ATPases and ABC transporters and their role in phospholipid transport.* Biochim Biophys Acta, 2013. **1831**(3): p. 555-74.

190. Bosch, I., et al., *Phosphatidylcholine and phosphatidylethanolamine behave as substrates of the human MDR1 P-glycoprotein.* Biochemistry, 1997. **36**(19): p. 5685-94.

191. Bleasby, K., et al., *Expression profiles of 50 xenobiotic transporter genes in humans and pre-clinical species: a resource for investigations into drug disposition.* Xenobiotica, 2006. **36**(10-11): p. 963-88.

192. Axiotis, C.A., et al., *Immunohistochemical detection of P-glycoprotein in endometrial adenocarcinoma.* Am J Pathol, 1991. **138**(4): p. 799-806.

193. Gori, I., et al., *Augmented epithelial multidrug resistance-associated protein 4 expression in peritoneal endometriosis: regulation by lipoxin A(4).* Fertil Steril, 2013. **99**(7): p. 1965-73 e2.

194. Pastor-Anglada, M., et al., *Cell entry and export of nucleoside analogues.* Virus Res, 2005. **107**(2): p. 151-64.

195. Robbins, B.L., et al., *Anti-human immunodeficiency virus activity and cellular metabolism of a potential prodrug of the acyclic nucleoside phosphonate 9-R-(2-phosphonomethoxypropyl)adenine (PMPA), Bis(isopropyloxymethylcarbonyl)PMPA.* Antimicrob Agents Chemother, 1998. **42**(3): p. 612-7.

196. Jackson, A., et al., *Tenofovir, Emtricitabine Intracellular and Plasma, and Efavirenz Plasma Concentration Decay Following Drug Intake Cessation: Implications for HIV Treatment and Prevention.* Jaids-Journal of Acquired Immune Deficiency Syndromes, 2013. **62**(3): p. 275-281.

197. Balzarini, J., et al., *Activity of acyclic nucleoside phosphonate analogues against human immunodeficiency virus in monocyte/macrophages and peripheral blood lymphocytes.* Biochem Biophys Res Commun, 1991. **178**(1): p. 329-35.

198. Cranage, M., et al., *Prevention of SIV rectal transmission and priming of T cell responses in macaques after local pre-exposure application of tenofovir gel.* PLoS Med, 2008. **5**(8): p. e157; discussion e157.

199. Rohan, L.C., et al., *In Vitro and Ex Vivo Testing of Tenofovir Shows It Is Effective As an HIV-1 Microbicide.* Plos One, 2010. **5**(2): e9310.

200. Balzarini, J., et al., *Differential antiherpesvirus and antiretrovirus effects of the (S) and (R) enantiomers of acyclic nucleoside phosphonates: potent and selective in vitro and in vivo antiretrovirus activities of (R)-9-(2-phosphonomethoxypropyl)-2,6-diaminopurine.* Antimicrob Agents Chemother, 1993. **37**(2): p. 332-8.

201. VIREAD, *Oral TFV perscribing information. http://rsc.tech-res.com/docs/default-source/pi-list-doc/pi_tenofovirdisoproxilfumarate(viread)pi_feb2016.pdf?Status=Master&sfvrsn=0. 2016.* (Accessed 18/May/2017).

202. Kearney, B.P., J.F. Flaherty, and J. Shah, *Tenofovir disoproxil fumarate: clinical pharmacology and pharmacokinetics.* Clin Pharmacokinet, 2004. **43**(9): p. 595-612.

203. Patterson, K.B., et al., *Penetration of tenofovir and emtricitabine in mucosal tissues: implications for prevention of HIV-1 transmission.* Sci Transl Med, 2011. **3**(112): p. 112re4.

204. Karim, S.S., et al., *Drug concentrations after topical and oral antiretroviral pre-exposure prophylaxis: implications for HIV prevention in women.* Lancet, 2011. **378**(9787): p. 279-81.

205. Ray, A.S., M.W. Fordyce, and M.J. Hitchcock, *Tenofovir alafenamide: A novel prodrug of tenofovir for the treatment of Human Immunodeficiency Virus.* Antiviral Res, 2016. **125**: p. 63-70.

206. Hijazi, K., et al., *Expression of Genes for Drug Transporters in the Human Female Genital Tract and Modulatory Effect of Antiretroviral Drugs.* PLoS One, 2015. **10**(6): p. e0131405.

207. Fletcher, P., et al., *Inhibition of human immunodeficiency virus type 1 infection by the candidate microbicide dapivirine, a nonnucleoside reverse transcriptase inhibitor.* Antimicrob Agents Chemother, 2009. **53**(2): p. 487-95.

208. Herrera, C., et al., *Reverse Transcriptase Inhibitors as Potential Colorectal Microbicides.* Antimicrobial Agents and Chemotherapy, 2009. **53**(5): p. 1797-1807.

209. Van Herrewege, Y., et al., *In vitro evaluation of nonnucleoside reverse transcriptase inhibitors UC-781 and TMC120-R147681 as human immunodeficiency virus microbicides.* Antimicrob Agents Chemother, 2004. **48**(1): p. 337-9.

210. Fletcher, P., et al., *The nonnucleoside reverse transcriptase inhibitor UC-781 inhibits human immunodeficiency virus type 1 infection of human cervical tissue and dissemination by migratory cells.* J Virol, 2005. **79**(17): p. 11179-86.

211. Nel AM, et al., *Pharmacokinetics and Safety Assessment of Anti-HIV Dapivirine Vaginal Microbicide Rings with Multiple Dosing.* J AIDS Clin Res 2009. **5**(355).

212. Ghosh, A.K., et al., *Bis-tetrahydrofuran: a privileged ligand for darunavir and a new generation of hiv protease inhibitors that combat drug resistance.* ChemMedChem, 2006. **1**(9): p. 939-50.

213. Back, D., V. Sekar, and R.M. Hoetelmans, *Darunavir: pharmacokinetics and drug interactions.* Antivir Ther, 2008. **13**(1): p. 1-13.

214. Fujimoto, H., et al., *P-glycoprotein mediates efflux transport of darunavir in human intestinal Caco-2 and ABCB1 gene-transfected renal LLC-PK1 cell lines.* Biol Pharm Bull, 2009. **32**(9): p. 1588-93.

215. Schon, A., M. del Mar Ingaramo, and E. Freire, *The binding of HIV-1 protease inhibitors to human serum proteins.* Biophys Chem, 2003. **105**(2-3): p. 221-30.

216. Molina, J.M. and A. Hill, *Darunavir (TMC114): a new HIV-1 protease inhibitor.* Expert Opin Pharmacother, 2007. **8**(12): p. 1951-64.

217. Tibotec, *PREZISTA™ (darunavir) Prescribing Information. Available from: http://www.tibotectherapeutics.com/PREZISTA_pi.pdf*. 2006. Accessed 22/May/2017)

218. Sekar V, Guzman S, and *e.a.* Stevens T, *Absolute bioavailability of TMC114, administered in the absence and presence of low-dose ritonavir.* The 7th International Workshop on Clinical Pharmacology of HIV Therapy. Abstract p86., 20–22 April 2006.

219. Clotet, B., et al., *Efficacy and safety of darunavir-ritonavir at week 48 in treatment-experienced patients with HIV-1 infection in POWER 1 and 2: a pooled subgroup analysis of data from two randomised trials.* Lancet, 2007. **369**(9568): p. 1169-78.

220. Murphy, D.J., et al., *Pre-clinical development of a combination microbicide vaginal ring containing dapivirine and darunavir.* J Antimicrob Chemother, 2014.

221. Kuramoto, H., S. Tamura, and Y. Notake, *Establishment of a Cell Line of Human Endometrial Adenocarcinoma in-Vitro.* American Journal of Obstetrics and Gynecology, 1972. **114**(8): p. 1012-1019.

222. Gali, Y., et al., *Development of an in vitro dual-chamber model of the female genital tract as a screening tool for epithelial toxicity.* J Virol Methods, 2010. **165**(2): p. 186-97.

223. Srinivasan, B., et al., *TEER measurement techniques for in vitro barrier model systems.* J Lab Autom, 2015. **20**(2): p. 107-26.

224. NIH, *Tissue repository guidelines (Accessed 18/May/2017).*

225. Hubatsch, I., E.G. Ragnarsson, and P. Artursson, *Determination of drug permeability and prediction of drug absorption in Caco-2 monolayers.* Nat Protoc, 2007. **2**(9): p. 2111-9.

226. Dezzutti, C.S., et al., *Is wetter better? An evaluation of over-the-counter personal lubricants for safety and anti-HIV-1 activity.* PLoS One, 2012. **7**(11): p. e48328.

227. Mesquita, P.M., et al., *Disruption of tight junctions by cellulose sulfate facilitates HIV infection: model of microbicide safety.* J Infect Dis, 2009. **200**(4): p. 599-608.

228. Lawrence, P., et al., *Selective transmigration of monocyte-associated HIV-1 across a human cervical monolayer and its modulation by seminal plasma.* AIDS, 2012. **26**(7): p. 785-96.

229. Gali, Y., et al., *In vitro evaluation of viability, integrity, and inflammation in genital epithelia upon exposure to pharmaceutical excipients and candidate microbicides.* Antimicrob Agents Chemother, 2010. **54**(12): p. 5105-14.

230. Arien, K.K., G. Vanham, and Y. Gali, *A dual-chamber model of the female genital tract to evaluate epithelial toxicity of candidate anti-HIV microbicides.* Curr Protoc Cell Biol, 2011. **Chapter 26**: 52:26.13:26.13.1–26.13.17. (Accessed 22/May/2017)

231. Pinto, M., et al., *Enterocyte-like differentiation and polarization of the human colon carcinoma cell line Caco-2 in culture.* Biol. Cell., 1983. **47**: p. 323-330.

232. Hidalgo, I.J., T.J. Raub, and R.T. Borchardt, *Characterization of the Human-Colon Carcinoma Cell-Line (Caco-2) as a Model System for Intestinal Epithelial Permeability.* Gastroenterology, 1989. **96**(3): p. 736-749.

233. Artursson, P., K. Palm, and K. Luthman, *Caco-2 monolayers in experimental and theoretical predictions of drug transport.* Advanced Drug Delivery Reviews, 1996. **22**(1-2): p. 67-84.

234. Forbes, B., et al., *The human bronchial epithelial cell line 16HBE14o-as a model system of the airways for studying drug transport.* International Journal of Pharmaceutics, 2003. **257**(1-2): p. 161-167.

235. Sambuy, Y., et al., *The Caco-2 cell line as a model of the intestinal barrier: influence of cell and culture-related factors on Caco-2 cell functional characteristics.* Cell Biol Toxicol, 2005. **21**(1): p. 1-26.

236. Boegh, M., et al., *Mucosal drug delivery: barriers, in vitro models and formulation strategies.* Journal of Drug Delivery Science and Technology, 2013. **23**(4): p. 383-391.

237. Corning, *http://csmedia2.corning.com/LifeSciences/Media/pdf/transwell_guide.pdf*. (Accessed 22/May/2017)

238. Zucco, F., et al., *An inter-laboratory study to evaluate the effects of medium composition on the differentiation and barrier function of Caco-2 cell lines.* Altern Lab Anim, 2005. **33**(6): p. 603-18.

239. Furuse, M., et al., *Claudin-based tight junctions are crucial for the mammalian epidermal barrier: a lesson from claudin-1-deficient mice.* Journal of Cell Biology, 2002. **156**(6): p. 1099-1111.

240. Balda, M.S., et al., *Functional dissociation of paracellular permeability and transepithelial electrical resistance and disruption of the apical-basolateral intramembrane diffusion barrier by expression of a mutant tight junction membrane protein.* Journal of Cell Biology, 1996. **134**(4): p. 1031-1049.

241. Balda, M.S. and K. Matter, *Tight junctions at a glance.* Journal of Cell Science, 2008. **121**(22): p. 3677-3682.

242. McCarthy, K.M., et al., *Occludin is a functional component of the tight junction.* Journal of Cell Science, 1996. **109**: p. 2287-2298.

243. Yu, A.S.L., et al., *Knockdown of occludin expression leads to diverse phenotypic alterations in epithelial cells.* American Journal of Physiology-Cell Physiology, 2005. **288**(6): p. C1231-C1241.

244. Ikenouchi, J., et al., *Tricellulin constitutes a novel barrier at tricellular contacts of epithelial cells.* Journal of Cell Biology, 2005. **171**(6): p. 939-945.

245. Krug, S.M., et al., *Tricellulin Forms a Barrier to Macromolecules in Tricellular Tight Junctions without Affecting Ion Permeability.* Molecular Biology of the Cell, 2009. **20**(16): p. 3713-3724.

246. Van Itallie, C.M. and J.M. Anderson, *Architecture of tight junctions and principles of molecular composition.* Semin Cell Dev Biol, 2014. **36**: p. 157-65.

247. Hamazaki, Y., et al., *Multi-PDZ domain protein 1 (MUPP1) is concentrated at tight junctions through its possible interaction with claudin-1 and junctional adhesion molecule.* J Biol Chem, 2002. **277**(1): p. 455-61.

248. Poliak, S., et al., *Distinct claudins and associated PDZ proteins form different autotypic tight junctions in myelinating Schwann cells.* J Cell Biol, 2002. **159**(2): p. 361-72.

249. Umeda, K., et al., *ZO-1 and ZO-2 independently determine where claudins are polymerized in tight-junction strand formation.* Cell, 2006. **126**(4): p. 741-54.

250. Rehder, D., et al., *Junctional adhesion molecule-A participates in the formation of apico-basal polarity through different domains.* Experimental Cell Research, 2006. **312**(17): p. 3389-3403.

251. Babinska, A., et al., *F11-receptor (F11R/JAM) mediates platelet adhesion to endothelial cells: Role in inflammatory thrombosis.* Thrombosis and Haemostasis, 2002. **88**(5): p. 843-850.

252. Mandell, K.J. and C.A. Parkos, *Junctional adhesion molecule-1 (JAM1) homodimer formation is important for regulation of epithelial barrier function.* Faseb Journal, 2004. **18**(4): p. A14-A14.

253. Naik, M.U., et al., *Signaling through JAM-1 and alpha(nu)beta(3) is required for the angiogenic action of bFGF: dissociation of the JAM-1 and alpha(nu)beta(3) complex.* Blood, 2003. **102**(6): p. 2108-2114.

254. Cera, M.R., et al., *Increased DC trafficking to lymph nodes and contact hypersensitivity in junctional adhesion molecule-A-deficient mice.* J Clin Invest, 2004. **114**(5): p. 729-38.

255. Laukoetter, M.G., et al., *JAM-A regulates permeability and inflammation in the intestine in vivo.* Journal of Experimental Medicine, 2007. **204**(13): p. 3067-3076.

256. Cereijido, M., et al., *Polarized Monolayers Formed by Epithelial-Cells on a Permeable and Translucent Support.* Journal of Cell Biology, 1978. **77**(3): p. 853-880.

257. Martinez-Palomo, A., et al., *Experimental Modulation of Occluding Junctions in a Cultured Transporting Epithelium.* Journal of Cell Biology, 1980. **87**(3): p. 736-745.

258. Lacaz-Vieira, F. and M.M. Jaeger, *Protein kinase inhibitors and the dynamics of tight junction opening and closing in A6 cell monolayers.* J Membr Biol, 2001. **184**(2): p. 185-96.

259. Gonzalez-Mariscal, L., et al., *Role of calcium in tight junction formation between epithelial cells.* Am J Physiol, 1990. **259**(6 Pt 1): p. C978-86.

260. Ivanov, A.I., et al., *Role for actin filament turnover and a myosin II motor in cytoskeleton-driven disassembly of the epithelial apical junctional complex.* Mol Biol Cell, 2004. **15**(6): p. 2639-51.

261. Gonzalez-Mariscal, L., R. Tapia, and D. Chamorro, *Crosstalk of tight junction components with signaling pathways.* Biochim Biophys Acta, 2008. **1778**(3): p. 729-56.

262. Spring, K.R., *Routes and mechanism of fluid transport by epithelia.* Annual Review of Physiology, 1998. **60**: p. 105-119.

263. Shen, L., et al., *Tight junction pore and leak pathways: a dynamic duo.* Annu Rev Physiol, 2011. **73**: p. 283-309.

264. LeBleu, V.S., B. Macdonald, and R. Kalluri, *Structure and function of basement membranes.* Exp Biol Med (Maywood), 2007. **232**(9): p. 1121-9.

265. Hughes, C.S., L.M. Postovit, and G.A. Lajoie, *Matrigel: a complex protein mixture required for optimal growth of cell culture.* Proteomics, 2010. **10**(9): p. 1886-90.

266. https://www.corning.com/worldwide/en/products/lifesciences/products/surfaces/matrigel-matrix.html. (Accessed 22/May/2017)

267. Kleinman, H.K. and G.R. Martin, *Matrigel: basement membrane matrix with biological activity.* Semin Cancer Biol, 2005. **15**(5): p. 378-86.

268. Vachon, P.H., J. Durand, and J.F. Beaulieu, *Basement membrane formation and re-distribution of the beta 1 integrins in a human intestinal co-culture system.* Anat Rec, 1993. **235**(4): p. 567-76.

269. Vachon, P.H., et al., *Cellular fibronectin expression is down-regulated at the mRNA level in differentiating human intestinal epithelial cells.* Exp Cell Res, 1995. **216**(1): p. 30-4.

270. Lotz, M.M., et al., *Intestinal epithelial restitution. Involvement of specific laminin isoforms and integrin laminin receptors in wound closure of a transformed model epithelium.* Am J Pathol, 1997. **150**(2): p. 747-60.

271. Larregieu, C.A. and L.Z. Benet, *Drug discovery and regulatory considerations for improving in silico and in vitro predictions that use Caco-2 as a surrogate for human intestinal permeability measurements.* AAPS J, 2013. **15**(2): p. 483-97.

272. Thie, M., et al., *Interactions between trophoblast and uterine epithelium: monitoring of adhesive forces.* Hum Reprod, 1998. **13**(11): p. 3211-9.

273. Capaldo, C.T. and A. Nusrat, *Cytokine regulation of tight junctions.* Biochim Biophys Acta, 2009. **1788**(4): p. 864-71.

274. Ma, T.Y., et al., *TNF-α-induced increase in intestinal epithelial tight junction permeability requires NF-κB activation.* American Journal of Physiology - Gastrointestinal and Liver Physiology, 2004. **286**(3): p. G367-G376.

275. Chen, M.L., et al., *Disruption of tight junctions and induction of proinflammatory cytokine responses in colonic epithelial cells by Campylobacter jejuni.* Infect Immun, 2006. **74**(12): p. 6581-9.

276. Le Ferrec, E., et al., *In vitro models of the intestinal barrier - The report and recommendations of ECVAM Workshop 46.* Atla-Alternatives to Laboratory Animals, 2001. **29**(6): p. 649-668.

277. Yang, Y.F., N. Wu, and X.W. Yang, *[Establishment of Caco-2 cell monolayer model with collagen coating 6-well plates for study of traditional Chinese medicine prescription].* Zhongguo Zhong Yao Za Zhi, 2014. **39**(3): p. 515-9.

278. Belec, L., et al., *Proinflammatory cytokine expression in cervicovaginal secretions of normal and HIV-infected women.* Cytokine, 1995. **7**(6): p. 568-74.

279. Lambert-Niclot, S., et al., *Factors associated with the selection of mutations conferring resistance to protease inhibitors (PIs) in PI-experienced patients displaying treatment failure on darunavir.* Antimicrob Agents Chemother, 2008. **52**(2): p. 491-6.

280. http://www.hiv-druginteractions.org/checker. (Accessed 22/May/2017)

281. Santos, S.d., et al., *Amphiphilic Molecules in Drug Delivery Systems*, in *Drug Delivery Systems: Advanced Technologies Potentially Applicable in Personalised Treatment*, J. Coelho, Editor. 2013, Springer Netherlands: Dordrecht. p. 35-85.

282. Levitt, L.J., et al., *Production of granulocyte/macrophage-colony-stimulating factor by human natural killer cells. Modulation by the p75 subunit of the interleukin 2 receptor and by the CD2 receptor.* J Clin Invest, 1991. **88**(1): p. 67-75.

283. Dezzutti, C.S., et al., *Reformulated tenofovir gel for use as a dual compartment microbicide.* Journal of Antimicrobial Chemotherapy, 2012. **67**(9): p. 2139-2142.

284. Moss, J.A., et al., *Pharmacokinetics of a multipurpose pod-intravaginal ring simultaneously delivering five drugs in an ovine model.* Antimicrob Agents Chemother, 2013. **57**(8): p. 3994-7.

285. Gutmann, H., et al., *Breast cancer resistance protein and P-glycoprotein expression in patients with newly diagnosed and therapy-refractory ulcerative colitis compared with healthy controls.* Digestion, 2008. **78**(2-3): p. 154-62.

286. Wojtal, K.A., et al., *Changes in mRNA expression levels of solute carrier transporters in inflammatory bowel disease patients.* Drug Metab Dispos, 2009. **37**(9): p. 1871-7.

287. Uwai, Y., et al., *Renal transport of adefovir, cidofovir, and tenofovir by SLC22A family members (hOAT1, hOAT3, and hOCT2).* Pharm Res, 2007. **24**(4): p. 811-5.

288. Klaassen, C.D. and L.M. Aleksunes, *Xenobiotic, bile acid, and cholesterol transporters: function and regulation.* Pharmacol Rev, 2010. **62**(1): p. 1-96.

289. Calabro, A.R., R. Konsoula, and F.A. Barile, *Evaluation of in vitro cytotoxicity and paracellular permeability of intact monolayers with mouse embryonic stem cells.* Toxicol In Vitro, 2008. **22**(5): p. 1273-84.

290. Konsoula, R. and F.A. Barile, *Correlation of in vitro cytotoxicity with paracellular permeability in Caco-2 cells.* Toxicol In Vitro, 2005. **19**(5): p. 675-84.

291. Lim, M.J., et al., *Cytotoxicity testing of multipurpose contact lens solutions using monolayer and stratified cultures of human corneal epithelial cells.* Eye Contact Lens, 2009. **35**(6): p. 287-96.

292. Gennari, A., et al., *Sensitive endpoints for evaluating cadmium-induced acute toxicity in LLC-PK1 cells.* Toxicology, 2003. **183**(1-3): p. 211-20.

293. Ayehunie, S., et al., *Development of an in vitro alternative assay method for vaginal irritation.* Toxicology, 2011. **279**(1-3): p. 130-8.

294. Costin, G.E., et al., *Vaginal irritation models: the current status of available alternative and in vitro tests.* Altern Lab Anim, 2011. **39**(4): p. 317-37.

295. Poonia, B., et al., *Cyclic changes in the vaginal epithelium of normal rhesus macaques.* J Endocrinol, 2006. **190**(3): p. 829-35.

296. Clark, M.R., et al., *Preclinical evaluation of UC781 microbicide vaginal drug delivery.* Drug Deliv Transl Res, 2011. **1**(2): p. 175-82.

297. Fatakdawala, H. and S.A. Uhland, *Hydrogen peroxide mediated transvaginal drug delivery.* Int J Pharm, 2011. **409**(1-2): p. 121-7.

298. Ayehunie, S., et al., *Organotypic human vaginal-ectocervical tissue model for irritation studies of spermicides, microbicides, and feminine-care products.* Toxicol In Vitro, 2006. **20**(5): p. 689-98.

299. Al-Sadi, R.M. and T.Y. Ma, *IL-1beta causes an increase in intestinal epithelial tight junction permeability.* J Immunol, 2007. **178**(7): p. 4641-9.

300. Thews, O., et al., *Impact of extracellular acidity on the activity of P-glycoprotein and the cytotoxicity of chemotherapeutic drugs.* Neoplasia, 2006. **8**(2): p. 143-52.

301. Sauvant, C., et al., *Acidosis induces multi-drug resistance in rat prostate cancer cells (AT1) in vitro and in vivo by increasing the activity of the p-glycoprotein via activation of p38.* Int J Cancer, 2008. **123**(11): p. 2532-42.

302. Wartenberg, M., et al., *Regulation of the multidrug resistance transporter P-glycoprotein in multicellular prostate tumor spheroids by hyperthermia and reactive oxygen species.* Int J Cancer, 2005. **113**(2): p. 229-40.

303. Boskey, E.R., et al., *Origins of vaginal acidity: high D/L lactate ratio is consistent with bacteria being the primary source.* Hum Reprod, 2001. **16**(9): p. 1809-13.

304. Okada, H., et al., *Vaginal absorption of a potent luteinizing hormone-releasing hormone analogue (leuprolide) in rats II: mechanism of absorption enhancement with organic acids.* J Pharm Sci, 1983. **72**(1): p. 75-8.

305. Okada, H., T. Yashiki, and H. Mima, *Vaginal absorption of a potent luteinizing hormone-releasing hormone analogue (leuprolide) in rats III: Effect of estrous cycle on vaginal absorption of hydrophilic model compounds.* J Pharm Sci, 1983. **72**(2): p. 173-6.

306. Larsen, B. and G.R. Monif, *Understanding the bacterial flora of the female genital tract.* Clin Infect Dis, 2001. **32**(4): p. e69-77.

307. Spear, G.T., et al., *Identification of rhesus macaque genital microbiota by 16S pyrosequencing shows similarities to human bacterial vaginosis: implications for use as an animal model for HIV vaginal infection.* AIDS Res Hum Retroviruses, 2010. **26**(2): p. 193-200.

Appendix

Chapter 3

Challenges in Microbicide Drug Delivery: Identifying Targets and Evolving Strategies

Karolin Hijazi,[a] Constandinos Carserides,[b] and Charles Kelly[b]

[a]*University of Aberdeen Dental School, Foresterhill Campus, Cornhill Road Aberdeen, AB25 2ZR, Scotland, United Kingdom*
[b]*Dental Institute, King's College London, 2nd Floor Hodgkin Building, Guy's Campus London, SE1 1UL, United Kingdom*

k.hijazi@abdn.ac.uk

3.1 Introduction

Current development of microbicides against HIV-1 is largely focused on antiretroviral (ARV) drugs. The relative success of the CAPRISA 004 trial of vaginally applied tenofovir (TFV) gel provides a rationale for developing microbicides that target intracellular events in virus replication [1]. While the reverse transcriptase inhibitors (RTIs) TFV and dapivirine are currently in Phase 3 clinical trials as single drugs, efforts are also under way to develop combination microbicides that include two or possibly more drugs. The potential advantages of combinations include increased efficacy and presentation of a higher barrier to drug resistance.

Drug Delivery and Development of Anti-HIV Microbicides
Edited by José das Neves and Bruno Sarmento

ISBN 978-981-4463-56-0 (Hardcover), 978-981-4463-57-7 (eBook)
www.panstanford.com

Development of such products also presents a number of challenges. To date, microbicides under development have targeted earlier events in infection, including HIV-1 attachment and fusion and production of double-stranded complementary DNA (cDNA) by reverse transcriptase (RT). Efficacy of microbicides may be improved by inclusion of compounds that have not been considered previously but that target later events such as integration of the viral genome or maturation of virus particles. Microbicides must deliver effective concentrations of drug to sub-mucosal target cells. In turn, this may need improved understanding of factors that influence drug distribution in tissues including the effects of drug uptake and efflux transporters. Desirable drugs in combination microbicides may have widely differing and incompatible physicochemical properties or may show unfavorable drug–drug interactions. Such incompatibilities present challenges for formulation.

In this chapter, we discuss findings from early events in HIV transmission that identify target cells for the prevention of infection. We review microbicides and targets currently under investigation as well as studies demonstrating in vitro the benefits of combining ARV drugs. We also discuss factors that may influence tissue distribution of drugs and challenges that must be addressed in the formulation of microbicides.

3.2 HIV Transmission at Mucosal Surfaces

Early HIV-1 infection events at the mucosal portal of entry have been studied in non-human primate (NHP) models. The similarities of simian immunodeficiency virus (SIV) transmission and propagation to HIV-1 and the similarities in anatomy and immunology of the genital tract of macaques to humans have made these models a valuable tool for identifying critical events that follow mucosal exposure to HIV-1 and precede clinical signs and symptoms of disease [2].

Transmission studies where rhesus macaques were inoculated intra-vaginally with high doses of SIV revealed that virus entry across the epithelial barrier results in productive infection of a small founder population of $CD4^+$ T cells at 3–4 days after challenge [3,4]. Exposure to the virus inoculum led to increased expression of macrophage inflammatory protein 3α (MIP-3α or CCL20) in

endocervial epithelium and recruitment of plasmacytoid dendritic cells (pDC). In turn, pDC may recruit and activate further $CD4^+$ T cells through production of MIP-1α (CCL3) and MIP-1β (CCL4) [4]. Expansion of the founder $CD4^+$ T cells (stimulated by innate immune and inflammatory mediators) then results in infection of draining lymph nodes and secondary lymphoid organs from day six on [3].

Ex vivo cervicovaginal tissue explant models of HIV infection have confirmed the role of dermal $CD4^+$ T cells as predominant targets of virus particles, but also suggested that Langerhans cells and dendritic cells may contribute to viral dissemination to lymphoid tissues [5] and enhance amplification of viral replication in $CD4^+$ T cells at mucosal sites [6].

The small size of the infected founder population was also confirmed in a study where animals received multiple low dose intra-rectal challenges with virus stocks containing a median of 48 different SIV Env sequences [7]. Single-genome amplification confirmed that the founder $CD4^+$ T cells populations were productively infected by one or a few viruses. These conclusions are in agreement with studies demonstrating that most HIV-1 infections are initiated by a single virus genotype [8].

Early events following rectal mucosa exposure to SIV, as well as subsequent kinetics of viral replication and dissemination, exhibit significantly different characteristics compared to vaginal infection. Breaches within the epithelial barrier and potential interaction with intraepithelial migrating cells may be major mechanisms of HIV transmission across the rectal mucosal barrier. HIV may also cross the rectal epithelium by transcytosis through epithelial cells [9] and M cells [10], and opening of tight junctions by analogy with other viruses [11,12]. The rectal epithelial layer is therefore likely to be more susceptible to virus entry compared to vaginal epithelium. The time required for dissemination of infection appears to be significantly shorter than that observed in infection of cervicovaginal mucosae. Analyses of viral dissemination in a simian-human immunodeficiency virus (SHIV) challenge model demonstrated proviral DNA in secondary lymphoid organs at 3 days post-inoculation [13]. In a more recent study where rhesus macaques were challenged intra-rectally with relatively low doses of pathogenic SIV, infectious virus was recovered in secondary lymphoid organs at four hours after rectal challenge [14]. At this time point virus was present in both lymphoid aggregates and

lamina propria of the rectum suggesting viral entry *via* digestive epithelium as well as *via* follicle-associated epithelium. Similar to vaginal infection, the primary target cells for HIV replication in the lamina propria were T cells, but the virus was also found associated with dendritic cell-specific intercellular adhesion molecule-3-grabbing non-integrin (DC-SIGN) positive cells and macrophages. These findings have also been confirmed in a further SHIV challenge model study where the effect of intravaginal inoculation was compared to intravenous and intrarectal challenges with the same SHIV strain [15].

These findings indicate that an effective microbicide must either disable HIV in the vaginal or rectal lumen or be delivered submucosally (while preserving integrity of the epithelial barrier) to prevent infection of submucosal $CD4^+$ T cells.

3.3 Microbicides: Current State of the Art

First-generation microbicides were relatively non-specific and aimed at disrupting HIV-1 virus particles (surfactants) or inhibiting virus attachment (polyanionic compounds) but did not show efficacy in clinical trials [16–20]. The CAPRISA (Centre for the AIDS Programme of Research in South Africa) 004 Phase 2b clinical trial of TFV 1% gel as a vaginal microbicide demonstrated 39% protection and provided the first proof-of-principle for the concept that microbicides could prevent infection [1]. Since TFV is a nucleotide RTI (NtRTI), this trial also provides a rationale for the development of microbicides that target intracellular events. Current efforts to develop microbicides are focused largely on compounds that specifically target different stages of HIV infection. Microbicides in development have been described in a number of previous reviews [21–24]. A brief outline with emphasis on mechanisms/targets follows.

3.3.1 HIV Fusion

The interactions between HIV-1 envelope protein and host cell receptors (CD4 and CCR5) have been targeted by a range of candidate microbicides including antibodies, single domain (llama-derived) antibodies, peptides and small molecule inhibitors aimed at preventing virus attachment and fusion. That vaginally applied

antibodies with neutralizing activity could prevent infection was demonstrated in a NHP challenge model using the monoclonal antibody b12 (directed against the CD4 binding site of gp120) [25] and subsequently with a combination of three monoclonal antibodies (2G12, 2F5, and 4E10) [26]. The combination of three monoclonal antibodies formulated as a vaginal gel was shown to be safe in a Phase 1 clinical trial [27]. A peptide mimic of the site of CD4 that binds to gp120 has also been shown effective in a NHP model of SHIV vaginal challenge [28].

Small molecule inhibitors of viral fusion that bind to gp120 are also under investigation as microbicides. The compound BMS-806 also showed efficacy in NHP model of SHIV vaginal challenge [29]. Inhibitors of this class do not prevent gp120 binding to CD4 (in contrast to the antibody and peptide inhibitors described above) but bind to gp120 and prevent the conformational changes required for membrane fusion [30].

Different classes of microbicides that target the co-receptor CCR5 are under development. A series of analogues of regulated on activation, normal T cell expressed and secreted (RANTES or CCL5) protein, a chemokine ligand of CCR5, have been developed that inhibit fusion either by receptor internalization or by receptor blockage [31,32]. Compounds in this series include PSC-RANTES [33], 6P4-RANTES, and 5P12-RANTES [34], and have shown protection in NHP vaginal challenge studies. In contrast to PSC-RANTES, which requires chemical modification of the *N*-terminus, 6P4-RANTES and 5P-12 RANTES are modified by inclusion of additional (naturally occurring) amino acids at the *N*-terminus thus allowing for large-scale production by microbial fermentation. Small molecule inhibitors of CCR5 binding are also being investigated as potential microbicides. Maraviroc, the only drug in this class approved for therapy, was also protective as a microbicide in a NHP model of vaginal challenge [35].

3.3.2 Reverse Transcriptase

The HIV-1 enzyme RT, that produces double-stranded viral cDNA, has been successfully targeted by nucleoside and nucleotide RTIs (NRTIs and NtRTIs, respectively) for treatment in HIV infection. As above, TFV (an NtRTI licensed for therapeutic use) is the only compound to demonstrate efficacy in humans when tested as a

vaginal microbicide [1]. In pre-clinical studies, TFV had also been protective against rectal [36] and vaginal [37] challenge in NHP models. However, in a further Phase 2b human safety and efficacy trial (the VOICE trial, MTN-003) that also tested TFV vaginal gel (as well as oral forms of TFV) no protection was observed [38]. The low level of adherence to TFV use was reported as likely to be the most significant factor in the lack of protection. Serum levels of drug were determined in a large subset of trial participants and TFV was detected in only 23% of participants in the vaginal gel arm [38,39]. Another Phase 3 trial (FACTS 001 study) of TFV gel using the same dosing schedule as CAPRISA 004 began in October 2011 and is in progress [40].

Non-nucleoside RTIs (NNRTIs) are non-competitive inhibitors that bind to an induced allosteric hydrophobic pocket approximately 15 Å from the RT active site [41]. Four NNRTIs, dapivirine (TMC120), UC-781, MIV-150, and MC-1220 are being investigated as potential microbicides. Dapivirine, currently the most advanced in clinical development, has been formulated in a vaginal ring (see below) for sustained delivery and is being tested in two linked Phase 3 safety and efficacy trials (The Ring Study, International Partnership for Microbicides; ASPIRE, Microbicide Trials Network) with completion expected in 2015 [42,43]. UC-781 formulated as gels has been generally well tolerated in vaginal [44,45] and rectal [46] Phase 1 trials. In pre-clinical studies both MIV-150 [47,48] and MC-1220 [49] prevented infection in NHP models of vaginal transmission.

3.3.3 RNase H

HIV-1 RT is a heterodimer comprising p66 and p51 polypeptides. The p66 polypeptide includes both RT (*N*-terminal domain) and RNase H (*C*-terminal domain) activity. The p51 polypeptide is itself derived by *C*-terminal proteolytic cleavage of a separate p66 polypeptide and plays a role in RNA/DNA hybrid positioning and hydrolysis [50]. RNase H activity is essential for production of double-stranded viral cDNA and a number of studies have described inhibitors of RNase H that may have potential as microbicides. Some NNRTIs show partial inhibition of RNase H activity in addition to inhibiting RT activity with both effects being

the result of binding to the single NNRTI inding site on RT [51]. A synthetic oligonucleotide has been investigated that binds specifically to the highly conserved polypurine tract (PPT) in the HIV genome and activates RNase H activity within the viral particle [52]. Pre-incubation of HIV with the oligonucleotide led to reduced infectivity in vitro [52] and conferred protection in a humanized severe combined immunodeficient (hu-SCID) mouse model of intraperitoneal challenge [53]. The need for improving oligonucleotide uptake by the virus and the high production cost remain hurdles to be overcome in further development of this class of inhibitors.

3.3.4 Integrase

HIV-1 integrase enzyme integrates reversed-transcribed (viral) DNA into the host genome. Raltegravir is the only inhibitor of integrase in use for therapy and has shown efficacy as a vaginal microbicide in a macaque model of SHIV challenge [54]. Since the integrase complex involves several (host-derived) cellular co-factors, inhibitors that may prevent binding of integrase to key factors have been investigated in pre-clinical studies. Small molecule inhibitors of integrase binding to lens epithelium-derived growth factor (LEDGF/p75) have been described as both inhibiting integrase activity and virus replication [55] although again, further optimization will be necessary for product development.

3.3.5 Protease

HIV-1 protease is essential for the conversion of non-infectious immature virus particles to mature infectious virus, a process initiated by cleavage of gag and gag-pol polyproteins. The successful use of protease inhibitors (PIs) as a component in highly active antiretroviral therapy (HAART) together with their high potency and high barrier to resistance have stimulated interest in developing them as microbicides [56,57]. In vitro studies of saquinavir demonstrated neutralizing activity both in cell and tissue explant systems with half-maximal inhibitory concentration (IC_{50}) values in the low micromolar range.

3.4 Combination Microbicides

The focus on ARV-based microbicides raises concerns regarding efficacy against transmission of strains of HIV that are resistant to ARV drug and the possibility of driving resistance to these last. In response to this, the inclusion of ARV drugs in combination in a single microbicide formulation has been investigated. The advantages of combinations are that they may be effective in preventing transmission of strains resistant to one of the drugs and that they present a higher barrier to the development of resistant strains since more mutations would be required than for a single drug. The possibility of drug–drug interactions that reduce antiviral activity and the likelihood that drugs with very different physicochemical properties may need to be co-formulated present potential obstacles for product development.

Support for the concept of a microbicide incorporating drug combinations was provided by a study in which small molecule inhibitors BMS-806 (binds to gp120 and prevents conformational changes required for fusion) and CMPD167 (binds to CCR5 and inhibits binding of gp120) were tested together with C52L (bacterially expressed modified form of the fusion inhibitor T-20) in a macaque vaginal challenge model with SHIV [29]. Drug combinations were tested for neutralizing activity in vitro showing additive or synergistic activity. In challenge experiments, significant protection was evident whether compounds were applied singly or in combination but there were some indications that combinations were more effective.

Drugs that act on the same target, namely RTIs, have also been investigated in combination. Dual combinations of TFV, dapivirine, and UC-781 have been tested in vitro in cell culture and colorectal explant tissues [58]. In each case, combination was more potent than individual drugs in tested models and NNRTI (dapivirine or UC-781) plus NtRTI (TFV) combinations were effective against strains of HIV-1 resistant to either class of drug. In an extension of this study, the NRTI emtricitabine was included to allow comparisons of triple and quadruple combinations of RTIs [59]. Triple combinations were more effective than double, while quadruple combinations showed no significant improvement over triple. In these studies, no antagonistic effects of drug combinations were evident. Gel formulations of UC-781 plus TFV were tested

in ectocervical explants showing both tissue compatibility and antiviral activity [60].

3.5 Factors Affecting Drug Distribution in Mucosal Tissues

3.5.1 Drug Transport and Metabolism

To be effective, ARV drug-based microbicides that target intracellular events in HIV-1 infection must be delivered to the sub-mucosal $CD4^+$ T cells that have been identified as forming the initial foci of infection (as outlined in Section 3.2) and therefore must first pass through the mucosal epithelium. The distribution of drugs in mucosal tissues may be influenced by the activity of specific cell membrane transporters whose primary function is the transport of nutrients and solutes. Solute transporters are grouped in two superfamilies, namely, solute carrier (SLC) transporters and ATP-binding cassette (ABC) transporters. Human SLC transporters are further divided into 52 different sub-families comprising a total of 395 transporter genes [61] while ABC transporters (48 genes) are grouped into 7 subfamilies.

SLC transporters show relatively broad and in some cases overlapping substrate specificities and are mainly responsible for the transport of drugs into cells. Those implicated in the transport of ARV drugs include the organic anion-transporting polypeptides (OATP, subfamily SLCO), organic anion (OAT, SLC22) and organic cation (OCT, SLC22) transporters, concentrative (CNT, SLC28) and equilibrative (ENT, SLC29) nucleoside transporters as well as peptide transporters (PEPT, SLC15) [62,63]. A common structural feature of SLC transporters is the large number (11–13) of predicted transmembrane domains. Efflux of drugs is mediated principally by ABC transporters including members of the P-glycoprotein (P-gp) subfamily (ABCB) as well as breast cancer resistant proteins (BCRP, ABCG subfamily) and multidrug resistance proteins (MRP, ABCC subfamily).

Because of their key role in determining drug distribution after systemic or oral administration, the expression and distribution of drug transporters in intestinal epithelia, hepatocytes, and kidney proximal tubules have been relatively well characterized and for some transporters the distribution on apical or basolateral surfaces

of epithelia have been described [64,65]. Polarized distribution of transporters allows transport of drugs across the epithelium with uptake at the apical surface by SLC transporters and efflux at the basolateral surface by MRP or other efflux transporters. Conversely, expression of P-gp at the apical surface of intestinal lumen may restrict net uptake of drugs. In mice deficient in intestinal P-gp, bioavailability following oral administration of the anti-cancer drug paclitaxel increased significantly compared with wild type mice confirming the role of P-gp in efflux of drug back to the intestinal lumen [66].

Drug transporters that may be relevant for rectal or vaginal microbicides have been described in the colon [67–69] and more recently in cervicovaginal tissue [70]. Data are summarized in Fig. 3.1. In the colon, while influx organic ion (OCT3 and OATPB) transporters are expressed on the apical surface, drug uptake may be restricted by the presence of efflux (P-gp and BDRP) transporters on the same surface. Conversely, on the basolateral surface, the activity of the efflux transporter (MRP3) may be compromised by influx transporters with the potential to reduce net transfer of drug across the epithelium. The apical and basolateral distribution of transporters in cervicovaginal epithelium has not been determined. However, the P-gp and BCRP efflux transporters are generally at the apical surface of epithelial cells while MRP1 is associated with basolateral surfaces [71]. MRP4 and MRP5 have been reported at both apical and basolateral surfaces in other tissues. Influx organic cation transporters (OCT2 and OCT3) have been reported on the apical surfaces of other epithelial cell types while the organic anion transporters have been reported on both apical and basolateral surfaces [71] as has the equilibrative nucleoside transporter ENT1 [62]. Drug transporters in peripheral blood $CD4^+$ T cells are well characterized including both influx and efflux transporters as also shown in Fig. 3.1 [62].

The influence of mucosal drug transporters on the distribution of topically applied ARV-based microbicides remains to be determined. Of the ARV drugs that are most advanced in clinical development as microbicides, TFV, as a polar small molecule, may cross the epithelium by the paracellular route but has also been identified as a substrate for influx organic anion transporters OAT1 and OAT3 and efflux transporter MRP4 [72,73]. Maraviroc

is a substrate for the influx transporter OATP1B1 [74], expression of which has not been reported for colorectal or cervicovaginal epithelium. Maraviroc is a substrate for the efflux transporter P-gp, which could potentially limit uptake. Hydrophobic drugs such as dapivirine and UC-781 may partition directly into epithelial and T cell membranes.

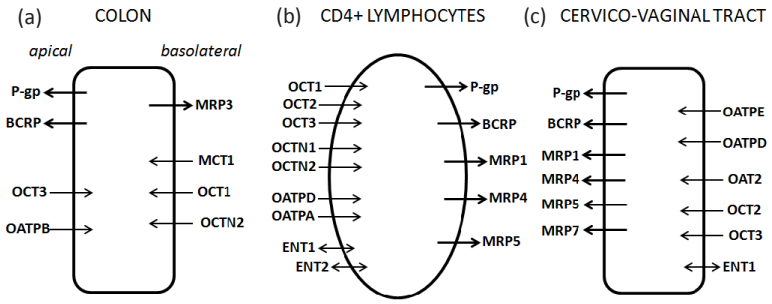

Figure 3.1 Efflux and uptake drug transporters that may be relevant for rectal or vaginal microbicides have been described in the (a) colon, (b) $CD4^+$ lymphocytes and (c) cervicovaginal tissue. The apical and basolateral distribution of transporters in cervicovaginal epithelium has not been determined.

More broadly, several nucleoside analogue ARV drugs are substrates for influx transporters of the SLC22 (organic cation and anion transporters) and SLC29 (ENT1 and ENT2) families as well as MRP4 and MRP5 efflux transporters that are expressed in cervicovaginal or colorectal epithelium [63]. PIs such as lopinavir, saquinavir, and darunavir are substrates for OATP1A1 and OATP1B1 (members of the SLCO family) and most members of this class of ARV drugs are substrates for P-gp as well as MRP1 and MRP2 efflux transporters [62]. ARV drugs may also modulate activity and expression of drug transporters. Several PIs inhibit OATP [75] and OCT transporters as well as P-gp, MRP, and BCRP efflux transporters [62,76]. In addition, some PIs induce P-gp expression. NRTIs, NtRTIs and NNRTIs also inhibit the activity of BCRP [76,77] and MRP [77] efflux transporters as well as some influx transporters [62]. While these observations point to the complexity of factors that may contribute to tissue disposition of drugs, they also point to the possibility of manipulating drug combinations to improve distribution and retention of ARV drugs at target tissues.

Metabolism by cytochrome P450 (CYP) isoforms further alters tissue levels of ARV drugs. Reverse transcription polymerase chain reaction (RT-PCR) analyses of human cervicovaginal tissue indicated that, while CYP1A1 and CYP1B1 isoforms were expressed, most isoforms, including CYP3A4 (the most highly expressed isoform in liver), were not [70]. In contrast, eight members of the UDP-glucuronosyltransferase (UGT) family of enzymes were expressed. Enzymes in this family catalyze the addition of hexose moieties to small molecules (including some drugs) which facilitates recognition and efflux by drug transporters [78]. Similar findings have been reported for colonic tissue where low messenger RNA (mRNA) levels were reported for most CYP isoforms, with the exception of CYP2J2 and CYP3A5 [79], while RT-PCR analyses suggested that 11 members of the UGT enzyme family were expressed [80]. Relatively low levels of CYP could be advantageous for maintaining tissue levels of locally applied microbicides.

3.5.2 Mucosal Inflammation

Inflammation of the genital tract that may result from alterations in microbiota or sexually transmitted diseases is associated with increased transmission of HIV-1 [81–83]. Contributing factors include a local increase in the number of HIV-1-susceptible target cells, increased activation of $CD4^+$ T cells and damage to the integrity of the epithelial barrier. Pro-inflammatory cytokines impair barrier function either by inducing apoptosis of epithelial cells or remodeling of tight junctions, thus resulting in increased paracellular leakiness [84,85], which in turn may impact on tissue drug distribution. Inflammation may also have an impact on the tissue distribution of ARV drugs by altering expression of drug transporters.

Studies of the effects of inflammation on expression of drug transporters generally focus on intestinal, hepatic, or placental transporters, and data for the female reproductive tract are not available. In inflamed tissue of duodenal biopsies from patients with ulcerative colitis, the expression of P-gp and BCRP efflux transporters is reduced as compared to non-affected mucosa or normal controls [86]. In colon biopsies from patients with ulcerative colitis, mRNA levels of the nucleoside transporters ENT1, ENT2 (SLC29 family), and CNT2 (SLC28) were significantly increased

as were mRNA levels of the organic anion transporters OATP2B1, OATPE (SLCO), and OCTN1 (SLC22) [87]. The net effect of these changes has not been determined although reduction in efflux transporters could lead to higher tissue levels of topically applied drugs.

3.6 Formulation Strategies

Understanding of the impact of drug transporters may contribute to optimized formulations for the delivery of ARV-based microbicides to target tissues. Potentially inhibitors or activators of specific efflux or uptake transporters could be included in formulations for improved delivery. Drug combinations present further challenges for formulation where the active pharmaceutical ingredients (APIs) may possess widely different physicochemical characteristics. Formulations of hydrophobic NNRTIs with TFV in a single gel have been reported. Gel formulations of UC-781 with TFV were developed that delivered in vitro (organotypic human vaginal-ectocervical tissue) and in vivo (vaginal administration in rabbits) tissue drug concentrations that were considerably in excess of in vitro IC_{50} values for each drug [88]. In this, and in earlier work [89] both the poor aqueous solubility and the oxidative degradation of UC-781 presented challenges.

Co-formulation of ARV drug combinations in intravaginal rings has also been reported. The advantage of these continuous use dosage forms is that incompatible drugs can be segregated. A silicone ring in which pods containing different drugs are inserted was used to co-formulate TFV and acyclovir [90]. A combination of maraviroc and dapivirine has also been formulated in thermoplastic (ethylene-vinyl acetate copolymer, EVAc) rings [91].

3.7 Conclusions and Future Perspectives

The challenge facing microbicide developers is to increase efficacy over the levels observed in the CAPRISA 004 trial and to understand the lack of protection in some subsequent efficacy trials. As discussed above, compliance is likely to be a key factor in determining efficacy. In turn, this points to the need for developing microbicide formulations with improved user acceptability. In this regard,

results of the Ring Study/ASPIRE trial of dapivirine formulated for sustained delivery by intravaginal ring will be of considerable interest. Further improvements in efficacy may come from development of combination microbicides. These may be particularly important where drugs are in use for both treatment and prevention so as to prevent transmission of resistant virus.

In view of studies (discussed above) that immune activation may enhance HIV acquisition and the finding that exposure to HIV-1 upregulates production of inflammatory cytokines by mucosal epithelial cells leading to disruption of tight junctions and translocation of virus [92], inclusion of inhibitors of immune activation in microbicide formulations may be a consideration. Protection against SIV transmission in the macaque model by vaginal application of glycerol monolaurate, which inhibits production of pro-inflammatory cytokines, provides a rationale for such an approach [4]. In addition, drug delivery may be improved by formulations designed to modulate drug transporter activity.

ARV drugs currently being developed as microbicides are either also used for treatment or belong to the same classes of drugs that are used for treatment. In the longer term, it would be preferable to have different classes of drug for prophylaxis or treatment. It would therefore be prudent to continue the development of some of the other classes of microbicide molecules including domain antibodies, peptides, RANTES analogues or small molecules (outlined above) that have entirely different mechanisms of action. In the longer term again, other cellular moieties may be targeted with novel classes of drugs. Genome wide screening studies [93–95] have collectively identified 1,254 cellular factors that may be essential for viral replication in host cells [96]. Meta-analysis of the genes identified in screening studies and those in the National Center for Biotechnology Information interaction database identified 259 genes that overlapped in at least two studies while network analysis identified a total of 1,657 cellular proteins that formed interactions with other host cell factors (implicated in HIV replication) or HIV-encoded proteins [96].

Acknowledgments

The authors are supported by grants from the European Commission: HEALTH-F3-2012-305316 (MOTIF) (C. K., K. H.) and

HEALTH-F3-2009-242135 (CHAARM) (C. K.). C. K. is grateful to Charlotte Vickers for assistance.

References

1. Abdool Karim, Q., Abdool Karim, S. S., Frohlich, J. A., Grobler, A. C., Baxter, C., Mansoor, L. E., Kharsany, A. B. M., Sibeko, S., Mlisana, K. P., Omar, Z., Gengiah, T. N., Maarschalk, S., Arulappan, N., Mlotshwa, M., Morris, L., and Taylor, D. (2010). Effectiveness and safety of tenofovir gel, an antiretroviral microbicide, for the prevention of HIV infection in women, *Science*, **329**, 1168–1174.
2. Zhang, Z., Schuler, T., Zupancic, M., Wietgrefe, S., Staskus, K. A., Reimann, K. A., Reinhart, T. A., Rogan, M., Cavert, W., Miller, C. J., Veazey, R. S., Notermans, D., Little, S., Danner, S. A., Richman, D. D., Havlir, D., Wong, J., Jordan, H. L., Schacker, T. W., Racz, P., Tenner-Racz, K., Letvin, N. L., Wolinsky, S., and Haase, A. T. (1999). Sexual transmission and propagation of SIV and HIV in resting and activated $CD4^+$ T cells, *Science*, **286**, 1353–1357.
3. Miller, C. J., Li, Q., Abel, K., Kim, E. Y., Ma, Z. M., Wietgrefe, S., La Franco-Scheuch, L., Compton, L., Duan, L., Shore, M. D., Zupancic, M., Busch, M., Carlis, J., Wolinsky, S., and Haase A. T. (2005). Propagation and dissemination of infection after vaginal transmission of simian immunodeficiency virus, *J. Virol*., **79**, 9217–9227.
4. Li, Q., Estes, J. D., Schlievert, P. M., Duan, L., Brosnahan, A. J., Southern, P. J., Reilly, C. S., Peterson, M. L., Schultz-Darken, N., Brunner, K. G., Nephew, K. R., Pambuccian, S., Lifson, J. D., Carlis, J. V., and Haase, A. T. (2009). Glycerol monolaurate prevents mucosal SIV transmission, *Nature*, **458**, 1034–1038.
5. Ballweber, L., Robinson, B., Kreger, A., Fialkow, M., Lentz, G., McElrath, M. J., and Hladik, F. (2011). Vaginal langerhans cells nonproductively transporting HIV-1 mediate infection of T cells, *J. Virol*., **85**, 13443–13447.
6. Hladik, F., Sakchalathorn, P., Ballweber, L., Lentz, G., Fialkow, M., Eschenbach, D., and McElrath, M. J. (2007). Initial events in establishing vaginal entry and infection by human immunodeficiency virus type-1, *Immunity*, **26**, 257–270.
7. Keele, B. F., Li, H., Learn, G. H., Hraber, P., Giorgi, E. E., Grayson, T., Sun, C., Chen, Y., Yeh, W. W., Letvin, N. L., Mascola, J. R., Nabel, G. J., Haynes, B. F., Bhattacharya, T., Perelson, A. S., Korber, B. T., Hahn, B. H., and Shaw G. M. (2009). Low-dose rectal inoculation of rhesus macaques

by SIVsmE660 or SIVmac251 recapitulates human mucosal infection by HIV-1, *J. Exp. Med*., **206**, 1117–1134.

8. Keele, B. F., Giorgi, E. E., Salazar-Gonzalez, J. F., Decker, J. M., Pham, K. T., Salazar, M. G., Sun, C., Grayson, T., Wang, S., Li, H., Wei, X., Jiang, C., Kirchherr, J. L., Gao, F., Anderson, J. A., Ping, L. H., Swanstrom, R., Tomaras, G. D., Blattner, W. A., Goepfert, P. A., Kilby, J. M., Saag, M. S., Delwart, E. L., Busch, M. P., Cohen, M. S., Montefiori, D. C., Haynes, B. F., Gaschen, B., Athreya, G. S., Lee, H. Y., Wood, N., Seoighe, C., Perelson, A. S., Bhattacharya, T., Korber, B. T., Hahn, B. H., and Shaw, G. M. (2008). Identification and characterization of transmitted and early founder virus envelopes in primary HIV-1 infection, *Proc. Natl. Acad. Sci. U. S. A*., **105**, 7552–7557.
9. Bomsel, M. (1997). Transcytosis of infectious human immunodeficiency virus across a tight human epithelial cell line barrier, *Nat. Med*., **3**, 42–47.
10. Fotopoulos, G., Harari, A., Michetti, P., Trono, D., Pantaleo, G., and Kraehenbuhl, J. P. (2002). Transepithelial transport of HIV-1 by M cells is receptor-mediated, *Proc. Natl. Acad. Sci. U. S. A*., **99**, 9410–9414.
11. Coyne, C. B., Shen, L., Turner, J. R., and Bergelson, J. M. (2007). Coxsackievirus entry across epithelial tight junctions requires occludin and the small GTPases Rab34 and Rab5, *Cell Host Microbe*, **2**, 181–192.
12. Walters, R. W., Freimuth, P., Moninger, T. O., Ganske, I., Zabner, J., and Welsh, M. J. (2002). Adenovirus fiber disrupts CAR-mediated intercellular adhesion allowing virus escape, *Cell*, **110**, 789–799.
13. Miyake, A., Ibuki, K., Enose, Y., Suzuki, H., Horiuchi, R., Motohara, M., Saito, N., Nakasone, T., Honda, M., Watanabe, T., Miura, T., and Hayami, M. (2006). Rapid dissemination of a pathogenic simian/human immunodeficiency virus to systemic organs and active replication in lymphoid tissues following intrarectal infection, *J. Gen. Virol*., **87** (Pt 5), 1311–1320.
14. Ribeiro Dos Santos, P., Rancez, M., Prétet, J. L., Michel-Salzat, A., Messent, V., Bogdanova, A., Couëdel-Courteille, A., Souil, E., Cheynier, R., and Butor, C. (2011). Rapid dissemination of SIV follows multisite entry after rectal inoculation, *PLoS One*, **6**, e19493.
15. Shakirzyanova, M., Tsai, L., Ren, W., Gettie, A., Blanchard, J., and Cheng-Mayer, C. (2012). Pathogenic consequences of vaginal infection with CCR5-tropic simian-human immunodeficiency virus SHIVSF162P3N, *J. Virol*., **86**, 9432–9442.
16. Van Damme, L., Govinden, R., Mirembe, F. M., Guédou, F., Solomon, S., Becker, M. L., Pradeep, B. S., Krishnan, A. K., Alary, M., Pande, B., Ramjee, G., Deese, J., Crucitti, T., and Taylor, D. (2008). Lack of

effectiveness of cellulose sulfate gel for the prevention of vaginal HIV transmission, *N. Engl. J. Med*., **359**, 463–472.

17. Van Damme, L., Ramjee, G., Alary, M., Vuylsteke, B., Chandeying, V., Rees, H., Sirivongrangson, P., Mukenge-Tshibaka, L., Ettiègne-Traoré, V., Uaheowitchai, C., Karim, S. S., Mâsse, B., Perriëns, J., and Laga, M. (2002). Effectiveness of COL-1492, a nonoxynol-9 vaginal gel, on HIV-1 transmission in female sex workers: A randomised controlled trial, *Lancet*, **360**, 971–977.
18. Peterson, L., Nanda, K., Opoku, B. K., Ampofo, W. K., Owusu-Amoako, M., Boakye, A. Y., Rountree, W., Troxler, A., Dominik, R., Roddy, R., and Dorflinger, L. (2007). SAVVY (C31G) gel for prevention of HIV infection in women: A phase 3, double-blind, randomized, placebo-controlled trial in Ghana, *PLoS One*, **2**, e1312.
19. Skoler-Karpoff, S., Ramjee, G., Ahmed, K., Altini, L., Plagianos, M. G., Friedland, B., Govender, S., De Kock, A., Cassim, N., Palanee, T., Dozier, G., Maguire, R., and Lahteenmaki, P. (2008). Efficacy of Carraguard for prevention of HIV infection in women in South Africa: A randomised, double-blind, placebo-controlled trial, *Lancet*, **372**, 1977–1987.
20. McCormack, S., Ramjee, G., Kamali, A., Rees, H., Crook, A. M., Gafos, M., Jentsch, U., Pool, R., Chisembele, M., Kapiga, S., Mutemwa, R., Vallely, A., Palanee, T., Sookrajh, Y., Lacey, C. J., Darbyshire, J., Grosskurth, H., Profy, A., Nunn, A., Hayes, R., and Weber, J. (2010). PRO2000 vaginal gel for prevention of HIV-1 infection (Microbicides Development Programme 301): A phase 3, randomised, double-blind, parallel-group trial, *Lancet*, **376**, 1329–1337.
21. Kelly, C. G., and Shattock, R. J. (2011). Specific microbicides in the prevention of HIV infection, *J. Int. Med*., **270**, 509–519.
22. Nuttall, J. (2010). Microbicides in the prevention of HIV infection: Current status and future directions, *Drugs*, **70**, 1231–1243.
23. Shattock, R. J., and Rosenberg, Z. (2012). Microbicides: Topical prevention against HIV, *Cold Spring Harb. Perspect. Med*., **2**, a007385.
24. Morris, G. C., and Lacey, C. J. (2010). Microbicides and HIV prevention: Lessons from the past, looking to the future, *Curr. Opin. Infect. Dis*., **23**, 57–63.
25. Veazey, R. S., Shattock, R. J., Pope, M., Kirijan, J. C., Jones, J., Hu, Q., Ketas, T., Marx, P. A., Klasse, P. J., Burton, D. R., and Moore, J. P. (2003). Prevention of virus transmission to macaque monkeys by a vaginally applied monoclonal antibody to HIV-1 gp120, *Nat. Med*., **9**, 343–346.
26. Moog, C., Dereuddre-Bosquet, N., Teillaud, J. L., Biedma, M. E., Holl, V., Vanham, G., Heyndrickx, L., Van Dorsselaer, A., Katinger, D., Vcelar,

B., Zolla-Pazner, S., Mangeot, I., Kelly, C., Shattock, R. J., and Le Grand, R. (2014). Protective effect of vaginal application of neutralizing and nonneutralizing inhibitory antibodies against vaginal SHIV challenge in macaques, *Mucosal Immunol*., **7**, 46–56.

27. Morris, G., Chindrove, S., Woodhall, S., Wiggins, R., Vcelar, B., and Lacey, C. (2010). A prospective randomized double blind placebo-controlled phase 1 pharmacokinetic and safety study of a vaginal microbicide gel containing three potent broadly neutralizing antibodies (2F5, 2G12, 4E10) (MabGel), *2010 International Microbicides Conference*, Pittsburgh, PA, USA.
28. Dereuddre-Bosquet, N., Morellato-Castillo, L., Brouwers, J., Augustijns, P., Bouchemal, K., Ponchel, G., Ramos, O. H., Herrera, C., Stefanidou, M., Shattock, R., Heyndrickx, L., Vanham, G., Kessler, P., Le Grand, R., and Martin, L. (2012). MiniCD4 microbicide prevents HIV infection of human mucosal explants and vaginal transmission of SHIV(162P3) in cynomolgus macaques, *PLoS Pathog*., **8**, e1003071.
29. Veazey, R. S., Klasse, P. J., Schader, S. M., Hu, Q., Ketas, T. J., Lu, M., Marx, P. A., Dufour, J., Colonno, R. J., Shattock, R. J., Springer, M. S., and Moore, J. P. (2005). Protection of macaques from vaginal SHIV challenge by vaginally delivered inhibitors of virus-cell fusion, *Nature*, **438**, 99–102.
30. Si, Z., Madani, N., Cox, J. M., Chruma, J. J., Klein, J. C., Schön, A., Phan, N., Wang, L., Biorn, A. C., Cocklin, S., Chaiken, I., Freire, E., Smith, A. B., III, and Sodroski, J. G. (2004). Small-molecule inhibitors of HIV-1 entry block receptor-induced conformational changes in the viral envelope glycoproteins, *Proc. Natl. Acad. Sci. U. S. A*., **101**, 5036–5041.
31. Pastore, C., Picchio, G. R., Galimi, F., Fish, R., Hartley, O., Offord, R. E., Mosier, D. E. (2003). Two mechanisms for human immunodeficiency virus type 1 inhibition by N-terminal modifications of RANTES, *Antimicrob. Agents Chemother*., **47**, 509–517.
32. Hartley, O., Gaertner, H., Wilken, J., Thompson, D., Fish, R., Ramos, A., Pastore, C., Dufour, B., Cerini, F., Melotti, A., Heveker, N., Picard, L., Alizon, M., Mosier, D., Kent, S., and Offord, R. (2004). Medicinal chemistry applied to a synthetic protein: Development of highly potent HIV entry inhibitors, *Proc. Natl. Acad. Sci. U. S. A*., **101**, 16460–16465.
33. Lederman, M. M., Veazey, R. S., Offord, R., Mosier, D. E., Dufour, J., Mefford, M., Piatak, M., Jr., Lifson, J. D., Salkowitz, J. R., Rodriguez, B., Blauvelt, A., and Hartley, O. (2004). Prevention of vaginal SHIV transmission in rhesus macaques through inhibition of CCR5, *Science*, **306**, 485–487.

34. Veazey, R. S., Ling, B., Green, L. C., Ribka, E. P., Lifson, J. D., Piatak, M., Jr., Lederman, M. M., Mosier, D., Offord, R., and Hartley, O. (2009). Topically applied recombinant chemokine analogues fully protect macaques from vaginal simian-human immunodeficiency virus challenge, *J. Infect. Dis*., **199**, 1525–1527.
35. Veazey, R. S., Ketas, T. J., Dufour, J., Moroney-Rasmussen, T., Green, L. C., Klasse, P. J., and Moore, J. P. (2010). Protection of rhesus macaques from vaginal infection by vaginally delivered maraviroc, an inhibitor of HIV-1 entry via the CCR5 co-receptor, *J. Infect. Dis*., **202**, 739–744.
36. Cranage, M., Sharpe, S., Herrera, C., Cope, A., Dennis, M., Berry, N., Ham, C., Heeney, J., Rezk, N., Kashuba, A., Anton, P., McGowan, I., and Shattock, R. (2008). Prevention of SIV rectal transmission and priming of T cell responses in macaques after local pre-exposure application of tenofovir gel, *PLoS Med*., **5**, e157.
37. Parikh, U. M., Dobard, C., Sharma, S., Cong, M. E., Jia, H., Martin, A., Pau, C. P., Hanson, D. L., Guenthner, P., Smith, J., Kersh, E., Garcia-Lerma, J. G., Novembre, F. J., Otten, R., Folks, T., and Heneine, W. (2009). Complete protection from repeated vaginal simian-human immunodeficiency virus exposures in macaques by a topical gel containing tenofovir alone or with emtricitabine, *J. Virol*., **83**, 10358–10365.
38. Marrazzo, J. M., Ramjee, G., Nair, G., Palanee, T., Mkhize, B., Nakabiito, C., Taljaard, M., Piper, J., Gomez, K., and Chirenje, M. (2013). Pre-exposure prophylaxis for HIV in women: Daily oral tenofovir, oral tenofovir/emtricitabine, or vaginal tenofovir gel in the VOICE study (MTN 003), *20th Conference on Retroviruses and Opportunistic Infections*, Atlanta, GA, USA.
39. Microbicide Trials Network (2013). Daily HIV prevention approaches didn't work for African women in the VOICE study. Available from URL: http://www.mtnstopshiv.org/node/4877 (last accessed Oct 10, 2013).
40. Facts Consortium (2013). Facts 001 study. Available from URL: http://www.facts-consortium.co.za/?page_id=83 (last accessed Oct 10, 2013).
41. Sluis-Cremer, N., and Tachedjian, G. (2008). Mechanisms of inhibition of HIV replication by non-nucleoside reverse transcriptase inhibitors, *Virus Res*., **134**, 147–156.
42. International Partnership for Microbicides. The Ring Study. Available from URL: http://www.ipmglobal.org/the-ring-study (last accessed Oct 10, 2013).
43. Microbicide Trials Network. (2011). MTN-020. A multi-center, randomized, double-blind, placebo-controlled phase 3 safety and

effectiveness trial of a vaginal matrix ring containing dapivirine for the prevention of HIV-1 infection in women. Available from URL: http://www.mtnstopshiv.org/sites/default/files/attachments/MTN-020%20Version1%200_28September2011_CLEAN.pdf (last accessed Oct 10, 2013).

44. Schwartz, J. L., Kovalevsky, G., Lai, J. J., Ballagh, S. A., McCormick, T., Douville, K., Mauck, C. K., and Callahan, M. M. (2008). A randomized six-day safety study of an antiretroviral microbicide candidate UC781, a non-nucleoside reverse transcriptase inhibitor, *Sex. Transm. Dis*., **35**, 414–419.
45. Bunge, K., Macio, I., Meyn, L., Noguchi, L., Parniak, M. A., Schwartz, J. L., Moncla, B., and Hillier, S. (2012). The safety, persistence, and acceptability of an antiretroviral microbicide candidate UC781, *J. Acquir. Immune Defic. Syndr*., **60**, 337–343.
46. Anton, P. A., Saunders, T., Elliott, J., Khanukhova, E., Dennis, R., Adler, A., Cortina, G., Tanner, K., Boscardin, J., Cumberland, W. G., Zhou, Y., Ventuneac, A., Carballo-Diéguez, A., Rabe, L., McCormick, T., Gabelnick, H., Mauck, C., and McGowan, I. (2011). First phase 1 double-blind, placebo-controlled, randomized rectal microbicide trial using UC781 gel with a novel index of ex vivo efficacy, *PLoS One*, **6**, e23243.
47. Kenney, J., Aravantinou, M., Singer, R., Hsu, M., Rodriguez, A., Kizima, L., Abraham, C. J., Menon, R., Seidor, S., Chudolij, A., Gettie, A., Blanchard, J., Lifson, J. D., Piatak, M., Jr., Fernández-Romero, J. A., Zydowsky, T. M., and Robbiani, M. (2011). An antiretroviral/zinc combination gel provides 24 hours of complete protection against vaginal SHIV infection in macaques, *PLoS One*, **6**, e15835.
48. Singer, R., Mawson, P., Derby, N., Rodriguez, A., Kizima, L., Menon, R., Goldman, D., Kenney, J., Aravantinou, M., Seidor, S., Gettie, A., Blanchard, J., Piatak, M., Jr., Lifson, J. D., Fernández-Romero, J. A., Robbiani, M., and Zydowsky, T. M. (2012). An intravaginal ring that releases the NNRTI MIV-150 reduces SHIV transmission in macaques, *Sci. Transl. Med*., **4**, 150ra123.
49. Caron, M., Besson, G., Etenna, S. L., Mintsa-Ndong, A., Mourtas, S., Radaelli, A., Morghen Cde, G., Loddo, R., La Colla, P., Antimisiaris, S. G., and Kazanji, M. (2010). Protective properties of non-nucleoside reverse transcriptase inhibitor (MC1220) incorporated into liposome against intravaginal challenge of rhesus macaques with RT-SHIV, *Virology*, **405**, 225–233.
50. Chung, S., Miller, J. T., Lapkouski, M., Tian, L., Yang, W., and Le Grice, S. F. (2013). Examining the role of the HIV-1 reverse transcriptase p51 subunit in positioning and hydrolysis of RNA/DNA hybrids, *J. Biol. Chem*., **288**, 16177–16184.

51. Hang, J. Q., Li, Y., Yang, Y., Cammack, N., Mirzadegan, T., and Klumpp, K. Substrate-dependent inhibition or stimulation of HIV RNase H activity by non-nucleoside reverse transcriptase inhibitors (NNRTIs), *Biochem. Biophys. Res. Commun*., **352**, 341–350.
52. Matskevich, A. A., Ziogas, A., Heinrich, J., Quast, S. A., and Moelling, K. (2006). Short partially double-stranded oligodeoxynucleotide induces reverse transcriptase/RNase H-mediated cleavage of HIV RNA and contributes to abrogation of infectivity of virions, *AIDS Res. Hum. Retroviruses*, **22**, 1220–1230.
53. Heinrich, J., Schols, D., and Moelling, K. (2012). A short hairpin loop-structured oligodeoxynucleotide targeting the virion-associated RNase H of HIV inhibits HIV production in cell culture and in huPBL-SCID mice, *Intervirology*, **55**, 242–246.
54. Dobard, C., Sharma, S., Parikh, U., Hanson, D., Lipscomb, J., Novembre, F., Smith, J., Hendry, M., Garcia-Lerma, G., and Heneine, W. (2011). High protection against vaginal infection in macaques by PEP with gel containing RAL, *18th Conference on Retroviruses and Opportunistic Infections*, Boston, MA, USA.
55. Christ, F., Voet, A., Marchand, A., Nicolet, S., Desimmie, B. A., Marchand, D., Bardiot, D., Van der Veken, N. J., Van Remoortel, B., Strelkov, S. V., De Maeyer, M., Chaltin, P., and Debyser, Z. (2010). Rational design of small-molecule inhibitors of the LEDGF/p75-integrase interaction and HIV replication, *Nat. Chem. Biol*., **6**, 442–448.
56. Stefanidou, M., Herrera, C., Armanasco, N., and Shattock, R. J. (2012). Saquinavir inhibits early events associated with establishment of HIV-1 infection: Potential role for protease inhibitors in prevention, *Antimicrob. Agents Chemother*., **56**, 4381–4390.
57. Herrera, C., and Shattock, R. J. (2012). Potential use of protease inhibitors as vaginal and colorectal microbicides, *Curr. HIV Res*., **10**, 42–52.
58. Herrera, C., Cranage, M., McGowan, I., Anton, P., and Shattock, R. J. (2009). Reverse transcriptase inhibitors as potential colorectal microbicides, *Antimicrob. Agents Chemother*., **53**, 1797–1807.
59. Herrera, C., Cranage, M., McGowan, I., Anton, P., and Shattock, R. J. (2011). Colorectal microbicide design: Triple combinations of reverse transcriptase inhibitors are optimal against HIV-1 in tissue explants, *AIDS*, **25**, 1971–1979.
60. Cost, M., Dezzutti, C. S., Clark, M. R., Friend, D. R., Akil, A., and Rohan, L. C. (2012). Characterization of UC781-tenofovir combination gel products for HIV-1 infection prevention in an ex vivo ectocervical model, *Antimicrob. Agents Chemother*., **56**, 3058–3066.

61. Hediger, M. A., Clemencon, B., Burrier, R. E., and Bruford, E. A. (2013). The ABCs of membrane transporters in health and disease (SLC series): Introduction, *Mol. Aspects Med*., **34**, 95–107.
62. Kis, O., Robillard, K., Chan, G. N., and Bendayan, R. (2010). The complexities of antiretroviral drug–drug interactions: Role of ABC and SLC transporters, *Trends Pharmacol. Sci*., **31**, 22–35.
63. Pastor-Anglada, M., Cano-Soldado, P., Molina-Arcas, M., Lostao, M. P., Larráyoz, I., Martínez-Picado, J., and Casado, F. J. (2005). Cell entry and export of nucleoside analogues, *Virus Res*., **107**, 151–164.
64. International Transporter Consortium, Giacomini, K. M., Huang, S. M., Tweedie, D. J., Benet, L. Z., Brouwer, K. L., Chu, X., Dahlin, A., Evers, R., Fischer, V., Hillgren, K. M., Hoffmaster, K. A., Ishikawa, T., Keppler, D., Kim, R. B., Lee, C. A., Niemi, M., Polli, J. W., Sugiyama, Y., Swaan, P. W., Ware, J. A., Wright, S. H., Yee, S. W., Zamek-Gliszczynski, M. J., and Zhang, L. (2010). Membrane transporters in drug development, *Nat. Rev. Drug Discov*., **9**, 215–236.
65. Shitara, Y., Horie, T., and Sugiyama, Y. (2006). Transporters as a determinant of drug clearance and tissue distribution, *Eur. J. Pharm. Sci*., **27**, 425–446.
66. Sparreboom, A., van Asperen, J., Mayer, U., Schinkel, A. H., Smit, J. W., Meijer, D. K., Borst, P., Nooijen, W. J., Beijnen, J. H., and van Tellingen, O. (1997). Limited oral bioavailability and active epithelial excretion of paclitaxel (taxol) caused by P-glycoprotein in the intestine, *Proc. Natl. Acad. Sci. U. S. A*., **94**, 2031–2035.
67. Bourgine, J., Billaut-Laden, I., Happillon, M., Lo-Guidice, J. M., Maunoury, V., Imbenotte, M., and Broly, F. (2012). Gene expression profiling of systems involved in the metabolism and the disposition of xenobiotics: Comparison between human intestinal biopsy samples and colon cell lines, *Drug Metab. Dispos*., **40**, 694–705.
68. Englund, G., Rorsman, F., Rönnblom, A., Karlbom, U., Lazorova, L., Gråsjö, J., Kindmark, A., and Artursson, P. (2006). Regional levels of drug transporters along the human intestinal tract: Co-expression of ABC and SLC transporters and comparison with Caco-2 cells, *Eur. J. Pharm. Sci*., **29**, 269–277.
69. Hilgendorf, C., Ahlin, G., Seithel, A., Artursson, P., Ungell, A. L., and Karlsson, J. (2007). Expression of thirty-six drug transporter genes in human intestine, liver, kidney, and organotypic cell lines, *Drug Metab. Dispos*., **35**, 1333–1340.
70. Zhou, T., Hu, M., Cost, M., Poloyac, S., and Rohan, L. (2013). Expression of transporters and metabolizing enzymes in the female lower genital tract: Implications for microbicide research, *AIDS Res. Hum. Retroviruses*, **29**, 1496–503.

71. Klaassen, C. D., and Aleksunes, L. M. (2010). Xenobiotic, bile acid, and cholesterol transporters: Function and regulation, *Pharmacol. Rev*., **62**, 1–96.
72. Uwai, Y., Ida, H., Tsuji, Y., Katsura, T., and Inui, K. (2007). Renal transport of adefovir, cidofovir, and tenofovir by SLC22A family members (hOAT1, hOAT3, and hOCT2), *Pharm. Res*., **24**, 811–815.
73. Ray, A. S., Cihlar, T., Robinson, K. L., Tong, L., Vela, J. E., Fuller, M. D., Wieman, L. M., Eisenberg, E. J., and Rhodes, G. R. (2006). Mechanism of active renal tubular efflux of tenofovir, *Antimicrob. Agents Chemother*., **50**, 3297–3304.
74. Siccardi, M., D'Avolio, A., Nozza, S., Simiele, M., Baietto, L., Stefani, F. R., Moss, D., Kwan, W. S., Castagna, A., Lazzarin, A., Calcagno, A., Bonora, S., Back, D., Di Perri, G., and Owen, A. (2010). Maraviroc is a substrate for OATP1B1 in vitro and maraviroc plasma concentrations are influenced by SLCO1B1 521 T > C polymorphism, *Pharmacogenetics Genomics*, **20**, 759–765.
75. Annaert, P., Ye, Z. W., Stieger, B., and Augustijns, P. (2010). Interaction of HIV protease inhibitors with OATP1B1, 1B3, and 2B1, *Xenobiotica*, **40**, 163–176.
76. Weiss, J., Rose, J., Storch, C. H., Ketabi-Kiyanvash, N., Sauer, A., Haefeli, W. E., and Efferth, T. (2007). Modulation of human BCRP (ABCG2) activity by anti-HIV drugs, *J. Antimicrob. Chemother*., **59**, 238–245.
77. Weiss, J., Theile, D., Ketabi-Kiyanvash, N., Lindenmaier, H., and Haefeli, W. E. (2007). Inhibition of MRP1/ABCC1, MRP2/ABCC2, and MRP3/ABCC3 by nucleoside, nucleotide, and non-nucleoside reverse transcriptase inhibitors, *Drug Metab. Dispos*., **35**, 340–344.
78. Meech, R., Miners, J. O., Lewis, B. C., and Mackenzie, P. I. (2012). The glycosidation of xenobiotics and endogenous compounds: Versatility and redundancy in the UDP glycosyltransferase superfamily, *Pharmacol. Ther*., **134**, 200–218.
79. Bièche, I., Narjoz, C., Asselah, T., Vacher, S., Marcellin, P., Lidereau, R., Beaune, P., and de Waziers, I. (2007). Reverse transcriptase-PCR quantification of mRNA levels from cytochrome (CYP)1, CYP2 and CYP3 families in 22 different human tissues, *Pharmacogenetics Genomics*, **17**, 731–742.
80. Nakamura, A., Nakajima, M., Yamanaka, H., Fujiwara, R., and Yokoi, T. (2008). Expression of UGT1A and UGT2B mRNA in human normal tissues and various cell lines, *Drug Metab. Dispos*., **36**, 1461–1464.
81. Naranbhai, V., Abdool Karim, S. S., Altfeld, M., Samsunder, N., Durgiah, R., Sibeko, S., Abdool Karim, Q., and Carr, W. H. (2012). Innate immune activation enhances HIV acquisition in women, diminishing the effectiveness of tenofovir microbicide gel, *J. Infect. Dis*., **206**, 993–1001.

82. Sewankambo, N., Gray, R. H., Wawer, M. J., Paxton, L., McNaim, D., Wabwire-Mangen, F., Serwadda, D., Li, C., Kiwanuka, N., Hillier, S. L., Rabe, L., Gaydos, C. A., Quinn, T. C., and Konde-Lule, J. (1997). HIV-1 infection associated with abnormal vaginal flora morphology and bacterial vaginosis, *Lancet*, **350**, 546–550.
83. Galvin, S. R., and Cohen, M. S. (2004). The role of sexually transmitted diseases in HIV transmission, *Nat. Rev. Microbiol*., **2**, 33–42.
84. Mullin, J. M., Agostino, N., Rendon-Huerta, E., and Thornton, J. J. (2005). Keynote review: Epithelial and endothelial barriers in human disease, *Drug Discov. Today*., **10**, 395–408.
85. Rosenthal, R., Milatz, S., Krug, S. M., Oelrich, B., Schulzke, J. D., Amasheh, S., Günzel, D., and Fromm, M. (2010). Claudin-2, a component of the tight junction, forms a paracellular water channel, *J. Cell Sci*., **123** (Pt 11), 1913–1921.
86. Gutmann, H., Hruz, P., Zimmermann, C., Straumann, A., Terracciano, L., Hammann, F., Lehmann, F., Beglinger, C., and Drewe, J. (2008). Breast cancer resistance protein and P-glycoprotein expression in patients with newly diagnosed and therapy-refractory ulcerative colitis compared with healthy controls, *Digestion*, **78**, 154–162.
87. Wojtal, K. A., Eloranta, J. J., Hruz, P., Gutmann, H., Drewe, J., Staumann, A., Beglinger, C., Fried, M., Kullak-Ublick, G. A., and Vavricka, S. R. (2009). Changes in mRNA expression levels of solute carrier transporters in inflammatory bowel disease patients, *Drug Metab. Dispos*., **37**, 1871–1877.
88. Kiser, P. F., Mahalingam, A., Fabian, J., Smith, E., Damian, F. R., Peters, J. J., Katz, D. F., Elgendy, H., Clark, M. R., and Friend, D. R. (2012). Design of tenofovir-UC781 combination microbicide vaginal gels, *J. Pharm. Sci*., **101**, 1852–1864.
89. Damian, F., Fabian, J., Friend, D. R., and Kiser, P. F. (2010). Approaches to improve the stability of the antiviral agent UC781 in aqueous solutions, *Int. J. Pharm*., **396**, 1–10.
90. Baum, M. M., Butkyavichene, I., Gilman, J., Kennedy, S., Kopin, E., Malone, A. M., Nguyen, C., Smith, T. J., Friend, D. R., Clark, M. R., and Moss, J. A. (2012). An intravaginal ring for the simultaneous delivery of multiple drugs, *J. Pharm. Sci*., **101**, 2833–2843.
91. Loxley, A., Gokhale, A., McConnell, J., Okoh, O., Edwards, K. L., Mitchnick, M. (2010). Combination ethylene vinyl acetate intravaginal rings containing dapivirine and maraviroc, *2010 International Microbicides Conference*, Pittsburgh, PA, USA.
92. Nazli, A., Chan, O., Dobson-Belaire, W. N., Ouellet, M., Tremblay, M. J., Gray-Owen, S. D., Arsenault, A. L., and Kaushic, C. (2010). Exposure to

HIV-1 directly impairs mucosal epithelial barrier integrity allowing microbial translocation, *PLoS Pathog*., **6**, e1000852.

93. Brass, A. L., Dykxhoorn, D. M., Benita, Y., Yan, N., Engelman, A., Xavier, R. J., Lieberman, J., and Elledge, S. J. (2008). Identification of host proteins required for HIV infection through a functional genomic screen, *Science*, **319**, 921–926.
94. König, R., Zhou, Y., Elleder, D., Diamond, T. L., Bonamy, G. M., Irelan, J. T., Chiang, C. Y., Tu, B. P., De Jesus, P. D., Lilley, C. E., Seidel, S., Opaluch, A. M., Caldwell, J. S., Weitzman, M. D., Kuhen, K. L., Bandyopadhyay, S., Ideker, T., Orth, A. P., Miraglia, L. J., Bushman, F. D., Young, J. A., and Chanda, S. K. (2008). Global analysis of host-pathogen interactions that regulate early-stage HIV-1 replication, *Cell*, **135**, 49–60.
95. Zhou, H., Xu, M., Huang, Q., Gates, A. T., Zhang, X. D., Castle, J. C., Stec, E., Ferrer, M., Strulovici, B., Hazuda, D. J., and Espeseth, A. S. (2008). Genome-scale RNAi screen for host factors required for HIV replication, *Cell Host Microbe*, **4**, 495–504.
96. Bushman, F. D., Malani, N., Fernandes, J., D'Orso, I., Cagney, G., Diamond, T. L., Zhou, H., Hazuda, D. J., Espeseth, A. S., König, R., Bandyopadhyay, S., Ideker, T., Goff, S. P., Krogan, N. J., Frankel, A. D., Young, J. A., and Chanda, S. K. (2009). Host cell factors in HIV replication: Meta-analysis of genome-wide studies, *PLoS Pathog*., **5**, e1000437.